Study of Molecular Interactions at the Oil-water Interface

Jeferson Augusto Valencia-Dávila

A thesis submitted to the science faculty in partial fulfillment of the requirements for the degree of DOCTOR IN CHEMISTRY

Advisors
Marianny Y. Combariza, Chemist, PhD.
Cristian Blanco-Tirado, Chemist, PhD.

Universidad Industrial de Santander
Science Faculty
School of Chemistry
Doctorate in Chemistry
Bucaramanga
2019

DEDICATION

Dedicated to my mother, Luz Marina, who has always been a constant support. Her endless love has sustained me throughout my life.

To Catalina for all her love, I am thankful for having you in my life.

ACKNOWLEDGMENTS

I gratefully acknowledge the financial support provided by COLCIENCIAS through the graduate fellowship 567-2012. I also acknowledge to ECOPETROL for financial support from the research agreement grants 5211794 and 672-2011. I want to thank technical support from the Central research laboratory facilities at Guatiguara´s campus (Microscopy Lab, XRD Lab, Spectroscopy Lab) and the Mass Spectrometry Lab-Central Research Laboratory Facility at Universidad Industrial de Santander for infrastructural support.

I would like to express my gratitude to my advisors Dr. Marianny Combariza and Dr. Cristian Blanco for the guidance and mentorship during my doctorate.

Many thanks also to Dr. Harvey Yarranton who allowed me to work on his research group. Special thanks to Elaine Baydak for her asssistance and training during the experimental work at the University of Calgary.

I also wish to express my gratitude to Dr. Matthias Witt for his collaboration with the characterization of naphthenic acids by MALDI high resolution mass spectrometry.

I would like to thank Dr. Wanderson Romão and Dr. Boniek Gontijo for technical support from their research laboratory facilities at UFES and UFG in Brazil.

Finally, I want to express my gratitude to my family, girlfriend and friends for their support during my doctorate program. To all of them, thank you for your understanding and encouragement**.**

TABLE OF CONTENTS

LIST OF TABLES

LIST OF FIGURES

LIST OF APPENDICES

RESUMEN

TÍTULO: Estudio de interacciones moleculares en la interfase agua-aceite*
AUTOR: Jeferson A. Valencia Dávila**
PALABRAS CLAVE: Ácidos nafténicos, asfaltenos, espectrometría de masas MALDI, espectrometría de masas ESI, emulsiones, celulosa, membranas hidrofóbicas

DESCRIPCIÓN:

Los resultados de este trabajo de investigación y otros relacionados con el área de petroleómica del grupo de investigación GIFTEX buscan contribuir al mejoraramiento de los procesos de recobro mejorado, transporte y refinación de crudos pesados a nivel mundial. Uno de los problemas que afecta toda la cadena de producción de crudo es la formación de emulsiones agua-aceite, un fenómeno complejo debido a la diversidad y gran cantidad de compuestos presentes en los crudos. Esta investigación, busca entender la influencia de un grupo de compuestos polares conocidos como ácidos nafténicos en la formación de emulsiones (estabilizadas por asfaltenos) mediante la caracterización molecular por espectrometría de masas usando técnicas de ionización suave como la desorción por láser asisitida por una matriz (MALDI) y la ionización por electronebulización (ESI).

Por primera vez y usando una matriz comercial altamente básica fue posible detectar por MALDI FT-ICR/MS un mayor número y tipo de clases de ácidos nafténicos extraídos de un crudo colombiano, que no se habían reportado por la ténica tradicional ESI FT-ICR/MS. Adicionalmente, se determinó el efecto de los ácidos en la estabilidad de las emulsiones, la tension interfacial dinámica y las propiedades interfaciales de los asfaltenos mediante isotermas de presión de superficie. Los resultados permitieron entender posibles interacciones entre ácidos y asfaltenos en la interface aceite-agua.

Finalmente, se realizó la separación de emulsiones estabilizadas por asfaltenos y mezclas aceite-agua, a través de una membrana de celulosa hidrofóbica.

---

*Tesis de doctorado
**Facultad de Ciencias. Escuela de química. Directores: Marianny Y. Combariza, Química, Ph.D- Cristian Blanco Tirado, Químico, Ph.D.

ABSTRACT

TITLE: Study of molecular interactions at the oil-water interface*
AUTHOR: Jeferson A. Valencia Dávila**
KEYWORDS: Naphthenic acids, asphaltenes, MALDI mass spectromety, ESI mass spectrometry, W/O emulsions, cellulose, hydrophobic membranes

DESCRIPTION:

This research work and others related to the area of petroleomics of the GIFTEX research group seek to contribute to the improvement of the processes of enhanced recovery, transportation and refining of heavy crude oils worldwide. One of the problems affecting the entire oil production chain is the formation of water-in-oil emulsions; a complex phenomenon due to the diversity and large number of compounds present in the crude oils. This research seeks to understand the influence of a group of polar compounds known as naphthenic acids in the formation of emulsions (stabilized by asphaltenes) by molecular characterization using mass spectrometry coupled to soft ionization techniques such as matrix assisted laser desorption ionization (MALDI) and electrospray ionization (ESI).

For the first time and using a highly basic commercial matrix, it was possible to detect by MALDI FT-ICR/MS, a greater number and type of naphthenic acid classes extracted from a Colombian crude oil, which had not been reported by the traditional ESI FT-ICR / MS technique. Additionally, the effect of the acids on the stability of the emulsions, the dynamic interfacial tension and the interfacial properties of the asphaltenes were determined by surface pressure isotherms. The results allowed to understand possible interactions between acids and asphaltenes at the oil-water interface.

Finally, separations of immiscible mixtures and emulsions stabilized by asphaltenes, were successfully achieved through a hydrophobic cellulose membrane.

---

*Doctoral thesis

**Science Faculty. School of Chemistry. Advisors: Marianny Y. Combariza, Chemist, Ph.D-Cristian Blanco Tirado, Chemist, Ph.D

Introduction

The worldwide decrease in light crude oils reserves has promoted the development of new extraction techniques to recover heavy crude oils found in the reservoirs. Heavy crude oils are now essential to maintain oil production in Colombia. Therefore, their extraction has been increasing and adapting over time.

Heavy crude oils are difficult to process because they cause serious problems during transportation, production and refining due to their high viscosity that has been related to a high content of asphaltenes and also with the formation and stabilization of water-in-oil emulsions that increase even more the viscosity of the streams.

For this reason, the oil industry around the world seeks strategies to inhibit or break emulsions in order to increase the recovery factor. Several studies found in the literature pointed out that asphaltenes are responsible for the formation of stable emulsions. However, the role of other native surfactants present in the crude oils such as naphthenic acids (NA) is not completely understood. Therefore, the interaction of NA and asphaltenes is important, however it is necessary to have information about the molecular composition of the NA mixtures before studying their interfacial properties. In this way, analytical methods were developed in mass spectrometry (low, medium and high resolution) in order to determine the molecular composition.

Unlike other studies where naphthenic acids correspond to commercial standards, the samples used in this research corresponded to complex mixtures of naphthenic acids extracted directly from heavy crude oils. For the first time, the molecular characterization of these acids was performed

using matrix assisted laser desorption ionization (MALDI) source through the use of highly basic matrices such as 9-aminoacridine and 1,8-bis(dimethylamino) naphthalene.

Further analysis of naphthenic acids of different molecular weight by high resolution mass spectrometry (MALDI FT-ICR/MS) allowed the detection of new heteroatom families. These compound classes had not been detected previously with ESI source, typically used for the characterization of these mixtures. The methodology was tested with both time of flight (TOF) and fourier transform ion cyclotron (FT-ICR) mass analyzers.

Once the analytical methods were developed, the effect of NA on the asphaltenes intefacial films at the oil-water interface was determined. Interfacial tension measurements and surface pressure isotherms helped to understand this phenomenon in a more complete way.

Finally, a hydrophobic membrane was used to separate immiscible oil/water mixtures and emulsions stabilized by asphaltenes. A two-step method was utilized to prepare the hydrophobic cellulosic membrane involving a SiO_2 sol-gel process, to increase surface roughness, followed by grafting of hexadecyltrimethoxysilane groups to chemically enhance the membrane's water repellency.

1. Analysis of naphthenic acids by matrix assisted laser desorption ionization time of flight mass spectrometry

We report on a matrix-assisted laser desorption/ionization time of flight mass spectrometry (MALDI-TOF) method to analyze naphthenic acids (NA), from petrochemical samples, using 9-aminoacridine (9-AA) and a proton sponge 1,8-bis(dimethylamino) naphthalene (DMAN), as matrices. Singly charged deprotonated molecules of NA, $[M - H]^-$, dominated the negative ion MALDI mass spectra. The negative ions were pre-formed in solution through an acid/base Brönsted-Lowry reaction promoted by the highly basic matrices (9-AA and DMAN).

The DMAN afforded cleaner spectra with absence of clusters, aggregates or matrix interferences at low *m/z*; in addition, it provides molecular weight distributions similar to those observed with negative ion ESI. In contrast, MALDI spectra obtained with 9-AA exhibits matrix interferences at low mass, and bias towards aliphatic NA. Finally, we observe the presence of monomeric species in the low mass region and non-covalent aggregates at higher masses in the negative mode MALDI spectra with both matrices, much like with negative mode electrospray ionization (ESI).

We demonstrate that MALDI-TOF/MS is a viable tool for NA analyses with added advantages such as high throughput and exceptional tolerance to the presence of impurities and salts in the samples, when compared with ESI (See figure 1).

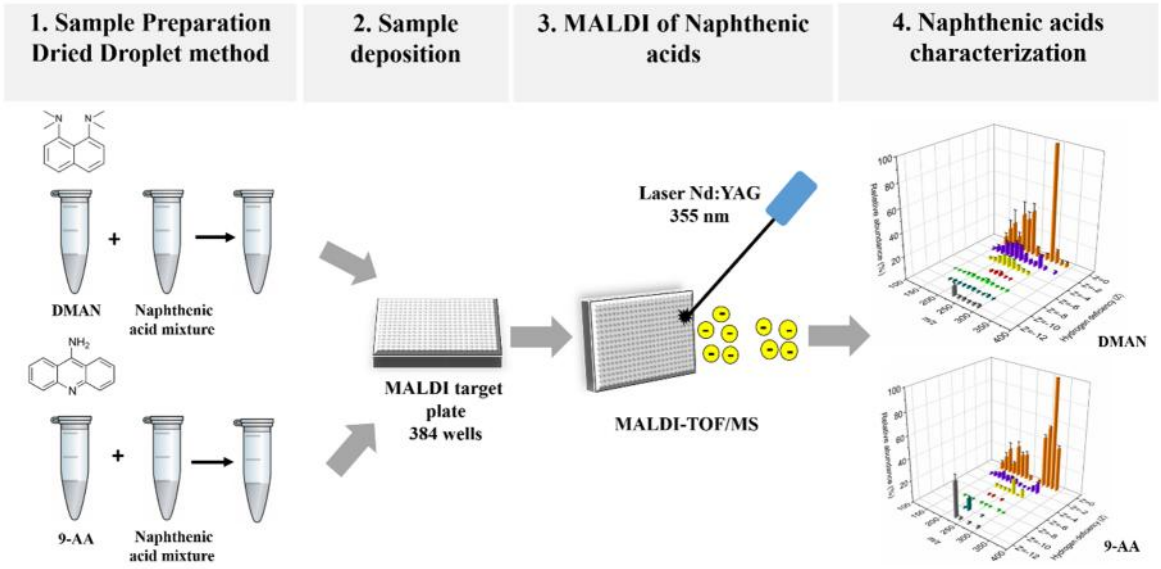

Figure 1. Analysis of NA by MALDI-TOF mass spectrometry.

1.1 Introduction

Naphthenic acids (NA) are possibly originated from the microbial oxidation of hydrocarbons, and are commonly found in immature and biodegraded heavy crude oils together with other polar compounds such as carbazoles and phenols. Some NA have been used as biomarkers by geochemists to indicate crude oil sources of origin (Hughey, Galasso, & Zumberge, 2007).

NA are complex mixtures of mono alkyl-substituted cyclic and acyclic compounds existing in various isomeric forms for a particular elemental composition. The formula $C_nH_{2n+z}O_2$ typically defines NA, where Z (an even negative integer) refers to the hydrogen deficiency and its modulus divided by two indicates the number of rings present in the acid structure.

NA and other polar molecules constitute around 3 to 5 wt % of the crude oil and, despite their low content, they are responsible for many problems in production and processing schemes. For

instance, flow assurance problems during recovery of heavy crude oil occur when pressure reduction in the well induces water degassing and release of dissolved carbon dioxide.

This phenomenon causes an increase in pH and dissociation of NA to form carboxylate ions. These anionic species readily react with inorganic cations (Na^+, Ca^{2+}) present in water, to form salts known as naphthenates (Igwebueze, Oduola, Smith, & Company, 2013; M. a. Mohammed & Sorbie, 2010; M. A. Mohammed, Sorbie, Shepherd, Solutions, & International, 2008; Nordgård, Magnusson, Hanneseth, & Sjöblom, 2009). Sodium naphthenates, in particular, are known to stabilize water in oil emulsions; while calcium naphthenates are generally sticky or solid deposits formed mostly of tetra acids known as ARNs (Baugh et al., 2005; Brocart, Bourrel, Hurtevent, Volle, & Escoffier, 2007; Mapolelo et al., 2011a; Sutton & Rowland, 2014).

These compounds, found across the whole oil production system (wellheads, electrostatic coalescers, oil/water separators, heat exchangers tubes and storage tanks) are responsible for unexpected refineries shutdowns and lengthily clean-up procedures that affect productivity (Mapolelo et al., 2011a). Additionally, because of their amphiphilic properties, naphthenates can stabilize water in oil (w/o) emulsions causing severe flow assurance problems related mainly to an increase in fluid viscosity (Alvarado, Wang, & Moradi, 2011; Ese & Kilpatrick, 2004; S. Gao, Moran, Xu, & Masliyah, 2010; Knudsen, Nordgård, Diou, & Sjöblom, 2012; Pauchard et al., 2009). Thus, characterization of NA is fundamental to better understand the stabilization mechanisms of w/o emulsions and to provide useful information to design new and effective demulsifying processes for heavy crude oils. In addition, NA identification is useful to establish correlations between undesirable NA-induced corrosion and the chemical nature of NA (Flego, Galasso, Montanari, & Gennaro, 2014; Klein, Rodgers, Teixeira, Teixeira, & Marshall, 2003; Laredo, López, Álvarez, Castillo, & Cano, 2004).

NA are considered a complex mixture and their characterization by mass spectrometry has been reported using different ionization techniques and a wide variety of analyzers (Gruber, L. D. A., Damasceno, F. C., Caramão, E. B., Jacques, R. A., Geller, A. M., & de Campos, 2012). For instance, electron ionization (EI) (Vaz de Campos, Oliveira, Filho, Piatnicki, & Caramão, 2006), chemical ionization (CI), electrospray ionization (Kuangnan Qian et al., 2008), nano- electrospray ionization (ESI) (Barrow, McDonnell, Feng, Walker, & Derrick, 2003), fast atom bombardment ionization (FAB) (Laredo, López, Álvarez, & Cano, 2004), atmospheric pressure chemical ionization (APCI) (Hsu, Dechert, Robbins, & Fukuda, 2000) and atmospheric pressure photoionization (APPI) (Barrow, Witt, Headley, & Peru, 2010) have been employed to assign NA in crude oil, distillates, bitumen, oil sands, process water(S. J. Rowland, Scarlett, Jones, West, & Frank, 2011) and even natural water.

Nowadays, ESI coupled to Fourier transform ion cyclotron resonance mass spectrometry (FT-ICR) (John V Headley, Peru, Barrow, & Derrick, 2007; S. M. Rowland, Robbins, Corilo, Marshall, & Rodgers, 2014; Q. Shi et al., 2010; Smith et al., 2008), is also widely used to characterize NA. Soft ionization methods for NA analysis offer not only high selectivity and sensitivity without fragmentation, but also solve problems related with GC/EI-MS approaches that required long extraction procedures and derivatization, resulting in an incomplete detection and extensive fragmentation of these species (Damasceno et al., 2014; Vaz de Campos et al., 2006).

Recently, laser desorption ionization (LDI) in negative ion mode coupled to FT-ICR (Cho, Witt, Kim, & Kim, 2012) was used to assign oxygenated compounds in three crude oils with different total acid number (TAN) values. This report concluded that the O_2 compound class readily forms negative ions due to the oxygen electronegativity and the acidity of the OH group that helps to stabilize the ion's charge. In addition, detection of non-aromatic O_x (x= 1, 2) compound classes,

as deprotonated molecules $[M - H]^-$, with DBE values from 1 to 3 supports this conclusion. However, as the DBE values increase NA radical anions become more abundant than the deprotonated molecules in the LDI spectrum. This suggests that as the analyte's aromaticity increases, electron capture becomes the dominant mechanism in negative ion mode ionization due to the high electron affinity of polyaromatic species.

Consequently, in a complex mixture, non-aromatic NA tend to exhibit low abundances and S/N ratios in LDI. This disadvantage could be addressed using a suitable matrix able not only to stabilize deprotonated molecules but also to absorb energy (337 or 355 nm) and promote efficient desorption of both non-aromatic and aromatic species. For example, several strong and weakly acidic metabolites such as fatty acids, amino acids, hormones and lipids were ionized in negative ion mode using 1,8-bis(dimethylamino) naphthalene (DMAN) as MALDI matrix (Shroff & Svatoš, 2009). This highly basic matrix allowed the identification of these analytes directly in complex biological samples such as leaves (*Arabidopsis thaliana*), insects bodies (*melanogaster* males and females) and even human blood, with detection limits as low as pico- and femto-moles (Shroff, Rulísek, Doubsky, & Svatos, 2009). DMAN is particularly suitable for analysis of low molecular weight metabolites due to the absence of interfering matrix signals or clusters in the low mass range; for this reason, it is also called an ion-less matrix.

Another matrix, 9-aminoacridine, has also been successfully employed to detect small metabolites such as aliphatic and aromatic carboxylic acids, phytohormones and amino acids in complex biological matrices with detection limits in the femto-mole range (Shroff, Muck, & Svatos, 2007; Vermillion-Salsbury & Hercules, 2002).

On the other hand, high molecular weight matrices are alternatives to overcome the problem of interfering ions in the low mass region, common when using traditional matrices such as 2,5-dihidroxy benzoic acid (DHB), α-cyano-4-hydroxycinnamic acid (CHCA) and sinapinic acidic to analyze acidic compounds.

The matrix meso-tetrakis-pentafluorophenyl-porphyrin (M_r ~974 Da) does not show clusters or matrix ions in the low mass region and has been employed to characterize, by MALDI-TOF/MS, low molecular weight compounds particularly saturated fatty acids (<1000 Da) (Ayorinde, Garvin, & Saeed, 2000). In addition, some high molecular weight metal phthalocyanines (Al, Ga, In) have also been used as a MALDI matrices to ionize, in negative ion mode, small molecules such as citric acid, stearic acid, salicylic acid, cholic acid, palmitic acid and gibberellic acid, without interference matrix peaks at low mass (S. Zhang et al., 2010).

In this contribution we explore the versatility of UV-MALDI for the analysis of NA from petrochemical samples using 9-aminoacridine and 1,8-bis(dimethylamino) naphthalene (DMAN, “proton sponge”) as basic matrices. To the best of our knowledge there are no reports in literature related to the characterization of NA by MALDI, which is surprising considering that the technique is commonly used for the characterization of polar analytes such as proteins, peptides, carbohydrates and polymers and, more recently, for the analysis of low molecular weight metabolites (including carboxylic acids). MALDI-TOF analyses have the advantage of high throughput and exceptional tolerance to the presence of impurities and salts in the samples in contrast with ESI, routinely used for NA analysis by MS.

1.2 Experimental section

1.2.1 Materials. 1,8-Bis(dimethylamino) naphthalene (DMAN), 9-aminoacridine (9-AA) and a mixture of naphthenic acids (Fluka 70340) were acquired from Sigma Aldrich (St. Louis, MO, USA). HPLC grade acetonitrile (ACN) and methanol (MeOH) were purchased from Merck (Germany). All chemicals are commercially available and were used as supplied. All aqueous solutions were prepared using deionized water with resistivity <18 MΩ/cm.

The ion exchange sugar (poly-1, 6-glucose) based resin QAE-Sephadex® A-25 (Chloride form) were acquired from Sigma-Aldrich (St. Louis, MO).

1.2.2 Sample preparation. For MALDI analysis, stock solutions of DMAN and 9-AA were prepared in ACN:H2O (1:1) at 0.5 mM and 2mM, respectively. A stock solution (2mM) of the NA standard mixture was also prepared in ACN:H2O (1:1). NA molar concentrations were calculated using an average molecular weight of 240 g/mol previously reported for the same NA standard mixture (Taylor, Havre, Sjöblom, Vindstad, & Sjo, 2003). The NA stock solution was mixed in appropriate amounts with 9-AA and DMAN to reach analyte:matrix molar ratios of 1:1, 1:4, 1:20, 1:40, 1:200 and 1:4000.

The NA/matrix solutions were homogenized on a vortex for 20 minutes and 1.0 µL of each resulting solution was deposited on a ground steel MALDI plate, and allow drying prior MS analysis, for final amounts of NA ranging from 1 nmol/well to 250 fmol/well.

A real naphthenic acid mixture was extracted from a heavy crude oil distillation cut (370-510 °C) using an anion exchange procedure according to the following: a sugar based resin (Sephadex A-25) was activated using a buffer solution of sodium carbonate/sodium bicarbonate with an

alkaline pH of 9.8. After this, the chloride initially attached to the resin is displaced by the bicarbonate ion (HCO_3^-); this process is known as resin activation. Subsequently, the distillate cut sample and the resin are dissolved in tolune and gently mixed for sixteen hours. After reaction completion, bicarbonate ions are replaced by the carboxylate anions in the samples. Several washes with toluene and a mixture of toluene/methanol (2:1 % v/v) are used to eliminate interferences before final elution of the NA with an acidic (1% v/v formic acid) toluene/methanol (1:1 % v/v) mixture. The elution solution was collected and the solvent excess was evaporated at 60°C to obtain a concentrated acid extract.

The NA extract was dissolved in ACN/MeOH (1:1) down to 0.5 mM using an average molecular weight of 538 g/mol. This solution was mixed, in equal volumes, with a solution of DMAN in ACN/MeOH (1:1) to reach a 1:1 analyte/matrix molar ratio. The resulting NA mixture/matrix solution was homogenized on a vortex for 20 minutes and 1.0 µL of the solution was deposited on a ground steel MALDI plate.

On the other hand, for ESI MS analysis 10 ppm solutions of the standard NA sample and the NA extracted from distillation cut (370-510 °C) in ACN/MeOH (1:1) were mixed with (1 % v/v) ammonium hydroxide (25% aqueous solution) to assist the deprotonation process.

1.2.3 Mass Spectrometry

1.2.3.1 ***MALDI.*** A Bruker Ultraflextreme MALDI TOF-TOF instrument (Bruker Daltonics, Billerica, MA) was used to perform MALDI analysis. The instrument is equipped with a 1 kHz Smart Beam Nd:YAG laser (355 nm) operated at 40 and 60% of the instrument arbitrary power scale (1.92 µJ/pulse and 4.17 µJ/pulse), as threshold values for NA signal detection with 9-AA and DMAN, respectively.

Lower laser power outputs resulted in no signal detection for the NA mixture regardless of the matrix:analyte ratios. Negative ion mass spectra, from m/z 100 to 1000, were acquired in reflectron mode with delayed extraction set at 100 ns and accelerating voltage of 20 kV.

Instrument calibration was performed using 1,5-diaminonaphthalene and a mixture of phthalocyanines, purchased from Sigma Aldrich (St. Louis, MO), covering the working mass range. Additionally, mass spectra were internally calibrated using a list of homologous series of naphthenic acids with different hydrogen deficiency.

To ensure unbiased data acquisition we used an autoexecution method within the FlexControl software (Bruker Daltonics, Billerica, MA) of the instrument; each reported analysis corresponds to the sum of 4000 mass spectra. Data analysis was performed using the FlexAnalysis software (Bruker Daltonics, Billerica MA, USA). The software automatically reports ion abundances, S/N ratios, signal resolution, peak area, and monoisotopic masses. Experimental and theoretical isotope patterns, calculated with ChemCalc (“http://www.chemcalc.org,” 2016), were compared to verify compound identification.

1.2.3.2 *ESI.* A Bruker AmaZon X ESI-Ion Trap mass spectrometer (Bruker Daltonics, Billerica MA, USA) was used to perform ESI analysis. The ESI ion source was operated in negative ion mode with a capillary voltage of 4.5 kV, source temperature of 350°C and nitrogen as nebulizing (2.0 µL/min) and drying gas (10 psi). Full scan mass spectra were acquired scanning from m/z 100 to 1000.

The NA solutions (10 ppm) in ACN:H_2O (1:1) and ACN:MeOH (1:1) were injected using a syringe pump at a flow rate of 2 µL/min. Mass spectral assignments for NA standard mixture were performed with a homemade FORTRAN 95 program by matching nominal masses, from

experimental mass spectra, with theoretical nominal masses calculated from a predefined set of naphthenic acid structures. ^{13}C even mass signals were excluded and only monoisotopic *m/z* signals were classified and assigned to specific hydrogen deficiency values (Z=0, -2, -4, -6, -8, -10 and -12). Final report includes naphthenic acids classification by Z values with their relative percentages within the whole sample.

1.3 Results and discussion

In negative ion ESI, common acidic compounds present in petrochemical samples such as naphthenic acids, carbazoles and phenols, are easily observed as singly deprotonated molecules $[M - H]^-$(Mapolelo et al., 2011a; Kuangnan Qian et al., 2008; Terra et al., 2014; Vaz, Abdelnur, Rocha, Gomes, & Pereira, 2013). In addition some sulfur- and nitrogen-containing species, N_XO_X, N_XS_X, $N_XS_XO_X$, S_XO_X, can also be detected (Hughey et al., 2007; K. Qian, Rodgers, Hendrickson, Emmett, & Marshall, 2001; Stanford, Kim, Rodgers, & Marshall, 2006; Teräväinen, Pakarinen, Wickström, & Vainiotalo, 2007).

Fig. 2 shows the ESI (-) mass spectrum of the commercial NAstandard from *m/z* 100 to 1000, mass profiles of monomeric naphthenic acids from Z=0 to Z=-12, relative abundances of each acid family in the sample and some typical naphthenic acid structures (Kuangnan Qian et al., 2008). NA in the ESI mass spectrum were detected as deprotonated molecules $[M - H]^-$ with a base peak at *m/z* 297.3 corresponding to a C_{19} (Z=0) aliphatic acid (Fig. 2a).

The presence of low abundance non-covalent singly charged aggregates (dimers and trimers) of deprotonated molecules sharing a proton are observed between *m/z* 400.0 and 1000.0. The inset in Fig. 2a shows two distinct distributions centered at average values of *m/z* 495.9 and *m/z* 799.1 which clearly indicate the presence of dimers and trimers, respectively (Smith et al., 2007).

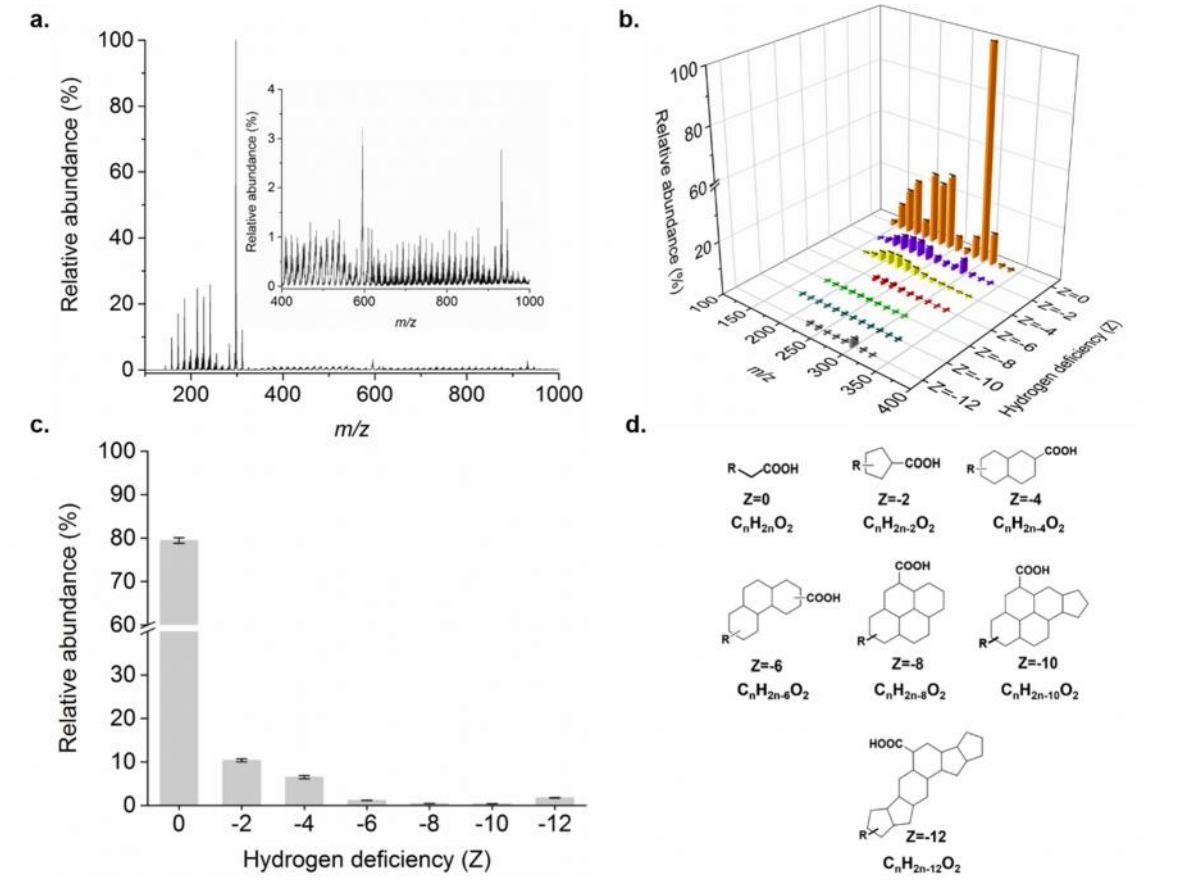

Figure 2. a) ESI(-) mass spectrum of NA, inset graph shows the presence of low abundance dimers and trimers; b) mass profiles; c) relative abundances vs hydrogen deficiency (Z) and d) basic structures of NA in the standard mixture.

In addition, Fig. 2b shows mass spectral profiles segregated in terms of hydrogen deficiency. This graph allows observation of individual contributions, *per* NA familiy, to the overall mass spectrum in the *m/z* 100 to 400 monomeric region (Table A1 of the appendix A contains standard deviation and error values for each type of NA detected).

On the other hand, Fig. 2c shows the normalized overall NA distribution in terms Z values. Clearly class Z=0, or aliphatic carboxylic acids, comprise most of the NA mixture (79.5%) followed by Z=-2 (10.4%), corresponding to 1-ring cyclic naphthenic acids. The Z=-4 family

(6.5%) with 2-rings, the Z=-6 family (1.2%) with three rings, the Z=-8 (0.4%) family with four rings, the Z=-10 (0.4%) family with five rings and the Z=-12 (1.7 %) family with six saturated rings comprise the remaining NA observed.

Average relative abundances in ESI, as shown in Fig. 2c, exhibit low standard deviations (σ). For instance, NA with Z=0 have average relative abundance with σ of 1.12, while for Z=-2 and Z=-4 NA σ corresponds to 0.61. For Z=-12, -6, -8 and -10 σ values are 0.09, 0.08, 0.02 and 0.02 respectively (Table A.2 of the appendix A section, contains relevant analytical information regarding ESI-IT analyses such as average relative abundances with standard deviation and error values for each type of naphthenic acid family in terms of hydrogen deficiency).

Ion signal in ESI of NA mixtures depend on the ionization efficiency (IE) of the individual acids. The IE, in turn, depends on the concentration of each species and their chemical nature (pKa, polarity, solubility, etc.), besides other parameters such as solvent composition and ESI experimental conditions (Henriksen, Juhler, Svensmark, & Cech, 2005; Leito et al., 2008; Oss, Kruve, Herodes, & Leito, 2010). For instance in the ESI analysis of carboxylic acids, phenols and steroids, the IE does not correlate well with compound classes and it rather depends on the analyte's chemical nature (such as length of alkyl chains in the case of carboxylic acids) and the spraying solvent (Henriksen et al., 2005).

In another report, the negative ESI response of a series of benzoic acids was found to correlate directly with P (the partition coefficient of the analytes in water/octanol) but not with their pKa (Kruve, Kaupmees, Liigand, & Leito, 2014). The IE in ESI(-) also depends on the spray stability, which is related with physical properties of the solvent (viscosity, surface tension, desolvation of droplets) (Huffman, Poltash, & Hughey, 2012). For instance, addition of acetonitrile as a co-

solvent for the analysis of NA, from oil sands processed water, resulted in an increased spray stability and improvement of mass spectral resolution (John V Headley et al., 2007).

Finally, a predictive computational model showed that anion charge delocalization and degree of ionization in solution are the most influential molecular parameters to calculate, with good agreement, the IE of phenols and carboxylic acids in negative ESI (Kruve et al., 2014). Clearly, ESI can be successfully employed for the characterization of many kinds of acidic species.

For NA, in particular, it has been applied to the analysis of these species in crude oils, vacuum distillates and in oil sands process-affected water, among others (Barrow, Headley, Peru, & Derrick, 2009; Gabryelski & Froese, 2003; John V Headley, Peru, & Barrow, 2009; Lo, Brownlee, & Bunce, 2003; Rudzinski, Oehlers, Zhang, & Najera, 2002). However, due to the high complexity of petrochemical mixtures, contamination of the ESI source is quite common as there is a continuous injection of the diluted sample. In addition solvent compatibility and spray stability are also issues related to spectrum reproducibility in ESI when the samples are highly hydrophobic (John V Headley et al., 2007). These issues result in time- and solvent- consuming cleaning procedures, in the first case, and poor data quality in the second.

In MALDI, a pulsed desorption ionization technique, analytes are desorbed from a solid solution in nanosecond-laser pulses that decrease the risk of source contamination. Besides, due to its high sensitivity, MALDI analyses require very few amounts of sample, and because of the outstanding duty cycle of a MALDI-TOF instrument the technique allows collection of many spectra in very short periods of time (1000 or 2000 spectra per second or more, depending on the laser frequency). For these reasons, MALDI represents a robust tool for the analysis of complex petrochemical samples with high throughput.

Recent application of MALDI to the successful characterization of small acidic metabolites through acid-base Brönsted-Lowry reactions, using UV-matrices with high basicity, inspired us to develop a methodology to assign NAs using MALDI-TOF/MS. We use DMAN, commonly known as a proton sponge, and 9-AA to deprotonate NA *via* an acid-base reaction that occurs in liquid phase with the formation of carboxylate ions ($R\text{-}COO^-$), according to the following mechanism (Karas, Glückmann, & Schäfer, 2000; Karas & Krüger, 2003; Shroff et al., 2009):

$$AH_{(l)} + M_{(l)} \rightleftharpoons A^-_{(l)} + MH^+_{(l)} \quad (1)$$

$$A^- \ldots MH^+_{(s)}/AH \ldots M_{(s)} \rightarrow UV\ ablation \rightarrow A^-_{(g)} + MH^+_{(g)} \quad (2)$$

Where A is the analyte and M is the matrix. The first reaction (Eq. (1)) shows an ion pair formed in the liquid phase whose existence depends on the matrix/analyte ratio, the acidity of the analytes (pK_a) and the basicity of the matrix (pK_b). The ion pair A^-/MH^+, initially formed in solution, can also exist in solid state since the presence of a strong base (matrix) ensures proton retention and anion stabilization in both solid and gas phases (Eq. (2)).

This acid-base mechanism is generally accepted and has been tested with matrices of different basicity and molecular structure with various analytes, using mass spectrometry, NMR and X-ray diffraction techniques (Shroff et al., 2009). According to these reports, the maximum production of analyte anions (A^-) is reached when equimolar proportions of the base and acid are used.

From an analytical point of view, a MALDI matrix with high proton affinity (PA) is of fundamental importance for developing methods where anion formation and stabilization are key. In our case DMAN and 9-AA have high PAs, of 1028 and 977 kJ/mol, respectively, and can

effectively abstract protons from relatively weak acids (such as naphthenic acids) (Calvano, Monopoli, Ditaranto, & Palmisano, 2013).

The proton sponge (DMAN), in particular, is considered a highly basic compound whose high basicity is related to the electronic repulsion between the lone pair of electrons on the nitrogens, and to steric effects due to the methyl groups' hindrance (Dávalos, Lago, Costa, Santos, & González, 2012; Ozeryanskii, Pozharskii, Antonov, & Filarowski, 2014). Although still under debate, it is widely accepted that high basicity in DMAN is related more to strain relief in the molecule, when protonated, than to strengthening of the hydrogen bond (Pozharskii & Ozeryanskii, 2012). Presumably, the protonated form of DMAN ($DMANH^+$) exists in solution in the form of two tautomers according to a double well potential derived from the H motion in the N-H-N bond (Perrin & Ohta, 2001; Pozharskii & Ozeryanskii, 2012; Schlosser, 1988).

On the other hand, the 9-AA is the most basic monoaminoacridines with a pKa value of 9.99. This molecule has an acridine core with an amino group on a carbon atom located at the position 9. The basicity of this compound is attributed to the stable resonant structure of the 9-aminoacridinium ion (see Fig. A.1 of the appendix A) formed by proton transfer from the analyte to the nitrogen atom. It has also been suggested that the introduction of amino groups in the acridine core, specifically at both positions 3 and 9, may increase the base strength due to a high number of possible resonant structures (Acheson, 2009).

The 9-AA was first used as a MALDI matrix, in 2002 by Vermillion-Salsbury *et al*., to detect low molecular weight acidic analytes (carboxylic acids phenols, sulfonates, amines, alcohols) and also larger molecules such as oligonucleotides, oligoamides and proteins (Vermillion-Salsbury & Hercules, 2002).

Our initial MALDI approach for NA analysis involved the use of equimolar analyte:matrix ratios, in a similar way as for the previously reported analysis of low-molecular weight acidic metabolites (Shroff et al., 2009; Shroff & Svatoš, 2009). This choice was also supported by experiments where additional analyte:matrix ratios of 1:4, 1:20, 1:40, 1:200 and 1:4000 were tested.

In agreement with Shroff et al., (Shroff et al., 2009; Shroff & Svatoš, 2009) we observed that only equimolar analyte:matrix ratios result in ionization of all NA, with a similar distribution as observed in ESI (Fig. 2). When we used lower and higher analyte:matrix ratios, in the best of cases the MALDI spectra do not represent the NA sample composition while in the worst case we do not observe NA signals at all. Fig. A.2 of the appendix A section shows MALDI(-) spectra for analyte:matrix ratios from 1:20 to 1:0.008 (for DMAN in this particular case).

Our results show that maximum signal abundances are observed when the analyte:matrix ratio of 1:1 is reached. This effect was also observed and reported by Shroff et al., where the abundances of two deprotonated ions, from trifluoacetic and stearic acids, reached their maximum value when mixed at equimolar ratios with DMAN and dimethyl aniline (DMA). Furthermore, when the concentration of the bases DMAN and DMA increases beyond one molar equivalent, the abundance of both anions decrease, probably due to a gas phase neutralization (Shroff et al., 2009).

We also found that the “threshold concentration”, understood as the lowest amount of matrix needed for observing representative NAs signals in MALDI, is four times higher for 9-AA than for DMAN. In other words, while we can use a 0.5 mM matrix solution for DMAN, for 9-AA we use 2 mM solutions. This is probably due to the low basicity of 9-AA (pKa= 9.99) when compared to DMAN (pKa=12.6).

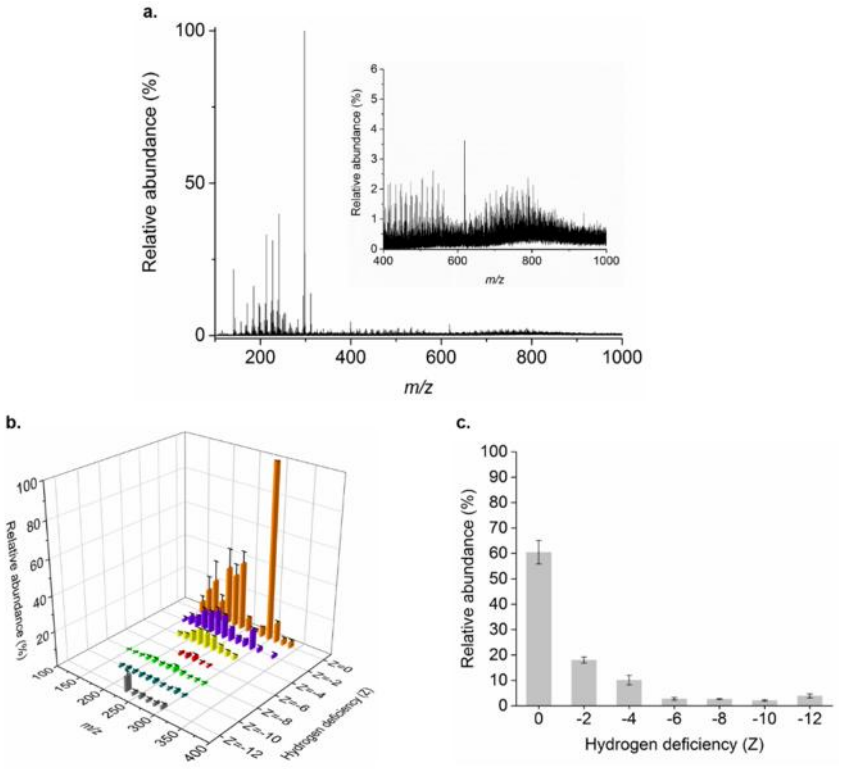

Figure 3. a) MALDI(-) MS analysis of a 1:1 NA:DMAN mixture (0.25 nmol/well and 4.17 µJ/pulse), inset graph shows the presence of low abundance dimers and trimers; b) mass profiles (Z); c) relative abundances vs hydrogen deficiency (Z) for the NA sample.

Fig. 3a shows the negative ion MALDI mass spectrum, from *m/z* 100 to 1000, for the NA sample mixed at an equimolar ratio (0.5 mM) with DMAN as matrix. Similarly, to the ESI analysis (Figure 2a), NA in the MALDI mass spectrum were detected as deprotonated molecules $[M - H]^-$ with a base peak at *m/z* 297.279 corresponding to a C_{19} (Z=0) aliphatic acid (Fig. 3a). Table A.3 of the appendix A section contains signal assignments for the monomeric $[M - H]^-$ species observed in the MALDI spectrum of Figure 3a. In addition, also like in ESI analysis, we observe the presence of low abundance non-covalent singly charged aggregates (dimers and trimers) of deprotonated molecules sharing a proton in the form of two distributions, with low relative abundance, at

approximately *m/z* 400-550 and *m/z* 625-850 (inset Fig. 3a). A reduction of sample concentration can result in a lower abundance of dimers and trimers. In addition, modification of experimental source conditions, as it has been reported in ESI, could result in the dissociation of the non-covalent aggregates observed in MALDI.

Use of DMAN results in a clean MALDI(-) mass spectrum, free of clusters or matrix ions in the low-mass region. MS profiles (Fig. 3b) show that compound distribution in MALDI, according to Z values, is comparable to the distributions observed in the ESI experiment (Fig. 2b), with Z= 0, Z= -2, Z= -4, Z= -6 as the main compound families in the NA sample (Table A.4 of the appendix A). The only major difference between the ESI and MALDI traces lies in the lower relative abundance and higher signal variability for the Z=0 NA family in MALDI (60.48 %, σ= 7.94) when compared to the ESI experiment (79.45 %, σ= 1.11) as seen in Fig. 3c. All other NA families with Z= -6, -8, -10, and Z= -12 present slightly higher relative abundances in MALDI than in ESI. In addition, the average relative abundances standard deviation (σ) in MALDI were always higher than the values measured in ESI MS analyses, as seen in Table A.5 of the appendix A section.

In MALDI, variations in relative abundances of the NA can be attributed to many variables such as analyte/matrix ratios, sample preparation, matrix pK_b, analyte pK_a, concentration, sweet spot formation and even slight differences in analyte volatility and adsorption of UV radiation (355nm), which are relevant during the desorption process from the solid phase. Relatively high σ values in MALDI signal abundances are common for the dried droplet method, used in this case, due mainly to sweet spot formation (Fukuyama, 2015; Y. L. Li & Gross, 2004) (Table A.4, from appendix A, contains standard deviations and error of the abundances for each NA detected). Dashtiev et al. followed the variation of positive/negative ion yield ratios of various analytes using six MALDI matrices with different acid/base properties. They found that positive/negative ion

yield ratios depend on experimental variables such as concentration, matrix/analyte ratios, microscopic morphology of the MALDI target, crystallization time, and sample crystallinity and homogeneity. Even the size of the matrix crystals influence the threshold laser fluence needed to desorb the sample (Hillenkamp, Wäfler, Jecklin, & Zenobi, 2009).

The inset in Fig. 3a shows the presence of low abundance dimers and trimers in the MALDI(-) spectrum of NAs using DMAN as matrix. The abundances of these aggregates increase as the amount of NA on the target increase (Fig. 4) or when the laser output increases as seen in Fig. A.3 of the appendix A.

Fig. 4 shows the effect of increasing sample amount (0.5 nmol/well) in the MALDI spectrum of NA with DMAN as matrix; this amount is twice as much as the one used for the MALDI spectrum shown in Fig. 3a.

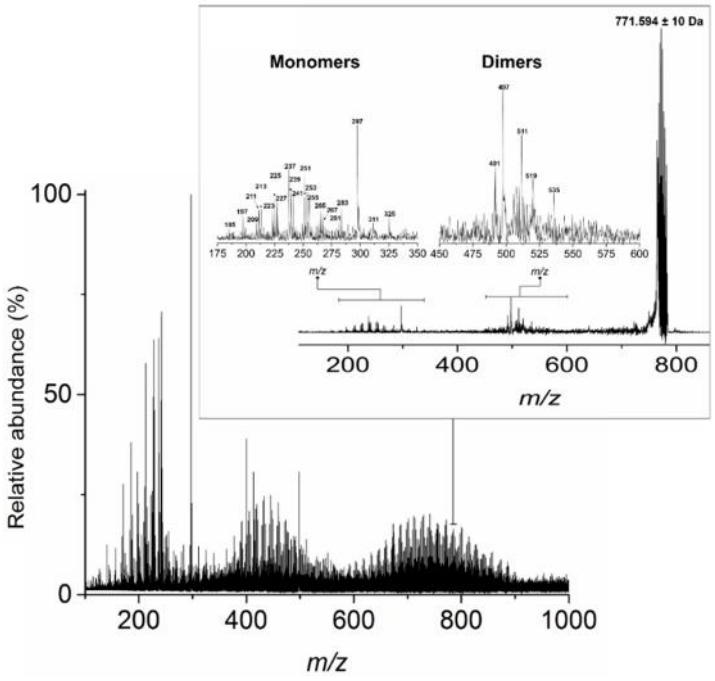

Figure 4. Effect of increasing on-target NA amount (0.5 nmol) on non-covalent aggregates formation. Inset shows the MS^2 spectrum of the precursor ion with m/z 771.594.

We observe a clear increase in the abundance of non-covalent aggregates; thus to investigate their nature we performed tandem MS experiments where we isolated an ion distribution centered at *m/z* 771.594 (with a ±10 Da window) corresponding to non-covalent trimers of the type $[3M - H]^-$, as seen in the inset in Fig. 4. Fragmentation of *m/z* 771.594 yielded two new distributions shifted to lower masses, specifically between *m/z* 150-350 and *m/z* 400-600 corresponding, respectively, to NAs monomers and dimers. The lower mass distribution in the MS^2 spectrum reflects the full scan mass spectrum in Fig. 3a and contains deprotonated monomeric NAs of low molecular weight and varied hydrogen deficiencies such as: *m/z* 185.154, 213.185, 227.201, 241.217, 255.232, 283.264, 297.279, 311.295 and 325.311 (Z=0); *m/z* 197.153, 211.168, 225.184, 253.217 and 267.232 (Z=-2); *m/z* 209.154, 223.170, 237.185, 251.200, 265.216 (Z=-4), 235.170, 263.203 (Z=-6). The medium mass distribution in the MS^2 spectrum, with signals at *m/z* 491.410,

497.457, 511.473, 519.440 and 535.472, corresponds to homo- and heterodimers of two deprotonated NA sharing a single proton.

For instance, the heterodimer at *m/z* 491.410 corresponds to the association of two deprotonated NA with *m/z* values of 237.185 (Z=-4) and 253.217 (Z=-2) to form the aggregate ($[C_{15}H_{26}O_2 - H]^-$ -- H^+-- $[C_{16}H_{30}O_2 - H]^-)^-$. The ion at *m/z* 497.457 is a homodimer formed by ions with *m/z* values of 241.217 (Z=0) and 255.232 (Z=0) in the form of ($[C_{15}H_{30}O_2 - H]^-$ -- H^+-- $[C_{16}H_{32}O_2 - H]^-)^-$. The heterodimer at *m/z* 519.440 arises from the non-covalent association of two acids with Z=-2 (*m/z* 253.217) and Z=-4 (*m/z* 265.216) sharing a proton to form the species ($[C_{16}H_{30}O_2 - H]^-$ -- H^+-- $[C_{17}H_{30}O_2 - H]^-)^-$. Finally, the heterodimer ($[C_{17}H_{30}O_2 - H]^-$ -- H^+-- $[C_{17}H_{34}O_2 - H]^-)^-$ with *m/z* 535.472 is formed by the NAs with Z=-4 (m/z 265.216) and Z=0 (*m/z* 269.248).

The formation of homo- and heterodimers in a commercial NA standard mixture has been previously reported, by ESI FT-ICR/MS (Da Campo, Barrow, Shepherd, Salisbury, & Derrick, 2009). The characteristics of the non-covalent dimers formed in ESI depend upon the NA monomeric composition; for instance, if the most abundant monomeric NAs in the sample are Z=-4, the homodimers formed will be mostly Z=-8 ($C_nH_{2n+Z}O_4$).

On the other hand, heterodimers with Z=-6 could result from association of Z=-2 and Z=-4 or Z=0 and Z=-6 monomers, while dimers with Z=-10 can result from association of monomeric NAs with Z=-4 and Z=-6, Z=-2 and Z=-8 or Z=0 and Z=-10.

We observe similar results, the dimers in MALDI arise from association of the most abundant monomeric NAs in the sample with Z=0, Z=-2 and Z=-4. For instance, the most abundant dimer in MALDI, using DMAN as matrix, is observed at *m/z* 497.457 and corresponds to the association of acids with Z=0 (*m/z* 241.217 and 255.232), this is not surprising considering that the Z=0 NA

family is the most abundant in the standard sample. In addition, to test the applicability of our MALDI approach for real samples analysis we isolated NA from a heavy crude oil distillation cut (370-510 °C) using an anion exchange procedure (see experimental section for details).

Fig 5a. and b. shows the MALDI (-) TOF and ESI (-) IT mass spectra from *m/z* 100 to 1000 for the real NA extract, respectively. Both spectra exhibit the molecular weight distribution spanning between *m/z* 200-700 with maxima around *m/*z 400. Insets shows zooms between *m/z* 340-400 revealing a typical distribution for NA. For instance, homologous series with mass signals differing 14 Da correspond to the addition of methylene units $–CH_2$ in NA belonging to species with the same hydrogen deficiency value.

On the other hand, homologous series from different families are separated by a mass difference of 2 Da indicating a change in hydrogen deficiency. The similarity between spectra in Fig. 5 suggests that MALDI can perform comparably than ESI for the analysis of NAs in real petrochemical samples.

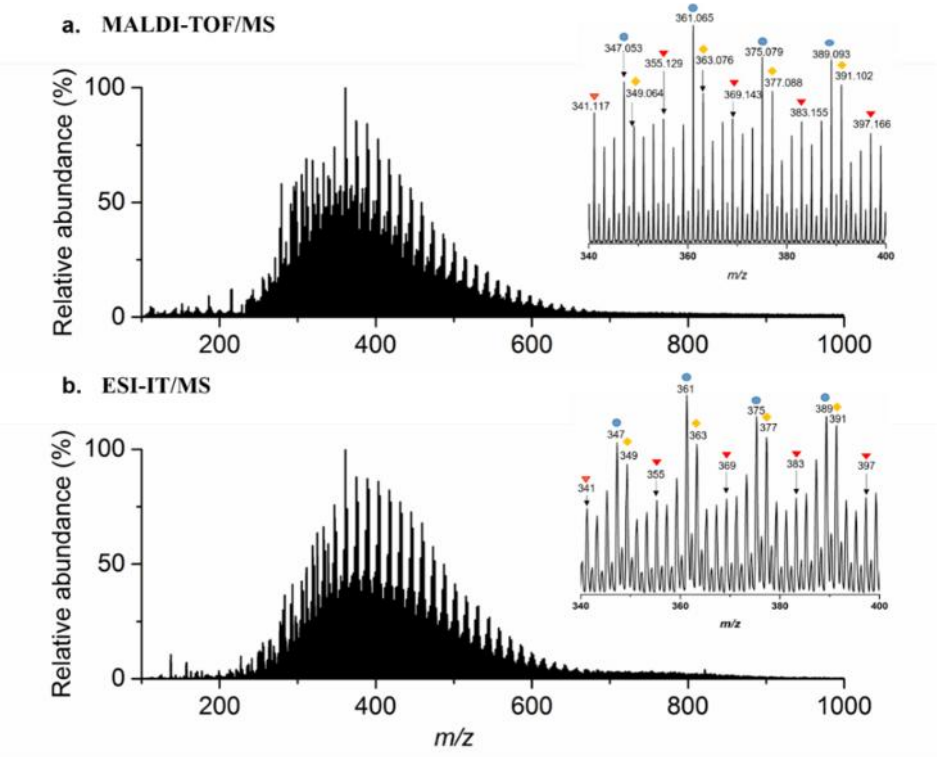

Figure 5. a) MALDI (-) and b) ESI (-) mass spectra for a real NA mixtrue extracted from a crude oil distillation cut (370-510 °C). Inset graphs correspond to an enlargement of the m/z 340-400 region of the spectra showing an identical NA distribution in ESI and MALDI. Labels on the signals correspond to homologous series of NAs with Z=-6 (circles) and Z=-4 (diamonds) and Z=0 (triangles).

9-AA is another basic matrix recently used to assign small acid molecules (<260 Da) by MALDI-TOF/MS (Shroff et al., 2007). Fig. 6a shows the negative ion MALDI spectrum, from *m/z* 100 to 1000, for the NA sample mixed at an equimolar ratio (2mM) with 9-AA as matrix.

The MALDI(-) profile observed with 9-AA is clearly different than the ESI(-) and DMAN MALDI(-) profiles (Fig. 2a and 3a). In Fig. 6a the MALDI MS of the NA mixture shows a base peak at *m/z* 193.074; this matrix-related ion is produced, according to Calvano *et al.*, (Calvano et

al., 2013) by initial formation of a matrix radical anion that reacts with a neutral matrix molecule to produce a deprotonated matrix molecule and a radical according to the following reaction (Eq. (3)):

$$9\text{-}AA^{-\cdot} + 9\text{-}AA \rightarrow [9\text{-}AA - H]^{-} + [9\text{-}AA + H]^{\cdot} \quad (3)$$

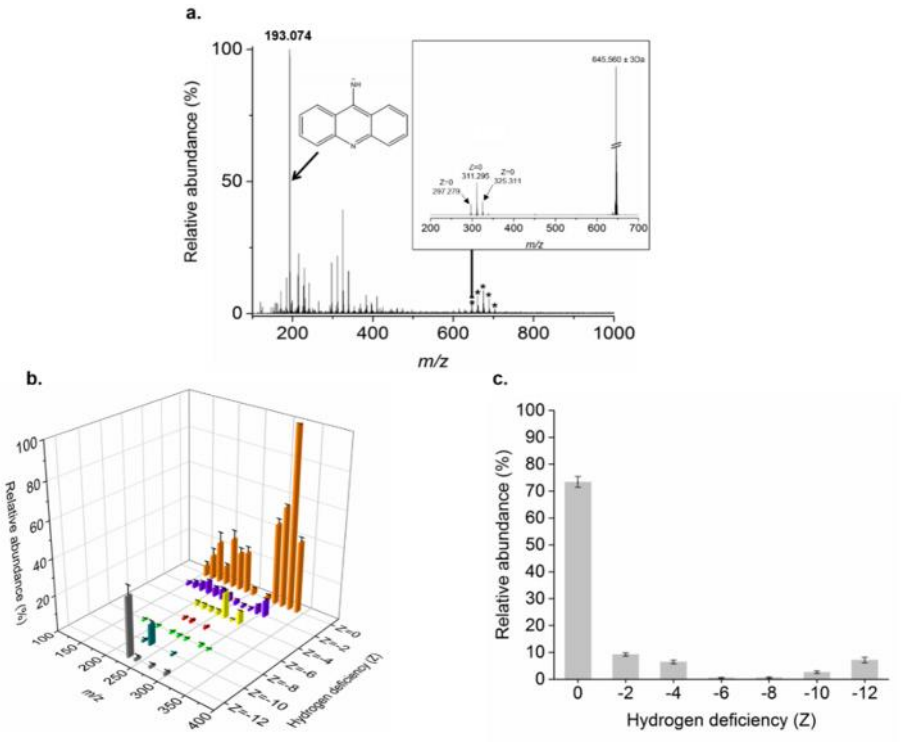

Figure 6. a) MALDI(-) MS analysis of a 1:1 NA:9-AA mixture (1 nmol/well and 1.92µJ/pulse), inset graph shows the MS2 spectrum of the precursor ion with m/z 645.560; b) mass profiles; c) relative abundances vs hydrogen deficiency (Z) of NAs.

Also in Fig. 6a we observe three distinctive distributions in the MALDI(-) profile when using 9-AA as matrix. The first distribution, ranging from m/z 100 to 280, corresponds exclusively to monomeric NA detected as deprotonated molecules [M - H]-. The second distribution is formed almost exclusively by high-abundance signals of aliphatic NA (CnH2n+zO2, Z=0) at m/z 297.279,

311.295, 325.311 and 339.295 where n is equal to 19, 20, 21 and 22, respectively. The third distribution, comprised of signals at m/z 645.560, 659.556, 673.572, 687.581, 701.604, was identified as homo/hetero dimers of monomeric NA.

Fig. 6b shows that compound distributions, according to Z values, in MALDI with 9-AA as matrix are very different than those for ESI and MALDI with DMAN as matrix. Clearly, 9-AA selectively ionizes NA with Z=0 and preferably the ones at the high end of the distribution (higher *m/z* values). For instance, in MALDI with DMAN deprotonated molecules corresponding to monomeric NAs with Z=0, with *m/z* values of 311.295, 325.310 and 339.326, exhibit relative abundances of 10.94, 3.05, and 3.17 %, respectively.

The same ions in the MALDI spectrum with 9-AA have much higher relative abundances of 55.81, 100 and 39.59 %, respectively. Likewise, with 9-AA NA with Z=-10 and -12 were detected with a higher relative abundance, 2.65 and 7.18 % respectively, than with DMAN with 2.09 and 3.91 %, respectively. In contrast, with 9-AA, families with Z=-2, -4, -6 and -8 show lower relative abundances than with DMAN, as seen in Fig. 6c (for more details see tables A.6, A.7 and A.8 of the appendix A).

The inset in Fig. 6a shows the isolation, within a window mass range of ± 3 Da, and dissociation, by CID, of the non-covalent aggregate at *m/z* 645.560. The MS^2 spectrum of *m/z* 645.560 shows three product ions corresponding to deprotonated aliphatic acids (Z=0) with *m/z* 297.279, 311.295 and 325.311. Hence, the aggregate with *m/z* 645.54 could correspond to two distinctive species: a heterodimer formed by two deprotonated molecules with *m/z* 297.279 and *m/z* 325.311 sharing a sodium atom ($[C_{19}H_{38}O_2 - H]^-$ -- Na^+-- $[C_{21}H_{42}O_2 - H]^-)^-$ or a homodimer formed by two deprotonated molecules with *m/z* 311.29 sharing a sodium atom ($2[C_{20}H_{40}O_2 - H]^- - Na^+)^-$.

Fig. A3 of the appendix A shows MS^2 spectra for dimers with *m/z* 659.556, 673.572 and 687.581. The dimer at *m/z* 659.556 corresponds either to the heterodimer ($[C_{20}H_{40}O_2 - H]^-$ -- Na^+-- $[C_{21}H_{42}O_2 - H]^-$), from the association of two deprotonated acid molecules with *m/z* 311.295 and *m/z* 325.311, or the heterodimer ($[C_{19}H_{38}O_2 - H]^-$ -- Na^+-- $[C_{22}H_{44}O_2 - H]^-)^-$ formed by monomeric acids with *m/z* 297.279 and *m/z* 339.326. The signal detected at *m/z* 673.572 is a homodimer formed by the association of two deprotonated molecules of the aliphatic acid with *m/z* 325.311 as $(2[C_{21}H_{42}O_2 - H]^- - Na^+)^-$. This signal can also be attributed to the noncovalent association of the acids with *m/z* 311.295 and *m/z* 339.326 to form the heterodimer ($[C_{20}H_{40}O_2 - H]^-$ -- Na^+-- $[C_{22}H_{44}O_2 - H]^-)^-$. Also, the dimer at *m/z* 673.572 is formed by the acids with *m/z* 297.279 and *m/z* 353.249, and the signal at *m/z* 687.581 corresponds to the heterodimer ($[C_{21}H_{42}O_2 - H]^-$ -- Na^+-- $[C_{22}H_{44}O_2 - H]^-)^-$ formed by the deprotonated acids with *m/z* 325.311 and *m/z* 339.326. This signal can also be attributed to the heterodimer ($[C_{20}H_{40}O_2 - H]^-$ -- Na^+-- $[C_{23}H_{46}O_2 - H]^-)^-$ formed by the monomeric acids with *m/z* 311.295 and *m/z* 353.249. The signal at *m/z* 701.604 could result either from the association of two acid molecules with *m/z* 339.326 ($2[C_{22}H_{44}O_2 - H]^- - Na^+)^-$ or a heterodimer ($[C_{21}H_{42}O_2 - H]^-$ -- Na^+-- $[C_{23}H_{46}O_2 - H]^-)^-$ formed by the acids with *m/z* 325.249 and *m/z* 353.249.

Figure A4 of the appendix A also shows the presence of trimers in the full scan mass spectrum (laser output of 50%, 2.85 µJ/pulse) for the NA mixed at an equimolar ratio (2 mM) with 9-AA. The inset graph in Figure A.4 shows the MS^2 spectrum of the trimer at *m/z* 1001.783 corresponding to any of the following species: ($[C_{20}H_{40}O_2]$--$[C_{20}H_{40}O_2 - H]^-$ -- K^+-- $[C_{22}H_{44}O_2 - H]^-)^-$, ($[C_{21}H_{42}O_2]$--$[C_{21}H_{42}O_2 - H]^-$ -- K^+-- $[C_{20}H_{40}O_2 - H]^-)^-$ or ($[C_{19}H_{38}O_2]$--$[C_{21}H_{42}O_2 - H]^-$ -- K^+-- $[C_{22}H_{44}O_2 - H]^-)^-$; interestingly this trimer is formed exclusively by Z=0 monomeric units.

NAs dimers can also exist in solution, as it has been reported using FTIR spectroscopy. A band with high absorption at 1703 cm^{-1} was associated with the presence of dimers while a low absorption band at 1742 cm^{-1} corresponds to monomeric acids. In both cases, the bands are associated to the stretching of the carbonyl group (Da Campo et al., 2009). For this reason, Da Campo et al.,(Da Campo et al., 2009) believe that non-covalent aggregates such as NA dimers are present natively in crude oils and their fractions. Likewise, cationized (Na^+ and K^+) homo/heterodimers were reported for fatty acids $C_{19}H_{38}O_2$ and $C_{21}H_{42}O_2$ (nonadecanoic and heneicosanoic acids) in negative ion mode using SALDI (surface-assisted Laser Desorption Ionization) with a porous silicon surface (DIOS/MS) (Budimir, Blais, Fournier, & Tabet, 2006).

This study also suggests an alkali cation selectivity depending on the size of the aggregates. For instance, Na^+ is mostly found in dimeric species whereas K^+ is preferably solvated by deprotonated trimers. Formation and survival of these multimers are also influenced by laser output and their stability in liquid and gas phase. Regarding the later it was also found that the monomer *vs* homo/hetero dimer ratios decrease when the extraction delay is increased, meaning that longer extraction times result in decreased survival yields of these species.

Our results also show that formation of these non-covalent aggregates (dimers and trimers) increase as the amount of NA on the target increase as well as the laser output as seen in Figure A.4 of the appendix A. The same behavior was observed with DMAN. However, there is a fundamental difference between aggregates formed in MALDI with DMAN and 9-AA; with the former we observe aggregates sharing a proton while with the later we observe aggregates sharing a sodium or potassium cation.

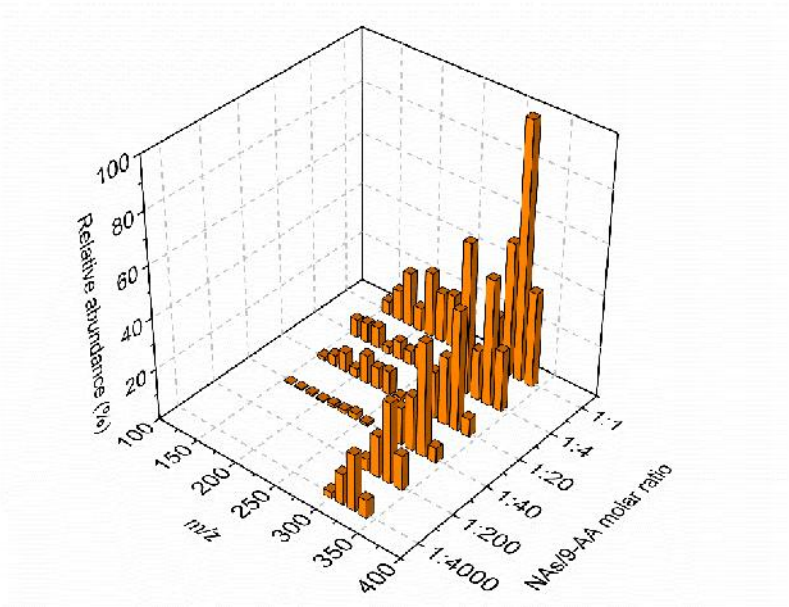

Figure 7. Effect of analyte: matrix ratios in the relative abundance of NA with Z=0 using 9-AA as negative ion MALDI matrix.

Considering the fact that 9-AA shows preferential ionization of Z=0 NA, we also tested the performance of this matrix using different analyte/matrix ratios. Fig. 7 shows the analyte:matrix dependence of the mass profiles and relative abundances for monomeric aliphatic (Z=0) NA. We observe NA signals up to analyte/matrix ratios of 1:4000; in addition, with 9-AA it is possible to selectively detect Z=0 NA (*m/z* 297.279, 311.295, 325.311 and 339.326) down to 250 fmol on target.

1.4 Conclusions

We demonstrated that negative ion MALDI mass spectrometry is a viable tool for NAs analysis. Our approach involves the use of equimolar analyte:matrix ratios, in a similar way as for the previously reported analysis of low-molecular weight acidic metabolites.

Using a standard NA mixture, we observed singly deprotonated molecular ions $[M - H]^-$ of cyclic and aliphatic naphthenic acids, with Z= 0, -2, -4, -6 using both 9-AA and DMAN as MALDI matrices.

The proton sponge (DMAN) produces a cleaner mass spectrum with absence of clusters, aggregates or matrix interferences at low *m/z*; more importantly, this matrix provides molecular weight distributions similar to those observed with negative ion ESI.

On the other hand, 9-AA exhibits matrix interferences at low mass, and promote selective ionization of NAs with Z=0. Finally, we consider that MALDI-MS presents advantages over ESI, for NAs analysis, such as high throughput (up to 384 samples in our case) with minimal contamination of the MALDI source and high reproducibility. This methodology could be applied to NAs analysis from different petrochemical sources, RICO reaction products, OSPW and natural contaminated waters, among others.

1.5 Acknowledgements

The authors acknowledge financial support from the research agreement grant No. 672-2011 between the Universidad Industrial de Santander, COLCIENCIAS and Ecopetrol. We also acknowledge a graduate fellowship from COLCIENCIAS Program No. 567. Finally, we acknowledge technical support from the Mass Spectrometry Lab, Central research laboratory facility at Guatiguara’s campus Universidad Industrial de Santander.

2. Molecular characterization of naphthenic acids from heavy crude oils using MALDI FT-ICR mass spectrometry

Naphthenic acid (NA) fractions from heavy crude oils are typically analyzed in mass spectrometry via electrospray ionization (ESI). Here, we show that NA analysis is also possible by MALDI using a highly basic matrix (proton sponge). When compared with ESI, that allowed detection of six compound families, MALDI resulted in the observation of twenty-two compound families. Besides, MALDI analysis affords compositional-dependent information.

Unlike ESI, where all NA are detected as deprotonated molecules, in MALDI we observe both deprotonated molecules and radical anions. This indicates that ion formation in NA by MALDI can occur by either acid-base and electron-capture mechanisms, or both. Interestingly, the preferred ionization channel seems to be compound class dependent; for instance, the acid base mechanism (which allows detection of deprotonated NA species through a Brönsted-Lowry reaction) applies exclusively to NAs with high H/C ratios along the whole O/C range.

On the other hand, for less saturated compounds both mechanisms apply, while the electron capture channel occurs exclusively in species with low H/C and high O/C ratios or high H/C and low O/C ratios (envelope of the van Krevelen plots, see figure 8).

In summary, we demonstrate that MALDI(-) is an alternative method for the analysis of complex petrochemical samples offering additional advantages, when compared with ESI, such as increasing compositional space accessibility for polar samples, high throughput and exceptional tolerance to the presence of impurities and salts in the samples. Furthermore, exploration on semi-quantitative approaches in MALDI can provide additional advantages such as those offered by LC-ESI MS, currently used to quantify naphthenic acids.

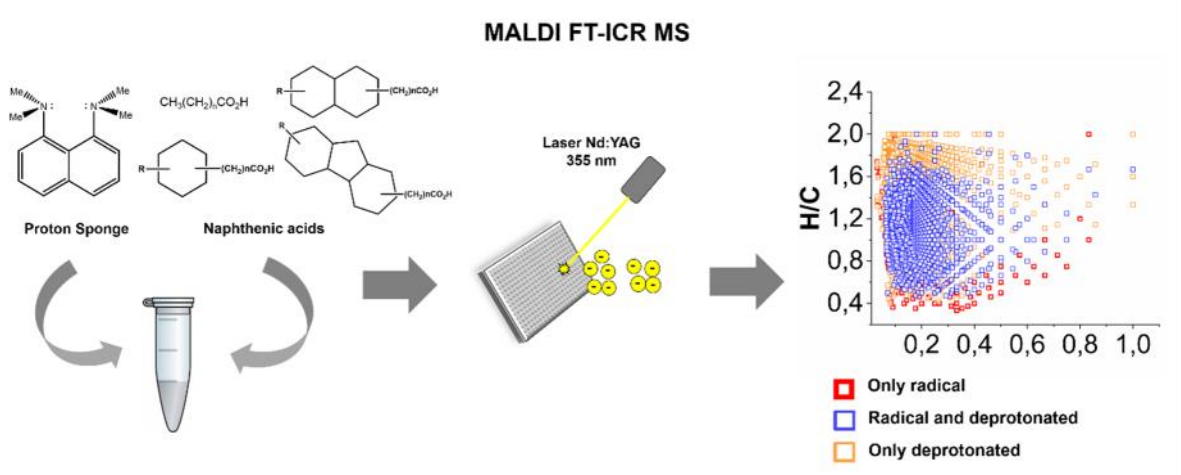

Figure 8. Analysis of naphthenic acids by MALDI high resolution mass spectrometry.

2.1 Introduction

Naphthenic acids (NA) are reactive molecules related to corrosion phenomena in refinery units such as atmospheric and vacuum distillation, transfer lines, furnaces, and crude oil heaters (Speight, 2007). Some studies suggest concentration-dependent synergistic effects between sulfur compounds and NA can enhance or inhibit corrosion (Flego et al., 2014). Thus, knowledge about NA chemical composition is vital to determine their potential to corrode materials, such as carbon steel (Flego et al., 2014; Laredo, López, Álvarez, Castillo, et al., 2004). Also, chemical speciation of NA is fundamental to understand and treat problems associated with calcium naphthenate formation, which forms solid deposits during crude oil processing. In addition, NA chemical features such as aromaticity and carbon number are important to establish relations between their amphiphilic behavior in liquid/liquid systems and their role in the stabilization or destabilization of water in oil (w/o) and/or oil in water (o/w) emulsions (Arla et al., 2007; Ese & Kilpatrick, 2004; Havre, Sjöblom, & Vindstad, 2003; Hemmingsen et al., 2006a; Östlund, Nydén, Auflem, & Sjöblom, 2003a; Varadaraj & Brons, 2007a; Wu, 2003).

Mass spectrometry coupled to traditional ionization techniques such as electron ionization (EI) (Vaz de Campos et al., 2006) , fast atom bombardment (FAB) (Laredo, López, Álvarez, Castillo, et al., 2004), chemical ionization (CI) (Fan, 1991) and atmospheric pressure chemical ionization (APCI) have been used to analyze NA in petrochemical (distillates, crude oil) (John V. Headley, Peru, & Barrow, 2016) and environmental samples such as oil sands processed water (OSPW) (John V Headley et al., 2009, 2007). In addition, gas chromatography (GC and GCxGC) coupled with EI mass spectrometry has also been used to characterize NA in petroleum (Robson, Sutton, McCormack, Chilcott, & Rowland, 2017; S. J. Rowland, West, Scarlett, & Jones, 2011), and natural waters (D. Jones et al., 2013; S. J. Rowland, Scarlett, et al., 2011). However, currently electrospray (ESI) is the method of choice to characterize NA in petrochemical samples. Many reports show that this type of ionization is selective, in negative ion mode, towards acidic compounds with functional groups such as carboxylic acids, phenols and carbazoles (Mapolelo et al., 2011b; Rodgers & Marshall, 2007).

ESI selectivity alone might be enough to detect all acidic compound classes in complex mixtures, eliminating the need for fractionation, however that is not the case. There is plenty of proof demonstrating that a single ionization technique (*e.g.* ESI) does not provide complete chemical characterization in complex mixtures due to interferences, and more importantly: differences in ionization efficiencies between the myriad of chemical species present in the samples. Hence, nowadays combined ionization methods (in lieu of a universal ionization source) and fractionation strategies are used to obtain a more comprehensive description of polar complex mixtures by high resolution mass spectrometry. For instance, when analyzing an OSPW sample by APPI and ESI (both operated in negative and positive ion modes) Barrow et al., concluded that APPI detects additional compound classes such as hydrocarbons, S_1 and N_1, whereas ESI is more

limited in terms of range and number of compound classes observed (Barrow et al., 2010). Also, oxygenated compounds, particularly naphtheno-aromatic acids with high hydrogen deficiencies dominated the mass spectra regardless of the ionization method; however, in APPI showed increased ion abundances (Barrow et al., 2010). Headley et al., also used APPI to characterize naphthenic acids extracted from an OSPW sample using a β-cyclodextrin cross linked with three different diisocyanate units (John V. Headley et al., 2014). APPI(+) could detect new compound classes such as HC, NO_1, NO_2, NO_3, NO_4, NO_5, N_2O and N_2O_2 which had not been previously detected by ESI. In addition, with APPI(-) compound families O_5, O_6, O_7 and SO_4 were detected.

Regarding the O_2 class compounds, APPI(-) showed the same species observed by ESI; however, in APPI(+) an enrichment of species with high DBE values was observed. Oxygenated compounds have been also studied by ESI- FT ICR MS in other complex mixtures such as NOM from river water samples (Bae et al., 2011). In these type of samples the oxygenated compounds detected contain between 6 and 14 oxygen atoms. In addition, the maximum DBE value for O_8, O_{10}, O_{12} species was found to increase by one unit for every two additional oxygen atoms (Bae et al., 2011).

As to ionization methods relying on desorption processes, recently LDI-FTICR analysis in negative ion mode was used to characterize whole crude oils (Cho et al., 2012). The authors found that LDI in negative ion mode is more selective towards the ionization of S_1 and O_o (o=1-2) compounds than LDI in positive ion mode. In other contribution, a commercial NOM sample was analyzed by ESI FT ICR and MALDI FT ICR mass spectrometry using DMAN as a matrix (Cao et al., 2015). The results show that unsaturated constituents of NOM with O/C ratios <0.5 are

preferentially ionized in MALDI negative mode, whereas polar constituents of NOM with higher O/C ratio are preferentially ionized in ESI negative mode.

This contribution shows that MALDI (-) can provide molecular information not accessed by ESI. Simultaneously, sample fractionation also allows detection of new compound classes in complex mixtures, expanding the range of their molecular characterization (S. M. Rowland et al., 2014).

Several methods have been reported to extract and fractionate NA from crude oils, distillates and petrochemical samples (Saab et al., 2005; L. Wang et al., 2013). For instance, ionic liquids of tetraalkylammonium and tetraalkylphosphonium amino acids have been used to extract NA through formation of a zwitterionic complex by reaction between the quaternary (N or P) cations and the carboxylic anion. NA are recovered using carbonic acid and the ionic liquid is regenerated. Experimental variables such as loading, saturation limits, losses of the ionic liquid and incomplete regeneration decrease the extraction efficiency of this process (Anderson et al., 2013; L. J. Shi, Shen, & Wang, 2008; Y. Sun & Shi, 2012).

Liquid-liquid extraction procedures have been also used to isolate NA from crude oils using ethanolic aqueous solutions at different pH (7, 10, and 14) (Colati et al., 2013). Interestingly, as the pH of the solution increased the average molecular weight of NA, shifted to higher values (from 270 to 390) and their ESI mass spectra also broadens the mass range (*m/z* 200 to 650). Although, this type of extraction is useful to reduce the total acid number (TAN) of crude oils in around 85-92 %, it requires high solvent volumes and problems of emulsion formation are likely to occur (Colati et al., 2013).

Adsorption chromatography is another method employed to extract NA using silica packed in a column, previously activated with a hot solution of potassium hydroxide. After the crude oil is loaded, neutral-basic compounds are eluted with chloroform whereas acid compounds are drained off by the addition of formic acid to chloroform (L. Wang et al., 2013; Y. Zhang et al., 2011).

Extraction chromatography, or extrography, has also been used to extract NA, but it requires large amounts of solvents and lengthy separations (L. Wang et al., 2013). Also, ion exchange methods are useful to isolate, with high efficiency, carboxylic acids from petroleum and calcium naphthenates from deposits with a hydrophilic resin (Sephadex A-25) (Mediaas et al., 2003; M. a. Mohammed & Sorbie, 2009).

Alternatively, solid phase extraction (SPE) has been gaining attention as a practical, rapid and quantitative method to extract polar compounds such as NA, phenols and carbazoles (D. M. Jones, Watson, Meredith, Chen, & Bennett, 2001). Low volumes of solvents needed to elute compounds and low sample concentration are among the best advantages of this fractionation method. Generally, SPE employs a functionalized stationary phase that can be a strong anion exchange quaternary amine (D. M. Jones et al., 2001), an ionic silica hybrid material containing the pyridinium group (SiPy) (De Conto et al., 2014) or an amino propyl silica phase (Zhu, He, He, Zhu, & Feng, 2017).

Recently, fractionation of NA followed by HRMS showed that low molecular weight acids are more efficiently ionized than molecules with a higher molecular weight (S. M. Rowland et al., 2014). This suggests that complex mixture fractionation is a successful approach to expand molecular characterization.

In this contribution we use a previously reported SPE procedure to extract and fractionate NA as a function of molecular weight (S. M. Rowland et al., 2014), and used MALDI(-) FTICR analysis (with a highly basic matrix) for compositional information. MALDI(-) data was compared to ESI(-) and we demonstrate that the former allows a more complete compositional description for the NA fractions than the latter.

2.2 Experimental section

2.2.1 Materials, reagents and samples. A heavy crude oil sample was provided by the Colombian Petroleum Institute (ICP-Ecopetrol). The sample had a total acid number (TAN) of 5,26 mg KOH/g crude, an API of 12,1, and nitrogen and sulfur contents of 0,49 and 1,44 % w, respectively. Dichloromethane (DCM), methanol (MeOH), toluene (MePh), acetonitrile (ACN) formic acid (HCOOH, 98 %) and ammonium hydroxide (NH_4OH, 28 % in H_2O) were purchased from Merck (Darmstadt, Germany) chemicals with HPLC grade. All of them were used as supplied. 1,8-Bis(dimethylamino) naphthalene (DMAN) was acquired from Sigma Aldrich (St. Louis, MO, USA).

Fractionation and isolation of NA from the crude oil were carried out by solid phase extraction (SPE), using aminopropyl cartridges (Biotage-ISOLUTE®-NH_2, 2 g/15 ml).

2.2.2 Isolation of naphthenic acids by SPE. SPE extraction involved dissolution of 500 mg of the crude oil in dichloromethane and loading of the sample onto the activated aminopropyl silica cartridge. Non-acidic species were eluted with mixtures of dichloromethane (DCM) whereas NA extracts, the most polar fractions in the sample, were isolated by sequential elution using mixtures comprised of DCM/MeOH/Water/FA in different ratios, according to an elution protocol

previously reported (S. M. Rowland et al., 2014). For further details about the elution solvent mixtures used see Table B1 of appendix B.

2.2.3 Sample preparation. For MALDI analysis, stock solutions of 1,8-bis(dimethylamino) naphthalene in ACN/MeOH (1:1) were mixed at 1:1 molar ratio with stock solutions of NA (0.5 mM) in ACN:MeOH (1:1). The NA/matrix solutions were homogenized on a vortex for 20 minutes. Then, 1.0 μL of each mixture was deposited on a ground steel MALDI plate and let dry for 15 minutes prior to MS analysis.

For ESI FT ICR MS analysis, naphthenic acid extracts obtained by solid phase extraction were firstly dissolved in toluene and subsequently diluted with a mixture of toluene/methanol (1:1 % v/v) to a concentration between 0.5-1 mg/mL. Ammonium hydroxide (1% v/v) was added to the final mixture to assist with the deprotonation of NA.

2.2.4 Mass Spectrometry analysis. Mass spectrometric analysis was performed on a FT-ICR mass spectrometer (SolariX 7 T, Bruker Daltonics, Billerica, MA) equipped with ESI and MALDI sources both operated in negative ion mode. MALDI mass spectra were recorded by the accumulation of 50-200 laser shots with 19% laser power with minimum laser focus.

The ESI ion source was operated in negative ion mode with a capillary voltage of 4.5 kV, source temperature of 250 °C and nitrogen as nebulizing (5.0 L/min) and drying gas (1 bar). 200 transients were averaged for final mass spectra in a mass range from *m/z* 100– 1200 with 8 MW acquisition size and 16 MW processing size. Mass spectra were externally calibrated using a NaTFA solution (*m/z* from 100 to 1200).

All mass spectra were additionally internally recalibrated using a homologous series of oxygenated compounds (O_2) in Data analysis 4.2 software (See appendix B, Table B2, for mass calibration lists). All mass assignments were done using composer software 1.0.6 (Sierra Analytics, Modesto, CA, USA).

2.3 Results and discussion

Figure 9 shows MALDI and ESI mass spectra for six NA fractions extracted by SPE from the crude oil sample. The SPE extraction protocol allows fractionation based on molecular weight (S. M. Rowland et al., 2014); Figure 9 clearly shows that the average molecular weight, in both ESI and MALDI mass spectra, for NA fractions 1 to 6 effectively increases. It should be noted that the quadrupole was set to *m/z* 700 for the mass spectrum acquisition of fraction F6 which causes a low mass cut-off at around *m/z* 500. This setting was used to improve the S/N of this fraction in the mass range of *m/z* 700-1000. Interestingly, MALDI MWDs are slightly shifted to higher *m/z* values, when compared with ESI. In addition, some low *m/z* species, not detected in ESI, are clearly seen in the MALDI spectra, particularly in fractions 1, 3 and 4. However, in general, both MALDI and ESI show MWD for NA fractions ranging from *m/z* 100 to *m/z* 1200.

Figure 10 shows compositional information derived from MALDI and ESI MS in the form of compound class histograms where, for instance, the code O_o refers to charged species detected as true molecular ions or radical anions ($[M^{-\bullet}]$) and O_o-H corresponds to deprotonated molecules ($[M - H]^-$). Clearly, MALDI allows observation of more compound classes than ESI (22 *vs* 6 families).

Common compound families, to both in ESI and MALDI, include O_2, O_3, O_4, O_2S, O_3S and NO_2. These heteroatom classes have been previously reported in other samples of NA extracted from different sources such as oil sands processed water (OSPW), crude oils, bitumen, interfacial

materials and sodium/calcium naphthenates (Barrow, Peru, McMartin, & Headley, 2016; Barrow et al., 2010; Cho et al., 2012; Clingenpeel, Rowland, Corilo, Zito, & Rodgers, 2017; Colati et al., 2013; J. V. Headley, Peru, Fahlman, Colodey, & McMartin, 2013; John V. Headley et al., 2014; Mapolelo et al., 2011b; Noestheden et al., 2014; Pauchard et al., 2009; R. C. L. Pereira et al., 2014).

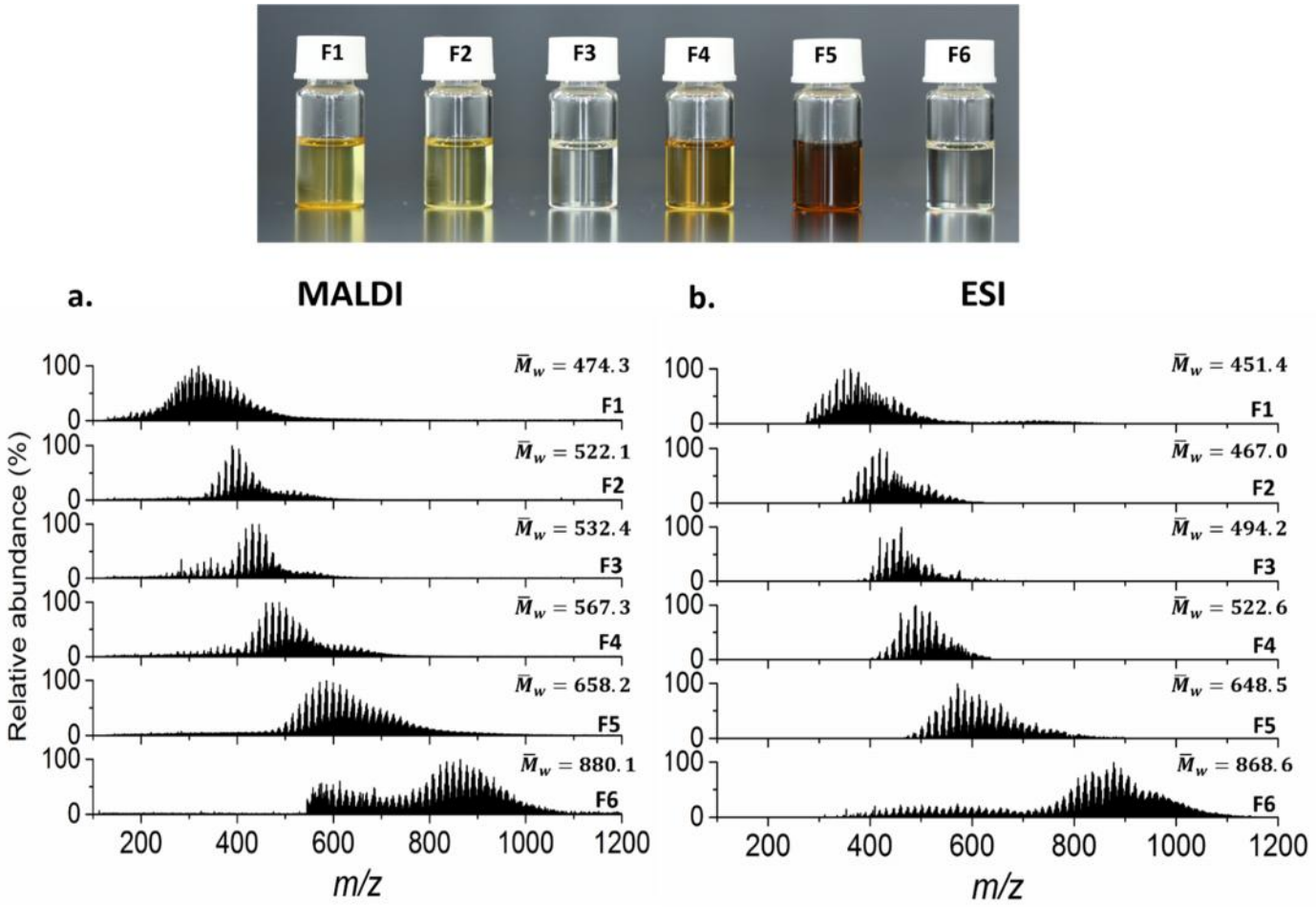

Figure 9. Mass spectra of NA SPE fractions (1-6) obtained by (a) MALDI and (b) ESI with M_w values. Top image shows the appearance of NA fractions solutions (toluene/methanol 50:50, 1 mg/ml) after SPE.

Table B3 of the appendix B, compiles the available information regarding compound classes detected in the aforementioned samples using APPI(-), LDI(-) and ESI(-) coupled to different mass analyzers. In summary, all of these ionization sources provide comparable information regarding nitrogen-containing species; however, sulfur and non-polar aromatic compounds are preferentially ionized and observed by APPI and LDI (Barrow et al., 2010; Purcell, Rodgers, Hendrickson, & Marshall, 2007).

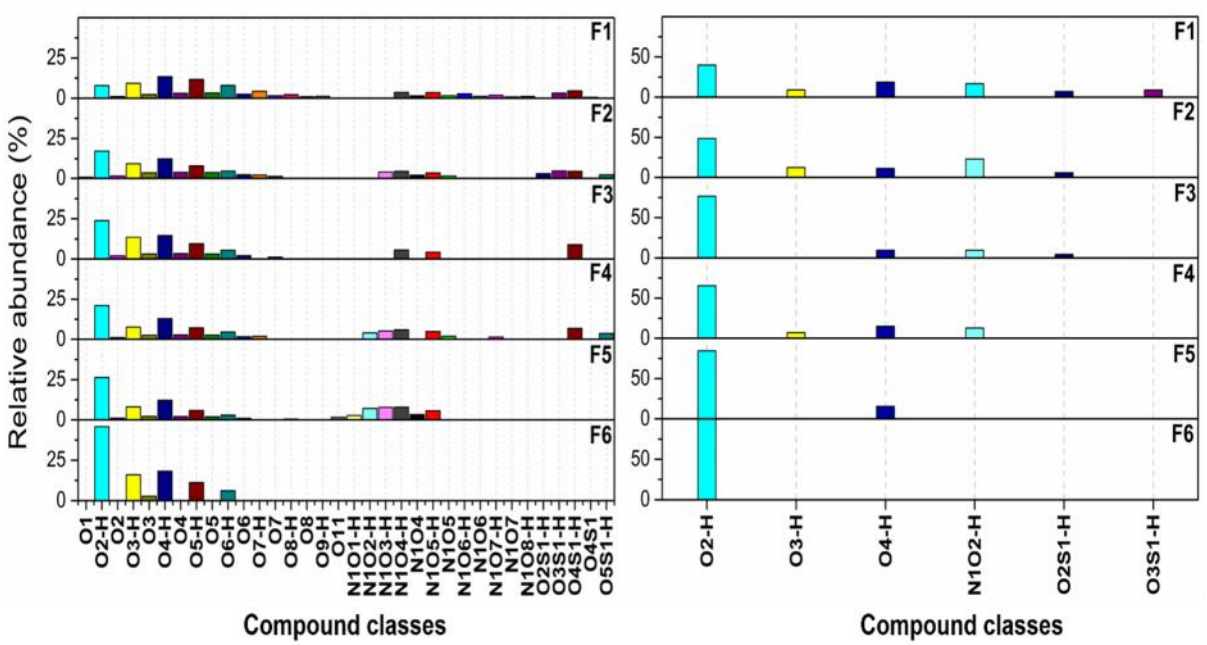

Figure 10. Comparative histograms showing compound classes detected in NA fractions (1-6) by MALDI (left) and ESI (right).

Interestingly, MALDI grants access to 16 additional compound families not observed in ESI such as O, O_5, O_6, O_7, O_8, O_9, O_{11}, NO, NO_3, NO_4, NO_5, NO_6, NO_7, NO_8, O_4S and O_5S. Our observation, using MALDI, of highly oxygenated O_o (o= 1-9, 11) compound classes in all NA fractions agrees with a recent report where the same kinds of compounds, O_o (o= 8,10,12), were

detected in natural organic matter (NOM) from rivers and oceans also with MALDI FT-ICR (Cao et al., 2015).

The presence of highly oxygenated species O_o (o= 2-11) was recently reported by Barrow et al (Barrow et al., 2016) in oil sands processed water using APPI FT-ICR MS in negative ion mode. It is believed that carboxylic acids in petroleum are produced either by incomplete catagenesis or biodegradation by bacteria (Ramirez-Corredores, 2017). Tomcsyk and Winans attributed the presence of highly oxygenated species O_o (o= 2-6) in a crude oil to various degrees of successive oxidation. However, as oxidation proceeds, addition of more acid groups (o > 6) is also possible (Hughey et al., 2007; Tomczyk, Winans, Shinn, & Robinson, 2001). Generally, biodegraded oils exhibit high total acid numbers (TAN); such is the case of the oil used to extract the acidic fractions in this contribution (TAN: 5.26 mg KOH/g). However, TAN values also can increase at low reservoir depths, so the formation of acids in the sample may be also due to biodegradation inside the reservoir or bacterial degradation (Ramirez-Corredores, 2017).

The overall relative abundances for the O_o species (as $M^{-\bullet}$ and $[M - H]^-$) in MALDI are between 70-80 % for fractions 1-3; 66 % for fractions 4 and 5; and 100 % for fraction 6. Also, MALDI data shows an extended N_nO_o (n=1, o=1-8) series with relative abundance values of 18 %, 15 %, 10 %, 23 % and 34 % for fractions 1, 2, 3, 4 and 5, respectively. Finally, another heteroatomic extended series O_oS_s (o=1-5, s=1) was observed by MALDI with relative abundances of 8 %, 14 %, 9 % and 10 % for fractions 1, 2, 3 and 4.

Figure 10 provides evidence, that ESI only produces deprotonated species of oxygenated classes O_2, O_3 and O_4 with combined relative abundances of 67 % and 72 % for fractions 1 and 2, respectively; and around 86 % for fractions 3 and 4. For fraction 6 the deprotonated O_2 class made

up 100% of the detected ions. In addition, in ESI O_oS_s (o=2-3; s=1) and NO_2 classes (also in the form of deprotonated molecules) accounted for a small percentage of the relative abundance in the mass spectra of the fractions 1-4. Figure B1, of the appendix B shows the percentage of molecular assignments for deprotonated ions in ESI. Formation of deprotonated species is the only possible ionization channel in ESI for negative ion formation, due to the basic mechanism of charge acquisition in ESI (Banerjee & Mazumdar, 2012; Konermann, Ahadi, Rodriguez, & Vahidi, 2013; Kruve et al., 2014). Also, Figure 10 shows an interesting pattern: unlike ESI, where all NAs are detected as deprotonated molecules, in MALDI we observe both deprotonated molecules and radical anions. This indicates that ion formation in NA by MALDI can occur by either acid-base and electron-capture mechanisms, or both (Karas et al., 2000; Karas & Krüger, 2003; Knochenmuss, 2006). It is true that we observe very high relative abundances for oxygenated species (O_o) detected as deprotonated molecules in MALDI; however, we also observe significant abundances of molecular ions (radical anions) for the same classes. This suggests that NA deprotonation, *via* acid-base reactions with the highly basic organic matrix (DMAN), is a favored ionization channel for O_o species; but ion formation can also go through electron-capture ionization. Table B6 shows the total number of formulas detected in common by MALDI and ESI.

A clearer picture of NA ion types produced in MALDI is provided in Figure 11, where percentages of molecular formulas assigned for only deprotonated molecules, only radical anions and both types of ions for the O_o (o=2-6) classes in fractions 1-6 are shown. In fractions 1-4 molecular formulas corresponding to only deprotonated molecules and only radical anions are higher (55 to 59 %) than those for both types of ions (41 to 47 %). Fraction 5 exhibits a 47 % of formulas detected as only deprotonated molecules and only radical ions, with 53 % corresponding to species that can form both types. Interestingly, in fraction 6 only deprotonated molecules

constitute 96 % of the oxygenated species and 3 % only radicals, while a surprisingly low 1 % corresponds to both types (Table B4 of the appendix B contains the number and percentage of molecular formulas for O_o (o=2-6) compound classes detected as only radicals, only deprotonated and both type of ions for each SPE fraction by MALDI FT-ICR. Table B5 shows the number of formulas assigned for each type of ion for the rest of the classes N_nO_o, and O_oS_s detected by MALDI).

Explaining the formation of deprotonated molecules is relatively straightforward, considering the sample preparation protocol used for MALDI(-) where a highly basic matrix (DMAN, pKa=12.6), mixed in solution with the NA sample (pKa~ 4-5), can easily deprotonate the acidic NA species through a Brönsted-Lowry reaction to yield preformed ions in condensed phase (Ozeryanskii et al., 2014; Schlosser, 1988; Valencia-Dávila, Blanco-Tirado, & Combariza, 2017). These charged species can be transferred into the gas phase upon laser interaction with the sample (Shroff et al., 2009; Shroff & Svatoš, 2009).

Radical anion formation, on the other hand, is a complex process involving either secondary charge transfer reactions in the gas phase (between a negative charged species with low electron affinity to an analyte neutral molecule with higher electron affinity) or multiphoton absorption (through an energy pooling mechanism) by the analyte that causes electron ejection and capture by another adjacent analyte molecule (Cawley & Flenker, 2008; Molin, Seraglia, Dani, Moneti, & Traldi, 2011; Streletskii et al., 2005). It is very likely that this process only occurs for analytes (NA), since the DMAN do not produce radical anions upon LDI (see Figure B6 of the appendix B).

Interestingly, a previous study indicates that aromatic or condensed species present in a natural organic matter (NOM) sample have high electron affinity so they can abstract electrons from other molecules to form highly stable aromatic radical anions (Cao et al., 2015; Rienstra-Kiracofe, Barden, Brown, & Schaefer, 2001). The existence of both radical and deprotonated species of the same molecule in NA fractions is perhaps due to the presence of both deprotonable acid groups and polyaromatic cores (Yamagaki & Watanabe, 2012).

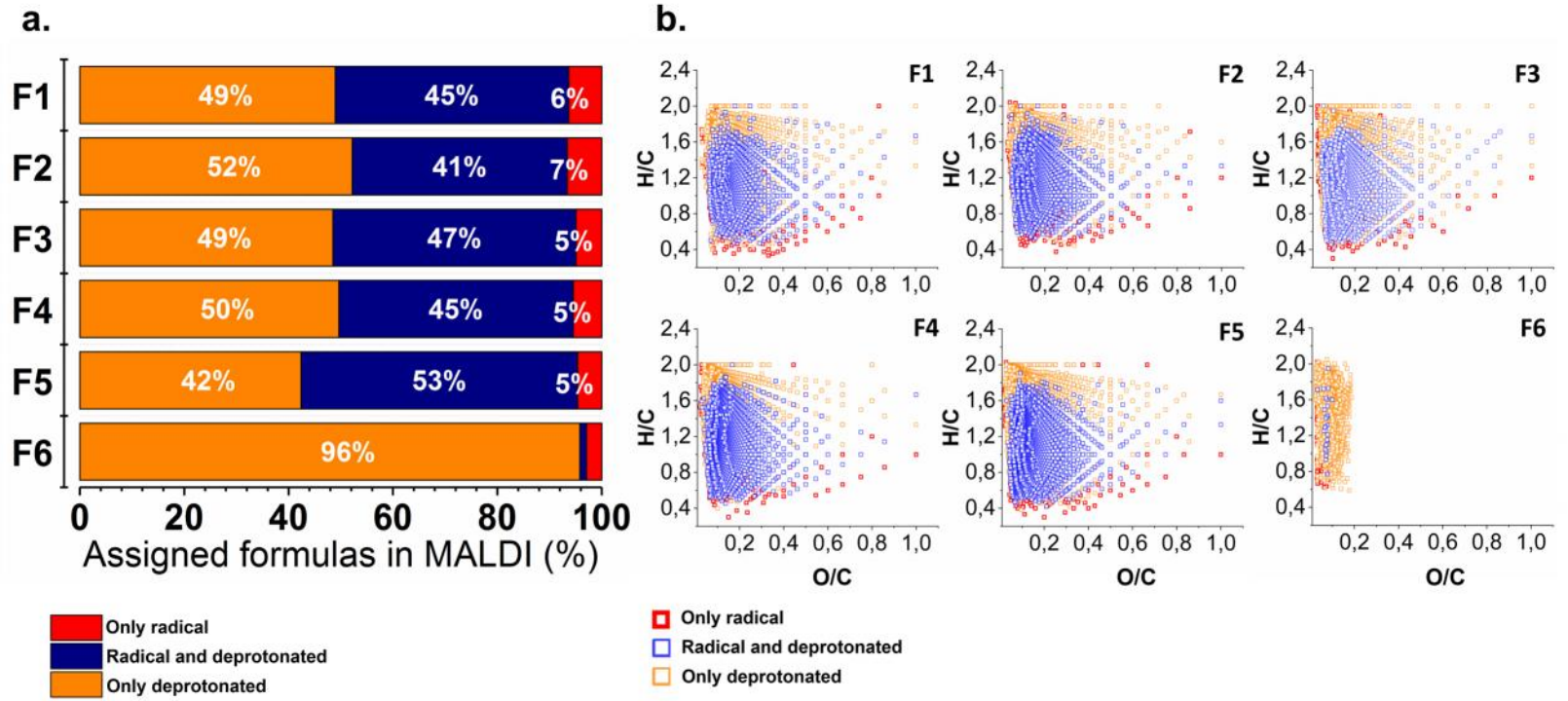

Figure 11. a) Percentage of molecular formulas assigned O_o (o =2-6) in MALDI as only radical, only deprotonated and both type of ions (radical and deprotonated). b) overlapped van Krevelen plots for all O_o (o =2-6) classes in NA fractions (1-6). (See Figure S2 of of the supplementary information for van Krevelen plots corresponding to individual O_o compound classes)

The van Krevelen diagrams for all O_o compound classes in Figure 11, consisting of a plot of H/C versus O/C ratios, allow observation of compositional differences between the NA fractions. In our case we overlapped the types of ions we observe in MALDI (deprotonated molecules in orange, radical anions in red and both types in blue) for all O_o (o=1-9, 11) compound classes to determine their places in the diagram, in doing so it is evident that the preferred ionization channel seems to be compound class dependent and that molecular composition has a fundamental role in the type of ion a NA can form in MALDI (for van Krevelen plots of individual O_o compound classes see Figure B2 of the appendix B).

Highly saturated ($1.6 < H/C < 2$) oxygenated compounds (orange bullets) ionize through an acid-base mechanism resulting in formation of deprotonated molecules; most of these ions are clustered at relatively low O/C ratios, meaning they have high C content – or are the heaviest within the class. On the other hand, for less saturated compounds ($0.4 < H/C < 1.6$) both mechanisms apply regardless of O/C ratio (blue bullets). Finally, the electron capture channel only occurs exclusively in species with either low H/C and high O/C ratios or high H/C and low O/C ratios (red bullets enveloping the outside of the van Krevelen plots). These species are highly unsaturated (aromatic) compounds possibly with high electron affinity that allows electron capture from neutrals or free radical anions during the MALDI ionization process, where photoexcitation, photoionization and charge transfer processes are involved.

Figure B3 from the appendix B shows that O_2 classes detected as both $[M - H]^-$ and $[M]^{-\cdot}$ in all fractions by MALDI, include aliphatic (DBE=1), non-aromatic (DBE= 2,3) and polyaromatic acids with DBE values up to 30. Clearly, deprotonated molecules exhibit lower DBE values (up to 20) than radical anions (up to 30) within the same compound family. In contrast, Figures B4 and B5 of the appendix B show the van Krevelen and DBE vs carbon number diagrams for the O_2

compounds detected in all fractions by ESI. These diagrams show the presence, almost exclusively, of saturated compounds with H/C values above 1.0 and DBE values below 10; this indicates that some compounds (unsaturated with high DBE values > 15) belonging to highly oxygenated families cannot be observed by ESI, despite their acidity, and that MALDI provides a way to increase compositional information for these polar fractions (as seen in Figure 11).

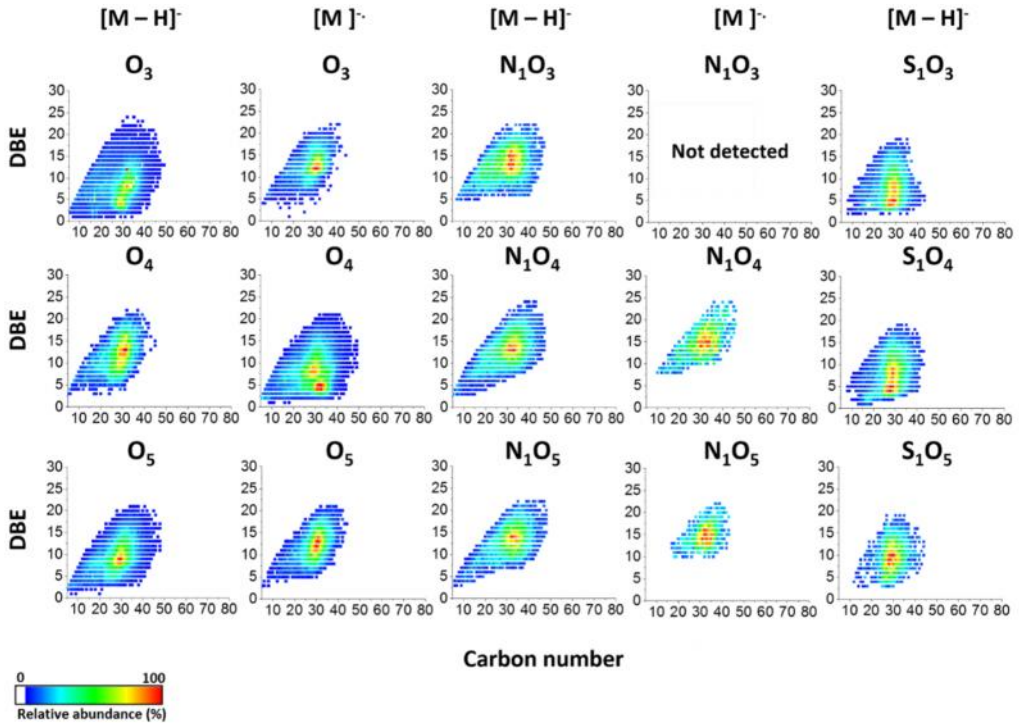

Figure 12. Neutral DBE versus carbon atom number plots of of N- and S- containing poly-oxygenated homologous series in fraction 2 detected by MALDI.

MALDI(-) also allows detection of additional heteroatom classes such as N_nO_o and O_oS_S possibly due to the presence of deprotonable or electronegative moieties in the structures (Mapolelo et al., 2011b). Figure 12 compares the distribution of N- and S- containing poly-oxygenated homologous series in terms of radical anion and deprotonated molecules for fraction 2 of NA detected by MALDI. Using the O_o (*o*= 3,4,5) compound family as starting point we observe that N-containing compound classes (N_1O_3, N_1O_4, N_1O_5) are shifted towards higher DBE

values. This indicate that N moieties in these families are present in the form of conjugated structures. Radical anions for the N_1O_o (*o*= 4-5) families were detected. In contrast, S-containing analogs exhibit lower DBE values, suggesting that these heteroatoms are probably not part of aromatic units in the structures. Radical anions for the S_1O_o (*o*= 3-5) families were not detected in this case.

Figure 13 shows the DBE versus carbon number plots for O_4 and O_5 compound classes with their N and S analogs for all fractions. In general, O_4 species have DBE values ranging from 1 to 27, with maxima around 5 -10, and carbon atom numbers between 1-75. As fraction increases, species with higher relative abundances shift to the right in carbon atom number. For instance, in fraction 1 species with DBE values from 3-12 and carbon atoms between 10 and 27 were detected, whereas in fraction 5 the most abundant species exhibited the same DBE range with carbon numbers between 40 and 60. In addition, only O_4 species with certain DBE and carbon numbers are ionized more efficiently than other species of the same class, and for this reason exhibit a high relative abundance. Interestingly, fractions 2 and 3 exhibited a bimodal distribution of O_4 species. The former has species with DBE= 4- 5 (#C 28-30) and DBE 8- 9 (#C 30-35) and the latter, species with DBE=7-10 (#C 30-35) and DBE= 4-5 (#C 35-38). In both fractions, bimodal distributions arise perhaps from the high abundance of two different core structures within the corresponding O_4 class.

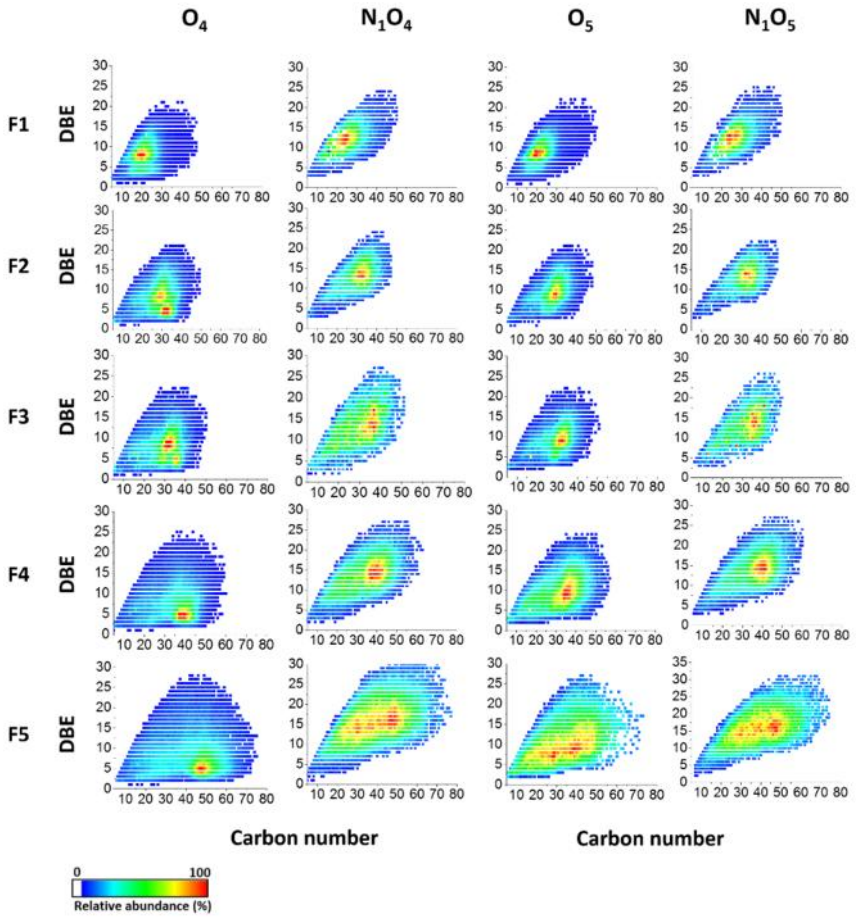

Figure 13. Neutral DBE versus carbon atom number plots for O4 and O5 species with their N- and S- analogs, as observed by MALDI in fractions 1-5.

Regarding the NO_4 homologues, species with DBE=11-13 and carbon atom number from 20 to 25 were detected with high relative abundance in the fraction 1. In contrast, O_4 species from fraction 5 exhibited values of DBE from 12 to 20 with carbon atom numbers between 20 to 50. Furthermore, the relative abundance is more uniform across the DBE and carbon number range in comparison with O_4 and O_5 compound classes. In general, O_4 and O_5 species showed similar petroleomes and DBE ranges. This trend was also observed for N_1O_4 and N_1O_5 compound classes.

2.4 Conclusions

MALDI FT-ICR is an alternative technique for complex mixtures characterization with the ability to increase compositional space accessibility for NA; we observed 22 compound classes in MALDI and only 6 compound classes in ESI. In addition, MALDI FT-ICR analysis of NA provides access to compositional-dependent information; unlike ESI, where all NA are detected as deprotonated molecules.

MALDI allowed observation of three types of compounds: the first group ionizes only through formation of deprotonated molecules, the second group can form both deprotonated molecules and radical anions, and the third ionizes exclusively to form radical anions. This indicates that ion formation in NA by MALDI (-) using a highly basic matrix (DMAN) occurs by both acid-base and electron capture reactions. The preferred ionization channel seems to be compound class dependent; for instance, the acid-base mechanism applies exclusively to NAs with high H/C ratios (1.6 to 2.0) along the whole O/C range (0.02 to 1.1).

On the other hand, for less saturated compounds (H/C 0.4 to 1.6) both mechanisms apply along the whole O/C range. Interestingly, the electron capture channel only occurs exclusively in species with low H/C and high O/C ratios or high H/C and low O/C ratios (envelope of the Van Krevelen plots).

Finally, MALDI a technique originally conceived for polymer and protein analysis, is versatile, robust and can be easily implemented for NA ionization as demonstrated in this contribution. The use of a basic matrix ensures absence of interferences in the low-mass region which are typically observed with traditional matrices. However, work on this area still requires addressing some weaknesses such as: desorption issues as the molecular weight increases, which may lead to the

use of high laser outputs and induce analyte fragmentation. In addition, low signal reproducibility in MALDI could make a semi-quantitative approach difficult to implement since it is not only dependent on analyte´s molecular features (such as acidity in this case) but also on sample homogeneity on the target, matrix photo physical properties, solubility and crystal formation, among others. In this regard, we are currently working on chemical modification of the basic matrices to obtain derivatives with improved physicochemical characteristics, that can resolve issues related to sample homogeneity and signal reproducibility allowing development of semi-quantitative approaches in MALDI.

2.5 Acknowledgements

The authors acknowledge Guatiguará Technology Park and the Mass Spectrometry Lab-Central Research Laboratory Facility at Universidad Industrial de Santander for infrastructural support. We also acknowledge the Colombian Petroleum Institute (ICP-Ecopetrol) for supplying the crude oil sample. JAVD acknowledges COLCIENCIAS (Grant 567- 2012) for a graduate fellowship.

3. Influence of naphthenic acids in asphaltene heptol/water interfaces and emulsion stability

The effect of naphthenic acids –NA (standards and real mixtures) on the interfacial properties of asphaltene films at the oil-water interface was evaluated using dynamic interfacial tension, surface pressure isotherms and emulsion stability analysis. Results suggested a correlation between interfacial film properties and emulsion stability. In this sense, addition of real NA resulted in less stable emulsions due to a weakening of the interfacial asphaltene films.

The effect of real NA on the asphaltene interface depends on concentration, heteroatom content and chemical structure rather than molecular weight. The mechanism of weakenig films and

emulsion destabilization upon NA addition may involve interactions between NA and asphaltenes (acid-base interactions, dipole-dipole interactions, π-π interactions) leading to aggregation inhibition and/or displacement of asphaltene molecules at the interface, especially when NA are present in excess.

Interestingly, we also found that NA activity at the interface depends on asphaltenes heteroatom content and ability to self-associate. In addition, we observe that only certain asphaltene molecules are interfacially- active. However, these characteristics are not neccesarily linked with a reduction of the interfacial tension.

When using a standard NA sample (with z values from 0 to -12) we observed rapid diffusion to the oil-water interface; however, the effect on the interfacial asphaltene film was lower when compared with the 5-β-cholanic acid (Z=-8), the second standard acid used in this study. It is believed that weakening of asphaltenes films, by the presence of 5-β-cholanic acid, occurs through an adsorption barrier mechanism or a slowdown adsorption of asphaltenes as a result of a faster diffusion of the acids at the interface. Overall, asphaltene-acid interactions at oil-water interface are clearly complex in nature and have to be treated carefully on a case-to-case basis.

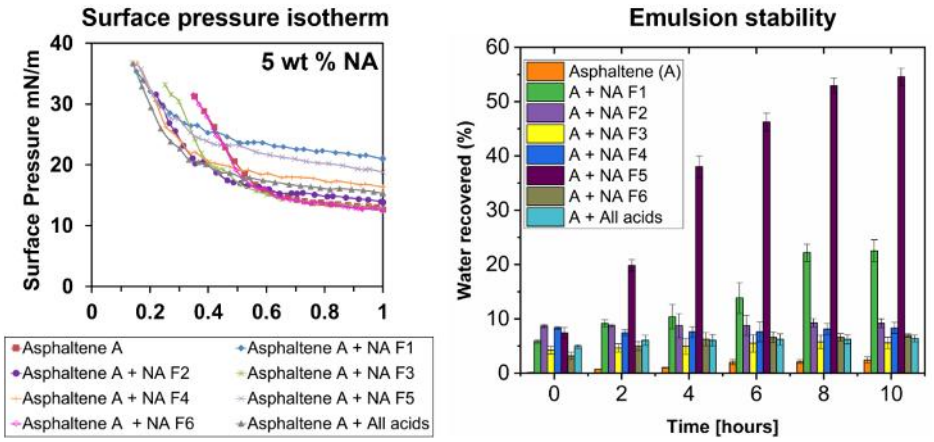

Figure 14. Effect of real napthenic acids on interfacial asphaltenes films and emulsion stability.

3.1 Introduction

Water-in-oil emulsions (w/o) are highly viscous dispersions formed during transportation and upstream processing of heavy crude oils, these mixtures are associated with increased stream viscosity, plugging and fouling issues (Guo, Li, & Yu, 2016) . Also, in downstream operations, emulsions are responsible for sludge formation at desalting units as well as corrosion in refiney units and catalyst deactivation during upgrading operations (Islam, 2015; J. Pereira et al., 2015). Tight w/o emulsions are also found during oil sands processing when bitumen is extracted from the sand grains employing alkaline hot water (Masliyah, Zhou, Xu, Czarnecki, & Hamza, 2008; Rao & Liu, 2013). Due to the economic impact associated with the presence of emulsions during bitumen and crude oil production, there is need to understand how emulsions are stabilized in order to propose strategies for their breaking or inhibition. Currently, it is believed that asphaltenes are the main contributors to w/o emulsion stabilization, because their chemical structure and aggregation properties (Kilpatrick, 2012).

Asphaltenes are poly-aromatic molecules with heteroatoms such as nitrogen, sulfur, oxygen (N, S, O) and metals (Ni, V) present on either island (Pomerantz, Wu, Mullins, & Zare, 2015; Sabbah, Morrow, Pomerantz, & Zare, 2011) or archipelago architectures (Alvarez-Ramírez & Ruiz-Morales, 2013; Chacón-Patiño, Rowland, & Rodgers, 2018; Murgich, Abanero, & Strausz, 1999; Strausz, Mojelsky, Faraji, Lown, & Peng, 1999; Strausz, Mojelsky, & Lown, 1992; Strausz, Peng, & Murgich, 2002).

The surface activity of asphaltenes has been attributed to the presence of aromatic and polar moieties; however, only a small fraction of asphaltenes reach the oil-water interface (Czarnecki & Moran, 2005; Xu, Dabros, Hamza, & Shefantook, 1999) upon w/o emulsion formation. Currently,

it is believed that polar asphaltenes constituted by ~6 or 7 fused aromatic rings are readily adsorbed as a monolayer at the oil-water interface, (L. Y. Zhang, Lopetinsky, Xu, & Masliyah, 2005) where the aromatic core is lying flat and the alkyl chains, located at the periphery, are oriented towards the oil phase (Rane et al., 2015; Rane, Pauchard, Couzis, & Banerjee, 2013; Sztukowski, Jafari, Alboudwarej, & Yarranton, 2003).

Gravimetric methods shown that the asphaltene monolayer coverage at the interface is about 3.5 mg/m^2; at high asphaltene concentrations the surface coverage increases eventually reaching a plateau (O Gafonova & Yarranton, 2001). This is attributed to self-association and nanoaggregate formation, in the bulk oil phase, that can interact with the aliphatic chains of the asphaltene monolayer at the interface (Langevin & Argillier, 2016; Mullins et al., 2012; Rane et al., 2013).

A monolayer asphaltene coverage was also reported by Rane *et al.*, (Rane et al., 2015) employing an equation of state where the interfacial tension and instantaneous elasticity were found to be an exclusive function of the surface coverage unrelated to adsorption conditions such as time, solvent viscosity and asphaltenes concentration below and above the critical nanoaggregation concentration (CNAC).

On the other hand, it has been established that adsorption of asphaltenes at the interface at short aging times is reversible but as the time increases the adsorption turns irreversible: asphaltenes remain on the interface and do not migrate to the aqueous or oil phase. This was confirmed by Freer *et al.*, (Freer & Radke, 2004) when and oil-equilibrated brine was replaced by fresh brine (not contacted with asphaltenes) the authors observed an increase in interfacial tension of only 1.5 mN/m.

The irreversible adsorption of asphaltenes was also confirmed by the formation of a rigid mechanical film that is observed as a “skin” with wrinkles when an aged oil droplet, bearing asphaltenes, crumples upon regular contractions applied by a pendant drop shape analyzer apparatus. The formation of this rigid film has been attributed to a crosslinking or gelation of asphaltenes resulted from π-π stacking interactions of their aromatic cores. As a consequence, it has been widely hypothesized that long term stability of emulsions is attained by the formation of this film around water droplets, that induce a steric repulsion between them –preventing approaches- and thus retarding the coalescence rate.

Shear elasticitiy rheology measurements have also provided evidence of gelation because a transition between a fluid-like interface to a solid-like interface is similar to the cross-linking that occurs in polymers at the gel point. Similarly, interfacial dilatational elasticity supports the gelation of asphaltenes at the interface because it does not follow the Lucassen-van den Tempel (LVDT) model at longer aging times, when asphaltenes exhibit an irreversible behavior. This fact indicated that adsorption of asphaltenes do not show a diffusional relaxation and consequently they do not behave as a typical surfactants (Lucassen & Van Den Tempel, 1972; Sztukowski & Yarranton, 2005).

On the other hand, shear elasticity and compression elasticity modulus (E) require time to evolve because asphaltenes undergo a slow cross-linking at the interface; a fact that does not correlate with the formation of stable emulsions just after a few minutes of mixing even at low asphaltene concentrations (Langevin & Argillier, 2016; F. Liu et al., 2017). Besides, shear elasticity is only observable at high asphaltene concentrations whereas dilatational elasticity decreases sharply at the same concentration range. Furthermore, dilatational modulus has shown higher values at low asphaltene concentration or short times whilst shear modulus is greater at

higher concentrations and long times. This would indicate that at least one of the techniques is not consistent with the hypothesis of a cros-linking of asphaltenes at the interface.

Recently, consensus about these issues were addressed by Liu *et al.,* (F. Liu et al., 2017), where transitioning to a softy-glass (arise from asphaltene cross-linking) interface in dilatational rheology was attained to the loss of the laplacian form of an oil droplet (bearing asphaltenes) that occurs when surface pressure exceeded a certain value (20-22 mN/m) under static adsorption conditions. Above this range, the oil-water interface behavior deviates from the equation of state proposed by Rane et al., (Rane et al., 2015) and cross-linking of asphaltenes begins after a maximum packing has been achieved. Therefore, discrepancy between the slow rise of shear elasticity and a fast emulsion stabilization can be attributed to the evolution of the surface coverage. The former occurs, at a static interface, under adsorption kinetics (diffusion kinetics) and the latter depends upon advection due to mixing and coalescence kinetics. In this sense, differences with shear rheology can be explained because surface coverage does not reach a maximum packing during static adsorption conditions. This suggests that surface pressure, in dilatational rheology, mainly depends on surface coverage and its evolution during oscillations.

Although, most of the studies found in the literature state that asphaltenes exhibit a non-diffusional behavior, Liu *et al.,* (F. Liu et al., 2017) believe that dilatational rheology results and deviations from the LVDT model can be explained by diffusional relaxation models. This is due to the fact that asphaltenes are defined as a complex fraction with diverse molecular structures of different interfacial activities. Instead, the non-diffusional character of asphaltenes arise from the differences in timescales between diffusion and interfacial tension that evolve fast initially and then slow at long times, suggesting a prolonged adsorption of surface active asphaltenes.

So far, we have shown different perspectives aimed to explain asphaltenes behavior at oil-water interfaces and its implication in emulsion stability. However, crude oil and bitumen are complex mixtures and other native surfactants such as resins, naphthenic acids and solids can reach the oil-water interface to participate in the formation, stabililization or breaking of water-in-oil emulsions (w/o) (Anisimov et al., 2014; Dicharry, Arla, Sinquin, Graciaa, & Bouriat, 2006; Elsharkawy, Al-Sahhaf, & Fahim, 2012; Spiecker, Gawrys, Trail, & Kilpatrick, 2003; Xia, Lu, & Cao, 2004; X. Yang, Verruto, & Kilpatrick, 2007). For instance, Östlund *et al.,* (Östlund, Nydén, Auflem, & Sjöblom, 2003b) showed, using NMR, that naphthenic acids and asphaltenes can associate *via* acid-base interactions depending upon the chemical structure of the asphaltenes. In other contribution, Arla *et al.*, (Arla et al., 2007) found that naphthenic acids stabilize w/o emulsions under certain conditions of pH and water content. Later, the same authors concluded that naphthenic acids and asphaltenes form an interfacial gel (liquid crystal) associated with the long term stability of w/o emulsions (Arla, Flesisnki, Bouriat, & Dicharry, 2011).

On the other hand, Moradi *et al.,* (Moradi, Topchiy, Lehmann, & Alvarado, 2013) pointed out that the synergistic effect between naphthenic acids and asphaltenes to stabilize emulsions is still controversial. They believed that acidic compunds with surface activity adsorb at the oil-water interface creating a barrier that impedes adsorption of asphaltenes; thus, reducing the rigidity of the interfacial film and decreasing emulsion stability.

Competitive adsorption of naphthenic acids and asphaltenes at the oil-water interface has also been proposed (Teklebrhan, Jian, Choi, Xu, & Sjöblom, 2016). In this case, displacement of asphaltenes produces “soft” interfaces that, in some cases, decrease emulsion stability. However, this phenomenon can change depending upon the type of asphaltenes and naphthenic acids as well as their concentration and the pH of the aqueous phase. In addition, due to the surface activity of

NA, these compunds can also dissociate in water and react with cations (e.g Ca^{2+}, Na^{+}) to form naphthenates which can accumulate at the oil-water interface (Kiran, Ng, & Acosta, 2011). Recently, it has been demonstrated that these salts lead to formation of lamellar liquid crystals at the interface which stabilize w/o emulsions. Similarly, Havre *et al.*,(Havre & Sjöblom, 2003) suggested that highly stable emulsions are formed by a combination of naphthenic acids, naphthenates and asphaltenes where multilayer formation and particle stabilization are proposed as stabilization mechanisms.

Interestingy, high molecular weight naphthenic acids can have a better stabilizing effect on the emulsions (Havre & Sjöblom, 2003). In addition, naphthenic acids with high molecular weight and structurally similar to asphaltenes formed tight w/o emulsions despite their hidrophobicity when compared with low molecular weight species (Clingenpeel et al., 2017). Few reports suggest the existence of chemical interactions between naphthenic acids and asphaltenes leading to complexes that dominate the interface. For instante, it has been hypothesized that nitrogen-containing asphaltenes and carboxylic acid groups in naphthenic acids undergo strong acid-base molecular interactions (Varadaraj & Brons, 2007b, 2007c).

Due to the fact that the influence of naphthenic acids and asphaltenes at the oil-water interface is not fully understood, in this chapter we provide insights into the effect of real naphthenic acid mixtures at an oil-water interface formed by C_7 solid-free asphalthenes isolated from two south american heavy crude oils, using dynamic interfacial tension measurements and surface pressure isotherms. To the best of our knowledge this is the first report where the effect of real naphthenic acid (and their fractions) samples on asphaltene film properties is tested and correlated with emulsion stability and molecular composition analyses. Most of the studies found in literature have employed standard mixtures of both fractions.

3.2 Experimental section

3.2.1 Materials, reagents and samples. Two heavy crude oil samples labelled A and B were provided by the Colombian Petroleum Institute-Ecopetrol. No chemicals were added to the crude oils and most of the water was removed previously.

Precipitation of asphaltenes from both samples was carried out using highly pure n-heptane (99.4 %), following a standard protocol (ASTM D6560-12).

Aminopropyl cartridges (NH_2- 2 g, volumen capacity 15 ml), purchased from Biotage-ISOLUTE®, were employed to extract six naphthenic acid (NA) fractions of different molecular weights from Crude oil B (total acid number of 5,26 mg KOH/g) using a solid phase extraction (SPE) method previously reported (S. M. Rowland et al., 2014). A whole NA sample, without fractionation by molecular weight, was also extracted from crude oil B using SPE. For elution of NA, in both procedures, HPLC-grade solvents such as dichloromethane (DCM), methanol (MeOH), toluene (MePh), acetonitrile (ACN) and formic acid (HCOOH, 98 %) were purchased from Merck (Darmstadt, Germany).

A standard mixture of NA (Fluka 70340) and 5β-cholanic acid standard were acquired from Sigma Aldrich (St. Louis, MO, USA) and used as received. Filter paper Whatman N° 2 (Diameter 24 cm, 8 µm) was used to filtrate asphaltenes. High purity toluene (99.99%) and n-heptane (99.4 %) solvents were purchased from VWR international and used to prepare the organic phase for model emulsions, interfacial tension measurements, extraction and purification of asphaltenes. All materials and solvents were used as supplied.

3.2.2 Asphaltene extraction. Asphaltene samples (A and B) were extracted from the corresponding heavy crude oils using an excess of n-heptane. Briefly, 1 g of each crude oil sample

was mixed with 40 mL n-heptane until complete dissolution. The mixture was stored in the dark and the precipitated unwashed asphaltenes were collected by gravitiy filtration. Then, asphaltenes are washed out with volumes of 25 mL of n-heptane for several days until the filtrate is clear.

For solids removal, asphaltenes were re-dissolved in toluene and solutions were centrifuged. Supernatant solutions were collected and toluene was evaporated, at room temperature, to produce a "solids-free" asphaltene fraction. The percentage weight content of asphaltenes in crude oil samples A and B was 21.9 ± 0.3 wt % and 5.5 ± 0.2 wt %, with toluene insolubles of 0.2 ± 0.1 wt % and 0.8 ± 0.2 wt %, respectively.

3.2.3 Isolation and fractionation of naphthenic acids. 500 mg of crude oil B was dissolved in dichloromethane and loaded onto an activated aminopropyl silica cartridge. Non-acidic species were eluted with mixtures of dichloromethane (DCM) whereas acidic extracts, the most polar fractions in the sample, were isolated by molecular weight using sequential elution mixtures comprised of DCM/MeOH/H2O/HCOOH in different ratios, according to an elution protocol previously reported (S. M. Rowland et al., 2014; Valencia-Dávila, Witt, Blanco-Tirado, & Combariza, 2018). Average molecular weight of the six acidic fractions extracted by SPE were previously determined by MALDI-FT ICR MS and are shown in Table 1.

Table 1. *Average molecular weight of the six acidic fractions extracted by SPE.*

N° Fraction	Molecular weight ($\bar{M}_w$)
1	474.3
2	522.1
3	532.4
4	567.3
5	658.2
6	880.1

On the other hand, extraction of total naphthenic acids from crude oil B was also done by SPE eluting non-polar molecules with dichloromethane, followed by the elution of low acidity species with a mixture of DCM/MeOH. Finally, the acids were extracted using a solvent ternary mixture of DCM/MeOH/ HCOOH. In both extraction procedures the NA recovery was 95 % and 96%, respectively.

3.2.4 Dynamic Interfacial tension and surface pressure isotherms. The dynamic interfacial tension and surface pressure isotherms were measured using a drop shape analyzer (DSA, IT Concept), coupled to the Windrop software (Figure C1, from appendix C, shows the drop shape analyzer apparatus). In summary, a droplet (12 μL) of the organic phase (heptol 25/75) bearing asphaltenes and/or acids is formed on the tip of a U-shaped needle and placed in an optical glass cuvette containing a brine solution (1541 mg/L NaCl, 628 mg/L CaCl2, 128 mg/L NaHCO3). The droplet was illuminated by a light source and a high-speed camera (CCD- charged coupled design) was used to capture the droplet profile which allows to calculate interfacial tension, drop surface area and volume over time. All experiments were conducted at room temperature and 1 atm pressure. Dymamic interfacial tension was measured from 0 to 3600 s and diffusion effects were eliminated previously by adding two drops of oil phase into the water phase and letting the solutions sit for 60 minutes until equilibration.

Surface pressure isotherms acquisition begins, after 1 hour or more of droplet aging, doing stepwise compressions by withdrawing fluid from the droplet, reversing the direction of the drive motor of the DSA apparatus. Between each measuring step 30 s of interface stabilization is allowed before interfacial tension and droplet surface area measurements. Compressions were suspended once the droplet crumpled or was too small to measure. Surface pressure isotherms were constructed by plotting the surface pressure as a function of film ratio A/A_0, (ratio of the area of

the interface after compression, A, to the initial area, A_0) at any given aging time. Surface pressure (denoted as π) is the difference between the interfacial tension of a pure solvent γ_o (heptol in all cases) and the interfacial tension of the solvent γ with an adsorbed surfactant (asphaltenes and/or naphthenic acids). Surface pressure (π) is calculated according to equation 1:

$$\pi = \gamma_o - \gamma \quad (1)$$

Surface pressure isotherms are analogue to 2-D pressure–volume isotherms and typically have 2-D phase transitions of an irreversibly adsorbed monolayer of surface active agents such as asphaltenes which remains on the surface even during compression. Generally, surface pressure is expected to be constant during compression of reversibly adsorbed monolayers. Crumpling film ratios (CR) for irreversibly adsorbed films correspond to the data point with the lowest film ratio A/A_0 value on the surface pressure isotherms. The reported crumpling ratio values are averages of two measurements.

3.2.5 Preparation of model emulsions. All emulsions were prepared with 40 vol % aqueous phase and 60 vol % of organic phase. To prepare the organic phase, 10 g/L (0.01 wt % respect to the oil phase) of solids-free asphaltenes A or B were first dissolved in toluene and sonicated for 20 min to ensure complete dissolution. Then, n-heptane was added to reach a proportion of 25 vol % n-heptane and 75 vol % toluene in all cases. To test the effect of other surfactants on emulsion stability, six acidic fractions (F1-F6), a whole NA fraction label as F-all acids, 5β-cholanic acid and a standard naphthenic acid mixture are added individually to the oil phase at 5 wt %. Then, the mixtures were sonicated for 5 min to ensure homogeneity. Finally, a brine with a composition similar to that of formation water found in a Colombian oil reservoir (1541 mg/L NaCl, 628 mg/L CaCl2, 128 mg/L NaHCO3) was added dropwise to the oil phase while an homogenizer (CAT

520D) was operated at 18000 rpm for 5 min. Using the same emulsion preparation conditions as above, we also tested the effect of the whole NA fraction from crude oil B (at 5 wt %) on the films composed by asphaltenes A and B (both at 10 g/L or 0.01 wt%).

3.2.6 Emulsion stability tests. Emulsions settled for 1.5 hours were then added to glass tubes, sealed and centrifuged for 5 min at 3500 rpm (Heraus Megafuge). The tubes were immersed in a water bath at 60 °C for 2 h and further centrifuged for 5 min. Heating and centrifuge steps were repeated after completing 5 cycles (10 hours). The volume of free water was recorded at the end of each cycle. The more water recovered after each cycle, the less stable the emulsion. The amount of free water is reported as a percentage of the amount of initial water in the emulsion.

3.3 Results and discussion

3.3.1 Differences between naphthenic acid and asphaltenes interfacial films. Figure 15 shows the surface pressure isotherms for the asphaltenes A (left side) and the whole NA sample and the fractions (F1-F6) from crude oil B. The surface pressure isotherm of asphaltene A exhibits two regimes, the first one corresponds to a film with an initial high compressibility at high film ratio (A/A_0) values, but as compression proceeds the slope becomes steeper at low film ratios (A/A_0) indicating a phase change to low compressibility a behavior typical of rigid films. These characteristics indicate that asphaltenes were irreversibly adsorbed and that they did not leave the interface upon compression. In contrast, surface pressure isotherms of NA fractions: 1, 2, 4, 5 and the fraction labeled as *all acids,* are typical of a reversible behavior without clear phase transitions and crumpling points. These fractions exhibited high surface pressure values between 25-38 mN/m (lower interfacial tension values), suggesting high surface activity. Conversely, fractions 3 and 6 show an irreversible behavior because their films crumpled upon compressions. In other words, molecules present in these two fractions reached the oil-water interface but did not leave the

interface after compressions, making possible to form a solid-like film until reaching the crumpling point (Figure C2 of appendix C shows the oil droplet images for fractions 3 and 6 taken at the crumpling point with their corresponding crumpling ratio values).

This behavior was not observed on the other NA fractions. In additon, fractions 3 and 6 had lower surface pressure values (*i.e* high interfacial tension values) beginning from 9 mN/m and extending until 38 mN/m. The sample containing *all acidic* species exhibits intermediate surface pressure values lying between two set of samples: F1, F2, F4, F5 and F3.

Interestingly, at low concentrations (1.5 wt % and 0.1 wt %) all NA fractions (Figure C3 of the appendix C) exhibit surface pressure isotherms typical of a reversible behavior, without crumpling points and low surface pressure values. Particularly, at 0.1 wt % all isotherms were almost horizontal with surface pressure values between 0- 20 mN/m due to a low number of molecules reaching the oil-water interface and quickly escaping it.

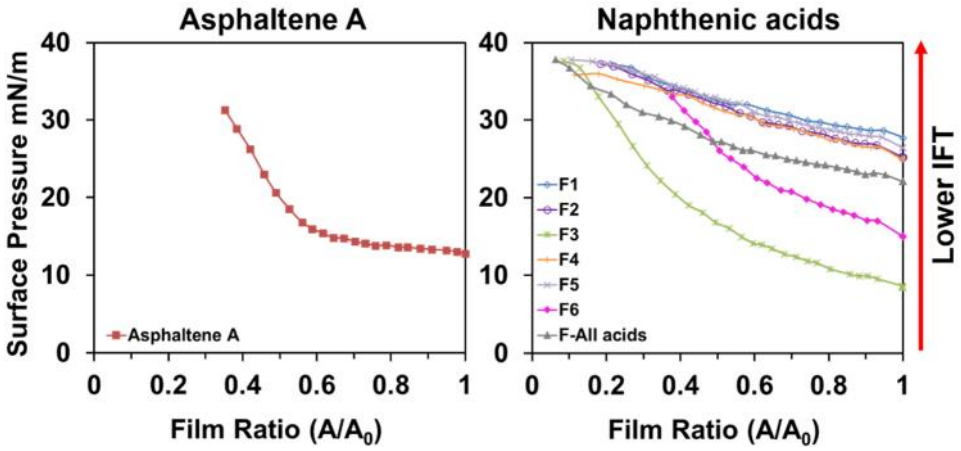

Figure 15. Surface pressure isotherms of asphaltene A (10 g/L) (left side) and acids (right side) at 5 wt % in heptol (25/75). All samples were aged 1 hour.

On the other hand, figure C4 of the appendix C shows the dynamic interfacial tension (IFT) profiles for all acidic fractions at 5, 1.5 and 0.1 wt % compared to asphaltene A. In general, lower IFT values were registered for fractions 1, 2, 4, 5 and the fraction with *all acids* at a concentration of 5 wt % whereas at 0.5 wt% asphaltene A was found to be more interfacially active than all acidic fractions. In addition, dynamic IFT profiles of NA fractions at 5 and 1.5 wt % showed a rapid decay within the first minutes and then a slower reduction towards equilibrium values over a long period of time. In contrast, at 0.1 wt % NA fractions with higher average molecular weight (F4, F5, F6) showed a slower reduction of the IFT that goes on beyond 50 min.

In some cases, IFT profiles of some acidic fractions (F1, F2, F4, F5, F-all acids) at 5 wt%, reached a minimum on the IFT that then slightly raised it to equilibrium values. This reduction can be attributed to an accumulation of acids at the interface before they are transferred to the aqueous phase. However, Farrooq et al., (Farooq, Simon, Tweheyo, Øye, & Sjöblom, 2013) pointed out that the absence of minima does not mean that transfer of soluble acids into the aqueous phase did not occur. It only indicates that there is no temporarily accumulation of the compounds at the interface, and most likely that the solublization of components in the water phase is smaller. It should be noted that F5, at 5 wt %, first reached the lowest IFT value (11.1 mN/m) at only 345 s (ca 6 min) in comparison with the other fractions at the same concentration. This fact indicate that NA contained in fraction 5 are the most interfacially active molecules among all fractions. In contrast, fraction 6 showed interfacial tension values similar to asphaltenes between 0-600 s, even at the highest concentration (5 wt %). On the other hand, F3 showed a lower surface activity than asphaltenes and the other acid fractions.

Differences between dynamic IFT profiles and surface pressure isotherms of acids and asphaltenes indicate that these species behave differently, perhaps because of asphaltenes ability

to self-associate through π-π interactions. In this sense, the next step is to examine in depth the effect of NA on asphaltenes films at the oil-water interface by monitoring changes on IFT, interfacial film properties and emulsion stability.

3.3.2 Influence of real NA samples on asphaltenes interfacial tension. Interfacial tension (IFT) is the amount of work per unit surface area required to bring molecules from bulk phases (oil or water) to create a new interface. Asphaltenes, particularly, reach the oil-water interface to reduce the IFT by interaction with water molecules through hydrogen bonding and/or dipole-dipole interactions as reported by Jian et al., (Jian et al., 2016) using an oxygen-rich asphaltene model compound known as Violanthrone-79 (VO-79). If this is the case any other surfactants present in the bulk, such as NA or even salts, could affect these molecular interactions. Literature reports related to this topic are diverse, with some authors suggesting that salt addition increase the IFT, while others observe an opposite trend. There is an specific study demonstrating that salinity has a weak effect on the IFT of hydrocarbons containing NA and asphaltenes (Bikky, 2012). In this section, we will focused on the effect of NA addition to asphaltene films at the oil-water interface, while keeping constant the salt content in the aqueous phase.

When comparing dynamic IFT profiles of NA (figure C-4 from the appendix C) with asphaltenes-NA systems shown in Figure 16, we observe that systems containing fractions 1, 4, 5 and F-*all acids* at 5 wt%, were able to decrease the IFT below 25 mN/m -the lowest IFT value observed for asphaltene A alone. However, IFT was higher than pure NA fractions (see figure C4 from appendix C for IFT of pure NA fractions). This fact would indicate that most of the acid molecules from the NA fractions reached the interface and displaced some asphaltene molecules. Particularly, the system with *all acids* was able to reduce the IFT below 25 mN/m probably due to the presence of a wider type of acids with different surface activities that can synergically compete

and displace asphaltenes from the interface more efficiently than fraction 2, 3 and 6 for example. Surprisinly, in spite of the high interfacial activity of the NA fraction 2 at 5 wt%, the asphaltene-F2 system had a dynamic IFT lower than asphaltenes but higher than the pure NA. This phenomenon most likely indicate that asphaltenes significantly mask the surface activity of these type of acids (F2) dominating the oil-water interface. In contrast, the systems with fractions 3 and 6 at 5 wt % showed dynamic IFT values similar to asphaltenes. This trend was also observed when NA fractions were at 1.5 wt%. However, at 0.1 wt %, the effect of the acids is not as significant and asphaltenes dominate completely the interfacial activity. Particularly, the IFT profiles of the system asphaltenes-F1 at 5 wt% showed some migration of molecules to the aqueous phase because the IFT initially decreases and then slightly increase to reach a plateau.

Overall, we did not find a systematic trend or link between the average molecular weight of the NA fractions and a reduction of the IFT. However, we think that displacement of asphaltenes from the interface is influenced by the presence of heteroatoms such as nitrogen and sulfur in the acidic fractions (compounds of the types NO_1, NO_2, NO_3, NO_4, NO_5, NO_6, NO_7, NO_8, O_2S, O_3S, O_4S, O_5S) as previously discussed in chapter two. These species were found to be aromatic in nature and although they exist in low concentrations in the NA samples, the heteroatoms present confer them higher interfacial activity than their oxygenated analogues (O_1, O_2, O_3, O_4, O_5, O_6, O_7, O_8); perhaps enough to displace asphaltenes at the interface. In addition, some of these species were also found in isolated interfacial materials from w/o emulsions, ratifying the notion of high surface activity (Czarnecki, 2009; Stanford, Rodgers, Marshall, High, et al., 2007).

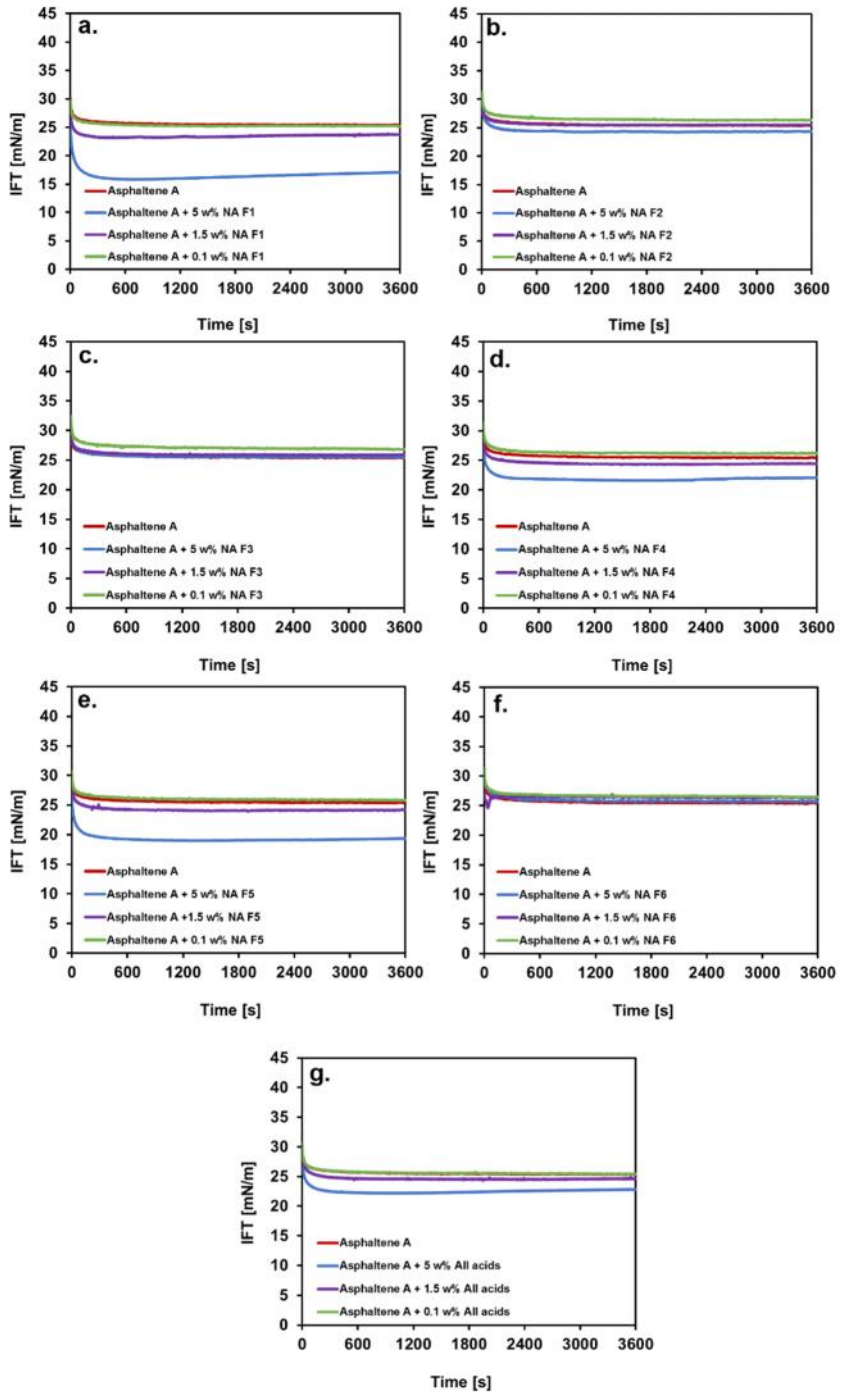

Figure 16. Effect of napthenic acid fractions a) F1, b) F2, c) F3, d) F4, e) F5, f) F6 and g) All acids on the dynamic interfacial tension of asphaltene A.

Interestingly, Varadaraj et al., (Varadaraj & Brons, 2007c) also reported that IFT of NA is influenced by their composition and chemical structure, which in turn determine the nature of molecular aggregation at the oil-water interface and their impact in emulsion stabilization. The same authors (Varadaraj & Brons, 2007a) suggested that interfacial activity of NA is improved in a crude oil medium, when compared with an aliphatic/aromatic solvent, as a result of a higher probability of chemical interactions between NA and the crude oil components.

3.3.3 Influence of naphthenic acids on asphaltenes interfacial film properties. Surface pressure isotherms of asphaltenes and asphaltenes/NA systems are shown in Figure 17. At 5 wt % (Figure 17a), NA notably affected the oil-water interface, weakening asphaltene films as evidenced by surface pressure isotherms with moderate slopes, phase transitions at lower film ratios (A/A0) values as well as lower crumpling ratios in comparison with the asphaltene A. Particularly, acids contained in fractions 1 and 5 (figure 17a) exhibited a stronger effect on the compressibility of the asphaltene interface. On the other hand, fraction 6 had a smaller effect than other fractions, since its surface pressure isotherms resemble that of an asphaltene-only system. Although, asphaltene films changed, all adsorbed irreversibly because the crumpling points were always observed (figure 17 a and b) even with the acidic fractions at high concentrations (5 and 1.5 wt%). In contrast, at low concentrations (0.1 wt %), the NA did not “weaken” the asphaltene film (figure 17 c) probably because only very few molecules of the NA molecules could reach the oil-water interface. Therefore, these asphaltene/acids films were also irreversibly adsorbed and their film properties were similar to those of the asphaltene.

These results suggest that the effect of additional surface-active agents on asphaltene films strongly depends on concentration. Hence, at concentrations ≥1.5 wt %, acidic fractions (F1-F5) can indeed weaken asphaltene films, increasing their compressibility. This can be caused by partial

displacement of asphaltenes or by molecular interactions between NA and asphaltenes that can effectively decrease the asphaltene´s self-association ability on the interface, reducing the rigidity of the films. We believe these mechanisms are highly dependent on the heteroatom content on both NA and asphaltenes.

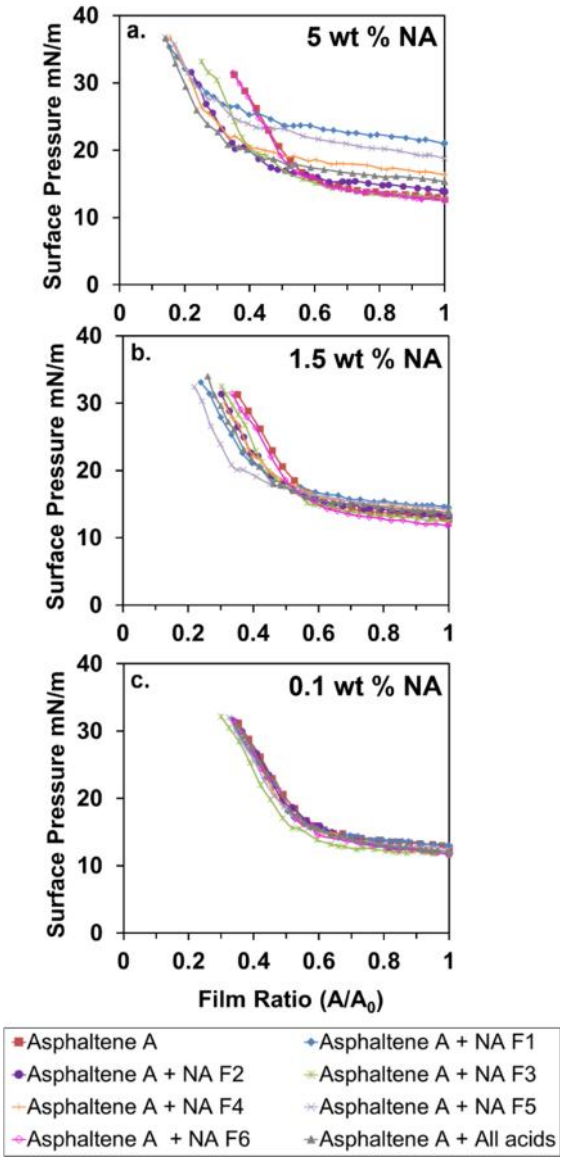

Figure 17. Effect of adding NA fractions at a) 5 wt%, b) 1.5 wt% and c) 0.1 wt% on the surface pressure isotherm of asphaltene A (10 g/L) in heptol (25/75). The samples were aged for 1 hour at 23 °C.

Formation of rigid films is associated with very stable emulsions because they are more resistant to coalescence. In contrast, weakened films favour approximation of water droplets thus leading to unstable emulsions. In the following section, we will describe how interfacial film properties can be related with emulsion stability.

3.3.4 Effect of naphthenic acids on crumpling ratios and emulsion stability. Yarranton et al., (Yarranton, Sztukowski, & Urrutia, 2007) found that aside from film properties such as interfacial compressibility and crumpling film ratio, surface pressure isotherms could provide information regarding rheological properties of interfacial films because the inverse of the initial interfacial compressibility is related to the interfacial modulus. In addition, the coalescence rate of emulsions can also be predicted by using surface pressure isotherm data, particularly with interfacial film compressibility that variates depending on film compression and aging (Yarranton, Urrutia, & Sztukowski, 2007). Furthermore, Diana et al., (Ortiz, Baydak, & Yarranton, 2010) developed a stability parameter that is a function of the crumpling ratio and surface pressure (interfacial tension) to provide a classification of surfactants according to their demulsifying properties and their effect on film properties at the oil-water interface. These previous findings demonstrated that the surface pressure isotherm is useful and although it is not a thermodynamic property, it is a measure of the time dependent film properties and may be relevant to emulsion stability.

In general, it has been observed that rigid films exhibit high crumpling ratio (CR) values and are more resistant to coalescence so they are associated with stable emulsions. Due to this relationship, the effect of NA (at 5 wt %) on the crumpling film ratio and emulsion stability was also examined in this study. Table C1 from the appendix C shows the crumpling film ratio of the asphaltene-acids systems. Clearly, all acids significantly decrease the crumpling film ratios (CR),

at 5 wt% concentration, but did not eliminate the irreversibility of the asphaltene film which exhibited a higher crumpling ratio (CR=0.35). At 5 wt%, acidic fractions change the crumpling asphaltene-acids film ratio from high to low values in the following order F6 >F3>F2>F4>all acids> F1>F5. The same trend was observed for the asphaltene-acids systems when acids were present at 1.5 wt%. In contrast, at the lowest concentration of acids (0.1 wt%) the crumpling film ratio values remained close to the one obtained for the asphaltene A without acids. This is because at high concentrations (≥1.5 wt %), NA partially replace asphaltenes at the interface weakening films and thus increasing the compressibility and decreasing the crumpling ratio.

Due to the fact that asphaltenes films are affected to a greater extend when NA are added at high concentration, figure 18 shows the effect of naphthenic acid fractions at 5 wt % on an emulsion stabilized by asphaltene A after 10 h of treatment. It is evident that the presence of NA results in a higher free water percentage in comparison with emulsion prepared with asphaltenes exclusively, that only released 2.4 % of water after 10 h of treatment. In contrast, NA fractions 1 and 5 had a stronger destabilizing effect releasing 22.6 % and 54.6 % of water, respectively. Outstanding demulsifying properties of fraction 5 are superior since it allowed to recover around 20 % of free water after two hours of treatment in comparison with only 9 % accounted for fraction 1, at the same time. Conversely, fractions 2 (9.2 %), 4 (8.3 %), 6 (7.0 %), a*ll acids* (6.4 %) and 3 (5.6 %) had the less effect on emulsion stability.

High water resolved obtained from emulsions prepared with fractions 1 and 5 coincide with the ability of these fractions to make flexible films, showing a correlation between the emulsion stability analysis and surface pressure isotherms data. Although salts in the aqueous phase can affect emulsion stability, Rocha et al., (Rocha et al., 2016) demonstrated that addition of salts from

0.002 to 1 wt% resulted in a slightly increase of emulsion stability. In addition, when the salt content increased above 1 wt %, the emulsion stability did not change significantly.

Interestingly, none of the acidic fractions could form w/o emulsions (data not shown) by themselves, as observed as well by other authors (El-Sayed, 2012). For instance, Hemmingsen et al., (Hemmingsen et al., 2006b) found that removing NA from crude oil increased emulsion stability, confirming they are not actively involved in the emulsion stabilization. Although, this finding agrees with the results obtained in this study, this can vary depending on the crude oil and asphaltene composition.

Recently, two models have been proposed to explain partioning mechanisms of asphaltenes and NA on the interface: The first involves the formation of a complex and the second is related with competition between these species (Bourrel & Passade-Boupat, 2018).

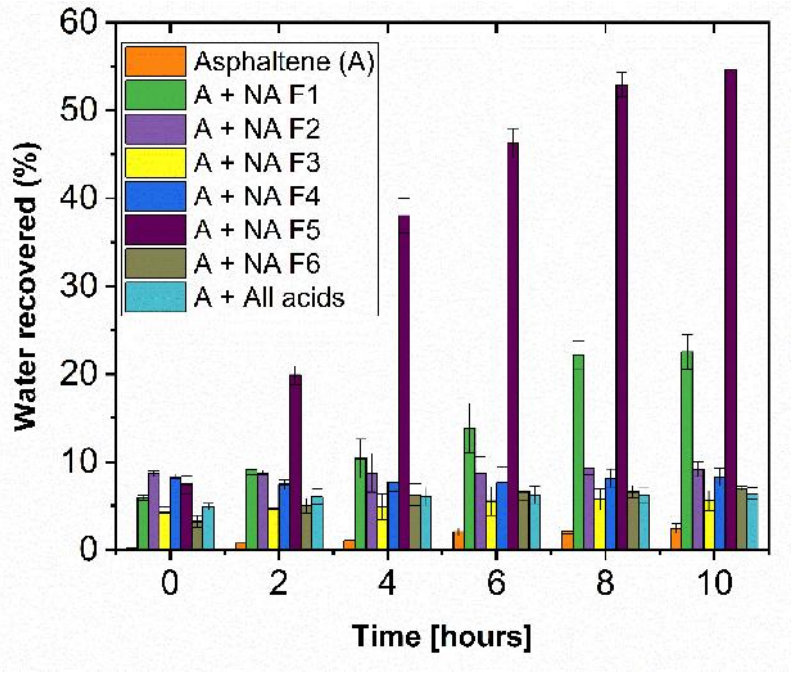

Figure 18. Effect of acidic fractions (5 wt%) on emulsion stability at 0, 2, 4, 6, 8 and 10 hours of treatment. Emulsions were prepared with asphaltene A (10g/L) in heptol (25/75) and 40 vol % of aqueous brine.

Varadaraj and Brons (Varadaraj & Brons, 2007c) proposed that nitrogen- containing asphaltenes and NA interact sinergistically, by strong acid-base interactions, to form a complex. They hipothetized that aggregation and packing of these complexes on the interface leads to a higher interfacial activity than in “free” asphaltenes. In a second study (Varadaraj & Brons, 2007a) they found that crude oil NA with a higher proportion of 250-425 Da molecular weight species were the most effective in reducing the interfacial tension and stabilizing water-in-oil emulsions.

In our study, all naphthenic acids destabilize emulsions and no correlation between molecular weight and demulsifying activity was found. On the other, Varadaraj et al., found that naphthenic acids extracted from crude oils are more surface active in a crude oil medium rather than a model hydrocarbon mixture such as an aliphatic/aromatic solvent system. This enhanced interfacial

activity was attributed by the interaction between acids and asphaltenes. This finding may indicate that other species in the crude oil can facilitate the interaction of these species to enhace the emulsion stability.

In other contribution, Heaps et al., (David T. Heaps, Madasu, Magers, & Buchanan, 2012; David Tristan Heaps, 2011) studied the interactions between standard naphthenic acids (methyl abietate, 5-β-cholanic acid and 5-β-cholanic acid-3-one) and asphaltenes using dynamic light scattering (DLS) and near infrared spectroscopy (NIR). Results from these techniques were correlated with the chemical structure of the asphaltenes and naphthenic acids and their interactions were determined using molecular modeling. The study monitored the flocculation of asphaltenes-acids toluene solutions by adding n-heptane as in a tritation procedure.

It was found that acids increased the precipitation onset of the asphaltenes in the order of 5β-cholanic acid-3-one < hydrogenated methyl abietate < methyl abietate < 5β-cholanic acid. They believe that acids have a peptizing effect that disperse asphaltenes due to the interactions between their corresponding polar groups, similar to a reduction in the interfacial activity of asphaltenes due to the solvation by resins in the oily phase (Anisimov et al., 2014; Spiecker et al., 2003). Molecular modeling results explained that 5β-cholanic acid increased the onset precipitation of asphaltenes due to a strong association between acidic and basic groups.

On the other hand, the presence of the π system in methyl abietate offered a more extensive interaction with the asphaltene than when the π system is absent as in the case of hydrogenated methyl abietate, explaining a greater extend of the onset asphaltene precipitation using methyl abietate. Interestingly, the ketone group in 5β-cholanic acid-3-one apparently interact in a different way with the asphaltenes than the other three naphthenic acids with larger dipole moment,

accelerating the precipitation of asphaltenes. In synthesis, naphthenic acids with a carboxylic acid functional group are able to form hydrogen bonds with electronegative heteroatoms present on the asphaltenes. Therefore, interaction with certain electronegative atoms present in the asphaltenes such as S_1, S_1O_1, N_1, N_2, O_2 varies depending on the chemical structure of the naphthenic acids.

Similarly, in other study (Teklebrhan et al., 2016), molecular dynamic simulations revealed that size and chemical structure of three naphthenic acids influence the interfacial activity of an asphaltene model compound (C5Pe, $C_{47}H_{48}N_2O_6$ Mw= 689 g/mol) at the oil-water interface. Due to the fact that NA interact with asphaltenes molecules *via* hydrogen bonds, the presence of a carboxylic acid group in the asphaltene-like model compound allowed to test the effect of NA−C5Pe association on C5Pe adsorption in a toluene−water interface. Interestingly, it was found that larger NA prefer to form hydrogen bonds with asphaltenes lowering their adsoption on the interface. In addition, small NA at high concentration avoided the adsorption of C5Pe nanoaggregates to the interface due to a blocking of their active sites, leading to less stable emulsions.

So far, these studies have shown different scenarios to explain the action of naphthenic acids in the presence of asphaltenes on water/oil interfaces. Similarly, we believe that weakening of asphaltenes films may happen through different mechanisms, step-wise or simultaneously. The first one involved the displacement of asphaltenes by differences on surface activities that generate a competition with acids for the the oil-water interface, similar to the action of some demulsifiers that due to their stronger interfacial activity penetrate into the interfacial film at the oil-water interface to breake and soften the film, enhancing the continuous phase drainage by decreasing the tension gradient (Kailey, 2016; Shehzad et al., 2018; Thomas, 2008; Zolfaghari, Fakhru'l-Razi, Abdullah, Elnashaie, & Pendashteh, 2016). The second possibility involves chemical interactions

such as hydrogen bond formation, dipole-dipole interactions, acid-base interactions or π-π interactions between acids and asphaltenes which can interfere in asphaltene aggregation at the oil/water interface. In addition, it is also possible that naphthenic acids can block the active sites of some molecules of asphaltenes via the above-mentioned molecular interactions, decreasing their adsorption with the water molecules and allowing some acids (possibly those enriched with heteroatoms) to reach the interface and remain anchored on it.

Particularly, fraction 6 contains larger NA molecules than fraction 5, however, it does not destabilize significantly the emulsion and its surface pressure isotherm was quite similar to the obtained for asphaltenes without acids i.e., asphaltenes film properties were not considerably affected by this fraction. Therefore, we hypothetized that these particular acids are highly aromatic and can self-associate through π-π interactions, as the asphaltenes also do.

Similar issues related to this finding were reported by Rowland et al., (Clingenpeel et al., 2017) using excitation emission matrix spectroscopy. It was found that most of the hydrophobic acids, present in an interfacial material sample, approached the size and aromaticity of bitumen asphaltenes and thus can also aggregate and overlap with asphaltenes on the interface.

Overall, emulsion stability and surface pressure isotherms suggested that any change on asphaltene films is influenced by the concentration, heteroatom content and chemical nature (extent of alkyl substitution and aromaticity) of the acids rather than a direct relation with the molecular weight. Furthermore, in agreement with the model proposed by Czarnecki et al.,(Czarnecki & Moran, 2005) we also believe that acid species with both maltenic and asphaltenic motifs could be more involved in the stabilization of w/o emulsions.

3.3.5 Effect of standard naphthenic acids on asphaltene films. We also examined the effect of two commercial naphthenic acids on the asphaltene A films in order to find a clearer insight about a possible relation between the chemical structure of acids and their abilitiy to change asphaltene films properties (compressibility and crumpling film ration) and destabilize water-in-oil emulsions. A naphthenic acid standard mixture mainly comprise of aliphatic acids (Hydrogen deficiency from Z=0 to Z= -12, Mw=240 g/mol) and the 5-β-Cholanic acid (hydrogen deficiency Z=-8, DBE=5, Mw=360 g/mol) were selected to study their effect on asphaltenes A films (detailed chemical characterization of the standard technical NA mixture is provided in chapter 1 (Valencia-Dávila et al., 2017). Figure C5 from the appendix C showed surface pressure isotherms for both NA tested.

Both samples exhibited a reversible behavior at all concentrations since their surface pressure isotherms did not exhibit slope changes, being almost horizontal. This is because molecules instead of remaining on the oil-water interface, came back to the bulk oil phase solution upon compressions. Furthermore, high surface pressure values in isotherm of 5-β-cholanic acid at 5 wt% indicated a higher interfacial activity in comparison with the NA standard mixture and asphaltenes (figure C6 a and b from the appendix C shows dynamic IFT of standard acids in heptol).

On the other hand, figure 19 shows the effect of these standard acids on interfacial asphaltene A films. Interestingly, 5-β-cholanic acid at all concentrations tested, shifted the isotherms to lower film ratio (A/A_0), affecting the interfacial compressibility as well as lowering the crumpling points values. However, it does not eliminate the irreversibiblity of the films, indicating that asphaltenes were also present on the interface. With a concentration of only 0.1 wt % in the oil phase, 5-β-cholanic acid (Figure 19b, green trace) affected the interfacial film properties in a greater extend that the NA standard mixture (figure 19a, green trace) present at the same concentration, which

surface pressure isotherm resembles to the asphaltenes. Particularly, at a concentration of 5 wt %, 5-β-cholanic acid affected considerably the compressibility, weakening the asphaltene film and decreasing the crumpling ratio until CR=0.05; the lowest value among the real acidic fractions and standard NA mixture tested in this study. Table C2 from the appendix C shows the crumpling ratio values for both asphaltenes/standard acid systems tested.

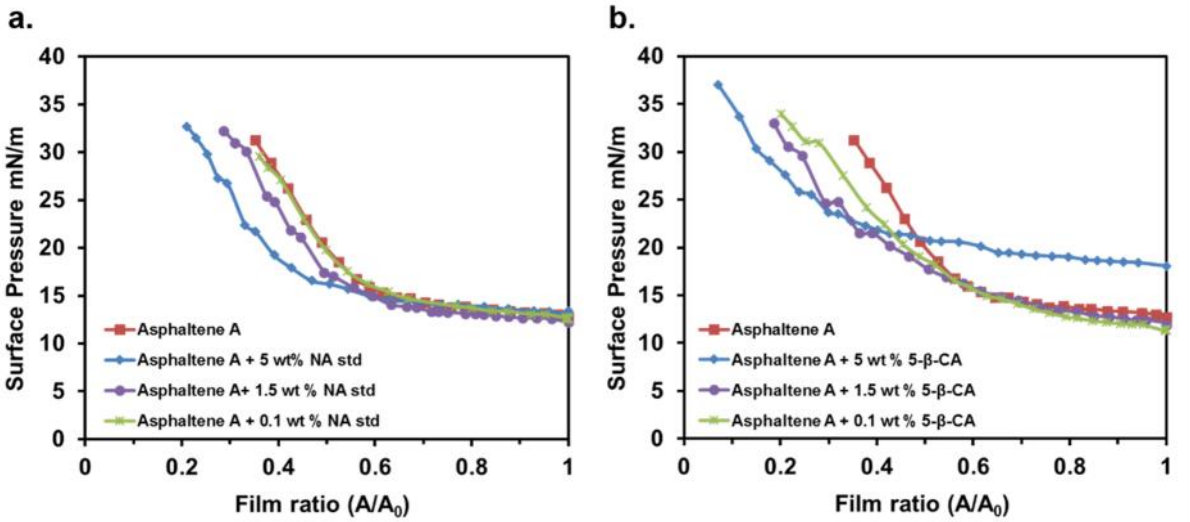

Figure 19. Effect of a) naphthenic acid standard mixture (NA std) and b) 5-β-cholanic acid (5-β-CA), at different concentrations, on asphaltene A films. All samples were dissolved in heptol (25/75) and aged 1 hour.

On the other hand, figure C6a from the appendix C shows that NA standard mixture reduced IFT and reached the equilibrium almost inmediate in contrast with the 5-β-CA that decays slowly at 1.5 and 0.1 wt %. In contrast, asphaltene/NA standard mixture (at 0.1, 1.5, 5 wt %) systems exhibited almost the same profile of the asphaltenes. (figure C6c from appendix C) This finding relies on the fact that aliphatic naphthenic acids Z = 0 which would be in a higher concentration, were not as interfacially active as asphaltenes so they did not reach the oil-water interface.

In contrast, asphaltenes/5-β-CA system (at 5 wt%) showed an IFT kinetics (see figure C6d from appendix C) similar to the 5-β-CA at 5 wt % in heptol/water, suggesting a high number of acid molecules at the interface. This fact indicates that, in this particular system, film asphaltene weakening is mainly due to a lower number of asphaltenes molecules on the interface possibly due to surface activity suppresion of asphaltenes by the action of 5-β-CA. Recall that none of the real acidic fractions could reduce the IFT in the presence of the asphaltenes until the values obtained for their corresponding pure acidic fractions.

Similarly, Sauerer et al., (Sauerer, Stukan, Buiting, Abdallah, & Andersen, 2018) found that stearic acid, at high concentration, blocked the access to the adsorption sites of the interface, leading to negligible adsorption of asphaltenes. This was due to a low diffusivity of asphaltenes that allowed to stearic acid molecules form rapidly well-organized interfacial structures, where hydrocarbon chains would be packed and extended into the oil phase. This brush-like organization would repel the asphaltenes from the interface. Besides, in spite of a larger adsorption energy of the asphaltenes, with adsorption equilibrium constants about two orders of magnitude higher than that of stearic acid, asphaltenes did not replaced slowly the stearic acid molecules as it was expected in a typical Gibbs-Langmuir approach. In contrast, Wang et al., (X. Wang et al., 2016) demonstrated, by studying the Langmuir interfacial isotherms, that stearic acid interact with asphaltenes at the oil-water interface. Interestingly, it was found that stearic acid asssociate strongly with asphaltenes at the interface to render films more flexible and soften. Such reduction of the interfacial rigidity was proportional to the amount of stearic acid and arise from a larger molecular interaction with asphaltenes that leads to a progressive reduction of molecular aggregates at the toluene/water interface as it was visualized by Brewster microscopy. It was also demonstrated, by washing experiments, that stearic acid-asphaltene adsorption at the interface was

irreversible. Morever, it was also found that stearic acid alone was not able to form rigid interfacial films in contrast with the asphaltenes.

The significant reduction of interfacial film rigidity exposed in the aforementioned study is more in accord with the 5-β-CA behavior at the interface than the observed for the NA standard mixture, mainly composed by aliphatic acids such as the stearic acid. This can be attributed to differences in concentration and also because NA mixture is a multicomponent sytem with naphthenic acids that have different diffusion coefficients and thus different rate of adsorption and desorption to and from the interface. Therefore, these conditions may facilitate a competition between acids for the interface that in sum led to a lower surface activity in comparison with the 5-β-cholanic acid. In addition, NA mixture contains acids with shorter hydrocarbon chains (# C<18) than stearic acid, thus, they can migrate to water subphase due to their larger solubility, adding complexity to the analysis.

On the other hand, real NA fractions, at 5 wt %, (F1, F2, F4, F5 and F-*all acids*) were more interfacially active than NA mixture and 5-β-cholanic acid. This could be explained by the presence of heteroatoms (N, S) present in the real mixtures, which are potential active sites where they can be linked to the interface. Conversely, F3 and F6 were found to be less surface active than 5-β-CA, probably due to a lower concentration of the compound classes O_2S_1 O_4S_1, N_1O_2, N_1O_4, N_1O_5 (see chapter 2) in the first fraction or due to an interfacial asphaltene-like behavior of the acids in the latter fraction (Valencia-Dávila et al., 2018).

3.3.6 Influence of naphthenic acids on asphaltenes extracted from two different crude oils.

So far, it has been shown how naphthenic acids from different molecular weight, heteroatom content and chemical structure interacted with one type of asphaltenes, changing the film

properties and emulsion stability. However, the effect of acids can change depending on the chemical composition of the asphaltenes. For example, Östlund et al., (Östlund et al., 2003b) studied the influence of two standard naphthenic acids (5β-cholanic acid and decahydro-1-naphthalene-pentanoic acid) on the aggregation of asphaltenes using near infrared spectroscopy (NIR). The results indicated that both NA had a dispersive effect that depended mostly on the asphaltene type.

Other studies have reported that interfacial behavior of asphaltenes also depend on their chemical structure. For instance, Singh et al., (Singh, Rampal, & Malani, 2018) reported that interfacial behavior of six asphaltene-like model compounds is influenced by their chemical structure and heteroatom type. It was found that heteroatoms such as oxygen (phenol) and nitrogen (pyrrole) inserted on an island motif and a quinoline on an archipelago type, facilitated the formation of hydrogen bonding between asphaltenes and water molecules, allowing them to be anchored on the interface. In contrast, asphaltenes with sulphur atoms (thiophene) both island and archipelago type as well as an oxygen (oxane) atom on an archipelago motif, left the interface and remained soluble on the oil phase. This is because these functional groups exhibited a low hydrophilicity of the heteroatom which make hydrogen bonding formation unlikely. In additon, orientational analysis performed by molecular dynamics, showed that N-based island type asphaltenes are parallel to the interface whilst O-based island type asphaltene and N-based archipelago type were perpendicular. However, in both type of orientations, the major part of the asphaltene molecules were immersed in the oil phase and anchored to the oil-water interface via the heteroatoms.

Due to the importance of asphaltenes composition on the acid-asphaltene interactions, we evaluated the effect of the fraction *all acids* on the interfacial behavior of the asphaltene B,

extracted from a heavy crude oil with high acidity but with a different compound class composition with respect to the asphaltene A. Recall, the acidic fraction (F-All acids) contained all NA extracted from the same crude oil B from which asphaltene B was isolated.

Figure 20 shows the surface pressure isotherms of asphaltene B compared to the asphaltenes B/acids systems, where the acidic fraction was added at three concentrations 0.1, 1.5 and 5 wt %. Initially, the isotherms revealed that asphaltenes B behave quite different with respect to asphaltenes A. For instance, films formed by asphaltene B exhibited a high compressibility region within a narrow surface pressure interval (27-30 mN/m) ranging from A/A_0=1 to A/A_0=0.24 film ratio. At this stage, asphaltenes molecules reach and leave the interface making imposible to compress them on the surface. As the area was reduced progressively the film exhibited a phase change ($A/A_0 < 0.24$), where asphaltene molecules were closely packed in a solid-like distribution. This resulted in higher surface pressure values and a low compressibility that decreases until reach the crumpling point. The surface activity of asphaltenes B was also higher (Figure C7 from appendix C) showing lower IFT values with a kinetics slower than the dynamic IFT of asphaltenes A (Figure C4 from appendix C) that decayed faster towards equilibrium values. This is mainly attributed to the differences on chemical composition and/or chemical structure rather than the size of asphaltenes. Recently, Sauerer et al., (Sauerer, Abdulghani, Abdallah, & Abdallah, 2018) found that despite similar aromatic sheet diameters of eleven asphaltenes extracted from very different formations within the Middle East, all samples showed variations in their interfacial activity.

Rergarding, surface pressure isotherms of asphaltene B/acids sytems, results suggested that acidic fraction (F-all acids) neither eliminated the irreversibility nor change the asphaltene B film properties (compressibility, crumpling ratio) significantly. In addition, dynamic IFT profiles (figure C7 from appendix C) resemble to the asphaltene B, suggesting that acids did not remain at

the interface even at the highest concentration (Figure C4 from appendix C shows the dynamic IFT), unlike the asphaltene A films. These results indicate that there was not any type of synergism or antagonism effect that leads to an enhancement or reduction of the interfacial activity of asphaltene B through molecular interactions that may involve formation of complexes with acids, asphaltenes solvatation and/or displacement of molecules at the oil-water interface.

In contrast, asphaltene A films were severely affected by this acidic fraction (≥1.5 wt %) demonstrating that differences on asphaltenes-acids interaction could be attributed to a different heteroatom content and maybe to the predominance of either an island or archipelago motif in the asphaltene fractions.

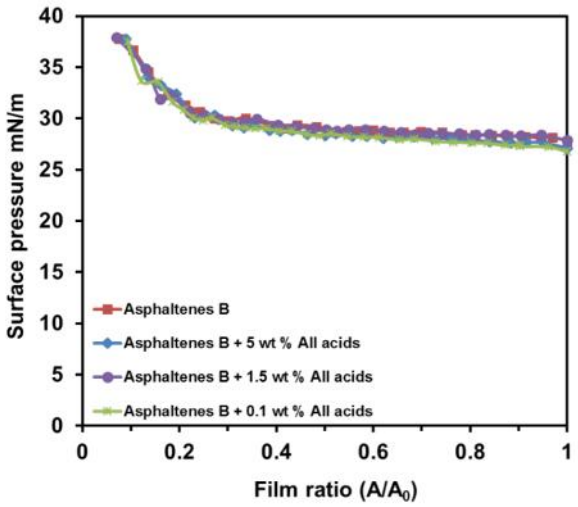

Figure 20. Effect of all acids fraction on interfacial asphaltene B films. All samples were dissolved in heptol (25/75) and aged for 1 hour.

The same factors mentioned above could also explain why some asphaltenes tend to aggregate more than others on the interface. As the irreversibility is related with the aggregation of asphaltenes and also with the ability to form a “skin”, films of asphaltene A and B were aged at

10, 30, 60, 120 and 240 min to establish how their film properties evolved along time. Figure 21 shows surface pressure isotherms for asphaltene A and B. Despite the fact that both asphaltenes exhibited crumpling points and were irreversibly adsorbed on the interface at all aging times, asphaltene A formed more rigid films with lower initial compressibilities (steeper slopes in the surface pressure isotherm), phase transition at higher film ratio values as well as higher crumpling ratio values as the aging time increases, in comparison with asphaltene B (Table C4 from appendix C shows the crumpling ratio for both asphaltenes as the aging time increases). This observation would have important effects on emulsion stability. This is because during coalescence the surface area of an emulsion decreases and interfacial films, irreversibly adsorbed, should be more resistant when the more they are compressed to resist coalescence. Therefore, a lower resistance to film compression would result in less stable emulsions. This fact may explain why asphaltene B were not able to stabilize w/o emulsions (data not shown) at longer times in comparison with asphaltene A. Furthermore, the increment in film rigidity along with the aging time would reveal an ease of aggregation of the asphaltene A at the interface.

On the other hand, the difference of surface pressure values between an aging time of 10 min and 240 min would indicate that asphaltene A require longer times to decrease IFT until equilibrium values, probably due to a possible reorganization of the asphaltenes where the more interfacially active molecules may replace the less active ones, which had arrived first at the interface (Jeribi, Almir-Assad, Langevin, Hénaut, & Argillier, 2002).

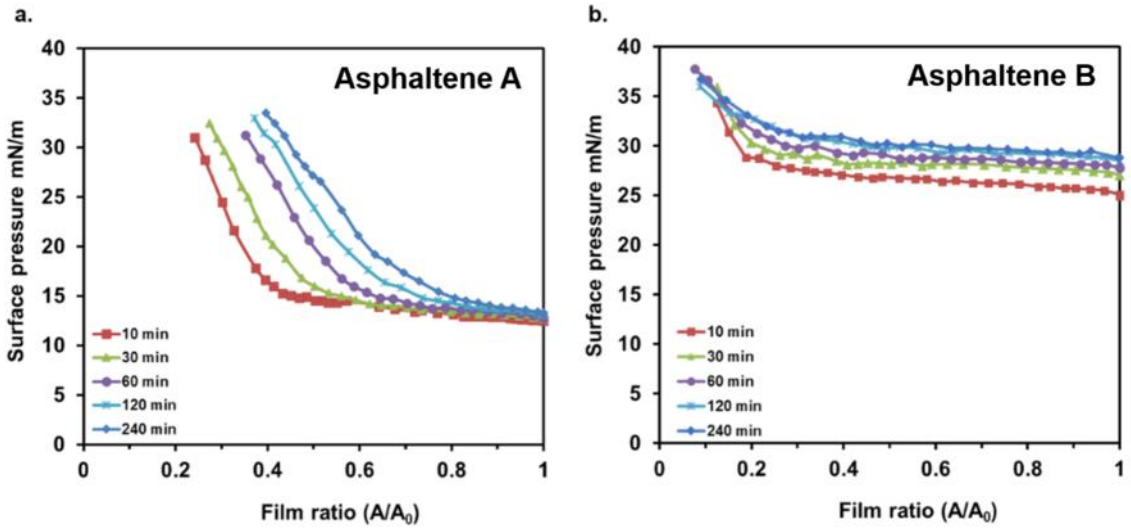

Figure 21. Effect of aging time on the surface pressure isotherms of asphaltenes A (a) and b (b) dissolved in heptol (25/75) at 10 g/L.

Another explanation for this is that only a small part of the asphaltene A were adsorbed at the interface, in accord with previous reports (Xu et al., 1999; F. Yang et al., 2014). To test this, we evaluated the surface pressure isotherm of the most interfacially adsorbed asphaltene A removed from a stabilized w/o emulsion by several washings with toluene following a procedure described in detail in the appendix C.

Figure C8 shows the surface pressure isotherms for the asphaltene A compared to the ones obtained for the most adsorbed asphaltenes and the supernatant solution both isolated from an asphaltene A-stabilized emulsion. The results indicate that the most adsorbed asphaltenes also have an irreversible behavior, however, they exhibited larger surface pressure values (lower IFT) along all film ratios than asphaltene A. In addition, compressibilities of phases 1 and 2 are different and phase transition occurred at a lower surface area i.e., most adsorbed asphaltenes rapidly packed in a solid-like distribution. Although the crumpling ratio was similar to the asphaltene A, images at this point showed an atypical droplet shape with respect to the asphaltene A which may due to

different viscoelastic properties of these films. Conversely, asphaltene molecules present in the supernatant solution showed a flat surface pressure isotherm with high compressibility between 1 to 0.35 film ratio values indicating a gas-like molecular behavior of the molecules on the surface which reach the oil-water interface and then come back to the oil solution. At $A/A_0<0.35$, asphaltenes in the supernatant solution began to pack until reaching the crumpling point. This fact suggested that molecules contained in the supernatant solution are poorly bond to water molecules whereas the most adsorbed asphaltenes, were strongly bound to the interface upon compressions.

Interestingly, whole fraction of asphaltene A showed intermediate surface pressure values between the most adsorbed asphaltenes (interfacial material) and those remaining on the supernatant solution suggesting that an irreversible adsorption can change when all myriad of asphaltene constituents are together. Probably, competition, between molecules with different activity for the oil-water interface, may have affected the way they bound to the interface.

Clearly, a larger portion of the asphaltenes are not present at the interface as it was found in other studies. For instance, Andersen et al., (Andersen, Mahavadi, Abdallah, & Buiting, 2017) confirmed that only specific types of asphaltenes are found at the interfaces because some of them are less surface active and therefore can be easily excluded. In addition, Rocha et al., (Rocha, Baydak, & Yarranton, 2018) found that the percentage of asphaltenes that are strongly involved in the stabilization of emulsion, varies and is dependent on the source origin.

On the other hand, figure C9 from appendix C showed that whole fraction of asphaltene A, the most adsorbed asphaltenes and those remaining in the supernatant solution showed similar dynamic IFT profiles. This suggests that molecules adsorbed at the interface are not neccesarily those that most reduce interfacial tension. In other words, only molecules with the ability to self-

associate and cross-link are adsorbed irreversibly at the oil-water interface to form rigid films and stabilize emulsions.

In general, literature suggests that asphaltenes responsible for stabilizing w/o emulsions are enriched in heteroatoms and metal groups and has a relatively high apparent molecular weight at the interface. For instance, Rocha et al., (Rocha et al., 2016) observed that stable emulsions were formed when the apparent molecular weight of the interfacial material exceeded 7000 g/mol, in other words molecules highly associated into nanoaggregates are found to be resposible for long-term emulsion stability.

3.4 Conclusions

Naphthenic acids (NA) at low concentrations (0.1 wt%) do not significantly affect the irreversible adsorption of asphaltene A at the heptol/water interface. Conversely, NA fractions at >0.1 wt% weaken the asphaltene A films consistent with destabilization of the emulsions. NA Fractions 1 and 5 act as demulsifiers whereas the other fractions and whole NA (F-all acids) slightly destabilize the w/o emulsions prepared with asphaltene A. It was found that destabilization properties of NA depend on the chemical composition and concentration rather than the molecular weight.

Surface pressure isotherms and dynamic IFT of asphaltene A/acids systems revealed that asphaltenes and NA adsorbed irreversibly. Furthermore, weakening of asphaltenes films could result from an inhibition in the aggregation or displacement by the action of the acids.

On the other hand, it was found that the effect of NA on the interfacial film formed by asphaltene B is negligible.

3.5 Acknowledgements

JAVD acknowledges COLCIENCIAS (Grant 567-2012) for a graduate fellowship. Special thanks for Elaine Baydak for experimental work assistance.

4. Separation of asphaltene-stabilized water in oil emulsions and immiscible oil/water mixtures using a hydrophobic cellulosic membrane

We present a two-step method to prepare a hydrophobic cellulosic membrane involving a SiO_2 sol-gel process, to increase surface roughness, followed by grafting of hexadecyltrimethoxysilane groups to chemically enhance the membrane's water repellency. The modification processes induced morphological and chemical changes as observed by scanning electron microscopy and infrared spectroscopy, respectively.

The hydrophobic membrane was used to separate immiscible oil/water mixtures with efficiencies over 99%. In addition, we tested the material for breaking an asphaltene–stabilized water in oil emulsion and registered separation efficiencies from 75% to 95%. The demulsification process depends on membrane surface hydrophobicity, emulsion viscosity and dispersed droplet size.

The hydrophobic/oleophilic cellulose membrane was efficiently reused over 18 times to break a water/oil (50% water) emulsion. This facile solution for breaking low viscosity w/o emulsions and immiscible water/oil mixtures could be easily scalable and used to develop efficient separation methods driven solely by gravity (see figure 22).

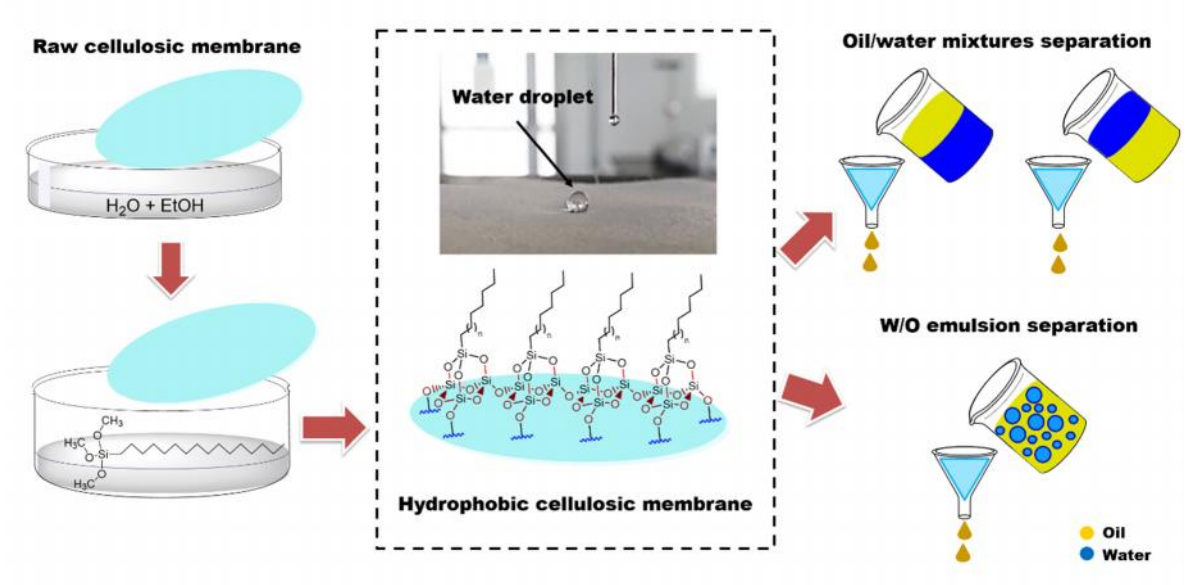

Figure 22. Separation of oil/water mixtures and w/o emulsion thorough a cellulosic membrane.

4.1 Introduction

The chemical composition of oil and formation water in oil reservoirs is variable, mostly depending on source rock. Recently we have shown that some chemical components in asphaltenes behave as surface active materials. For instance, in a recent publication we have shown that asphaltenes contain polar molecules with abundant heteroatoms, such as $N_nO_oS_s$, N_nO_o, O_o, that not only can stabilize emulsions but also form aggregates (Giraldo-Dávila, Chacón-Patiño, McKenna, Blanco-Tirado, & Combariza, 2018). As crude oil contains native surfactants and is normally processed along with formation water, stable emulsions are formed during pumping operations due to the shear stress experienced in valves and pipelines (Arla et al., 2007; Olga V. Gafonova & Yarranton, 2001; S. Gao et al., 2010; Kilpatrick, 2012; Knudsen et al., 2012; Stanford, Rodgers, Marshall, Czarnecki, et al., 2007; F. Yang et al., 2014).

Single and multiple emulsions are common to the petrochemical industry; the former are of the water in oil (w/o) or oil in water (o/w) types if the continuous phase is either oil or water,

respectively; the latter can be of the o/w/o or w/o/w types if an immiscible oil layer exists between two water layers (o/w/o) or *vice versa* (Kokal, 2005).

It is widely known that w/o emulsions behave like non-newtonian fluids; upon emulsion formation an increase in oil viscosity ensues, together with changes in rheology that can dramatically affect transport operations in pipelines (Al-Sabagh, Nasser, & Abd El-Hamid, 2013; Fingas & Fieldhouse, 2003).

Conventional heating, chemical additives and electrocoalescers are some of the most common ways to break these emulsified crude oil streams. In many cases, although there is a reduction in the water content, phase separation is not completely achieved (Havre, 2002) when using these alternatives individually; thus a combination of these methods can improve the results however at the expense of increasing operational and maintenance costs (Chan & Chen, 2002).

Reducing operational costs and increasing profitability during crude oil processing requires the use of efficient strategies to separate or inhibit the formation of w/o emulsions. Nowadays, demulsification using membranes has gained more attention due to low energy consumption when relying on gravity for the separation; additionally, the fact that oil and water are not contaminated by chemical additives after separation and that the process does not require extra safety cautions in contrast, for instance, with high voltage demulsification (D. Sun, Duan, Li, & Zhou, 1998; Tirmizi, Raghuraman, & Wiencek, 1996; W. Zhang et al., 2013).

The membranes used for the separation of mixtures and emulsions are made of materials with high chemical, thermal and mechanical stability. In addition, modifications on the surfaces of these materials are oriented towards the improvement of the separation efficiency, either by modifying the porosity to achieve a higher flux or by providing anti-fouling properties to avoid clogging

issues (Kota, Kwon, Choi, Mabry, & Tuteja, 2012). For instance, o/w nanoemulsions, stabilized by surfactants are separated via ultrafiltration using hydrophilic membranes with nanoporous surfaces between 2-50 nm of pore size. In this way, oil droplets dispersed with a typical size between 0.1-10 µm will not permeate the membrane and the water can be separated without oil impurities (W. Chen, Su, Zheng, Wang, & Jiang, 2009). Conversely, for the separation of water in oil emulsions, the membrane´s surface is generally modified with hydrophobic compounds to retain water allowing permeation of oily phases (Tirmizi et al., 1996).

Electrochemical deposition, electrochemical etching, vapor phase deposition, self-assembly, dipping, sol/gel processes and electrospinning techniques are among the most common procedures to confer superhydrophobicity/superoleophilicity and superhydrophilicity/superoleophobicity to composite materials. These properties are achieved by means of either increasing surface roughness and reducing surface energy or both (Z. Gao et al., 2015; Genzer & Efimenko, 2006; Ma & Hill, 2006; Song & Rojas, 2013; Xue, Cao, Liu, Feng, & Jiang, 2014).

Altering surface roughness, in the field of membrane design, is related to a change on surface topography. The introduction of roughness in soft materials, such as cellulose, is usually achieved by chemical grafting, sol gel dipping, nanoparticle deposition and chemical vapor deposition, among others (He, Lu, & Zhang, 2014; S. Li, Zhang, & Wang, 2008; Y. Peng & Guo, 2016). Surface energy reduction is generally accomplished by adding low surface energy compounds such as alkyl chains, silicone and fluorine compounds which provide hydrophobic properties to the membrane (Ramirez et al., 2011). Once these compounds are deposited on a surface, only liquids with equal or lower surface tension than the membrane can wet out and permeate it. This explains why water, with surface tension of 72.1 mN/m, is repelled by hydrophobic substrates, which typically exhibit a low surface energy. For this reason, organic solvents such as octane (γ= 21.6

mN/m) and hexadecane (γ= 27.5 mN/m) can permeate easily hydrophobic substrates due to similar intermolecular interactions with the functionalized surface (Chhatre et al., 2010; Mabry, Vij, Iacono, & Viers, 2008).

Different approaches have been used to provide hydrophobic properties to membranes made of cellulosic materials (Cunha, Freire, Silvestre, Neto, & Gandini, 2010; S. Li et al., 2008; Song & Rojas, 2013; Tuteja et al., 2007). For instance, a cotton fabric with a bi functional modification was used for the separation of hexadecane-water emulsions. One side of the membrane was treated with a polyamine polymer (poly (N,N-dimethyl aminoethyl methacrylate)) to increase the surface roughness and the other was grafted with a hydrophobic polymer. In this way, the side with the amine polymer helped coalesce oil droplets whereas the hydrophobic side allowed selective permeation of the oil, facilitating the separation. Although this approaching allowed rapid and efficient separations of o/w emulsions, fabrication is not simple limiting practical applications (Z. Wang, Wang, & Liu, 2016).

In another study, a filter paper functionalized with polytetrafluoroethylene nanoparticles was used as a membrane to separate o/w mixtures with high efficiency (99%) and good recyclability (Du, Wang, Chen, & Chen, 2014). Increasing surface roughness of cellulose was achieved by adhering nano-amorphous titanium dioxide (TiO_2) and an epoxy resin to the surface. Also, modification of cellulose, by immersion in an ethanolic solution of octadecyltrichlorosilane, conferred hydrophobicity to the material which was used to separate oil/water mixtures thanks to its high oil absorption capacity (Z. Gao et al., 2015).

Hydrophobic/oleophilic properties were given to a filter paper through a bi-silanization process that enabled separation of diesel-water and gasoline-water mixtures (J. Wang, Wong, Kwok, Li,

& Yu, 2016). Recently, o/w nanoemulsions were separated by ultrafiltration employing porous membranes made of cellulose nanosheets, formed from a solution of cellulose through freeze/drying, with thickness between 80 and 220 nm. This hydrophilic/oleophobic membrane exhibited a decrease in flow rates as the thickness of the membrane increased, which is a serious drawback (Zhou et al., 2014).

On the other hand, hydrophobic magnetic cellulose was used to separate oil/water mixtures and a toluene in water emulsion. In this case, magnetic and roughness properties were achieved by the introduction of a thin layer of Fe_3O_4 nanoparticles on the cellulose surface, while hydrophobicity was provided by self-assembly of a hexadecyltrimethoxysilane layer on the nanoparticle´s surface or directly over the cellulose by reaction with the hydroxyl groups (H. Peng et al., 2016).

Finally, a hexane in water emulsion stabilized by sodium dodecyl sulfate was successfully separated using a cellulose filter paper with hydrophilic/oleophobic wettability properties. The cellulosic substrate was coated with a layer of nanofibrillated cellulose hydrogel through a dipping/drying process. The hydrogel traps water creating a hydrated layer that hampers permeation of the oil phase due to differences in surface energy. However, this modification involves lengthy steps such as production of nanofibrillated cellulose with nanometric size (10-40 nm) and careful crosslinking of the hydrogel to avoid possible coating fractures (Rohrbach et al., 2014).

The above mentioned examples were all carried out with model solvent mixtures or emulsions, with very few dealing with use of composite materials, or modified surfaces, to separate real w/o emulsions. These emulsions in oil processing (stabilized by asphaltenes and by naphthenic acids) exhibit high viscosity and are extremely stable (Kilpatrick, 2012; Pradilla, Ramírez, Zanetti, &

Álvarez, 2017; Subramanian, May, & Firoozabadi, 2017). It is widely known in the petroleum industry that asphaltenes comprise a huge number of molecules interfacially active which form a thick layer around the water droplets impeding the coalescence and separation of w/o emulsions (Jian, Liu, Zeng, & Tang, 2017; Qiao et al., 2017).

In this contribution, we fabricated a hydrophobic cellulose membrane by changing surface roughness and reducing surface energy via attachment of SiO_2 to the surface by a sol-gel method, for the former, and grafting hexadecyltrimethoxysilane groups, for the latter. The morphological modifications were monitored by scanning electron microscopy whereas the chemical changes in the membrane were confirmed by infrared spectroscopy and contact angle measurements. This composite material enables oil/water mixtures separation by gravity and more importantly breaking of tight water in oil emulsions stabilized by asphaltenes with efficiencies between 75-95%.

4.2 Experimental section

4.2.1 Materials and reagents. Tetraethyl orthosilicate (TEOS- $SiC_8H_{20}O_4$) and hexadecyltrimethoxysilane (HDTMS-H_3C ($(CH_2)_{15}Si(OCH_3)_3$) were purchased from Sigma Aldrich (St. Louis, MO, USA). HPLC grade ammonium hydroxide (32% ammonia in water), ethanol (EtOH), dichloromethane (DCM), n-heptane, potasium chloride (KCl), dihydrate calcium chloride ($CaCl_2$. $2H_2O$) and sodium chloride (NaCl) salts were purchased from Merck (Darmstadt, Germany).

A cellulose filter paper (Schleicher & Schuell -Micro Science), with a nominal size pore ranging from 12 to 25 µm, was used for surface chemical functionalization. All solvents and reagents were

used as supplied. Commercial-grade diesel, gasoline and mineral oil were also used as received. Deionized water with a resistivity less than 18.2 mΩ/cm was used to prepare solutions.

4.2.2 Cellulose modification using the sol-gel process. The cellulose surface modification by roughness begins with a hydrolysis reaction of TEOS followed by a polycondensation at alkaline conditions. An ammonium hydroxide solution (3 mL, pH 11) was heated at 30° C under constant stirring and 1ml of TEOS was added dropwise. Then 10 mL of ethanol, previously heated at 40 °C, were added to the TEOS solution under constant stirring and the mixture was heated (30 °C) for 30 minutes to allow formation of a colorless xerogel. The cellulose filter paper was immersed in the xerogel for 1 hour after which it was removed and the solvent was allowed to evaporate at 80 ºC; the modified cellulose substrate was cured at 140°C during 3 minutes. After this treatment, the membrane was immersed in a 3.5% w/v HDTMS ethanolic solution for 24 hours and dried, afterwards, at 80 °C for 5 minutes.

4.2.3 Chemical characterization. Attenuated total reflection infrared spectra (FTIR-ATR) were taken on a Fourier transform infrared spectrometer Bruker Tensor 27 instrument (Billerica, MA), equipped with a Platinum Diamond ATR unit A225/Q (Billerica, MA), operated at a resolution of 2 cm^{-1} with 32 scans accumulated for each spectrum.

Surface morphology analysis was conducted using scanning electron microscopy on a FEI QUANTA FEG 650 (Oregon, USA) instrument equipped with a large field detector and an energy dispersive x-ray analyzer (SEM/EDX, Quanta® FEG 650 FEI). Samples were coated with a thin layer of carbon before imaging and the micrographs were taken at 10 kV.

Thermogravimetrical and differential scanning calorimetry (DSC) analyses were performed with a Discovery TGA instrument (Newcastle, England), using nitrogen at 50 mL/min and a heating rate 10 °C/min starting from room temperature up to 500 °C.

The static water contact angle was measured at ambient temperature using a drop shape analyzer instrument (Dataphysics, model OCA15EC) equipped with a high definition camera system. 3 µL of water were dropped onto the raw and modified cellulosic surfaces to measure the contact angle. The reported contact angle values from the raw and functionalized cellulose correspond to an average of three measurements taken at different positions on the paper surface

4.2.4 Preparation oil/water mixtures and w/o emulsions. Synthetic w/o emulsions were prepared using gasoline as the oil phase and an aqueous brine solution with composition similar to that of formation water found in Colombian oil reservoirs (6460 mg/L NaCl, 1390 mg/L $CaCl.2H_2O$ y 136 mg/L KCl). A 1000 mg/L asphaltene stock dissolved in toluene was used as surface-active material for preparing w/o emulsions. Different final content of asphaltene were used to achieve 0.02, 0.011, 0.002 mg/mL with respect to the total volume of the water and oil mixture. The asphaltenes were isolated from a heavy Colombian crude oil (API 9.6) following the ASTM D6560-12 procedure.

These asphaltenes solutions were added to the gasoline before adding aqueous brine to prepare w/o emulsions. Then the former solution was stirred in an Ultraturrax T-25 at 13000 rpm and the aqueous brine solution was added until reaching the desire water content of 20, 30 and 50% volume).

The type of emulsion was confirmed performing wettability tests in pure water and toluene. Since all the emulsions prepared easily dissolve in toluene they were catalogued as w/o. In

addition, conductivity measurements (HANNA, HI 933100) showed values below 7 µS/cm, typical of w/o emulsions, confirming the previous results. All w/o emulsions prepared were stable for up to three months. A 3-level factorial experimental design of 32 experiments was conducted (Statgraphics Centurion XVI version 16.1.18 software) to find the optimal experimental conditions (water content, pH, % volume asphaltene solution content in oil phase) to prepare highly stable water in oil emulsions. All details about the experimental design are shown in Tables D.1-D.4 and Fig. D.1 of the supplementary information.

Finally, oil/water immiscible mixtures were also prepared. For this purpose, five different oily phases such as gasoline, diesel, n-heptane, mineral oil and dichloromethane were mixed with water at 1:1 volume ratio. These mixtures, along with the stable w/o emulsions, were used to test the ability of the functionalized cellulose membrane to break and separate stable and unstable oil and water blends.

4.2.5 Emulsion characterization. For droplet size distribution measurements one droplet of the settled emulsion was always sampled from below 1 cm of the surface to ensure consistency of results. The emulsion droplet was placed, without dilution, at room temperature, on a glass slide to obtain an optical image using a stereomicroscope (Olympus, SZ61) coupled with a camera system (MOTICAM 2500) set at 8000x and 15000x magnification scales. Several images were acquired at different regions of the slide to find a representative image that was then processed by an image-processing script code in MATLAB (Zeng, Zhang, Bukirwa, Li, & Yang, 2015) to find the droplet size distribution and the average droplet size (see Fig. D.2 of the appendix D). In addition, the emulsion viscosity was measured using a viscometer (OFITE, 900) operated automatically through a computer system.

4.2.6 Separation of w/o emulsions and oil/water mixtures by gravity filtration. For separation of mixtures and w/o emulsions through gravity filtration, the functionalized cellulose membrane was folded into a conical shape and placed on a glass funnel. Each time a sample of 20 mL was added to the separation apparatus. The separation time was measured as the time it took from the first droplet of the non-polar phase to drain off the funnel to the time the last droplet was collected. For recyclability tests, after emulsion or mixture separation, the membrane was cleaned by repeated washings with naphtha and then with a mixture ethanol: water 1:1 ratio. After washing it was dried at 80°C during 20 min.

The water contact angle was measured after each cycle to follow changes in the hydrophobicity and to evaluate reusability properties of the membrane.

4.3 Results and discussion

4.3.1 SiO_2 deposition and HDTMS grafting onto cellulose. Most of the hydrophilic/oleophobic materials used routinely in industrial applications depend on fluoride-based chemicals and non-renewable synthetic materials (Rohrbach et al., 2014). However, new technical and environmental regulations promote the use of environmentally friendly hydrophobic materials based on renewable substrates.

Cellulose is a versatile biopolymer that can be modified, via a great number of surface reactions, to produce advanced functional materials with multiple advantages over synthetic counterparts such as outstanding chemical, thermal and mechanical properties (Castellanos, Blanco-Tirado, Hinestroza, & Combariza, 2012; Moon, Martini, Nairn, Simonsen, & Youngblood, 2011; Saheb & Jog, 1999). These advantages are highlighted in an ever growing number of publications related to surface modification of cellulosic substrates (Dufresne, 2017; Hubbe, Rojas, Lucia, Sain, &

Forest, 2008; Moon et al., 2011; Ragesh, Anand Ganesh, Nair, & Nair, 2014; Raquez et al., 2012; Xue et al., 2014).

As seen in Figure 23 we conferred hydrophobic properties to a cellulosic substrate using initially a sol-gel process aimed to modify the surface roughness of the cellulose, followed by grafting of hexadecyltrimethoxysilane (HDTMS) groups to chemically enhance the surface's water repellency; this method has been recently highlighted by Peng et al (Y. Peng & Guo, 2016) as environmentally benign.

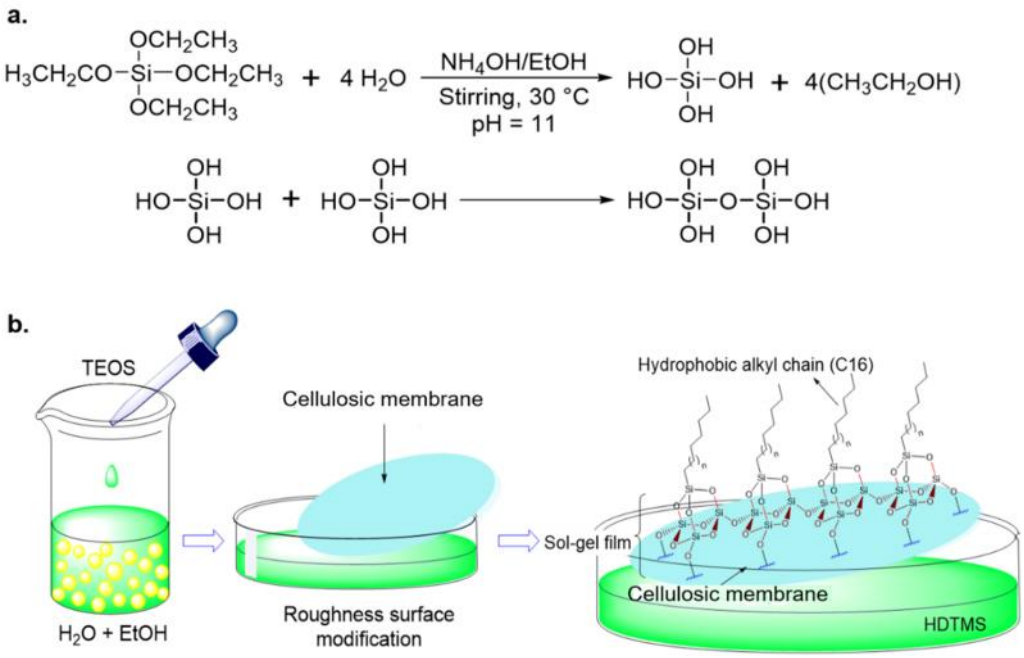

Figure 23. a) Base-catalyzed hydrolysis reaction of TEOS followed by a polycondensation reaction to form a xerogel. b) General process to modify a cellulosic membrane (via roughness and grafting of alkyl chains).

Fig. 23a shows the reactions involved in the sol-gel process whereas Fig. 1b shows the overall process with the insertion of HDTMS to modify the surface energy. The sol-gel process starts with formation of hydrated silica, or silicilic acid ($Si(OH)_4$), through a hydrolysis reaction between the

TEOS and water in a basic ethanolic solution (Figure 23a). Hench *et al.*, reported that tetrahedral silica undergoes a condensation reaction to form interconnected Si-O-Si bonds, and eventually colloidal particles in a low viscosity liquid known as a sol (Hench & West, 1990). Subsequent attachment of silanol groups (Si-OH) triggers a polycondensation reaction resulting in the formation of silicon oxide (SiO_2) particles arranged in a 3D network; at this point the viscosity of the mixture sharply increases due to formation of a gel known as xerogel (H. Yang et al., 2010). TEOS/water ratio, temperature and pH are all crucial factors influencing particle size and cross linking reactions in the xerogel (Hench & West, 1990). For instance, at pH values < 11 the solution turns cloudy and particle precipitation impedes gel formation. In addition, temperatures above 40 °C hinder sol formation due to a rapid evaporation of the ethanol. When the cellulosic membrane is immersed into the xerogel, the hydroxyl groups on the cellulose surface react with the polysiloxane units Si–O-Si (Hench & West, 1990; S. Li et al., 2008; Ruiz, 1999) eventually forming a film of silica on the surface. This reaction increases the cellulose nano-roughness, as a previous step towards grafting low surface energy compounds such as HDTMS.

After sol-gel treatment, the cellulose membrane is dipped in a HDTMS ethanolic solution to attach alkyl chains (C_{16}) on the SiO_2 film. Initially, a hydroxyl anion (OH^-) acts as a nucleophile attacking the silicon atom in the HDTMS to form a Si-OH bond, with the consequent release of a methoxy group OCH_3 due to the Si-OMe bond cleavage. Then, another hydroxyl anion OH^-, present in excess in the reaction mixture, takes a proton from the silanol group releasing water. The oxygen atom in the silanol, bearing a partial negative charge, reacts with the silicon atoms of the SiO_2 layer on the membrane´s surface, to finally graft the HDTMS (Hench & West, 1990; Latthe, Imai, Ganesan, & Venkateswara Rao, 2010; J. Wang et al., 2016).

4.3.2 Raw and modified surface characterization. Reactions in Figure 23a can be easily followed by monitoring the formation of Si-OH and O-Si-O bonds. The IR spectrum of the xerogel, shown in figure A.3 of the supplementary information, shows a broad band at 1061 cm^{-1} typical of asymmetric stretching vibrations of Si-O-Si bonds (Latthe et al., 2010). This band becomes wider after the hydrolysis reaction because initiates the polymerization of Si-O-Si bonds to form by nucleation colloidal particles or a sol which creates, as the reaction proceeds, a three dimension network that generates the xerogel (Buckley & Greenblatt, 1994) . For this reason, the IR band associated to the formation of this bond is normally used to follow the reaction progress (Y.-S. Li & Ba, 2008; Rubio, Rubio, & Oteo, 1998). On the other hand, the band at 450 cm^{-1} is due to out-of-plane (oop) vibrations of inter-tetrahedral O–Si-O linkages formed during the polycondensation reaction (Mendoza, 2000). Symmetrical stretching and oop vibrations of Si-O bonds, present in silanols groups, were also observed at 954 and 800 cm^{-1}, respectively. The low intensity broad band at 3750-2800 cm^{-1} from Si-OH bonds indicates that silanol groups are almost completely converted to O-Si-O bonds during the polymerization that takes place in the polycondensation reaction.

On the other hand, Fig. 24 shows IR spectra for raw and modified cellulose after treatment with the xerogel and grafting of the hydrophobic C_{16} alkyl chains. The IR spectrum for the raw cellulose exhibit a wide band at 3351 cm^{-1} typical of the OH groups (Youssef, Kamel, El-Sakhawy, & El Samahy, 2012). The IR spectrum (Fig. 2b) clearly reflects a change in the cellulosic surface chemical composition after deposition of the alkyl units. We observe two low intensity bands at 2963 cm^{-1} and 2901 cm^{-1} corresponding to characteristic symmetric and asymmetric stretching vibrations from the CH_2 units in the C_{16} hydrocarbon chains (absents in the IR of cellulose with xerogel and modified.). In addition, bands located at 1415, 1260 and 797 cm^{-1} are due to the

symmetric/asymmetric stretching of CH_2, Si-CH_2, Si-O-C bonds associated with the presence of hydrocarbon chains covalently attached to silicon atoms. The band at 1028 cm^{-1} is due to the Si-O-Si asymmetric stretching vibration bonds of the siloxane network on the modified cellulosic surface. This band is overlapped with the C-O bonds present in the raw cellulose membrane (Latthe et al., 2010; S. Li et al., 2008; H. Peng et al., 2016). The increasing band intensities of the Si–C and C–H bonds and the low band intensities at 3300 cm^{-1} and 1625 cm^{-1} for O–H bonds, clearly indicates the chemical modification of silica surface by the organic groups.

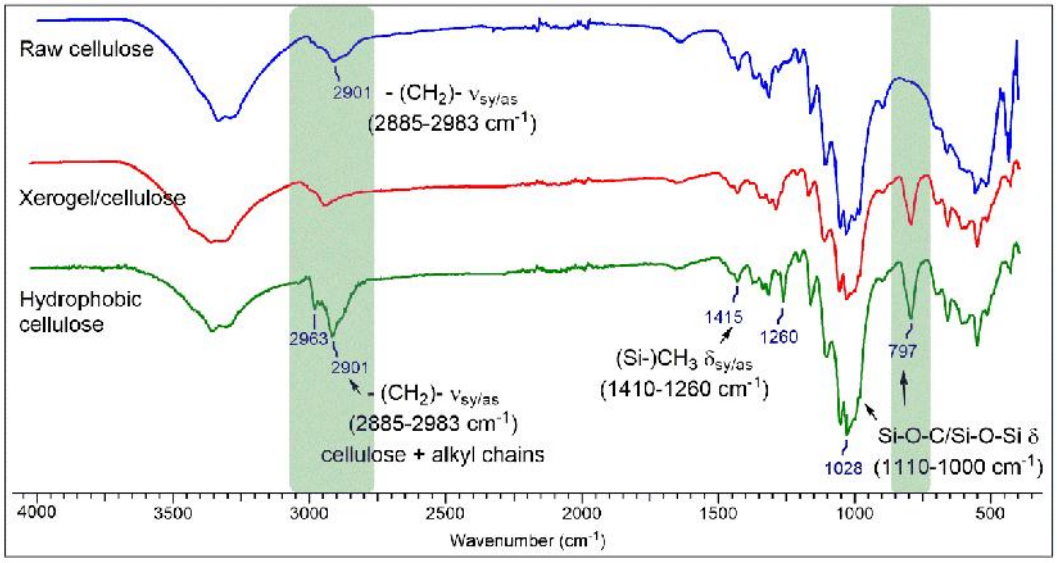

Figure 24. FT-IR spectra of the cellulosic substrate before and after chemical surface modification with the xerogel and the hexadecyltrimethoxy silane (HDMTS).

4.3.3 Thermogravimetric analysis and differential scanning calorimetry. Figure 25a shows the thermogram (TG) for the raw and functionalized cellulose membrane. For the raw cellulose (red trace Figure 25a) an initial weight loss, attributed to water release (4%), is observed between 31-87 °C. A second weight loss, starting at 310 °C, corresponds to the onset degradation temperature of the cellulose, which extends until a maximum weight loss of 93.8% between 493-500°C. The outstanding thermal stability of cellulose is explained by the linear arrangement of the

repeat D-glucose units. However, the thermal stability may also be influenced by the source of the cellulose and/or the presence of some remaining contaminants such as acids that might be used during the extraction (D. Liu et al., 2015; Shen & Gu, 2009). Interestingly, the residual mass less than 10% in the raw cellulose sample is attributed to the carbon remaining as char. This low percentage can be explained by the loss of water and additional release of CO and CO_2 gases through possible decarboxylation reactions (Brancatelli, Colleoni, Massafra, & Rosace, 2011).

On the other hand, the thermogram of the hydrophobic cellulose substrate (blue trace Figure 25a) exhibits a weight loss of 2% between 30-161 °C and 5% between 161-185 °C due to the loss of water and ethanol adsorbed during the formation of the sol-gel. In addition, morphological and chemical modifications applied to the cellulosic membrane resulted in an increment of the onset degradation temperature, from 310 °C in raw cellulose, to 321 °C in the hydrophobic. This indicates that the SiO_2 film deposited on the membrane´s surface is acting as a thermal insulator delaying cellulose decomposition. This behavior has also been observed in other cellulosic substrates functionalized with nanomaterials *via* sol-gel. For instance, Lui *et al.* reported that the onset degradation temperature for pure nano-fibrillated cellulose increases from 374 to 377 °C after an efficient silica coverage (D. Liu et al., 2015). Above 401.5 °C a residual weight of 73.6% in the modified cellulosic membrane corresponds to 6.2% of carbon char and 67.4% of silicon dioxide (SiO_2) that can only be decomposed at a high temperature of ca. 1200°C (Ismail Ab Rahman & Padavettan, 2012). In this sense, from an initial weight of 4.8 mg of the hydrophobic cellulosic membrane, 3.2 mg corresponds to the SiO_2 deposited *via* the sol-gel process.

These results agree with the TGA results presented by Liu et al. in a previous study where nanofibrillated cellulose (NFC) coated with silica loses only 30% of its initial mass compared with 90% for the pure NFC (D. Liu et al., 2015).

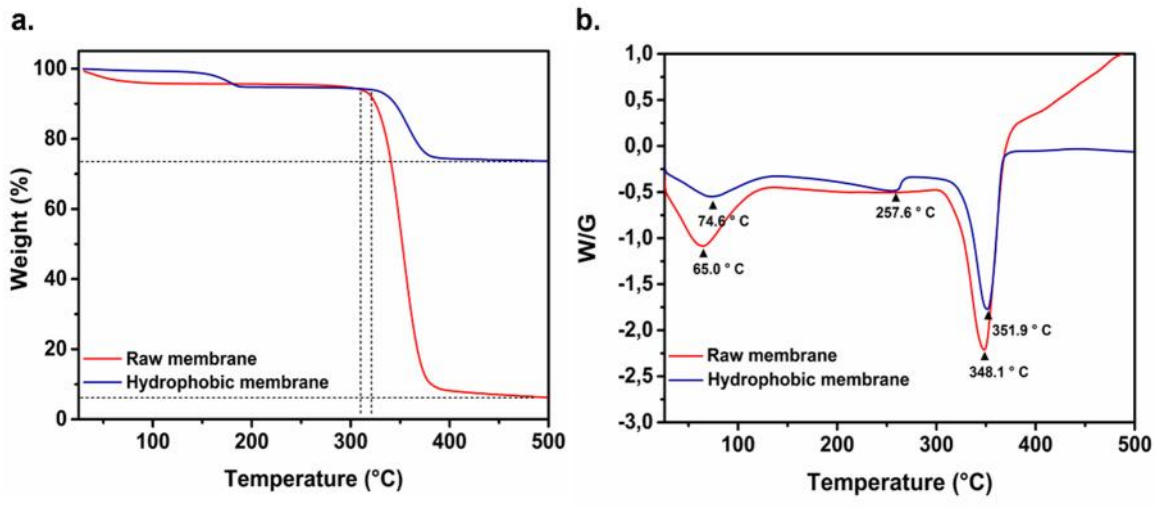

Figure 25. a) TGA and b) DSC analysis for the raw and hydrophobic cellulosic membrane.

On the other hand, DSC analysis (Figure 25b) shows two endothermic peaks, at 65.0 °C and 74.6 °C, for the raw and modified membrane, respectively. These peaks are associated with absorbed water loss. A second peak observed at 257.6 °C for the functionalized membrane can be attributed to the decomposition of organic groups (-CH_2) in the HDTMS alkyl chain as it was reported by Xiu *et al*. (Xiu, Hess, & Wong, 2008). Finally, a third signal, at 348.1 °C and 351.9 °C for the raw and modified cellulosic membrane, respectively, is associated to a depolymerization of the cellulose and its subsequently degradation (Brancatelli et al., 2011).

4.3.4 Scanning electron microscopy (SEM) and EDX analysis. Figure 26a shows the raw cellulose membrane composed of entangled single microfibers with widths between 15 - 30 µm, and various lengths. Figure 26b shows the modified cellulosic surface after the sol-gel/HDTMS treatment. The coating is clearly observed on the fibers as a bright layer, insets (Figures 26 c and d) show magnification of an individual microfiber where spherical SiO_2 nanoparticles are observed (20-100 nm) (I.A. Rahman et al., 2007) on the surface. The presence of these SiO_2 nanoparticles, uniformly distributed along the surface of the fibers, can efficiently increase the material´s surface

roughness as previously reported (Song & Rojas, 2013). In addition, covering all cellulosic fibers with modified Si nanoparticles, to create a monolayer, will add less than 100 nm to the fibers diameter, this will marginally affect the porosity of the original cellulose membrane which, as explain in section 2.1., has a pore size between 12 and 25 µm.

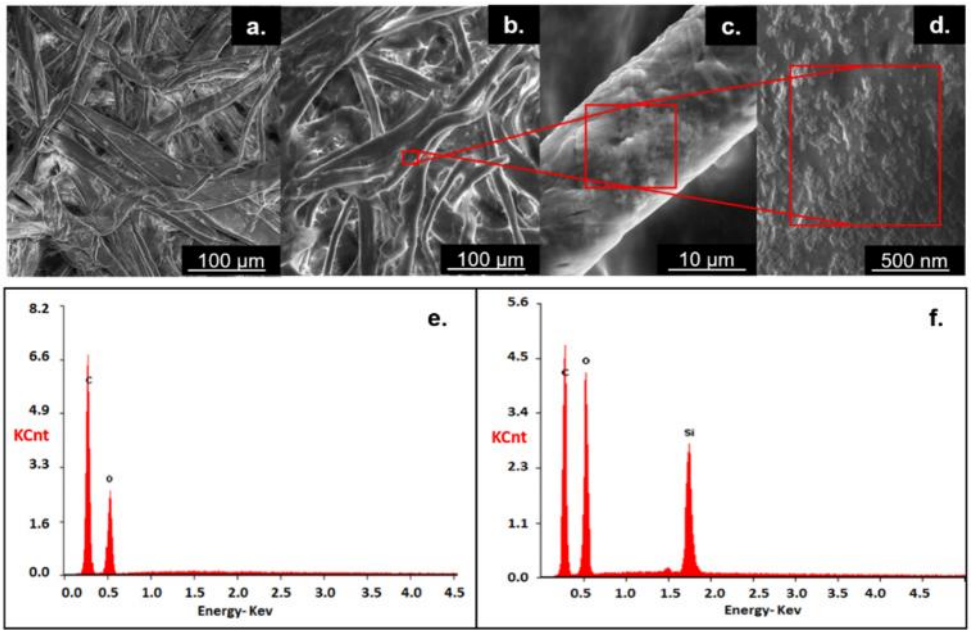

Figure 26. SEM images of the cellulosic substrate a) before and b) after chemical surface modification with the xerogel and hexadecyltrimethoxysilane (HDMTS). Zooming regions, magnification c) 8000x and d) 150000x, show discrete silicon dioxide particles (SiO_2). EDX spectra for the cellulosic substrate e) before and f) after chemical surface modification.

Qualitative surface atomic composition by energy dispersive x-ray spectroscopy (EDX) is shown in Figure 26e and f for the cellulosic substrate and the hydrophobic membrane. Raw cellulose is mainly composed of carbon (K_α 0.3) and oxygen (K_α 0.5); in contrast, the modified membrane exhibits an additional peak, characteristic of silicon atoms (K_α 1.8 eV) derived from the sol-gel reaction and the HDTMS grafting (Fig. 26f). In addition, an increase in the absolute signal intensity for O is also observed in Figure 26f.

4.3.5 Water contact angle measurements. Change in cellulose surface properties, as modification proceeds, was monitored by measuring the water contact angle. Before modification, a contact angle value of 9° ± 0.08 (Fig. 27a) reflects the biopolymer´s hydrophilicity as permeation of water through the cellulose easily occurs.

Raw cellulose is highly hydrophilic due to the biopolymer´s chemical structure composed of linear chains of glucopyranose units linked by β -1,4 glycosidic bonds (Song & Rojas, 2013). Each glucose unit has three –OH polar groups at carbon atoms 2, 3, and 6, which readily form inter and intra molecular hydrogen bonds. In contrast, when the SiO_2 film was deposited, the modified cellulose showed an increase in contact angle to 51°± 0.12 (Fig. 27b) due to surface roughness modification (Latthe et al., 2010). However, there is still certain tendency to be wetted by water due to the presence hydroxyl groups on the silica surface (Latthe et al., 2010). Finally, after chemical modification with the hydrophobic agent (HDTMS), the water contact angle value increased up to 121° ± 0.08 (Fig. 27c) confirming the true hydrophobic nature of the modified surface (Fig. 5d).

Roughness modification with the xerogel and chemical treatment with HDTMS efficiently alter the morphology and decrease the surface energy, respectively (Dorrer & Rühe, 2009; Kubiak, Wilson, Mathia, & Carval, 2011). High hydrophobicity is explained by the arrangement of the non-polar C_{16} alkyl chains over the surface, forming a low surface energy (Dorrer & Rühe, 2009; Kubiak et al., 2011), and by molecular repulsion forces between the apolar backbone carbon chain and polar water molecules which causes the repellency effect of this liquid (Ma & Hill, 2006; Marmur, 2003).

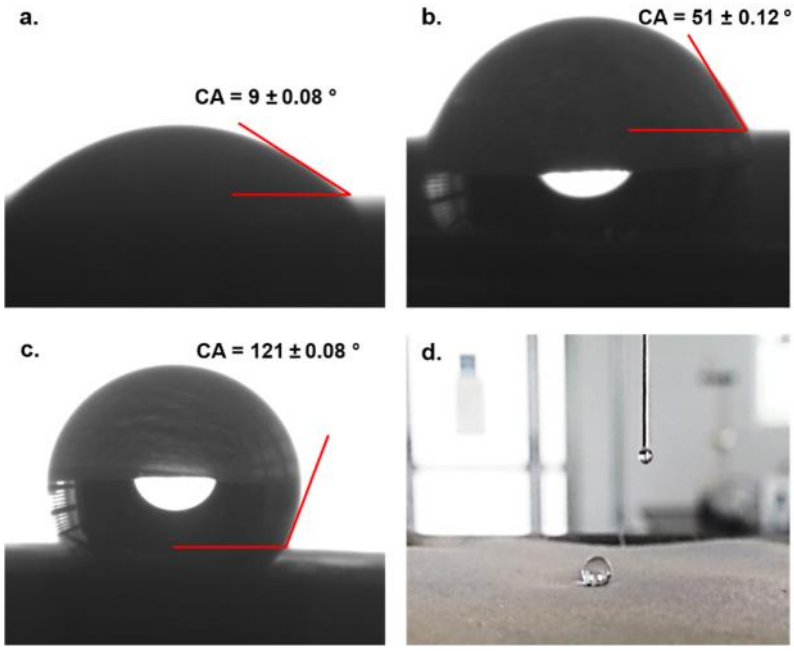

Figure 27. Water contact angle values with standard deviation values for the cellulosic substrate a) before and after chemical surface modification with the b) xerogel and c) HDMTS. A spherical water droplet d) over the filter paper visually demonstrates its hydrophobic properties.

4.4 Separation of immiscible oil/water mixtures

The modified cellulosic membrane was tested for separation of oil/water immiscible mixtures composed by different organic mixtures and solvents such as gasoline, diesel, heptane, mineral oil and dichloromethane (Fig. 28). The modified membrane was folded into a conical shape and placed on a conventional gravity filtration funnel. 20 ml of oil/water mixtures were individually loaded onto the funnel and the separation time was recorded as the period it took for the first oil droplet to go through the membrane until it stopped. The separation efficiency was expressed in terms of the recovered water was calculated by equation 1:

$$\% \text{ w} = \frac{V_r}{V_i} * 100 \qquad \text{(Eq 1)}$$

where V_r is the volume of recovered water after separation and V_i is the initial volume of water contained in the oil/water mixtures.

As seen in Figure 28, the hydrophobic membrane achieved high separation efficiencies for oil/water mixtures. However, the time required for separation depends on the permeation capacity of the membrane and, perhaps, the density of the compounds used as the oil phase. For water/oil mixtures where the oils are less dense than water (water on bottom) such as gasoline, diesel and heptane the process is quick (2 minutes) and efficient (100% recovery) (see Fig. D.4 of the appendix D for the separation sequence of these mixtures). This is because when the mixture is added to the modified membrane the oily solvents are the first to come into contact with the surface and due to similar surface tension between the organic solvents and the membrane, the oily phase spreads more quickly over the surface and penetrate into the membrane.

In contrast, for water on top mixtures such as with dichloromethane (density= 1.33 g/cm^3), the process is efficient (98% recovery) but slow (31 minutes). The same is true for mineral oil mixtures with water with recovery efficiency of 99% and time of 56 minutes. Increasing separation times are directly related to the viscosity of the oil phase. The mineral oil is more viscous than dichloromethane so it has a higher resistance to flow, increasing the time of separation. In addition, when these mixtures are loaded for separation, water droplets come in contact with the surface of the membrane first and are trapped between air bubbles in the rough surface and the organic phase. This creates a barrier that makes difficult for the molecules of dichloromethane or mineral oil to penetrate into the membrane, delaying the separation. This behavior is described mathematically by the Cassie-Baxter model applied to heterogeneous rough surfaces (S. Chen, Wang, & Chen, 2014; Karimnezhad, 2017; S. Wang, Li, & Lu, 2010).

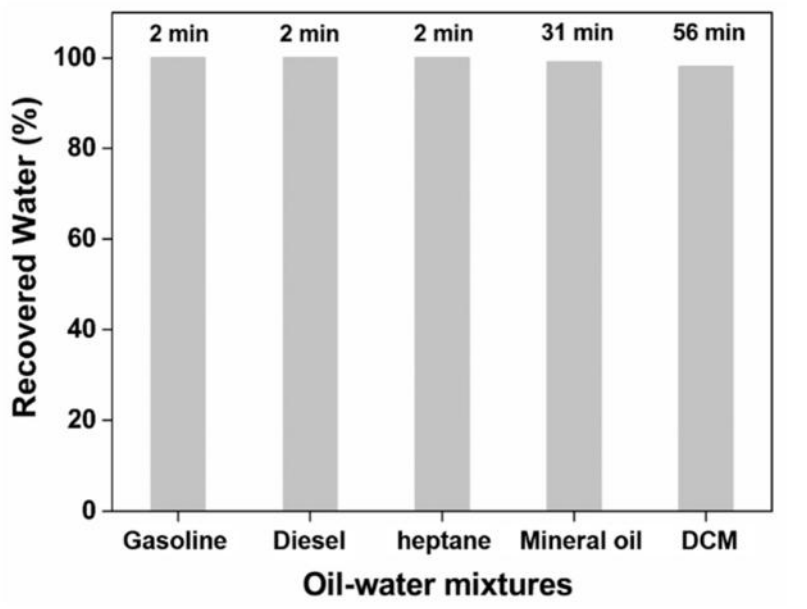

Figure 28. Water recovered after separation of several oil-water mixtures using the hydrophobic cellulose membrane.

4.4.1 Separation of w/o emulsions. Emulsions with three different water contents (20, 30 and 50% volume) were separated by gravity filtration using our functionalized cellulosic membrane (See Fig. D.6 of the appendix D). The average droplet size for these w/o emulsions were 9, 11 and 12 μm for the emulsions with 20, 30, and 50% volume, respectively. Fig. 29 shows the water recovery percentage for each type of emulsion and the total time of separation.

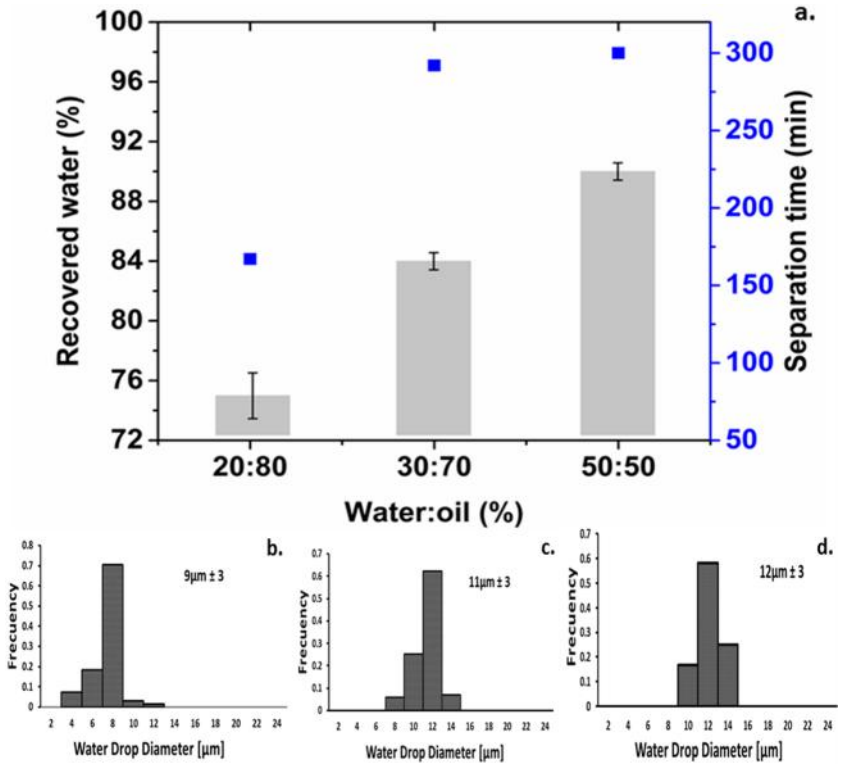

Figure 29. a) Water recovery from stable w/o in emulsions after gravity filtration using the hydrophobic cellulose membrane. Water Drop size distribution graphics before breaking the emulsion b) Emulsion 20:80. c) Emulsion 30:70 and d) Emulsion 50:50.

We observe that the efficiency in emulsion separation (understood as the water percentage recovered) correlates directly with water content and droplet size of the water dispersed in the oily phase, and inversely with time. The higher the water content and droplet size the more water recovered and the slowest the separation. The emulsion with less water content (20%) not only has small droplet size (9 µm) but also high droplet separation distances, hence water has a higher contact area with the organic phase than with the low energy surface membrane decreasing thus droplet coalescence and water recovery. However, the oily phase (80%) can easily interact with the membrane and initiate drainage faster through the membrane inducing the separation of the emulsion in less time (Kocherginsky, Tan, & Lu, 2003; D. Sun et al., 1998; Tirmizi et al., 1996).

On the other hand, the emulsion with more water content (50%) has bigger droplets (12 µm) and closer separation distances, hence water coalescence is favored and so is water recovery. However, the oily phase (50%) does not interact easily with the membrane and drainage is slower so emulsion separation takes more time.

Separation of w/o emulsions by filtration can also depend on emulsion viscosity. For instance, emulsion viscosity increases with water content (see Figure D.5 of the appendix D). In this sense, separation takes more time for viscous emulsions due to a resistance in flow through the membrane in gravity filtration systems.

4.4.2 Recyclability of hydrophobic cellulose filter paper. The hydrophobic membrane was tested for w/o emulsion separation (w/o 50 % volume) up to 18 cycles; Figure 30 shows the change in water contact angle and water recovery percentage *vs* usage cycle. We observed a 9.2% decrease in water contact angle, from 120 ° to 109 °, as the separation cycle goes from 1 to 18, while water recovery remained over 90% from cycles 1-13. Beyond cycle 13 water recovery falls to 85%, this decrease in water recovery coincides also with a sharp reduction in water contact angles perhaps due to removal some HDMTS during the washing procedures. This observation indicates that membrane hydrophobicity also influences emulsion separation.

Finally, we observed that the hydrophobic membrane could be reused until 18 cycles with only a slight change in separation efficiencies; in addition, the membrane presented good antifouling properties since the separation time was approximately between 290 to 308 minutes without considerable flux reduction after each cycle.

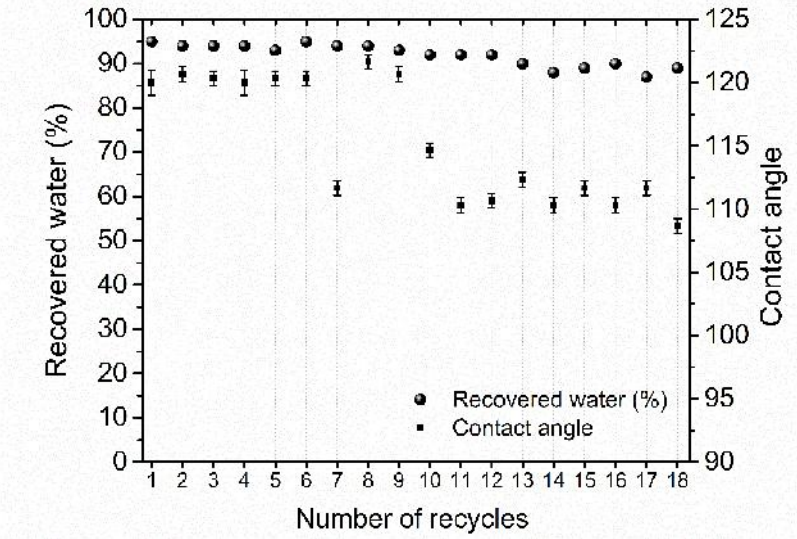

Figure 30. a) Recovered water and variation of water contact angles after the separation of a w/o emulsion (50% water) was performed 18 times.

4.5 Conclusions

Synthetic w/o emulsions and water/oil mixtures can be efficiently separated using a hydrophobic cellulose membrane. The membrane, with water contact angles of 120°, was prepared by modifying the cellulose surface roughness, via SiO_2 deposition, followed by surface energy reduction by grafting HDTMS.

The hydrophobic membrane can efficiently separate (100%) water/oil mixtures at different rates, with water on top mixtures separating slower than water on bottom blends. In addition, we prepared model emulsions by mixing gasoline containing asphaltenes with aqueous brine until obtaining a stable solution. Several ratios of water(brine):oil(gasoline) were used to determine the separation capabilities of the new membranes showing that it is possible to separate water with high efficiency (75-95%). High percentages of water recovery are obtained with increased water

amounts, and droplet sizes, in the emulsion. Short separation times are achieved for emulsions (and mixtures of fluids) with low viscosities and low water contents.

The modified cellulose membrane can be reused up to 18 cycles without losing its hydrophobic properties. We found that over 90% of water can be efficiently separated from model emulsions. Considering that preparation of this type of membranes is simple and that the water separation from emulsions can be done by gravity filtration, an energetically appealing methodology, we believe that modified cellulosic membranes can be optimized to break w/o emulsions in different industrial applications such as fuel purification and wastewater treatment.

4.6 Acknowledgements

The authors acknowledge financial support from the research agreement grant No. 5211794 subscribed between the Universidad Industrial de Santander and ECOPETROL. We also acknowledge a graduate fellowship from COLCIENCIAS Program No. 567. Finally, we acknowledge technical support from the Central research laboratory facilities at Guatiguara's campus (Microscopy Lab, XRD Lab, Spectroscopy Lab) from Universidad Industrial de Santander.

5. FUTURE WORK

Design of MALDI matrices with high basicity and higher UV absorption would be a new pathway to enhance the ionization of high molecular weight naphthenic acids without interferences in the low mass range. Exploring different fractionation methodologies such as MALDI-thin layer chromatography (TLC) could provide a complete and rapid molecular characterization. Moreover,

it would be ideal to create a UV-MALDI matrix that can ionize selectively naphthenic acids within a heavy crude oil without any type of fractionation.

Special attention should be focused on the naphthenic acids with an average molecular weight beyond 648 Da. According to interfacial tension measurements and surface pressure isotherms, these high molecular weight acids exhibited a similar behavior as the asphaltenes. It would be interesting to test this fraction through light scattering techniques to examine, in detail, their effect on aggregation and/or precipitation of asphaltenes. Furthermore, gravimetric quantification of the interfacial material adsorbed in stabilized emulsions by asphaltenes along with the presence of naphthenic acids, would allow to establish whether the weakening of asphaltene films occurs via a replacement or aggregation inhibition mechanism. The influence of naphthenic acids mixtures should also be studied on asphaltenes with a predominance of either island or archipelago chemical structure.

REFERENCES

Acheson, R. M. (2009). *The chemistry of heterocyclic compounds, acridines* (2nd Editio). United States: John Wiley & Sons.

Al-Sabagh, A. M., Nasser, N. M., & Abd El-Hamid, T. M. (2013). Investigation of Kinetic and Rheological Properties for the Demulsification Process. *Egyptian Journal of Petroleum*, *22*(1), 117–127. https://doi.org/10.1016/j.ejpe.2012.11.013

Alvarado, V., Wang, X., & Moradi, M. (2011). Role of Acid Components and Asphaltenes in Wyoming Water-in-Crude Oil Emulsions. *Energy & Fuels*, *25*(10), 4606–4613. https://doi.org/10.1021/ef2010805

Alvarez-Ramírez, F., & Ruiz-Morales, Y. (2013). Island versus archipelago architecture for asphaltenes: Polycyclic aromatic hydrocarbon dimer theoretical studies. *Energy and Fuels*, *27*(4), 1791–1808. https://doi.org/10.1021/ef301522m

Andersen, S. I., Mahavadi, S. C., Abdallah, W., & Buiting, J. J. (2017). Infrared Spectroscopic Analysis of the Composition of an Oil / Water Interfacial Film. *Energy & Fuels*, *31*(9), 8959–8966. https://doi.org/10.1021/acs.energyfuels.7b01022

Anderson, K., Goodrich, P., Hardacre, C., Hussain, a., Rooney, D. W., & Wassell, D. (2013). Removal of naphthenic acids from crude oil using amino acid ionic liquids. *Fuel*, *108*, 715–722. https://doi.org/10.1016/j.fuel.2013.02.030

Anisimov, M. a., Ganeeva, Y. M., Gorodetskii, E. E., Deshabo, V. a., Kosov, V. I., Kuryakov, V. N., … Yudin, I. K. (2014). Effects of Resins on Aggregation and Stability of Asphaltenes.

Energy & Fuels, *28*(10), 6200–6209. https://doi.org/10.1021/ef501145a

Arla, D., Flesisnki, L., Bouriat, P., & Dicharry, C. (2011). Influence of alkaline pH on the rheology of water/acidic crude oil interface. *Energy and Fuels*, *25*(3), 1118–1126. https://doi.org/10.1021/ef1015022

Arla, D., Sinquin, A., Palermo, T., Hurtevent, C., Graciaa, A., & Dicharry, C. (2007). Influence of pH and Water Content on the Type and Stability of Acidic Crude Oil Emulsions †. *Energy & Fuels*, *21*(3), 1337–1342. https://doi.org/10.1021/ef060376j

Ayorinde, F. O., Garvin, K., & Saeed, K. (2000). Determination of the fatty acid composition of saponified vegetable oils using matrix-assisted laser desorption/ionization time-of-flight mass spectrometry. *Rapid Communications in Mass Spectrometry*, *14*(7), 608–615. https://doi.org/10.1002/(SICI)1097-0231(20000415)14:7<608::AID-RCM918>3.0.CO;2-4

Bae, E., Yeo, I. J., Jeong, B., Shin, Y., Shin, K.-H., & Kim, S. (2011). Study of Double Bond Equivalents and the Numbers of Carbon and Oxygen Atom Distribution of Dissolved Organic Matter with Negative-Mode FT-ICR MS. *Analytical Chemistry*, *83*(11), 4193–4199. https://doi.org/10.1021/ac200464q

Banerjee, S., & Mazumdar, S. (2012). Electrospray Ionization Mass Spectrometry : A Technique to Access the Information beyond the Molecular Weight of the Analyte. *International Journal of Analytical Chemistry*, *2012*, 40. https://doi.org/10.1155/2012/282574

Barrow, M. P., Headley, J. V, Peru, K. M., & Derrick, P. J. (2009). Data Visualization for the Characterization of Naphthenic Acids within Petroleum Samples. *Energy & Fuels*, *23*(5), 2592–2599. https://doi.org/10.1021/ef800985z

Barrow, M. P., McDonnell, L. A., Feng, X., Walker, J., & Derrick, P. J. (2003). Determination of the Nature of Naphthenic Acids Present in Crude Oils Using Nanospray Fourier Transform Ion Cyclotron Resonance Mass Spectrometry: The Continued Battle Against Corrosion. *Analytical Chemistry*, *75*(4), 860–866. https://doi.org/10.1021/ac020388b

Barrow, M. P., Peru, K. M., McMartin, D. W., & Headley, J. V. (2016). Effects of Extraction pH on the Fourier Transform Ion Cyclotron Resonance Mass Spectrometry Profiles of Athabasca Oil Sands Process Water. *Energy & Fuels*, *30*(5), 3615–3621. https://doi.org/10.1021/acs.energyfuels.5b02086

Barrow, M. P., Witt, M., Headley, J. V, & Peru, K. M. (2010). Athabasca oil sands process water: characterization by atmospheric pressure photoionization and electrospray ionization fourier transform ion cyclotron resonance mass spectrometry. *Analytical Chemistry*, *82*(9), 3727–3735. https://doi.org/10.1021/ac100103y

Baugh, T. D., Co, C., Grande, K. V, Mediaas, H., Vindstad, J. E., Asa, S., & Wolf, N. O. (2005). SPE 93011 The Discovery of High-Molecular-Weight Naphthenic Acids (ARN Acid) Responsible for Calcium Naphthenate Deposits, (August 2004). https://doi.org/dx.doi.org/10.2118/93011-MS

Bikky, K. (2012). *Effect of Salinity on the Interfacial Tension of Model and Crude Oil Systems*. University of Calgary. Retrieved from http://hdl.handle.net/11023/195

Bourrel, M., & Passade-Boupat, N. (2018). Crude Oil Surface Active Species: Consequences for Enhanced Oil Recovery and Emulsion Stability. *Energy & Fuels*, *32*(3), 2642–2652. https://doi.org/10.1021/acs.energyfuels.7b02811

Brancatelli, G., Colleoni, C., Massafra, M. R., & Rosace, G. (2011). Effect of hybrid phosphorus-doped silica thin films produced by sol-gel method on the thermal behavior of cotton fabrics. *Polymer Degradation and Stability*, *96*(4), 483–490. https://doi.org/10.1016/j.polymdegradstab.2011.01.013

Brocart, B., Bourrel, M., Hurtevent, C., Volle, J., & Escoffier, B. (2007). ARN-Type Naphthenic Acids in Crudes: Analytical Detection and Physical Properties. *Journal of Dispersion Science and Technology*, *28*(3), 331–337. https://doi.org/10.1080/01932690601107161

Buckley, A. M., & Greenblatt, M. (1994). The Sol-Gel Preparation of Silica Gels. *Journal of Chemical Education*, *71*(7), 599. https://doi.org/10.1021/ed071p599

Budimir, N., Blais, J.-C., Fournier, F., & Tabet, J.-C. (2006). The use of desorption/ionization on porous silicon mass spectrometry for the detection of negative ions for fatty acids. *Rapid Communications in Mass Spectrometry : RCM*, *20*(4), 680–684. https://doi.org/10.1002/rcm.2363

Calvano, C. D., Monopoli, A., Ditaranto, N., & Palmisano, F. (2013). 1,8-Bis(dimethylamino)naphthalene/9-aminoacridine: A new binary matrix for lipid fingerprinting of intact bacteria by matrix assisted laser desorption ionization mass spectrometry. *Analytica Chimica Acta*, *798*, 56–63. https://doi.org/10.1016/j.aca.2013.08.050

Cao, D., Huang, H., Hu, M., Cui, L., Geng, F., Rao, Z., … Kang, Y. (2015). Comprehensive characterization of natural organic matter by MALDI- and ESI-Fourier transform ion cyclotron resonance mass spectrometry. *Analytica Chimica Acta*, *866*, 48–58. https://doi.org/10.1016/j.aca.2015.01.051

Castellanos, L. J., Blanco-Tirado, C., Hinestroza, J. P., & Combariza, M. Y. (2012). In situ synthesis of gold nanoparticles using fique natural fibers as template. *Cellulose*, *19*(6), 1933–1943. https://doi.org/10.1007/s10570-012-9763-8

Cawley, A. T., & Flenker, U. (2008). The application of carbon isotope ratio mass spectrometry to doping control. *Journal of Mass Spectrometry : JMS*, *43*(7), 854–864. https://doi.org/10.1002/jms

Chacón-Patiño, M. L., Rowland, S. M., & Rodgers, R. P. (2018). Advances in Asphaltene Petroleomics. Part 3. Dominance of Island or Archipelago Structural Motif Is Sample Dependent. *Energy and Fuels*, *32*(9), 9106–9120. https://doi.org/10.1021/acs.energyfuels.8b01765

Chan, C.-C., & Chen, Y.-C. (2002). Demulsification of W/O Emulsions By Microwave Radiation. *Separation Science and Technology*, *37*(15), 3407–3420. https://doi.org/10.1081/SS-120014434

Chen, S., Wang, J., & Chen, D. (2014). States of a Water Droplet on Nanostructured Surfaces. *The Journal of Physical Chemistry C*, *118*(32), 18529–18536. https://doi.org/10.1021/jp504070e

Chen, W., Su, Y., Zheng, L., Wang, L., & Jiang, Z. (2009). The improved oil/water separation performance of cellulose acetate-graft-polyacrylonitrile membranes. *Journal of Membrane Science*, *337*(1–2), 98–105. https://doi.org/10.1016/j.memsci.2009.03.029

Chhatre, S. S., Guardado, J. O., Moore, B. M., Haddad, T. S., Mabry, J. M., McKinley, G. H., & Cohen, R. E. (2010). Fluoroalkylated Silicon-Containing Surfaces−Estimation of Solid-Surface Energy. *ACS Applied Materials & Interfaces*, *2*(12), 3544–3554.

https://doi.org/10.1021/am100729j

Cho, Y., Witt, M., Kim, Y. H., & Kim, S. (2012). Characterization of crude oils at the molecular level by use of laser desorption ionization Fourier-transform ion cyclotron resonance mass spectrometry. *Analytical Chemistry*, *84*(20), 8587–8594. https://doi.org/10.1021/ac301615m

Clingenpeel, A. C., Rowland, S. M., Corilo, Y. E., Zito, P., & Rodgers, R. P. (2017). Fractionation of Interfacial Material Reveals a Continuum of Acidic Species That Contribute to Stable Emulsion Formation. *Energy and Fuels*, *31*(6), 5933–5939. https://doi.org/10.1021/acs.energyfuels.7b00490

Colati, K. a. P., Dalmaschio, G. P., de Castro, E. V. R., Gomes, A. O., Vaz, B. G., & Romão, W. (2013). Monitoring the liquid/liquid extraction of naphthenic acids in brazilian crude oil using electrospray ionization FT-ICR mass spectrometry (ESI FT-ICR MS). *Fuel*, *108*, 647–655. https://doi.org/10.1016/j.fuel.2013.02.007

Cunha, A. G., Freire, C. S. R., Silvestre, A. J. D., Neto, C. P., & Gandini, A. (2010). Preparation and characterization of novel highly omniphobic cellulose fibers organic–inorganic hybrid materials. *Carbohydrate Polymers*, *80*(4), 1048–1056. https://doi.org/10.1016/j.carbpol.2010.01.023

Czarnecki, J. (2009). Stabilization of Water in Crude Oil Emulsions. Part 2. *Energy & Fuels*, *23*, 1253–1257.

Czarnecki, J., & Moran, K. (2005). On the Stabilization Mechanism of Water-in-Oil Emulsions in Petroleum Systems. *Energy & Fuels*, *19*(4), 2074–2079.

Da Campo, R., Barrow, M. P., Shepherd, A. G., Salisbury, M., & Derrick, P. J. (2009). Characterization of Naphthenic Acid Singly Charged Noncovalent Dimers and Their Dependence on the Accumulation Time within a Hexapole in Fourier Transform Ion Cyclotron Resonance Mass Spectrometry. *Energy & Fuels*, *23*(11), 5544–5549. https://doi.org/10.1021/ef900594d

Damasceno, F. C., Gruber, L. D. a., Geller, A. M., Vaz de Campos, M. C., Gomes, A. O., Guimarães, R. C. L., … Caramão, E. B. (2014). Characterization of naphthenic acids using mass spectroscopy and chromatographic techniques: study of technical mixtures. *Anal. Methods*, *6*(3), 807–816. https://doi.org/10.1039/C3AY40851E

Dávalos, J. Z., Lago, A. F., Costa, J. C. S., Santos, L. M. N. B. F., & González, J. (2012). Thermochemical and structural properties of DMAN-"proton sponges." *Journal of Chemical Thermodynamics*, *54*(February 2016), 346–351. https://doi.org/10.1016/j.jct.2012.05.013

De Conto, J. F., Santos, M. R. O., Carvalho, A. S., Campos, K. V., Freitas, L. S., Benvenutti, E. V., … Egues, S. M. (2014). Naphthenic acids recovery from petroleum using ionic silica based hybrid material as stationary phase in solid phase extraction (SPE) process. *Adsorption*, *20*(8), 917–923. https://doi.org/10.1007/s10450-014-9634-8

Dicharry, C., Arla, D., Sinquin, A., Graciaa, A., & Bouriat, P. (2006). Stability of water/crude oil emulsions based on interfacial dilatational rheology. *Journal of Colloid and Interface Science*, *297*(2), 785–791. https://doi.org/10.1016/j.jcis.2005.10.069

Dorrer, C., & Rühe, J. (2009). Some thoughts on superhydrophobic wetting. *Soft Matter*, *5*(1), 51. https://doi.org/10.1039/b811945g

Du, C., Wang, J., Chen, Z., & Chen, D. (2014). Durable superhydrophobic and superoleophilic filter paper for oil-water separation prepared by a colloidal deposition method. *Applied Surface Science*, *313*, 304–310. https://doi.org/10.1016/j.apsusc.2014.05.207

Dufresne, A. (2017). Cellulose nanomaterial reinforced polymer nanocomposites. *Current Opinion in Colloid & Interface Science*, *29*, 1–8. https://doi.org/10.1016/j.cocis.2017.01.004

El-Sayed, M. (2012). Factors Affecting the Stability of Crude Oil Emulsions. In *Crude Oil Emulsions- Composition Stability and Characterization* (pp. 183–204). InTech. https://doi.org/10.5772/35018

Elsharkawy, A. M., Al-Sahhaf, T. a., & Fahim, M. a. (2012). Further Investigation into the Stability of Water-in-Crude Oil Emulsions Formed in Burgan Oilfield: Effect of Toluene, Resins to Asphaltenes Ratio, and Surfactant. *Journal of Dispersion Science and Technology*, *33*(6), 805–811. https://doi.org/10.1080/01932691.2011.584797

Ese, M., & Kilpatrick, P. K. (2004). Stabilization of Water-in-Oil Emulsions by Naphthenic Acids and Their Salts: Model Compounds, Role of pH, and Soap:Acid Ratio. *Journal of Dispersion Science and Technology*, *25*(3), 253–261. https://doi.org/10.1081/DIS-120038634

Fan, T. P. (1991). Characterization of naphthenic acids in petroleum by fast atom bombardment mass spectrometry. *Energy & Fuels*, *5*(3), 371–375. https://doi.org/10.1021/ef00027a003

Farooq, U., Simon, S., Tweheyo, M. T., Øye, G., & Sjöblom, J. (2013). Interfacial Tension Measurements Between Oil Fractions of a Crude Oil and Aqueous Solutions with Different Ionic Composition and pH. *Journal of Dispersion Science and Technology*, *34*(5), 701–708. https://doi.org/10.1080/01932691.2013.783618

Fingas, M., & Fieldhouse, B. (2003). Studies of the formation process of water-in-oil emulsions. *Marine Pollution Bulletin*, *47*(9–12), 369–396. https://doi.org/10.1016/S0025-326X(03)00212-1

Flego, C., Galasso, L., Montanari, L., & Gennaro, M. E. (2014). Evolution of Naphthenic Acids during the Corrosion Process. *Energy & Fuels*, *28*(3), 1701–1708. https://doi.org/10.1021/ef401973z

Freer, E. M., & Radke, C. J. (2004). RELAXATION OF ASPHALTENES AT THE TOLUENE/WATER INTERFACE: DIFFUSION EXCHANGE AND SURFACE REARRANGEMENT. *The Journal of Adhesion*, *80*(6), 481–496. https://doi.org/10.1080/00218460490477143

Fukuyama, Y. (2015). MALDI Matrix Research for Biopolymers. *MALDI MatrIx ResearcH For BIoPoLYmers*, *4*, 1–14. https://doi.org/10.5702/massspectrometry.A0037

Gabryelski, W., & Froese, K. L. (2003). Characterization of naphthenic acids by electrospray ionization high-field asymmetric waveform ion mobility spectrometry mass spectrometry. *Analytical Chemistry*, *75*(17), 4612–4623. https://doi.org/10.1021/ac026439m

Gafonova, O., & Yarranton, H. W. (2001). The Stabilization of Water-in-Hydrocarbon Emulsions by Asphaltenes and Resins. *Journal of Colloid and Interface Science*, *241*(2), 469–478. https://doi.org/10.1006/jcis.2001.7731

Gafonova, O. V., & Yarranton, H. W. (2001). The Stabilization of Water-in-Hydrocarbon Emulsions by Asphaltenes and Resins. *Journal of Colloid and Interface Science*, *241*(2), 469–478. https://doi.org/10.1006/jcis.2001.7731

Gao, S., Moran, K., Xu, Z., & Masliyah, J. (2010). Role of naphthenic acids in stabilizing water-in-diluted model oil emulsions. *The Journal of Physical Chemistry. B*, *114*(23), 7710–7718. https://doi.org/10.1021/jp910855q

Gao, Z., Zhai, X., Liu, F., Zhang, M., Zang, D., & Wang, C. (2015). Fabrication of TiO2/EP super-hydrophobic thin film on filter paper surface. *Carbohydrate Polymers*, *128*, 24–31. https://doi.org/10.1016/j.carbpol.2015.04.014

Genzer, J., & Efimenko, K. (2006). Recent developments in superhydrophobic surfaces and their relevance to marine fouling: a review. *Biofouling*, *22*(5–6), 339–360. https://doi.org/10.1080/08927010600980223

Giraldo-Dávila, D., Chacón-Patiño, M. L., McKenna, A. M., Blanco-Tirado, C., & Combariza, M. Y. (2018). Correlations between Molecular Composition and Adsorption, Aggregation, and Emulsifying Behaviors of PetroPhase 2017 Asphaltenes and Their Thin-Layer Chromatography Fractions. *Energy & Fuels*, *32*(3), 2769–2780. https://doi.org/10.1021/acs.energyfuels.7b02859

Gruber, L. D. A., Damasceno, F. C., Caramão, E. B., Jacques, R. A., Geller, A. M., & de Campos, M. C. V. (2012). Revisão. *Quim. Nova*, *35*(7), 1423–1433. https://doi.org/dx.doi.org/10.1590/S0100-40422012000700025

Guo, K., Li, H., & Yu, Z. (2016). In-situ heavy and extra-heavy oil recovery: A review. *Fuel*, *185*, 886–902. https://doi.org/10.1016/j.fuel.2016.08.047

Havre, T. E. (2002). *Formation of Calcium Naphthenate in Water / Oil Systems , Naphthenic Acid Chemistry and Emulsion Stability.* Norwegian University of Science and Technology.

Havre, T. E., & Sjöblom, J. (2003). Emulsion stabilization by means of combined surfactant multilayer (D-phase) and asphaltene particles. *Colloids and Surfaces A: Physicochemical and Engineering Aspects*, *228*(1–3), 131–142. https://doi.org/10.1016/S0927-7757(03)00302-9

Havre, T. E., Sjöblom, J., & Vindstad, J. E. (2003). Oil/Water-Partitioning and Interfacial Behavior of Naphthenic Acids. *Journal of Dispersion Science and Technology*, *24*(6), 789–801. https://doi.org/10.1081/DIS-120025547

He, M., Lu, A., & Zhang, L. (2014). Advances in Cellulose Hydrophobicity Improvement. In V. Komolprasert & P. Turowski (Eds.), *Food Additives and Packaging* (Vol. 1162, pp. 241–274). Washington, DC: American Chemical Society.

Headley, J. V., Peru, K. M., & Barrow, M. P. (2016). Advances in mass spectrometric characterization of naphthenic acids fraction compounds in oil sands environmental samples and crude oil - A review. *Mass Spectrometry Reviews*. https://doi.org/10.1002/mas.21472

Headley, J. V., Peru, K. M., Fahlman, B., Colodey, A., & McMartin, D. W. (2013). Selective solvent extraction and characterization of the acid extractable fraction of Athabasca oils sands process waters by Orbitrap mass spectrometry. *International Journal of Mass Spectrometry*, *345–347*, 104–108. https://doi.org/10.1016/j.ijms.2012.08.023

Headley, J. V., Peru, K. M., Mohamed, M. H., Wilson, L., McMartin, D. W., Mapolelo, M. M., … Marshall, A. G. (2014). Atmospheric Pressure Photoionization Fourier Transform Ion Cyclotron Resonance Mass Spectrometry Characterization of Tunable Carbohydrate-Based Materials for Sorption of Oil Sands Naphthenic Acids. *Energy & Fuels*, *28*(3), 1611–1616. https://doi.org/10.1021/ef401640n

Headley, J. V, Peru, K. M., & Barrow, M. P. (2009). Mass spectrometric characterization of naphthenic acids in environmental samples: a review. *Mass Spectrometry Reviews*, *28*(1), 121–134. https://doi.org/10.1002/mas.20185

Headley, J. V, Peru, K. M., Barrow, M. P., & Derrick, P. J. (2007). Characterization of Naphthenic Acids from Athabasca Oil Sands Using Electrospray Ionization: The Significant Influence of Solvents. *Analytical Chemistry*, *79*(16), 6222–6229. https://doi.org/10.1021/ac070905w

Heaps, D. T. (2011). *The Investigation of Asphaltene-Naphthenic Acid and Asphaltene-Surface Interactions*. University of Southern Mississippi.

Heaps, D. T., Madasu, P. K., Magers, D. H., & Buchanan, J. P. (2012). Investigation of the precipitation behavior of asphaltenes in the presence of naphthenic acids using light scattering and molecular modeling techniques. *Energy and Fuels*, *26*(3), 1862–1869. https://doi.org/10.1021/ef201719m

Hemmingsen, P. V., Kim, S., Pettersen, H. E., Rodgers, R. P., Sjöblom, J., & Marshall, A. G. (2006a). Structural Characterization and Interfacial Behavior of Acidic Compounds Extracted from a North Sea Oil. *Energy & Fuels*, *20*(5), 1980–1987. https://doi.org/10.1021/ef0504321

Hemmingsen, P. V., Kim, S., Pettersen, H. E., Rodgers, R. P., Sjöblom, J., & Marshall, A. G. (2006b). Structural Characterization and Interfacial Behavior of Acidic Compounds Extracted from a North Sea Oil. *Energy & Fuels*, *20*(5), 1980–1987. https://doi.org/10.1021/ef0504321

Hench, L. L., & West, J. K. (1990). The sol-gel process. *Chemical Reviews*, *90*(1), 33–72. https://doi.org/10.1021/cr00099a003

Henriksen, T., Juhler, R. K., Svensmark, B., & Cech, N. B. (2005). The relative influences of acidity and polarity on responsiveness of small organic molecules to analysis with negative ion electrospray ionization mass spectrometry (ESI-MS). *Journal of the American Society for Mass Spectrometry*, *16*(4), 446–455. https://doi.org/10.1016/j.jasms.2004.11.021

Hillenkamp, F., Wäfler, E., Jecklin, M. C., & Zenobi, R. (2009). Positive and negative analyte ion yield in matrix-assisted laser desorption/ionization revisited. *International Journal of Mass Spectrometry*, *285*(3), 114–119. https://doi.org/10.1016/j.ijms.2009.02.028

Hsu, C. S., Dechert, G. J., Robbins, W. K., & Fukuda, E. K. (2000). Naphthenic Acids in Crude Oils Characterized by Mass Spectrometry. *Energy & Fuels*, *14*(1), 217–223. https://doi.org/10.1021/ef9901746

http://www.chemcalc.org. (2016). Retrieved August 5, 2016, from http://www.chemcalc.org/

Hubbe, M. A., Rojas, O. J., Lucia, L. A., Sain, M., & Forest, T. A. (2008). Cellulosic nanocomposites: a review. *BioResources*, *3*(3), 929–980. https://doi.org/10.15376/biores.3.3.929-980

Huffman, B. A., Poltash, M. L., & Hughey, C. A. (2012). Effect of Polar Protic and Polar Aprotic Solvents on Negative-Ion Electrospray Ionization and Chromatographic Separation of Small Acidic Molecules. *Analytical Chemistry*, *84*(22), 9942–9950. https://doi.org/10.1021/ac302397b

Hughey, C. a., Galasso, S. a., & Zumberge, J. E. (2007). Detailed compositional comparison of acidic NSO compounds in biodegraded reservoir and surface crude oils by negative ion electrospray Fourier transform ion cyclotron resonance mass spectrometry. *Fuel*, *86*(5–6),

758–768. https://doi.org/10.1016/j.fuel.2006.08.029

Igwebueze, C., Oduola, L., Smith, O., & Company, P. (2013). SPE 164055 Calcium Naphthenate Solid Deposit Identification and Control in Offshore Nigerian Fields, 1–13. https://doi.org/dx.doi.org/10.2118/164055-MS

Islam, B. (2015). Petroleum sludge, its treatment and disposal: A review. *International Journal of Chemical Sciences*, *13*(4), 1584–1602.

Jeribi, M., Almir-Assad, B., Langevin, D., Hénaut, I., & Argillier, J. F. (2002). Adsorption Kinetics of Asphaltenes at Liquid Interfaces. *Journal of Colloid and Interface Science*, *256*, 268–272. https://doi.org/10.1006/jcis.2002.8660

Jian, C., Liu, Q., Zeng, H., & Tang, T. (2017). Effect of Model Polycyclic Aromatic Compounds on the Coalescence of Water-in-Oil Emulsion Droplets. *The Journal of Physical Chemistry C*, *121*(19), 10382–10391. https://doi.org/10.1021/acs.jpcc.7b01116

Jian, C., Poopari, M. R., Liu, Q., Zerpa, N., Zeng, H., & Tang, T. (2016). Reduction of Water/Oil Interfacial Tension by Model Asphaltenes: The Governing Role of Surface Concentration. *The Journal of Physical Chemistry B*, *120*(25), 5646–5654. https://doi.org/10.1021/acs.jpcb.6b03691

Jones, D. M., Watson, J. S., Meredith, W., Chen, M., & Bennett, B. (2001). Determination of Naphthenic Acids in Crude Oils Using Nonaqueous Ion Exchange Solid-Phase Extraction. *Analytical Chemistry*, *73*(3), 703–707. https://doi.org/10.1021/ac000621a

Jones, D., Scarlett, a G., West, C. E., Frank, R. a, Gieleciak, R., Hager, D., … Rowland, S. J.

(2013). Elemental and spectroscopic characterization of fractions of an acidic extract of oil sands process water. *Chemosphere*, *93*(9), 1655–1664. https://doi.org/10.1016/j.chemosphere.2013.03.011

Kailey, I. (2016). Properties and Performance of Newly Developed Demulsifiers in Oil Sands Froth Treatment. *Energy and Fuels*, *30*(11), 9233–9241. https://doi.org/10.1021/acs.energyfuels.6b01940

Karas, M., Glückmann, M., & Schäfer, J. (2000). Ionization in matrix-assisted laser desorption/ionization: singly charged molecular ions are the lucky survivors. *Journal of Mass Spectrometry*, *35*(1), 1–12. https://doi.org/10.1002/(SICI)1096-9888(200001)35:1<1::AID-JMS904>3.0.CO;2-0

Karas, M., & Krüger, R. (2003). Ion Formation in MALDI: The Cluster Ionization Mechanism. *Chemical Reviews*, *103*(2), 427–440. https://doi.org/10.1021/cr010376a

Karimnezhad, H. (2017). Fabrication of Hydrophobic Membrane for the Separation of n-Hexane/Water Mixture Using Novel Oleophilic Nanoparticle and Kevlar Fabric, as a Superior Support. *Journal of Water and Environmental Nanotechnology*, (3). https://doi.org/10.22090/jwent.2017.03.002

Kilpatrick, P. K. (2012). Water-in-Crude Oil Emulsion Stabilization: Review and Unanswered Questions. *Energy & Fuels*, *26*(7), 4017–4026. https://doi.org/10.1021/ef3003262

Kiran, S. K., Ng, S., & Acosta, E. J. (2011). Impact of Asphaltenes and Naphthenic Amphiphiles on the Phase Behavior of Solvent-Bitumen-Water Systems. *Energy & Fuels*, *25*, 2223–2231. https://doi.org/dx.doi.org/10.1021/ef1016285

Klein, G. C., Rodgers, R. P., Teixeira, M. A. G., Teixeira, A. M. R. F., & Marshall, A. G. (2003). Petroleomics: Electrospray ionization FT-ICR mass analysis of NSO compounds for correlation between total acid number, corrosivity, and elemental composition. *ACS Division of Fuel Chemistry, Preprints*, *48*(1), 14–15.

Knochenmuss, R. (2006). Ion formation mechanisms in UV-MALDI. *The Analyst*, *131*(9), 966. https://doi.org/10.1039/b605646f

Knudsen, A., Nordgård, E. L., Diou, O., & Sjöblom, J. (2012). Methods to Study Naphthenate Formation in w/o Emulsions by the Use of a Tetraacid Model Compound. *Journal of Dispersion Science and Technology*, *33*(10), 1514–1524. https://doi.org/10.1080/01932690903543329

Kocherginsky, N. M., Tan, C. L., & Lu, W. F. (2003). Demulsification of water-in-oil emulsions via filtration through a hydrophilic polymer membrane. *Journal of Membrane Science*, *220*(1–2), 117–128. https://doi.org/10.1016/S0376-7388(03)00223-0

Kokal, S. L. (2005). Crude Oil Emulsions: A State-Of-The-Art Review. *SPE Production & Facilities*, *20*(1), 5–13. https://doi.org/10.2118/77497-PA

Konermann, L., Ahadi, E., Rodriguez, A. D., & Vahidi, S. (2013). Unraveling the Mechanism of Electrospray Ionization. *Analytical Chemistry*, *85*(1), 2–9. https://doi.org/10.1021/ac302789c

Kota, A. K., Kwon, G., Choi, W., Mabry, J. M., & Tuteja, A. (2012). Hygro-responsive membranes for effective oil–water separation. *Nature Communications*, *3*, 1025. https://doi.org/10.1038/ncomms2027

Kruve, A., Kaupmees, K., Liigand, J., & Leito, I. (2014). Negative Electrospray Ionization via Deprotonation: Predicting the Ionization Efficiency. *Analytical Chemistry*, *86*(10), 4822–4830. https://doi.org/10.1021/ac404066v

Kubiak, K. J., Wilson, M. C. T., Mathia, T. G., & Carval, P. (2011). Wettability versus roughness of engineering surfaces. *Wear*, *271*(3–4), 523–528. https://doi.org/10.1016/j.wear.2010.03.029

Langevin, D., & Argillier, J. (2016). Interfacial behavior of asphaltenes. *Advances in Colloid and Interface Science*, *233*, 83–93. https://doi.org/10.1016/j.cis.2015.10.005

Laredo, G. C., López, C. R., Álvarez, R. E., & Cano, J. L. (2004). Naphthenic acids, total acid number and sulfur content profile characterization in Isthmus and Maya crude oils. *Fuel*, *83*(11–12), 1689–1695. https://doi.org/10.1016/j.fuel.2004.02.004

Laredo, G. C., López, C. R., Álvarez, R. E., Castillo, J. J., & Cano, J. L. (2004). Identification of Naphthenic Acids and Other Corrosivity-Related Characteristics in Crude Oil and Vacuum Gas Oils from a Mexican Refinery. *Energy & Fuels*, *18*(6), 1687–1694. https://doi.org/10.1021/ef034004b

Latthe, S. S., Imai, H., Ganesan, V., & Venkateswara Rao, a. (2010). Porous superhydrophobic silica films by sol–gel process. *Microporous and Mesoporous Materials*, *130*(1–3), 115–121. https://doi.org/10.1016/j.micromeso.2009.10.020

Leito, I., Herodes, K., Huopolainen, M., Virro, K., Künnapas, A., Kruve, A., & Tanner, R. (2008). Towards the electrospray ionization mass spectrometry ionization efficiency scale of organic compounds. *Rapid Communications in Mass Spectrometry*, *22*(3), 379–384.

https://doi.org/10.1002/rcm.3371

Li, S., Zhang, S., & Wang, X. (2008). Fabrication of superhydrophobic cellulose-based materials through a solution-immersion process. *Langmuir*, *24*(10), 5585–5590. https://doi.org/10.1021/la800157t

Li, Y.-S., & Ba, A. (2008). Spectroscopic studies of triethoxysilane sol–gel and coating process. *Spectrochimica Acta Part A: Molecular and Biomolecular Spectroscopy*, *70*(5), 1013–1019. https://doi.org/10.1016/j.saa.2007.09.050

Li, Y. L., & Gross, M. L. (2004). Ionic-liquid matrices for quantitative analysis by MALDI-TOF mass spectrometry. *Journal of the American Society for Mass Spectrometry*, *15*(12), 1833–1837. https://doi.org/10.1016/j.jasms.2004.08.011

Liu, D., Wu, Q., Andersson, R. L., Hedenqvist, M. S., Farris, S., & Olsson, R. T. (2015). Cellulose nanofibril core–shell silica coatings and their conversion into thermally stable nanotube aerogels. *J. Mater. Chem. A*, *3*(30), 15745–15754. https://doi.org/10.1039/C5TA03646A

Liu, F., Darjani, S., Akhmetkhanova, N., Maldarelli, C., Banerjee, S., & Pauchard, V. (2017). Mixture Effect on the Dilatation Rheology of Asphaltenes-Laden Interfaces. *Langmuir*, *33*(8), 1927–1942. https://doi.org/10.1021/acs.langmuir.6b03958

Lo, C. C., Brownlee, B. G., & Bunce, N. J. (2003). Electrospray-Mass Spectrometric Analysis of Reference Carboxylic Acids and Athabasca Oil Sands Naphthenic Acids. *Analytical Chemistry*, *75*(23), 6394–6400. https://doi.org/10.1021/ac030093d

Lucassen, J., & Van Den Tempel, M. (1972). Dynamic measurements of dilational properties of a

liquid interface. *Chemical Engineering Science*, *27*(6), 1283–1291. https://doi.org/10.1016/0009-2509(72)80104-0

Ma, M., & Hill, R. M. (2006). Superhydrophobic surfaces. *Current Opinion in Colloid & Interface Science*, *11*(4), 193–202. https://doi.org/10.1016/j.cocis.2006.06.002

Mabry, J. M., Vij, A., Iacono, S. T., & Viers, B. D. (2008). Fluorinated Polyhedral Oligomeric Silsesquioxanes (F-POSS). *Angewandte Chemie International Edition*, *47*(22), 4137–4140. https://doi.org/10.1002/anie.200705355

Mapolelo, M. M., Rodgers, R. P., Blakney, G. T., Yen, A. T., Asomaning, S., & Marshall, A. G. (2011a). Characterization of naphthenic acids in crude oils and naphthenates by electrospray ionization FT-ICR mass spectrometry. *International Journal of Mass Spectrometry*, *300*(2–3), 149–157. https://doi.org/10.1016/j.ijms.2010.06.005

Mapolelo, M. M., Rodgers, R. P., Blakney, G. T., Yen, A. T., Asomaning, S., & Marshall, A. G. (2011b). Characterization of naphthenic acids in crude oils and naphthenates by electrospray ionization FT-ICR mass spectrometry. *International Journal of Mass Spectrometry*, *300*(2–3), 149–157. https://doi.org/10.1016/j.ijms.2010.06.005

Marmur, A. (2003). Wetting on Hydrophobic Rough Surfaces: To Be Heterogeneous or Not To Be? *Langmuir*, *19*(20), 8343–8348. https://doi.org/10.1021/la0344682

Masliyah, J., Zhou, Z. J., Xu, Z., Czarnecki, J., & Hamza, H. (2008). Understanding Water-Based Bitumen Extraction from Athabasca Oil Sands. *The Canadian Journal of Chemical Engineering*, *82*(4), 628–654. https://doi.org/10.1002/cjce.5450820403

Mediaas, H., Grande, K. V, Hustad, B. M., Rasch, A., Rueslåtten, H. G., Vindstad, J. E., & Asa, S. (2003). SPE 80404 The Acid-IER Method - a Method for Selective Isolation of Carboxylic Acids from Crude Oils and Other Organic Solvents.

Mendoza, A. (2000). *SOLES Y GELES HIBRIDOS (ORGANICOS-INORGANICOS) DE SILICIO*. Universidad Autónoma Metropolitana (UAM).

Mohammed, M. a., & Sorbie, K. S. (2009). Naphthenic acid extraction and characterization from naphthenate field deposits and crude oils using ESMS and APCI-MS. *Colloids and Surfaces A: Physicochemical and Engineering Aspects*, *349*(1–3), 1–18. https://doi.org/10.1016/j.colsurfa.2009.07.047

Mohammed, M. a., & Sorbie, K. S. (2010). Thermodynamic modelling of calcium naphthenate formation: Model predictions and experimental results. *Colloids and Surfaces A: Physicochemical and Engineering Aspects*, *369*(1–3), 1–10. https://doi.org/10.1016/j.colsurfa.2010.08.034

Mohammed, M. A., Sorbie, K. S., Shepherd, A. G., Solutions, S. G., & International, B. V. (2008). Thermodynamic Modelling of Naphthenate Formation and Related pH Change Experiments. https://doi.org/dx.doi.org/10.2118/114034-PA

Molin, L., Seraglia, R., Dani, F. R., Moneti, G., & Traldi, P. (2011). The double nature of 1,5-diaminonaphthalene as matrix-assisted laser desorption/ionization matrix: some experimental evidence of the protonation and reduction mechanisms. *Rapid Communications in Mass Spectrometry : RCM*, *25*(20), 3091–3096. https://doi.org/10.1002/rcm.5201

Moon, R. J., Martini, A., Nairn, J., Simonsen, J., & Youngblood, J. (2011). *Cellulose*

nanomaterials review: structure, properties and nanocomposites. Chemical Society reviews (Vol. 40). https://doi.org/10.1039/c0cs00108b

Moradi, M., Topchiy, E., Lehmann, T. E., & Alvarado, V. (2013). Impact of ionic strength on partitioning of naphthenic acids in water–crude oil systems – Determination through high-field NMR spectroscopy. *Fuel*, *112*, 236–248. https://doi.org/10.1016/j.fuel.2013.05.024

Mullins, O. C., Sabbah, H., Pomerantz, A. E., Barre, L., Andrews, a. B., Ruiz-Morales, Y., … Barré, L. (2012). Advances in Asphaltene Science and the Yen − Mullins Model. *Energy & Fuels*, *26*, 3986−4003. https://doi.org/10.1021/ef300185p

Murgich, J., Abanero, J. A., & Strausz, O. P. (1999). Molecular recognition in aggregates formed by asphaltene and resin molecules from the Athabasca oil sand. *Energy and Fuels*, *13*(2), 278–286. https://doi.org/10.1021/ef980228w

Noestheden, M. R., Headley, J. V., Peru, K. M., Barrow, M. P., Burton, L. L., Sakuma, T., … Campbell, J. L. (2014). Rapid characterization of naphthenic acids using differential mobility spectrometry and mass spectrometry. *Environmental Science & Technology*, *48*(17), 10264–10272. https://doi.org/10.1021/es501821h

Nordgård, E. L., Magnusson, H., Hanneseth, A.-M. D., & Sjöblom, J. (2009). Model compounds for C80 isoprenoid tetraacids. *Colloids and Surfaces A: Physicochemical and Engineering Aspects*, *340*(1–3), 99–108. https://doi.org/10.1016/j.colsurfa.2009.03.002

Ortiz, D. P., Baydak, E. N., & Yarranton, H. W. (2010). Effect of surfactants on interfacial films and stability of water-in-oil emulsions stabilized by asphaltenes. *Journal of Colloid and Interface Science*, *351*(2), 542–555. https://doi.org/10.1016/j.jcis.2010.08.032

Oss, M., Kruve, A., Herodes, K., & Leito, I. (2010). Electrospray Ionization Efficiency Scale of Organic Compounds. *Analytical Chemistry*, *82*(7), 2865–2872. https://doi.org/10.1021/ac902856t

Östlund, J.-A., Nydén, M., Auflem, I. H., & Sjöblom, J. (2003a). Interactions between Asphaltenes and Naphthenic Acids. *Energy & Fuels*, *17*(1), 113–119. https://doi.org/10.1021/ef020103y

Östlund, J.-A., Nydén, M., Auflem, I. H., & Sjöblom, J. (2003b). Interactions between Asphaltenes and Naphthenic Acids. *Energy & Fuels*, *17*(1), 113–119. https://doi.org/10.1021/ef020103y

Ozeryanskii, V. A., Pozharskii, A. F., Antonov, A. S., & Filarowski, A. (2014). Out-Basicity of 1,8-bis(dimethylamino)naphthalene: the experimental and theoretical challenge. *Organic & Biomolecular Chemistry*, *12*(15), 2360. https://doi.org/10.1039/c3ob41986j

Pauchard, V., Sjöblom, J., Kokal, S., Bouriat, P., Dicharry, C., Müller, H., & Al-Hajji, A. (2009). Role of Naphthenic Acids in Emulsion Tightness for a Low-Total-Acid-Number (TAN)/High-Asphaltenes Oil †. *Energy & Fuels*, *23*(3), 1269–1279. https://doi.org/10.1021/ef800615e

Peng, H., Wang, H., Wu, J., Meng, G., Wang, Y., Shi, Y., … Guo, X. (2016). Preparation of Superhydrophobic Magnetic Cellulose Sponge for Removing Oil from Water. *Industrial and Engineering Chemistry Research*, *55*(3), 832–838. https://doi.org/10.1021/acs.iecr.5b03862

Peng, Y., & Guo, Z. (2016). Recent Advances in Biomimetic Thin Membranes Applied in Emulsified Oil/Water Separation. *J. Mater. Chem. A*. https://doi.org/10.1039/C6TA06922C

Pereira, J., Velasquez, I., Blanco, R., Sanchez, M., Pernalete, C., & Canelón, C. (2015). Crude Oil

Desalting Process. In *Advances in Petrochemicals*. InTech. https://doi.org/10.5772/61274

Pereira, R. C. L., Carvalho, M., Couto, B. C., Oliveira, C. K. De, Eberlin, M. N., & Vaz, B. G. (2014). Waxy Crude Oil Emulsion Gel : Chemical Characterization of Emulsi fi ed Phase Extract Components. *Energy & Fuels*.

Perrin, C. L., & Ohta, B. K. (2001). Symmetry of N-H-N hydrogen bonds in 1,8-bis(dimethylamino)naphthalene·H+ and 2,7-dimethoxy-1,8-bis(dimethylamino)naphthalene·H+. *Journal of the American Chemical Society*, *123*(27), 6520–6526. https://doi.org/10.1021/ja0036965

Pomerantz, A. E., Wu, Q., Mullins, O. C., & Zare, R. N. (2015). Laser-Based Mass Spectrometric Assessment of Asphaltene Molecular Weight, Molecular Architecture, and Nanoaggregate Number. *Energy & Fuels*, *29*(5), 2833–2842. https://doi.org/10.1021/ef5020764

Pozharskii, A. F., & Ozeryanskii, V. A. (2012). Proton Sponges and hydrogen transfer phenomena. *Mendeleev Communications*, *22*, 117–124. https://doi.org/10.1016/j.mencom.2012.05.001

Pradilla, D., Ramírez, J., Zanetti, F., & Álvarez, O. (2017). Demulsifier Performance and Dehydration Mechanisms in Colombian Heavy Crude Oil Emulsions. *Energy & Fuels*, *31*(10), 10369–10377. https://doi.org/10.1021/acs.energyfuels.7b01021

Purcell, J. M., Rodgers, R. P., Hendrickson, C. L., & Marshall, A. G. (2007). Speciation of nitrogen containing aromatics by atmospheric pressure photoionization or electrospray ionization fourier transform ion cyclotron resonance mass spectrometry. *Journal of the American Society for Mass Spectrometry*, *18*(7), 1265–1273. https://doi.org/10.1016/j.jasms.2007.03.030

Qian, K., Edwards, K. E., Dechert, G. J., Jaffe, S. B., Green, L. a, & Olmstead, W. N. (2008). Measurement of total acid number (TAN) and TAN boiling point distribution in petroleum products by electrospray ionization mass spectrometry. *Analytical Chemistry*, *80*(3), 849–855. https://doi.org/10.1021/ac701868v

Qian, K., Rodgers, R. P., Hendrickson, C. L., Emmett, M. R., & Marshall, A. G. (2001). Reading chemical fine print: Resolution and identification of 3000 nitrogen-containing aromatic compounds from a single electrospray ionization Fourier transform ion cyclotron resonance mass spectrum of heavy petroleum crude oil. *Energy and Fuels*, *15*(2), 492–498. https://doi.org/10.1021/ef000255y

Qiao, P., Harbottle, D., Tchoukov, P., Masliyah, J., Sjoblom, J., Liu, Q., & Xu, Z. (2017). Fractionation of Asphaltenes in Understanding Their Role in Petroleum Emulsion Stability and Fouling. *Energy & Fuels*, *31*(4), 3330–3337. https://doi.org/10.1021/acs.energyfuels.6b02401

Ragesh, P., Anand Ganesh, V., Nair, S. V., & Nair, a. S. (2014). A review on "self-cleaning and multifunctional materials." *Journal of Materials Chemistry A*, *2*(36), 14773. https://doi.org/10.1039/C4TA02542C

Rahman, I. A., & Padavettan, V. (2012). Synthesis of Silica nanoparticles by Sol-Gel: Size-dependent properties, surface modification, and applications in silica-polymer nanocompositesa review. *Journal of Nanomaterials*, *2012*. https://doi.org/10.1155/2012/132424

Rahman, I. A., Vejayakumaran, P., Sipaut, C. S., Ismail, J., Bakar, M. A., Adnan, R., & Chee, C.

K. (2007). An optimized sol–gel synthesis of stable primary equivalent silica particles. *Colloids and Surfaces A: Physicochemical and Engineering Aspects*, *294*(1–3), 102–110. https://doi.org/10.1016/j.colsurfa.2006.08.001

Ramirez-Corredores, M. M. (2017). Acidity in Crude Oils. In *The Science and Technology of Unconventional Oils* (pp. 295–385). Elsevier. https://doi.org/10.1016/B978-0-12-801225-3.00004-8

Ramirez, S. M., Diaz, Y. J., Campos, R., Stone, R. L., Haddad, T. S., & Mabry, J. M. (2011). Incompletely condensed fluoroalkyl silsesquioxanes and derivatives: Precursors for low surface energy materials. *Journal of the American Chemical Society*, *133*(50), 20084–20087. https://doi.org/10.1021/ja208506v

Rane, J. P., Pauchard, V., Couzis, A., & Banerjee, S. (2013). Interfacial rheology of asphaltenes at oil-water interfaces and interpretation of the equation of state. *Langmuir*, *29*(15), 4750–4759. https://doi.org/10.1021/la304873n

Rane, J. P., Zarkar, S., Pauchard, V., Mullins, O. C., Christie, D., Andrews, a. B., … Banerjee, S. (2015). Applicability of the Langmuir Equation of State for Asphaltene Adsorption at the Oil–Water Interface: Coal-Derived, Petroleum, and Synthetic Asphaltenes. *Energy & Fuels*, *29*(6), 3584–3590. https://doi.org/10.1021/acs.energyfuels.5b00179

Rao, F., & Liu, Q. (2013). Froth treatment in athabasca oil sands bitumen recovery process: A review. *Energy and Fuels*, *27*(12), 7199–7207. https://doi.org/10.1021/ef4016697

Raquez, J., Murena, Y., Goffin, A., Habibi, Y., Ruelle, B., Debuyl, F., & Dubois, P. (2012). Surface-modification of cellulose nanowhiskers and their use as nanoreinforcers into

polylactide : A sustainably-integrated approach. *Composites Science and Technology*, *72*(5), 544–549. https://doi.org/10.1016/j.compscitech.2011.11.017

Rienstra-Kiracofe, J. C., Barden, C. J., Brown, S. T., & Schaefer, H. F. (2001). Electron Affinities of Polycyclic Aromatic Hydrocarbons. *The Journal of Physical Chemistry A*, *105*(3), 524–528. https://doi.org/10.1021/jp003196y

Robson, W. J., Sutton, P. A., McCormack, P., Chilcott, N. P., & Rowland, S. J. (2017). Class Type Separation of the Polar and Apolar Components of Petroleum. *Analytical Chemistry*, acs.analchem.6b04202. https://doi.org/10.1021/acs.analchem.6b04202

Rocha, J. A., Baydak, E. N., & Yarranton, H. W. (2018). What Fraction of the Asphaltenes Stabilizes Water-in-Bitumen Emulsions ? *Energy & Fuels*, *32*, 1440–1450. https://doi.org/10.1021/acs.energyfuels.7b03532

Rocha, J. A., Baydak, E. N., Yarranton, H. W., Sztukowski, D. M., Ali-Marcano, V., Gong, L., … Zeng, H. (2016). Role of Aqueous Phase Chemistry, Interfacial Film Properties, and Surface Coverage in Stabilizing Water-in-Bitumen Emulsions. *Energy and Fuels*, *30*(7), 5240–5252. https://doi.org/10.1021/acs.energyfuels.6b00114

Rodgers, R. P., & Marshall, A. G. (2007). Petroleomics: Advanced Characterization of Petroleum-Derived Materials by Fourier Transform Ion Cyclotron Resonance Mass Spectrometry (FT-ICR MS). In O. C. Mullins, E. Y. Sheu, A. Hammami, & A. G. Marshall (Eds.), *Asphaltenes, Heavy Oils, and Petroleomics* (pp. 63–93). New York, NY: Springer New York.

Rohrbach, K., Li, Y., Zhu, H., Liu, Z., Dai, J., Andreasen, J., & Hu, L. (2014). A cellulose based hydrophilic, oleophobic hydrated filter for water/oil separation. *Chemical Communications*

(Cambridge, England), *50*(87), 13296–13299. https://doi.org/10.1039/c4cc04817b

Rowland, S. J., Scarlett, A. G., Jones, D., West, C. E., & Frank, R. a. (2011). Diamonds in the rough: identification of individual naphthenic acids in oil sands process water. *Environmental Science & Technology*, *45*(7), 3154–3159. https://doi.org/10.1021/es103721b

Rowland, S. J., West, C. E., Scarlett, A. G., & Jones, D. (2011). Identification of individual acids in a commercial sample of naphthenic acids from petroleum by two-dimensional comprehensive gas chromatography/mass spectrometry. *Rapid Communications in Mass Spectrometry : RCM*, *25*(12), 1741–1751. https://doi.org/10.1002/rcm.5040

Rowland, S. M., Robbins, W. K., Corilo, Y. E., Marshall, A. G., & Rodgers, R. P. (2014). Solid-Phase Extraction Fractionation To Extend the Characterization of Naphthenic Acids in Crude Oil by Electrospray Ionization Fourier Transform Ion Cyclotron Resonance Mass Spectrometry. *Energy & Fuels*, *28*(8), 5043–5048. https://doi.org/10.1021/ef5015023

Rubio, F., Rubio, J., & Oteo, J. L. (1998). A FT-IR Study of the Hydrolysis of Tetraethylorthosilicate (TEOS). *Spectroscopy Letters*, *31*(1), 199–219. https://doi.org/10.1080/00387019808006772

Rudzinski, W. E., Oehlers, L., Zhang, Y., & Najera, B. (2002). Tandem Mass Spectrometric Characterization of Commercial Naphthenic Acids and a Maya Crude Oil. *Energy & Fuels*, *16*(5), 1178–1185. https://doi.org/10.1021/ef020013t

Ruiz, F. (1999). *Formación y caracterización de materiales vítreos preparados por la técnica*. *Revista Mexicana de física* (Vol. 45).

Saab, J., Mokbel, I., Razzouk, A. C., Ainous, N., Zydowicz, N., & Jose, J. (2005). Quantitative Extraction Procedure of Naphthenic Acids Contained in Crude Oils. Characterization with Different Spectroscopic Methods. *Energy & Fuels*, *19*(2), 525–531. https://doi.org/10.1021/ef049930k

Sabbah, H., Morrow, A. L., Pomerantz, A. E., & Zare, R. N. (2011). Evidence for island structures as the dominant architecture of asphaltenes. *Energy and Fuels*, *25*(4), 1597–1604. https://doi.org/10.1021/ef101522w

Saheb, D. N., & Jog, J. P. (1999). Natural fiber polymer composites: A review. *Advances in Polymer Technology*, *18*(4), 351–363. https://doi.org/10.1002/(SICI)1098-2329(199924)18:4<351::AID-ADV6>3.0.CO;2-X

Sauerer, B., Abdulghani, A. J. Al, Abdallah, M. S., & Abdallah, W. (2018). Interfacial Activity of Characterized Middle Eastern Asphaltenes. *Energy & Fuels. Article ASAP*. https://doi.org/10.1021/acs.energyfuels.8b03085

Sauerer, B., Stukan, M., Buiting, J., Abdallah, W., & Andersen, S. (2018). Dynamic Asphaltene-Stearic Acid Competition at the Oil − Water Interface. *Langmuir*, *34*(19), 5558–5573. https://doi.org/10.1021/acs.langmuir.8b00684

Schlosser, M. (1988). Superbases for organic synthesis. *Pure and Applied Chemistry*, *60*(11), 1627–1634. https://doi.org/10.1351/pac198860111627

Shehzad, F., Hussein, I. A., Kamal, M. S., Ahmad, W., Sultan, A. S., & Nasser, M. S. (2018). Polymeric Surfactants and Emerging Alternatives used in the Demulsification of Produced Water: A Review. *Polymer Reviews*, *58*(1), 63–101.

https://doi.org/10.1080/15583724.2017.1340308

Shen, D. K., & Gu, S. (2009). The mechanism for thermal decomposition of cellulose and its main products. *Bioresource Technology*, *100*(24), 6496–6504. https://doi.org/10.1016/j.biortech.2009.06.095

Shi, L. J., Shen, B. X., & Wang, G. Q. (2008). Removal of Naphthenic Acids from Beijiang Crude Oil by Forming Ionic Liquids. *Energy & Fuels*, *22*(6), 4177–4181. https://doi.org/10.1021/ef800497p

Shi, Q., Zhao, S., Xu, Z., Chung, K. H., Zhang, Y., & Xu, C. (2010). Distribution of Acids and Neutral Nitrogen Compounds in a Chinese Crude Oil and Its Fractions: Characterized by Negative-Ion Electrospray Ionization Fourier Transform Ion Cyclotron Resonance Mass Spectrometry. *Energy & Fuels*, *24*(7), 4005–4011. https://doi.org/10.1021/ef1004557

Shroff, R., Muck, A., & Svatos, A. (2007). Analysis of low molecular weight acids by negative mode matrix-assisted laser desorption/ionization time-of-flight mass spectrometry. *Rapid Communications in Mass Spectrometry : RCM*, *21*(20), 3295–3300. https://doi.org/10.1002/rcm.3216

Shroff, R., Rulísek, L., Doubsky, J., & Svatos, A. (2009). Acid-base-driven matrix-assisted mass spectrometry for targeted metabolomics. *Proceedings of the National Academy of Sciences of the United States of America*, *106*(25), 10092–10096. https://doi.org/10.1073/pnas.0900914106

Shroff, R., & Svatoš, A. (2009). Proton Sponge: A Novel and Versatile MALDI Matrix for the Analysis of Metabolites Using Mass Spectrometry. *Analytical Chemistry*, *81*(19), 7954–

7959. https://doi.org/10.1021/ac901048z

Singh, M. B., Rampal, N., & Malani, A. (2018). Structural Behavior of Isolated Asphaltene Molecules at the Oil–Water Interface. *Energy & Fuels*, *32*(8), 8259–8267. https://doi.org/10.1021/acs.energyfuels.8b01648

Smith, D. F., Schaub, T. M., Kim, S., Rodgers, R. P., Rahimi, P., Teclemariam, A., & Marshall, A. G. (2008). Characterization of Acidic Species in Athabasca Bitumen and Bitumen Heavy Vacuum Gas Oil by Negative-Ion ESI FT - ICR MS with and without Acid - Ion Exchange Resin Prefractionation, *31*(4), 2372–2378.

Smith, D. F., Schaub, T. M., Rahimi, P., Teclemariam, A., Rodgers, R. P., & Marshall, A. G. (2007). Self-Association of Organic Acids in Petroleum and Canadian Bitumen Characterized by Low- and High-Resolution Mass Spectrometry †. *Energy & Fuels*, *21*(3), 1309–1316. https://doi.org/10.1021/ef060387c

Song, J., & Rojas, O. J. (2013). Approaching super-hydrophobicity from cellulosic materials : A Review. *Nordic Pulp and Paper Research Journal*, *28*(2), 216–238. https://doi.org/10.3183/NPPRJ-2013-28-02-p216-238

Speight, J. G. (2007). *The chemistry and technology of petroleum* (4th ed). Boca Raton: CRC Press/Taylor & Francis.

Spiecker, P. M., Gawrys, K. L., Trail, C. B., & Kilpatrick, P. K. (2003). Effects of petroleum resins on asphaltene aggregation and water-in-oil emulsion formation. *Colloids and Surfaces A: Physicochemical and Engineering Aspects*, *220*(1–3), 9–27. https://doi.org/10.1016/S0927-7757(03)00079-7

Stanford, L. A., Kim, S., Rodgers, R. P., & Marshall, A. G. (2006). Characterization of Compositional Changes in Vacuum Gas Oil Distillation Cuts by Electrospray Ionization Fourier Transform−Ion Cyclotron Resonance (FT−ICR) Mass Spectrometry. *Energy & Fuels*, *20*(4), 1664–1673. https://doi.org/10.1021/ef060104g

Stanford, L. A., Rodgers, R. P., Marshall, A. G., Czarnecki, J., Wu, X. A., & Taylor, S. (2007). Detailed Elemental Compositions of Emulsion Interfacial Material versus Parent Oil for Nine Geographically Distinct Light, Medium, and Heavy Crude Oils, Detected by Negative- and Positive-Ion Electrospray Ionization Fourier Transform Ion Cyclotron Resonan. *Energy & Fuels*, *21*(2), 973–981. https://doi.org/10.1021/ef060292a

Stanford, L. A., Rodgers, R. P., Marshall, A. G., High, N., Field, M., State, F., … Wu, X. A. (2007). Compositional Characterization of Bitumen / Water Emulsion Films by Negative- and Positive-Ion Electrospray Ionization and Field Desorption / Ionization Fourier Transform Ion Cyclotron Resonance Mass Spectrometry, *196*(1), 963–972.

Strausz, O. P., Mojelsky, T. W., Faraji, F., Lown, E. M., & Peng, P. (1999). Additional structural details on Athabasca asphaltene and their ramifications. *Energy and Fuels*, *13*(2), 207–227. https://doi.org/10.1021/ef980274w

Strausz, O. P., Mojelsky, T. W., & Lown, E. M. (1992). The molecular structure of asphaltene: an unfolding story. *Fuel*, *71*(12), 1355–1363. https://doi.org/10.1016/0016-2361(92)90206-4

Strausz, O. P., Peng, P., & Murgich, J. (2002). About the colloidal nature of asphaltenes and the MW of covalent monomeric units. *Energy and Fuels*, *16*(4), 809–822. https://doi.org/10.1021/ef0002795

Streletskii, A. V., Ioffe, I. N., Kotsiris, S. G., Barrow, M. P., Drewello, T., Strauss, S. H., & Boltalina, O. V. (2005). In-plume thermodynamics of the MALDI generation of fluorofullerene anions. *Journal of Physical Chemistry A*, *109*(4), 714–719. https://doi.org/10.1021/jp0462431

Subramanian, D., May, N., & Firoozabadi, A. (2017). Functional Molecules and the Stability of Water-in-Crude Oil Emulsions. *Energy & Fuels*, *31*(9), 8967–8977. https://doi.org/10.1021/acs.energyfuels.7b01039

Sun, D., Duan, X., Li, W., & Zhou, D. (1998). Demulsification of water-in-oil emulsion by using porous glass membrane. *Journal of Membrane Science*, *146*(1), 65–72. https://doi.org/10.1016/S0376-7388(98)00096-9

Sun, Y., & Shi, L. (2012). Basic ionic liquids with imidazole anion: New reagents to remove naphthenic acids from crude oil with high total acid number. *Fuel*, *99*, 83–87. https://doi.org/10.1016/j.fuel.2012.04.014

Sutton, P. A., & Rowland, S. J. (2014). Determination of the Content of C 80 Tetraacids in Petroleum. *Energy & Fuels*, *28*(9), 5657–5669. https://doi.org/10.1021/ef5012337

Sztukowski, D. M., Jafari, M., Alboudwarej, H., & Yarranton, H. W. (2003). Asphaltene self-association and water-in-hydrocarbon emulsions. *Journal of Colloid and Interface Science*, *265*(1), 179–186. https://doi.org/10.1016/S0021-9797(03)00189-9

Sztukowski, D. M., & Yarranton, H. W. (2005). Rheology of Asphaltene−Toluene/Water Interfaces. *Langmuir*, *21*(25), 11651–11658. https://doi.org/10.1021/la051921w

Taylor, P., Havre, T. E., Sjöblom, J., Vindstad, J. E., & Sjo, J. (2003). Oil / Water Partitioning and Interfacial Behavior of Naphthenic Acids. *Journal of Dispersion Science and Technology*, *24*(2003), 37–41. https://doi.org/dx.doi.org/10.1081/DIS-120025547

Teklebrhan, R. B., Jian, C., Choi, P., Xu, Z., & Sjöblom, J. (2016). Competitive Adsorption of Naphthenic Acids and Polyaromatic Molecules at a Toluene-Water Interface. *Journal of Physical Chemistry B*, *120*(50), 12901–12910. https://doi.org/10.1021/acs.jpcb.6b07938

Teräväinen, M. J., Pakarinen, J. M. H., Wickström, K., & Vainiotalo, P. (2007). Comparison of the Composition of Russian and North Sea Crude Oils and Their Eight Distillation Fractions Studied by Negative-Ion Electrospray Ionization Fourier Transform Ion Cyclotron Resonance Mass Spectrometry: The Effect of Suppression. *Energy & Fuels*, *21*(1), 266–273. https://doi.org/10.1021/ef060294v

Terra, L. A., Filgueiras, P. R., Tose, L. V, Romão, W., de Souza, D. D., de Castro, E. V. R., … Poppi, R. J. (2014). Petroleomics by electrospray ionization FT-ICR mass spectrometry coupled to partial least squares with variable selection methods: prediction of the total acid number of crude oils. *The Analyst*, *139*(19), 4908–4916. https://doi.org/10.1039/c4an00538d

Thomas, S. (2008). Destabilisation of Water-in-Crude Oil Emulsions by Silicone Copolymer Demulsifiers. *Oil & Gas Science and Technology*, *63*(1), 9–19. https://doi.org/10.2516/ogst

Tirmizi, N. P., Raghuraman, B., & Wiencek, J. (1996). Demulsification of Water / Oil / Solid Emulsions by Hollow-Fiber Membranes. *AIChe Journal*, *42*(5), 1263–1276. https://doi.org/doi.org/10.1002/aic.690420508

Tomczyk, N. A., Winans, R. E., Shinn, J. H., & Robinson, R. C. (2001). On the Nature and Origin

of Acidic Species in Petroleum. 1. Detailed Acid Type Distribution in a California Crude Oil. *Energy & Fuels*, *15*(6), 1498–1504. https://doi.org/10.1021/ef010106v

Tuteja, A., Choi, W., Ma, M., Mabry, J. M., Mazzella, S. A., Rutledge, G. C., … Cohen, R. E. (2007). Designing Superoleophobic Surfaces. *Science*, *318*(5856), 1618–1622. https://doi.org/10.1126/science.1148326

Valencia-Dávila, J. A., Blanco-Tirado, C., & Combariza, M. Y. (2017). Analysis of naphthenic acids by matrix assisted laser desorption ionization time of flight mass spectrometry. *Fuel*, *193*, 168–177. https://doi.org/10.1016/j.fuel.2016.12.048

Valencia-Dávila, J. A., Witt, M., Blanco-Tirado, C., & Combariza, M. Y. (2018). Molecular characterization of naphthenic acids from heavy crude oils using MALDI FT-ICR mass spectrometry. *Fuel*, *231*, 126–133. https://doi.org/10.1016/j.fuel.2018.05.061

Varadaraj, R., & Brons, C. (2007a). Molecular Origins of Heavy Crude Oil Interfacial Activity Part 2: Fundamental Interfacial Properties of Model Naphthenic Acids and Naphthenic Acids Separated from Heavy Crude Oils. *Energy & Fuels*, *21*(1), 199–204. https://doi.org/10.1021/ef060425s

Varadaraj, R., & Brons, C. (2007b). Molecular Origins of Heavy Oil Interfacial Activity Part 1: Fundamental Interfacial Properties of Asphaltenes Derived from Heavy Crude Oils and Their Correlation To Chemical Composition. *Energy & Fuels*, *21*(1), 195–198. https://doi.org/10.1021/ef0604240

Varadaraj, R., & Brons, C. (2007c). Molecular Origins of Heavy Oil Interfacial Activity Part 1: Fundamental Interfacial Properties of Asphaltenes Derived from Heavy Crude Oils and Their

Correlation To Chemical Composition. *Energy & Fuels*, *21*(1), 195–198. https://doi.org/10.1021/ef0604240

Vaz, B. G., Abdelnur, P. V., Rocha, W. F. C., Gomes, A. O., & Pereira, R. C. L. (2013). Predictive Petroleomics: Measurement of the Total Acid Number by Electrospray Fourier Transform Mass Spectrometry and Chemometric Analysis. *Energy & Fuels*, *27*(4), 1873–1880. https://doi.org/10.1021/ef301515y

Vaz de Campos, M. C., Oliveira, E. C., Filho, P. J. S., Piatnicki, C. M. S., & Caramão, E. B. (2006). Analysis of tert-butyldimethylsilyl derivatives in heavy gas oil from Brazilian naphthenic acids by gas chromatography coupled to mass spectrometry with electron impact ionization. *Journal of Chromatography. A*, *1105*(1–2), 95–105. https://doi.org/10.1016/j.chroma.2005.07.040

Vermillion-Salsbury, R. L., & Hercules, D. M. (2002). 9-Aminoacridine as a matrix for negative mode matrix-assisted laser desorption/ionization. *Rapid Communications in Mass Spectrometry*, *16*(16), 1575–1581. https://doi.org/10.1002/rcm.750

Wang, J., Wong, J. X. H., Kwok, H., Li, X., & Yu, H. Z. (2016). Facile preparation of nanostructured, superhydrophobic filter paper for efficient water/oil separation. *PLoS ONE*, *11*(3), 1–12. https://doi.org/10.1371/journal.pone.0151439

Wang, L., He, C., Zhang, Y., Zhao, S., Chung, K. H., Xu, C., … Shi, Q. (2013). Characterization of Acidic Compounds in Heavy Petroleum Resid by Fractionation and Negative-Ion Electrospray Ionization Fourier Transform Ion Cyclotron Resonance Mass Spectrometry Analysis. *Energy & Fuels*, *27*(8), 4555–4563. https://doi.org/10.1021/ef400459m

Wang, S., Li, M., & Lu, Q. (2010). Filter paper with selective absorption and separation of liquids that differ in surface tension. *ACS Applied Materials and Interfaces*, *2*(3), 677–683. https://doi.org/10.1021/am900704u

Wang, X., Pensini, E., Liang, Y., Xu, Z., Chandra, M. S., Ivar, S., … Buiting, J. J. (2016). Fatty acid-asphaltene interactions at oil / water interface. *Colloids and Surfaces A: Physicochemical and Engineering Aspects*, *513*, 168–177. https://doi.org/10.1016/j.colsurfa.2016.10.029

Wang, Z., Wang, Y., & Liu, G. (2016). Rapid and Efficient Separation of Oil from Oil-in-Water Emulsions Using a Janus Cotton Fabric. *Angewandte Chemie - International Edition*, *55*(4), 1291–1294. https://doi.org/10.1002/anie.201507451

Wu, X. (2003). Investigating the Stability Mechanism of Water-in-Diluted Bitumen Emulsions through Isolation and Characterization of the Stabilizing Materials at the Interface. *Energy & Fuels*, *17*(10), 179–190.

Xia, L., Lu, S., & Cao, G. (2004). Stability and demulsification of emulsions stabilized by asphaltenes or resins. *Journal of Colloid and Interface Science*, *271*(2), 504–506. https://doi.org/10.1016/j.jcis.2003.11.027

Xiu, Y., Hess, D. W., & Wong, C. P. (2008). UV and thermally stable superhydrophobic coatings from sol–gel processing. *Journal of Colloid and Interface Science*, *326*(2), 465–470. https://doi.org/10.1016/j.jcis.2008.06.042

Xu, Y., Dabros, T., Hamza, H., & Shefantook, W. (1999). DESTABILIZATION OF WATER IN BITUMEN EMULSION BY WASHING WITH WATER. *Petroleum Science and*

Technology, *17*(9–10), 1051–1070. https://doi.org/10.1080/10916469908949765

Xue, Z., Cao, Y., Liu, N., Feng, L., & Jiang, L. (2014). Special wettable materials for oil/water separation. *Journal of Materials Chemistry A*, *2*, 2445–2460. https://doi.org/10.1039/C3TA13397D

Yamagaki, T., & Watanabe, T. (2012). Hydrogen Radical Removal Causes Complex Overlapping Isotope Patterns of Aromatic Carboxylic Acids in Negative-ion Matrix-assisted Laser Desorption/Ionization Mass Spectrometry. *Mass Spectrometry*, *1*, A0005. https://doi.org/10.5702/massspectrometry.A0005

Yang, F., Tchoukov, P., Pensini, E., Dabros, T., Czarnecki, J., Masliyah, J., & Xu, Z. (2014). Asphaltene Subfractions Responsible for Stabilizing Water-in-Crude Oil Emulsions. Part 1: Interfacial Behaviors. *Energy & Fuels*, *28*(11), 6897–6904. https://doi.org/10.1021/ef501826g

Yang, H., Pi, P., Cai, Z. Q., Wen, X., Wang, X., Cheng, J., & Yang, Z. ru. (2010). Facile preparation of super-hydrophobic and super-oleophilic silica film on stainless steel mesh via sol-gel process. *Applied Surface Science*, *256*(13), 4095–4102. https://doi.org/10.1016/j.apsusc.2010.01.090

Yang, X., Verruto, V. J., & Kilpatrick, P. K. (2007). Dynamic Asphaltene−Resin Exchange at the Oil/Water Interface: Time-Dependent W/O Emulsion Stability for Asphaltene/Resin Model Oils. *Energy & Fuels*, *21*(3), 1343–1349. https://doi.org/10.1021/ef060465w

Yarranton, H. W., Sztukowski, D. M., & Urrutia, P. (2007). Effect of interfacial rheology on model emulsion coalescence I . Interfacial rheology. *Journal of Colloid and Interface Science*, *310*,

246–252. https://doi.org/10.1016/j.jcis.2007.01.071

Yarranton, H. W., Urrutia, P., & Sztukowski, D. M. (2007). Effect of interfacial rheology on model emulsion coalescence II . Emulsion coalescence. *Journal of Colloid and Interface Science*, *310*, 253–259. https://doi.org/10.1016/j.jcis.2007.01.098

Youssef, A. M., Kamel, S., El-Sakhawy, M., & El Samahy, M. A. (2012). Structural and electrical properties of paper-polyaniline composite. *Carbohydrate Polymers*, *90*(2), 1003–1007. https://doi.org/10.1016/j.carbpol.2012.06.034

Zeng, L., Zhang, Y., Bukirwa, C., Li, W., & Yang, Y. (2015). Study of mean diameter and drop size distribution of emulsion drops in a modified rotating disc contactor for an emulsion liquid membrane system. *RSC Adv.*, *5*(109), 89959–89970. https://doi.org/10.1039/C5RA16267J

Zhang, L. Y., Lopetinsky, R., Xu, Z., & Masliyah, J. H. (2005). Asphaltene Monolayers at a Toluene / Water Interface. *Energy & Fuels*, *19*(4), 1330–1336. https://doi.org/10.1021/ef0603129

Zhang, S., Liu, J., Chen, Y., Xiong, S., Wang, G., Chen, J., & Yang, G. (2010). A Novel Strategy for MALDI-TOF MS Analysis of Small Molecules. *Journal of the American Society for Mass Spectrometry*, *21*(1), 154–160. https://doi.org/10.1016/j.jasms.2009.09.024

Zhang, W., Shi, Z., Zhang, F., Liu, X., Jin, J., & Jiang, L. (2013). Superhydrophobic and superoleophilic PVDF membranes for effective separation of water-in-oil emulsions with high flux. *Advanced Materials*, *25*(14), 2071–2076. https://doi.org/10.1002/adma.201204520

Zhang, Y., Shi, Q., Li, A., Chung, K. H., Zhao, S., & Xu, C. (2011). Partitioning of Crude Oil

Acidic Compounds into Subfractions by Extrography and Identification of Isoprenoidyl Phenols and Tocopherols. *Energy & Fuels*, *25*(11), 5083–5089. https://doi.org/10.1021/ef2011854

Zhou, K., Zhang, Q. G., Li, H. M., Guo, N. N., Zhu, A. M., & Liu, Q. L. (2014). Ultrathin cellulose nanosheet membranes for superfast separation of oil-in-water nanoemulsions. *Nanoscale*, *6*(17), 10363. https://doi.org/10.1039/C4NR03227F

Zhu, G.-T., He, S., He, X.-M., Zhu, S.-K., & Feng, Y.-Q. (2017). A micro-solid phase extraction in glass pipette packed with amino-functionalized silica for rapid analysis of petroleum acids in crude oils. *RSC Adv.*, *7*(64), 40608–40614. https://doi.org/10.1039/C7RA06763A

Zolfaghari, R., Fakhru'l-Razi, A., Abdullah, L. C., Elnashaie, S. S. E. H., & Pendashteh, A. (2016). Demulsification techniques of water-in-oil and oil-in-water emulsions in petroleum industry. *Separation and Purification Technology*, *170*, 377–407. https://doi.org/10.1016/j.seppur.2016.06.026

APPENDICES

Appendix A. Analysis of naphthenic acids by matrix assisted laser desorption ionization time of flight mass spectrometry

1. Naphthenic acid extraction from a distillation cut (370-510 °c) using an anion exchange mechanism.

Materials and reagents

Methanol (MeOH), toluene (MePh), formic acid (HCOOH, 98 %) were all HPLC grade and purchased from Merck (Darmstadt, Germany) chemicals. All of them were used as supplied. The ion exchange sugar (poly-1, 6-glucose) based resin QAE-Sephadex® A-25 (Chloride form) were acquired from Sigma-Aldrich (St. Louis, MO) and employed for the naphthenic acid extraction from the distillation cut (370-510 °C). Whatman™ filter paper used to filtrate the resin was purchased from GE Healthcare life sciences (100 µm, 150 mm diameter).

A pH 9.8 buffer solution was prepared by mixing solutions of sodium carbonate (Merck Darmstadt, Germany) and sodium bicarbonate (Merck Darmstadt, Germany) previously prepared in deionized water with a resistivity less than 18.2 mΩ/cm, purified by a Millipore system.

Isolation of NAs by ion exchange resin

Naphthenic acid isolation from the crude oil distillation cut was achieved with an anion exchange mechanism that initiates with the activation of the sugar based resin using a buffer solution of sodium carbonate/sodium bicarbonate with an alkaline pH of 9.8. After this, the chloride initially attached to the resin is displaced by the bicarbonate ion (HCO_3^-); this anion exchange is known as the resin activation. Subsequently, the distillate cut and resin are dissolved in toluene and gently

mixed for sixteen hours. At the end of this point, bicarbonate ions will have been replaced by the carboxylate anions of the acids present in the crude oils. After that, several washes with toluene and a mixture of toluene/methanol (2:1 % v/v) allow to eliminate interferences before final elution of the acids, which is done using a solvent mixture of toluene/methanol (1:1 %v/v) with formic acid (1 % v/v). This final solution was collected and the solvent excess was evaporated at 60 °C to obtain a concentrated acid extract. This procedure was applied based on a previous reported procedure (Mediaas H, Grande K. V, Hustad B. M, Rasch A, Rueslåtten H. G, Vindstad J. E. The acid-IER Method- a Method for selective Isolation of Carboxylic Acids from Crude Oil and other Organic Solvents. Asa, S. 2003; 80404. doi: dx.doi.org/10.2118/80404-MS).

2. Tables and figures

Table A1. *Average of maximum relative abundances with standard deviation and error values for each m/z values of naphthenic acids detected by ESI-MS and classified by hydrogen deficiency.*

Z=0						
Nominal Mass	**Relative abundance (%)**			**Mean value**	**Standard deviation**	**Error**
	Mass spectra					
	1	**2**	**3**			
143	1.346	1.368	1.258	1.324	0.058	0.034
157	9.746	9.507	8.661	9.305	0.570	0.329
171	17.062	15.950	15.350	16.121	0.869	0.502
185	21.679	20.950	20.735	21.121	0.495	0.286
199	6.343	6.736	6.826	6.635	0.257	0.148
213	24.714	26.362	27.090	26.055	1.217	0.703
227	22.141	23.498	24.733	23.457	1.297	0.749
241	25.880	27.893	29.187	27.653	1.667	0.962

255	5.141	5.250	5.493	5.295	0.180	0.104
269	1.555	1.581	1.658	1.598	0.054	0.031
283	7.791	7.611	7.884	7.762	0.139	0.080
297	100	100	100	100	0.000	0.000
311	12.175	11.833	11.034	11.680	0.585	0.338
325	0.786	0.716	0.819	0.774	0.052	0.030
339	0.469	0.515	0.426	0.470	0.045	0.026

Z=-2

Nominal Mass	**Relative abundance (%)**			**Mean value**	**Standard deviation**	**Error**
	Mass spectra					
	1	**2**	**3**			
155	0.121	0.134	0.138	0.131	0.01	0.005
169	0.940	1.123	1.100	1.054	0.10	0.058
183	2.825	3.276	3.398	3.166	0.30	0.174
197	4.214	5.166	5.116	4.832	0.54	0.309
211	4.785	5.593	5.740	5.373	0.51	0.297
225	4.954	5.710	5.850	5.505	0.48	0.278
239	3.907	4.425	4.579	4.304	0.35	0.203
253	1.870	2.024	2.110	2.001	0.12	0.070
267	1.069	1.136	1.169	1.125	0.05	0.029
281	1.083	1.162	1.186	1.144	0.05	0.031
295	5.182	5.168	5.154	5.168	0.01	0.008
309	0.634	0.637	0.639	0.637	0.00	0.002
323	0.228	0.236	0.222	0.229	0.01	0.004
337	0.191	0.166	0.153	0.170	0.02	0.011

Z=-4

Nominal Mass	Relative abundance (%)			Mean value	Standard deviation	Error
	Mass spectra					
	1	2	3			
167	0.149	0.184	0.182	0.172	0.020	0.012
181	0.897	1.098	1.114	1.036	0.121	0.070
195	2.554	3.278	3.271	3.034	0.416	0.240
209	3.309	4.436	4.359	4.035	0.630	0.363
223	3.624	4.515	4.493	4.210	0.508	0.293
237	3.091	3.613	3.685	3.463	0.324	0.187
251	2.207	2.481	2.560	2.416	0.185	0.107
265	1.117	1.273	1.368	1.253	0.126	0.073
279	0.654	0.711	0.720	0.695	0.035	0.020
293	0.472	0.513	0.537	0.507	0.033	0.019
307	0.314	0.345	0.350	0.336	0.020	0.011
321	0.128	0.125	0.138	0.131	0.007	0.004
335	0.132	0.131	0.133	0.132	0.001	0.001

Z=-6

Nominal Mass	Relative abundance (%)			Mean value	Standard deviation	Error
	Mass spectra					
	1	2	3			
221	0.699	0.882	0.861	0.814	0.100	0.058
235	0.944	1.130	1.120	1.065	0.105	0.061
249	0.879	1.019	1.051	0.983	0.092	0.053
263	0.443	0.547	0.527	0.506	0.055	0.032
277	0.248	0.282	0.297	0.276	0.025	0.014
291	0.174	0.178	0.214	0.189	0.022	0.013
305	0.103	0.105	0.118	0.109	0.008	0.005

319	0.051	0.056	0.053	0.053	0.003	0.001
333	0.094	0.104	0.097	0.098	0.005	0.003

Z=-8

Nominal Mass	Relative abundance (%) Mass spectra			Mean value	Standard deviation	Error
	1	**2**	**3**			
177	0.055	0.077	0.076	0.069	0.012	0.007
191	0.105	0.133	0.132	0.123	0.016	0.009
205	0.177	0.196	0.202	0.192	0.013	0.008
219	0.173	0.177	0.191	0.180	0.009	0.005
233	0.221	0.252	0.265	0.246	0.022	0.013
247	0.234	0.252	0.258	0.248	0.013	0.007
261	0.169	0.171	0.187	0.176	0.010	0.006
275	0.117	0.120	0.112	0.116	0.004	0.002
289	0.096	0.091	0.084	0.090	0.006	0.003
303	0.060	0.057	0.063	0.060	0.003	0.002

Z=-10

Nominal Mass	Relative abundance (%) Mass spectra			Mean value	Standard deviation	Error
	1	**2**	**3**			
175	0.013	0.147	0.013	0.057	0.078	0.045
189	0.029	0.032	0.030	0.030	0.001	0.001
203	0.062	0.070	0.063	0.065	0.004	0.002
217	0.114	0.117	0.113	0.115	0.002	0.001
231	0.144	0.140	0.139	0.141	0.003	0.002
245	0.146	0.139	0.134	0.140	0.006	0.003
259	0.122	0.126	0.132	0.127	0.005	0.003

273	0.119	0.098	0.119	0.112	0.012	0.007
287	0.136	0.136	0.093	0.122	0.025	0.014
301	0.193	0.190	0.201	0.195	0.005	0.003
315	0.106	0.104	0.107	0.106	0.002	0.001
329	0.184	0.153	0.168	0.168	0.015	0.009

Z=-12

Nominal Mass	Relative abundance (%)			Mean value	Standard deviation	Error
	Mass spectra					
	1	**2**	**3**			
229	0.559	0.629	0.645	0.611	0.045	0.026
243	0.556	0.550	0.599	0.568	0.027	0.016
257	0.170	0.196	0.186	0.184	0.013	0.008
271	0.208	0.209	0.223	0.213	0.008	0.005
285	0.259	0.259	0.270	0.263	0.007	0.004
299	2.927	2.899	2.934	2.920	0.018	0.011
313	0.421	0.405	0.388	0.405	0.017	0.010
327	0.137	0.136	0.140	0.138	0.002	0.001

Table A2. *Average total relative abundances with standard deviation and error values for each type of naphthenic acids classified by hydrogen deficiency.*

Hydrogen Deficiency Z	Relative abundance (%)			Mean value	Standard deviation	Error
	Mass spectra					
	1	**2**	**3**			
0	80.570	79.453	78.332	79.452	1.119	0.646
-2	10.010	9.997	11.060	10.356	0.610	0.352
-4	5.773	6.868	6.791	6.478	0.611	0.353

-6	1.060	1.214	1.183	1.153	0.082	0.047
-8	0.419	0.455	0.453	0.442	0.020	0.012
-10	0.410	0.387	0.379	0.392	0.016	0.009
-12	1.759	1.625	1.801	1.728	0.092	0.053

Table A3. *Mass assignments for each m/z values of the naphthenic acids identified by MALDI-TOF/MS using DMAN as a matrix.*

Z=0			
Reference *m/z*	**Experimental *m/z***	**Relative abundance (%)**	**Error [ppm]**
157.123156	157.122855	3.8	5.81
171.138474	171.138505	9.8	1.92
185.153607	185.154155	14.8	0.18
199.167889	199.169805	9.6	2.96
213.183732	213.185455	33.0	9.62
227.199947	227.201105	29.7	8.08
241.217150	241.216755	39.0	5.10
255.233111	255.232405	6.7	1.64
269.246614	269.248055	1.9	2.77
283.262935	283.263705	4.6	5.35
297.278786	297.279355	100	2.72
311.295403	311.295005	13.0	1.91
325.311313	325.310655	6.6	1.28
339.325343	339.326305	9.8	2.02
Z=-2			

Reference *m/z*	**Experimental *m/z***	**Relative abundance (%)**	**Error [ppm]**
169.122855	169.121972	1.3	5.22
183.138505	183.137910	4.6	3.25
197.154155	197.152845	10.0	6.64
211.169805	211.168088	10.2	8.13
225.185455	225.183832	11.7	7.21
239.201105	239.200695	11.3	1.71
253.216755	253.217117	6.2	1.43
267.232405	267.232045	3.0	1.35
281.248055	281.246024	2.0	7.22
295.263705	295.264229	11.9	1.78

Z=-4

Reference *m/z*	**Experimental *m/z***	**Relative abundance (%)**	**Error [ppm]**
181.122855	181.121126	1.5	9.55
195.138505	195.136993	2.2	7.75
209.154155	209.153769	5.0	1.85
223.169805	223.169824	7.6	0.08
237.185455	237.184670	2.1	3.31
251.201105	251.200173	6.5	3.71
265.216755	265.216498	3.8	0.97
279.232405	279.230754	2.1	5.91

Z=-6

Reference *m/z*	**Experimental *m/z***	**Relative abundance (%)**	**Error [ppm]**

221.154155	221.153045	1.5	5.02
235.169805	235.170068	2.4	1.12
249.185455	249.183182	2.8	9.12
263.201105	263.203233	1.9	8.08
277.216755	277.215068	1.6	6.09

Z=-8

Reference *m/z*	**Experimental *m/z***	**Relative abundance (%)**	**Error [ppm]**
149.060254	149.061567	0.10	8.81
163.075904	163.076832	0.26	5.69
177.091554	177.092345	0.38	4.47
191.107204	191.105342	1.23	9.74
205.122854	205.122466	1.58	1.89
219.138504	219.137321	0.93	5.40
233.154154	233.156131	1.31	8.48
247.169804	247.168321	2.49	6.00
261.185455	261.183213	1.20	8.58
275.201105	275.203124	0.47	7.34
289.216755	289.218354	0.60	5.53
303.232405	303.234232	0.66	6.03

Z=-10

Reference m/z	**Experimental *m/z***	**Relative abundance (%)**	**Error [ppm]**
175.075905	175.074567	0.78	7.64
189.091555	189.089955	1.33	8.46
203.107205	203.105201	1.01	9.87

217.122855	217.121955	1.08	4.15
231.138505	231.139851	1.29	5.83
245.154155	245.151579	1.60	10.51
259.169805	259.168245	0.68	6.02
273.185455	273.187903	0.52	8.96
287.201105	287.212563	1.44	39.90
301.216755	301.212657	0.47	13.60
	Z=-12		
Reference m/z	**Experimental *m/z***	**Relative abundance (%)**	**Error [ppm]**
229.122855	229.126175	8.69	14.49
243.138505	243.139243	1.50	3.04
257.154155	257.153457	1.72	2.71
271.169805	271.167580	1.18	8.21
285.185455	285.187543	1.34	7.32
299.201105	299.204174	1.88	10.26

Table A4. *Maximum relative abundances (*average value of three measurements) with standard deviation and error values for each m/z values of naphthenic acids classified by hydrogen deficiency and identified by MALDI-TOF/MS with DMAN as a matrix.*

Z=0			
m/z	**Relative abundance (%)***	**Standard deviation**	**Error**
157	6.58	6.03	3.48
171	15.64	13.70	7.91
185	22.54	20.59	11.89
199	11.41	6.77	3.91
213	33.29	19.54	11.28
227	30.29	11.43	6.60
241	38.89	11.91	6.87
255	7.83	1.02	0.59
269	2.02	1.20	0.69
283	5.22	0.57	0.33
297	100.00	0.00	0.00
311	10.94	2.24	1.29
325	3.05	1.64	0.95
339	3.17	2.22	1.28
Z=-2			
m/z	**Relative abundance (%)***	**Standard deviation**	**Error**

155	1.28	2.22	1.28
169	4.48	2.99	1.73
183	6.41	0.44	0.26
197	11.04	3.21	1.85
211	11.92	1.52	0.88
225	14.07	3.60	2.08
239	13.09	1.68	0.97
253	7.34	0.92	0.53
267	3.78	0.19	0.11
281	3.61	0.19	0.11
295	11.40	1.90	1.10
309	2.15	1.90	1.10

Z=-4

m/z	**Relative abundance (%)***	**Standard deviation**	**Error**
181	1.90	0.37	0.21
195	2.81	0.73	0.42
209	5.99	0.20	0.11
223	8.81	0.89	0.52
237	8.04	2.84	1.64
251	7.44	1.66	0.96

265	4.35	0.95	0.55
279	2.76	0.95	0.55
293	2.11	0.95	0.55

Z=-6

m/z	**Relative abundance (%)***	**Standard deviation**	**Error**
221	1.30	0.12	0.07
235	1.92	0.14	0.08
249	2.49	2.35	1.36
263	0.63	1.08	0.63
277	0.54	0.94	0.54

Z=-8

m/z	**Relative abundance (%)***	**Standard deviation**	**Error**
149	0.10	0.18	0.10
163	0.26	0.27	0.16
177	0.38	0.47	0.27
191	1.23	0.94	0.54
205	1.58	1.25	0.72
219	0.93	0.42	0.24
233	1.31	0.43	0.25
247	2.49	1.84	1.06

261	1.20	0.48	0.28
275	0.47	0.41	0.24
289	0.60	0.58	0.33
303	0.66	0.57	0.33

Z=-10

m/z	**Relative abundance (%)***	**Standard deviation**	**Error**
175	0.78	0.57	0.33
189	1.33	0.14	0.08
203	1.01	0.47	0.27
217	1.08	0.45	0.26
231	1.29	0.63	0.36
245	1.60	0.51	0.29
259	0.68	0.66	0.38
273	0.52	0.48	0.28
287	1.44	1.13	0.65
301	0.47	0.49	0.28

Z=-12

m/z	**Relative abundance (%)***	**Standard deviation**	**Error**
229	8.69	3.87	2.23
243	1.50	1.33	0.77

257	1.72	0.59	0.34
271	1.18	1.04	0.60
285	1.34	0.39	0.22
299	1.88	1.69	0.98

Table A.5. *Average total relative abundances with standard deviation and error values for each family of naphthenic acids, classified by hydrogen deficiency.*

Z	Relative abundance (%)			Mean value	Standard deviation	Error
	Mass spectra					
	1	**2**	**3**			
0	66.690	63.233	51.525	60.482	7.948	4.589
-2	16.116	17.835	20.096	18.016	1.996	1.153
-4	7.768	8.757	13.841	10.122	3.259	1.881
-6	2.155	2.296	3.812	2.754	0.918	0.530
-8	2.811	2.295	2.771	2.625	0.287	0.166
-10	1.621	2.181	2.481	2.094	0.437	0.252
-12	2.839	3.404	5.475	3.906	1.387	0.801

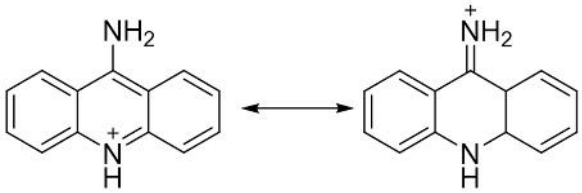

Figure A1. Chemical structure of the 9-aminoacridinium ion and its resonant structure

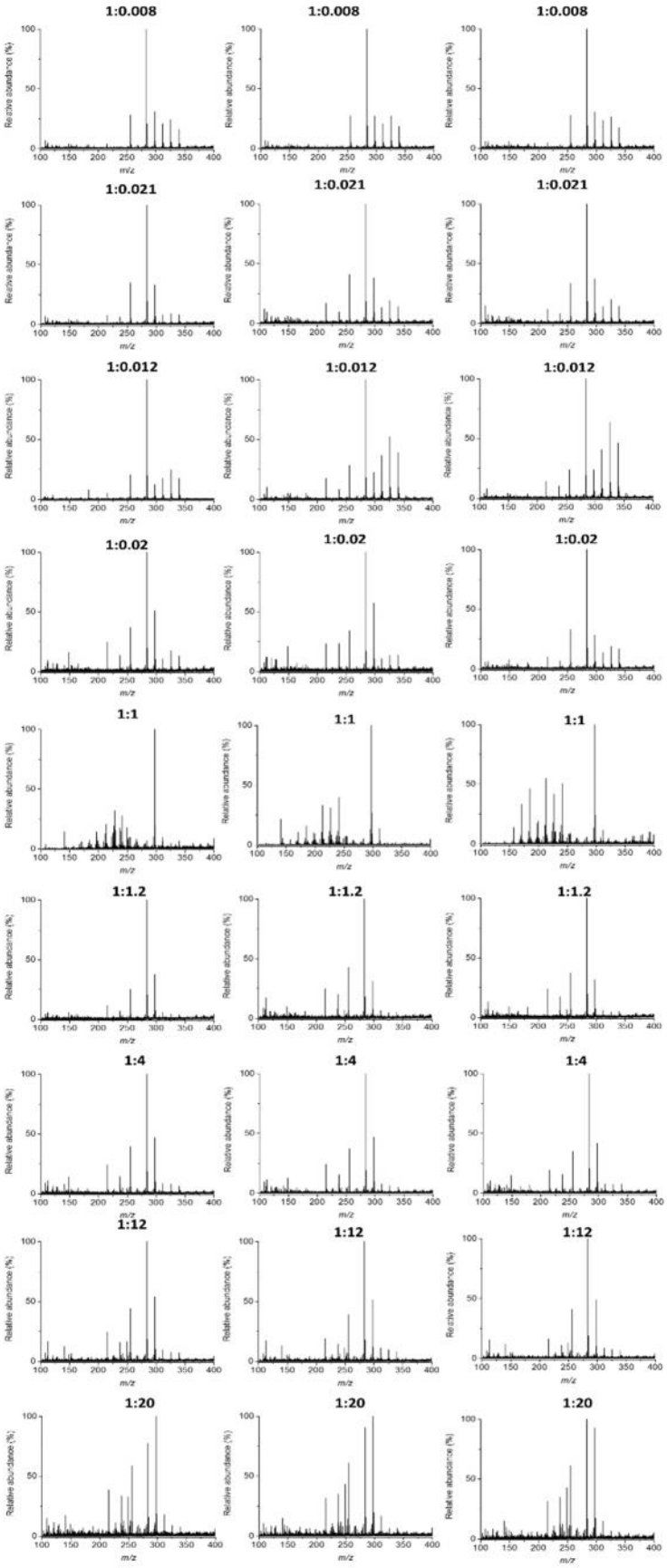
1:0.008
1:0.008
1:0.008
1:0.021
1:0.021
1:0.021
1:0.012
1:0.012
1:0.012
1:0.02
1:0.02
1:0.02
1:1
1:1
1:1
1:1.2
1:1.2
1:1.2
1:4
1:4
1:4
1:12
1:12
1:12
1:20
1:20
1:20
Relative abundance (%)
m/z

Figure A2. MALDI-TOF mass spectra of the standard NA mixture at a constant concentration (0.5 mM) but varying the matrix concentration resulting in several analyte/matrix ratios ranging from 1:0.008 to 1:20.

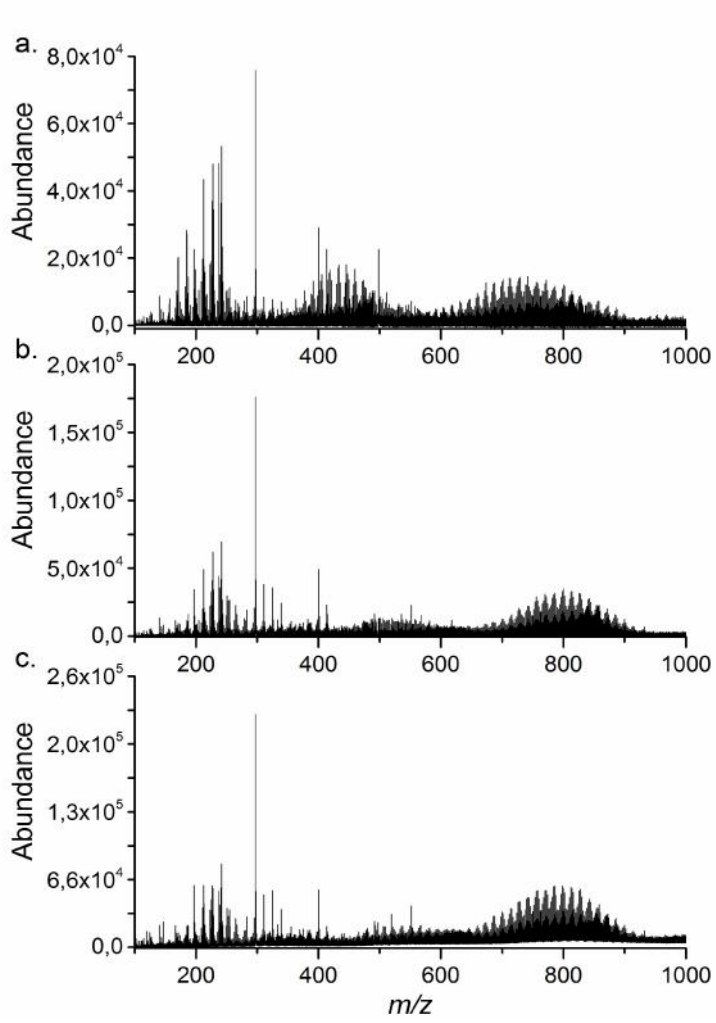

Figure A3. MALDI-TOF mass spectra of NAs (0.5 nmol/µL) acquired at different laser fluences: (a) 60% (4.17 µJ/pulse), (b) 65%, (c) 70% using DMAN as matrix and summing 4000 mass spectra in all cases.

Table A6. *Average total relative abundances with standard deviation and error values for each family of naphthenic acids present in a commercial standard mixture and identified by MALDI TOF/MS using 9-aminocridine (9-AA) as the matrix.*

Z	Relative abundance (%)			Mean value	Standard deviation	Error
	Mass spectra					
	1	**2**	**3**			
0	70.238	77.134	72.987	73.453	3.472	2.004
-2	10.164	8.229	9.340	9.245	0.971	0.560
-4	5.616	5.999	7.728	6.447	1.125	0.650
-6	0.322	0.636	0.667	0.542	0.191	0.110
-8	0.932	0.255	0.699	0.628	0.344	0.198
-10	3.566	2.171	2.203	2.647	0.796	0.460
-12	9.163	5.797	6.584	7.181	1.761	1.017

Table A7. *Maximum relative abundances (*average value of three measurements) with standard deviation and error values for each m/z values of naphthenic acids identified by MALDI-TOF/MS using 9-AA.*

Z=0			
m/z	Relative abundance (%)*	Standard deviation	Error
157	6.10	3.69	2.13
171	13.52	7.33	4.23
185	22.83	10.48	6.05
199	10.53	2.16	1.25
213	28.02	8.42	4.86

227	21.22	5.08	2.94
241	22.88	6.09	3.52
255	3.71	0.39	0.23
269	0.91	0.81	0.47
283	2.69	0.42	0.25
297	45.11	5.18	2.99
311	55.81	2.29	1.32
325	100.00	0.00	0.00
339	39.59	4.56	2.63
	Z=-2		
m/z	Relative abundance (%)*	Standard deviation	Error
155	1.45	0.67	0.39
169	3.15	1.45	0.84
183	4.36	1.48	0.85
197	7.01	1.09	0.63
211	4.82	1.09	0.63
225	5.49	1.40	0.81
239	4.40	0.74	0.43
253	2.33	0.71	0.41
267	1.16	1.05	0.61
281	0.96	1.02	0.59
295	4.69	0.16	0.09
309	8.97	1.80	1.04
	Z=-4		
m/z	Relative abundance (%)*	Standard deviation	Error
209	2.38	0.55	0.32
223	2.48	0.59	0.34

237	2.26	0.65	0.38
251	2.25	0.99	0.57
265	14.36	3.24	1.87
279	0.60	0.52	0.30
293	6.87	0.80	0.46
	Z=-6		
m/z	Relative abundance (%)*	Standard deviation	Error
221	0.79	0.69	0.40
235	1.20	0.25	0.15
263	0.97	0.14	0.08
	Z=-8		
m/z	Relative abundance (%)*	Standard deviation	Error
177	0.55	0.71	0.41
205	0.42	0.73	0.42
233	0.83	0.31	0.18
247	0.57	0.58	0.34
261	0.59	0.55	0.32
289	0.93	1.04	0.60
303	0.27	0.46	0.27
	Z=-10		
m/z	Relative abundance (%)*	Standard deviation	Error
217	0.84	0.86	0.50
231	11.44	3.06	1.77
273	0.60	1.04	0.60
	Z=-12		

m/z	Relative abundance (%)*	Standard deviation	Error
229	32.80	9.70	5.60
243	1.30	2.25	1.30
271	1.18	1.31	0.76
299	1.55	0.93	0.54

Table A8. *Mass assignments of napthtenic acids identified by MALDI-TOF/MS using 9-AA.*

Z=0			
Reference *m/z*	**Experimental *m/z***	**Relative abundance (%)**	**Error [ppm]**
157.123450	157.122855	6.10	3.79
171.136954	171.138505	13.52	9.06
185.152564	185.154155	22.83	8.59
199.169246	199.169805	10.53	2.81
213.184604	213.185455	28.02	3.99
227.203234	227.201105	21.22	9.37
241.219321	241.216755	22.88	10.64
255.229432	255.232405	3.71	11.65
269.249685	269.248055	0.91	6.05
283.259345	283.263705	2.69	15.39
297.268754	297.279355	45.11	35.66
311.283433	311.295005	55.81	37.17
325.299256	325.310655	100.00	35.04
339.319356	339.326305	39.59	20.48
Z=-2			

Reference *m/z*	**Experimental *m/z***	**Relative abundance (%)**	**Error [ppm]**
155.104437	155.107205	1.45	17.85
169.126236	169.122855	3.15	19.99
183.136734	183.138505	4.36	9.67
197.153243	197.154155	7.01	4.63
211.172432	211.169805	4.82	12.44
225.187432	225.185455	5.49	8.78
239.203564	239.201105	4.40	10.28
253.224324	253.216755	2.33	29.89
267.242765	267.232405	1.16	38.77
281.257244	281.248055	0.96	32.67
295.252732	295.263705	4.69	37.16
309.269396	309.279355	8.97	32.20
Z=-4			
Reference *m/z*	**Experimental *m/z***	**Relative abundance (%)**	**Error [ppm]**
209.147275	209.154155	2.38	32.89
223.165469	223.169805	2.48	19.43
237.189216	237.185455	2.26	15.86
251.212467	251.201105	2.25	45.23
265.213895	265.216755	14.36	10.78
279.230064	279.232405	0.60	8.38
293.233459	293.248055	6.87	49.77
Z=-6			

Reference *m/z*	**Experimental *m/z***	**Relative abundance (%)**	**Error [ppm]**
221.152561	221.154155	0.79	7.21
235.174245	235.169805	1.20	18.88
263.202322	263.201105	0.97	4.62

Z=-8

Reference *m/z*	**Experimental *m/z***	**Relative abundance (%)**	**Error [ppm]**
177.094498	177.091554	0.55	16.62
205.125934	205.122854	0.42	15.02
233.146575	233.154154	0.83	32.51
247.176296	247.169804	0.57	26.27
261.179486	261.185455	0.59	22.85
289.224463	289.216755	0.93	26.65
303.235255	303.232405	0.27	9.40

Z=-10

Reference *m/z*	**Experimental *m/z***	**Relative abundance (%)**	**Error [ppm]**
217.125443	217.122855	0.84	11.92
231.133452	231.138505	11.44	21.86
273.172355	273.185455	0.60	47.95

Z=-12

Reference *m/z*	**Experimental *m/z***	**Relative abundance (%)**	**Error [ppm]**
229.131453	229.122855	32.80	37.53
243.133245	243.138505	1.30	21.63

271.185313	271.169805	1.18	57.19
299.212543	299.201105	1.55	38.23

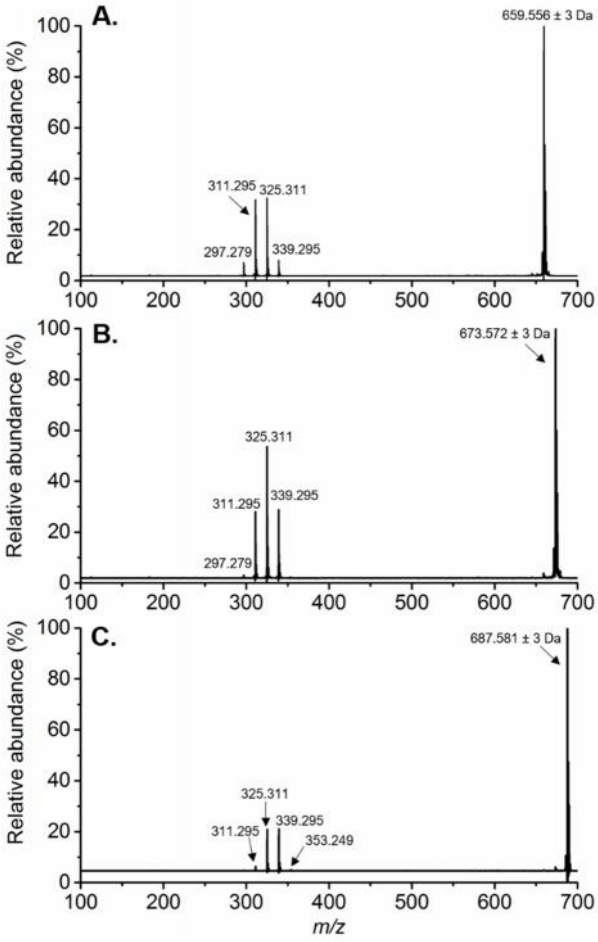

Figure A3. MALDI-TOF-CID tandem mass spectra of NAs dimers detected with 9-AA at *m/z* A) 659.556, B) 673.572, C) 687.581.

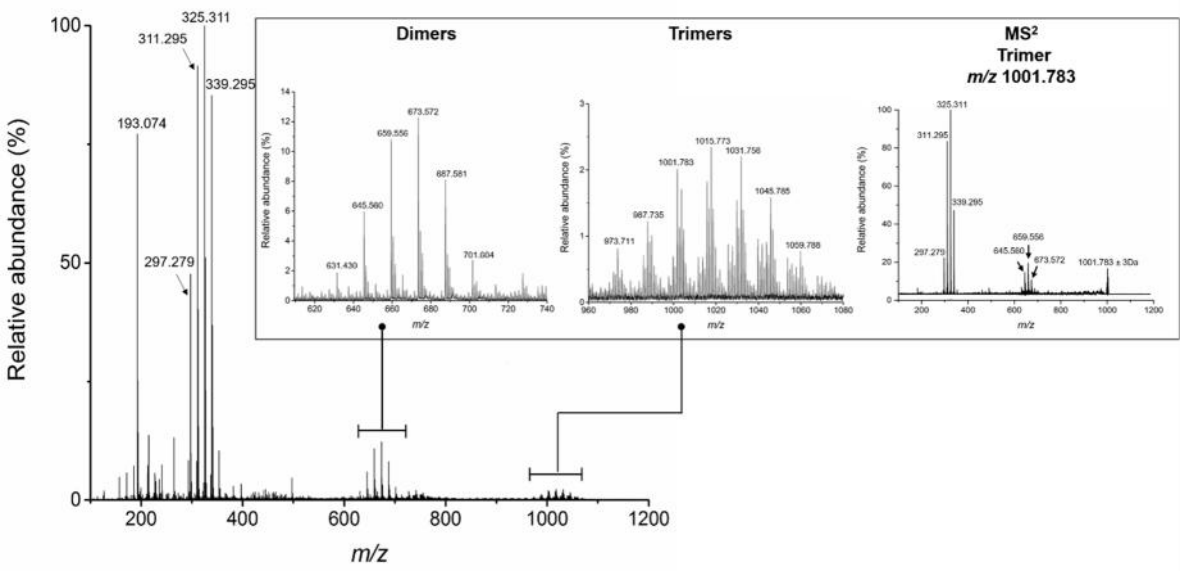

Figure A4. MALDI-TOF/MS mass spectrum of NAs dimers detected with 9-AA at an equimolar mixture (2mM-2mM) using a laser fluence of 50% (2.85 µJ/pulse). Inset graph shows the CID mass spectrum of the trimer with m/z 1001.783.

Appendix B. Molecular characterization of naphthenic acids from heavy crude oils using MALDI FT-ICR mass spectrometry

Table B1. *SPE protocol used to isolate naphthenic acids from a heavy crude oil. DCM: Dichloromethane; MeOH (Methanol); Formic acid (FA); H_2O (water).*

Solvent systems	Elution volume (ml)	Solvent composition % v/v	Species eluted
DCM	30	100	Non-acidic species/interferences
DCM/MeOH	15	50/50	Non-acidic species
MeOH	15	100	Non-acidic species
MeOH/H_2O	15	67/33	Non-acidic species
MeOH/ H_2O/FA	15	67.3/27.3/5	NA fraction 1
MeOH/ H_2O/FA	15	77.3/17.3/5	NA fraction 2
MeOH/ H_2O/FA	15	87.3/7.3/5	NA fraction 3
MeOH/FA	15	95/5	NA fraction 4
DCM/MeOH/FA	15	5/90/5	NA fraction 5
DCM/MeOH/FA	15	17.3/77.3/5	NA fraction 6

Table B2. *Homologous series of deprotonated molecules from O_2 class used to calibrate internally the mass spectra in negative ion mode.*

FRACTION 1				
Calibration list: **$C_xH_yO_2$ DBE 5.5**				
Calibration mode: **Quadratic**				
Standard deviation: **0.054**				
Formula	**Ref. Mass**	**Exp. Mass**	**Error [ppm]**	**Abundance**
C30H52O2	443.389454	443.318666	0.016	16913550
C30H52O2	443.389454	443.318666	0.016	16913550
C31H54O2	457.405105	457.334369	-0.024	18134248
C31H54O2	457.405105	457.334369	-0.024	18134248
C32H56O2	471.420755	471.350102	0.004	16375087
C32H56O2	471.420755	471.350102	0.004	16375087
C33H58O2	485.436405	485.365827	0.014	19326230
C34H60O2	499.452055	499.381530	-0.020	13970508
C35H62O2	513.467705	513.397250	-0.019	12870276
C36H64O2	527.483355	527.413005	0.048	9826220
C37H66O2	541.499005	541.428698	-0.002	4824090
C38H68O2	555.514655	555.444440	0.038	4722732
C39H70O2	569.530305	569.460133	-0.008	4479042
C40H72O2	583.545955	583.475804	-0.091	3098812
C41H74O2	597.561605	597.491515	-0.101	3305978
C42H76O2	611.577255	611.507364	0.114	3583026

C43H78O2	625.592905	625.523004	-0.013	4004658
C44H80O2	639.608555	639.538783	0.082	4065973
C45H82O2	653.624205	653.554458	0.014	5534328
C46H84O2	667.639855	667.570159	-0.012	6320694
C47H86O2	681.655506	681.585830	-0.081	5116331
C48H88O2	695.671156	695.601635	0.046	5036207
C49H90O2	709.686806	709.617361	0.058	5701511
C50H92O2	723.702456	723.632987	-0.070	7171729
C51H94O2	737.718106	737.648800	0.062	5064240
C52H96O2	751.733756	751.664477	0.008	4929217
C53H98O2	765.749406	765.680141	-0.061	4404390
		FRACTION 2		
Calibration list: **$C_xH_yO_2$ DBE 5.5**				
Calibration mode: **Linear**				
Standard deviation: **0.014**				
C33H58O2	485.436405	485.436405	-0.023	13210506
C32H56O2	471.420755	471.422712	0.006	14368666
C32H56O2	471.420755	471.422712	0.006	14368666
C31H54O2	457.405105	457.406995	-0.012	25693760
C31H54O2	457.405105	457.406995	-0.012	25693760
C30H52O2	443.389454	443.391297	0.016	32818874
C30H52O2	443.389454	443.391297	0.016	32818874
C29H50O2	429.373804	429.375584	0.008	35728460
C28H48O2	415.358154	415.359872	0.005	40668728

C27H46O2	401.342504	401.344161	0.008	39906508
C26H44O2	387.326854	387.328435	-0.029	29929966
C25H42O2	373.311204	373.312735	0.003	16650668
C24H40O2	359.295554	359.297023	0.008	5563981
C23H38O2	345.279904	345.281308	0.007	2352378
C22H36O2	331.264254	331.265587	-0.009	1132757

FRACTION 3

Calibration list: **$C_xH_yO_2$ DBE 6.5**

Calibration mode: **Linear**

Standard deviation: **0.008**

C27H44O2	399.326854	399.328498	-0.000	2753614
C28H46O2	413.342504	413.343209	-0.002	5467929
C29H48O2	427.358154	427.359919	0.000	13511725
C30H50O2	441.373804	441.375625	-0.000	15316780
C31H52O2	455.389454	455.391337	0.015	20014008
C32H54O2	469.405105	469.407028	-0.012	17554182
C33H56O2	483.420755	483.422732	-0.004	17656000
C34H58O2	497.436405	497.438430	-0.003	12485072
C35H60O2	511.452055	511.454130	0.004	10671409
C36H62O2	525.467705	525.469822	0.001	7479256

FRACTION 4

Calibration list: **$C_xH_yO_2$ DBE 5.5**

Calibration mode: **Linear**

Standard deviation: **0.038**				
C28H48O2	415.358154	415.359780	-0.062	489417
C29H50O2	429.373804	429.375534	0.068	1007166
C30H52O2	443.389454	443.391208	0.009	2189018
C30H52O2	443.389454	443.391208	0.009	2189018
C31H54O2	457.405105	457.406895	-0.016	3941784
C31H54O2	457.405105	457.406895	-0.016	3941784
C32H56O2	471.430755	471.422612	0.029	3567942
C32H56O2	471.430755	471.422612	0.029	3567942
C33H58O2	485.436405	485.438274	-0.042	4124048
C34H60O2	499.452055	499.453995	0.015	4228721
C35H62O2	513.467705	513.469675	-0.010	4769620
C36H64O2	527.483355	527.485362	-0.017	4118978
C37H66O2	541.499005	541.501038	-0.041	2754884
C38H6802	555.514655	555.516782	0.061	1698404
C39H70O2	569.530305	569.532426	-0.017	1856793
		FRACTION 5		
Calibration list: **$C_xH_yO_2$ DBE 5.5**				
Calibration mode: **Linear**				
Standard deviation: **0.069**				
C56H104O2	807.796356	807.798934	0.012	1126378
C55H102O2	793.780706	793.783280	0.028	768574
C54H100O2	779.765056	779.767553	-0.048	1631577
C53H98O2	765.749406	765.751807	-0.151	2062394

C52H96O2	751.733756	751.736244	-0.010	2131653
C51H94O2	737.718106	737.720644	0.084	2008775
C50H92O2	723.702456	723.705002	0.128	2779273
C49H90O2	709.686806	709.689193	-0.059	2643669
C48H88O2	695.671156	695.673506	-0.078	3521665
C47H86O2	681.655506	681.657890	0.008	4288948
C46H84O2	667.639855	667.642258	0.077	4888629
C45H82O2	653.624205	653.626577	0.076	5704657
C44H80O2	639.608555	639.610839	-0.013	5016404
C43H78O2	625.592905	625.595179	0.020	6311540
C42H76O2	611.577255	611.579460	-0.039	6870752
C41H74O2	597.561605	597.563806	0.009	7866513
C40H72O2	583.545955	583.548117	0.004	7618691
C39H70O2	569.530305	569.532395	-0.059	8601260
C38H68O2	555.514655	555.516765	0.042	6581807
C37H66O2	541.499005	541.501001	-0.096	4554545
C36H64O2	527.483355	527.485399	0.069	6061044
C35H62O2	513.467705	513.469668	-0.006	3668029

FRACTION 6

Calibration list: **$C_xH_yO_2$ DBE 5.5**

Calibration mode: **Linear**

Standard deviation: **0.071**

C32H56O2	471.420755	471.422786	-0.069	5602400
C32H56O2	471.420755	471.422786	-0.069	5602400

C33H58O2	485.436405	485.438497	-0.036	6088114
C34H60O2	499.452055	499.454237	0.056	6370980
C35H62O2	513.467705	513.469902	0.000	7221770
C36H64O2	527.483355	527.485617	0.047	6767106
C37H66O2	541.499005	541.501321	0.072	6742642
C38H68O2	555.514655	555.516930	-0.072	6701890
C39H70O2	569.530305	569.532699	0.076	9264215
C40H72O2	583.545955	583.548419	0.134	6690202
C41H74O2	597.561605	597.564081	0.096	7624449
C42H76O2	611.577255	611.579744	0.064	7278759
C43H78O2	625.592905	625.595410	0.041	6361768
C44H80O2	639.608555	639.611020	-0.066	5676321
C45H82O2	653.624205	653.626709	-0.046	6713390
C46H84O2	667.639855	667.642399	-0.022	7139307
C47H86O2	681.655506	681.658144	0.081	4815424
C48H88O2	695.671156	695.673802	0.061	4559592
C49H90O2	709.686806	709.689385	-0.063	6046111
C50H92O2	723.702456	723.705056	-0.059	7175711
C51H94O2	737.718106	737.720686	-0.107	8849954
C52H96O2	751.733756	751.736398	-0.043	9621876
C53H98O2	765.749406	765.752049	-0.059	12957769
C54H100O2	779.765056	779.767668	-0.113	17164038
C55H102O2	793.780706	793.783333	-0.105	22736396
C56H104O2	807.796356	807.799013	-0.077	31745470
C57H106O2	821.812006	821.814673	-0.072	33754752

C56H104O2	807.796356	807.799013	-0.077	31745470
C57H106O2	821.822006	821.814673	-0.071	33754752
C58H108O2	835.827656	835.830343	-0.054	36632724
C59H110O2	849.843306	849.846066	0.028	32252900
C60H112O2	863.858956	863.861685	-0.011	38219856
C61H114O2	877.874606	877.877354	0.011	44293556
C62H116O2	891.890257	891.893022	0.030	39300076
C63H118O2	905.905907	905.908698	0.061	33290966
C64H120O2	919.921557	919.924401	0.122	27478574
C65H122O2	933.937207	933.939961	0.030	21408144
C66H124O2	947.952857	947.955636	0.064	21309586
C67H128O2	961.968507	961.971288	0.074	20334284

Table B3. *Review of the heteroatom classes in naphthenic acids detected in crude oils, oil sands processed water, bitumen, interfacial materials and naphthenates.*

Ionization source	Mass analyzer	Sample	Compound classes	Reference
ESI (-)	9.4 T FT ICR	Crude oil	O_1, O_2, O_1S_1, O_2S_1, O_3S_1, O_3S_2, O_4S_1, N_1, N_1S_1, N_1S_2, N_1O_2.	Energy & Fuels **2009**, 23, 1269–1279
		Acid extracts	O_2, O_3, O_4, N_1, N_1S_1, N_1O_2	
		Interfacial material	O_2, O_3, O_4, O_3S_1, O_3S_2, O_4S_1.	
ESI (-)	12 T FT ICR	Oil sands processed water (OSPW)	O_2, O_2S, O_2S_2	Anal. Chem. **2010**, 82, 3727–3735
ESI (-)	9.4 T FT ICR	Crude oil and bitumen	N_1, N_1O_1, N_1O_2, N_1S_1, N_2, O_1, O_1S_1, O_2, O_2S_1, O_2S_2, O_3, O_3S_1, O_3S_2, O_4, O_4S_1	Int J Mass Spectrom. **2011**, 300, 149–57

		Acids isolated form Sodium naphthenates	O_2	
ESI (-)	9.4 T FT ICR	Crude oil and their NA extracts	N_1, N_1O_2, O_2	Fuel **2013**, 108, 647–655
ESI (-)	LTQ Orbitrap	Oil sands processed water (OSPW)	O_2, O_2S, O_3, O_4, O_4S, O_5, O_6	Int J Mass Spectrom. **2013** (345-347), 104-108
ESI (-)	9.4 T FT ICR	NAs extracts isolated from bitumen	O_2, O_3, O_4, O_2S, O_3S, O_2S_2, O_3S_2	Energy & Fuels **2014**, 28, 5043−5048
ESI (-)	7.2 T FT ICR	Interfacial material from waxy crude oil emulsions	N, N_2, NO, NO_2, NO_3, NS, O, O_2, O_3, O_3S, O_4S	*Energy & Fuels*, **2014**, 28 (12), 7352–7358
ESI (-)	DMS-qToF	Oil sands processed water (OSPW)	O_2, O_4, O_7, O_8, N_1O_5, O_2S, O_5S_1, O_8S_1, O_2S_2	Environ. Sci. Technol. **2014**, 48, 10264−10272
ESI (-)	9.4 T FT-ICR	Interfacial material	O_2, O_2S_1, O_2S_2, O_2S_3, O_3, O_3S_1, O_3S_2, O_3S_3, O_4, O_4S_1, O_4S_2, O_4S_3, O_5, O_5S_1, O_5S_2, O_5S_3, O_6S_1, O_6S_2, N_1O_2, $N_1O_2S_1$, N_1O_3, N_1O_4	Energy Fuels **2017**, 31, 5933−5939
APPI (-)	12 T FT ICR	Oil sands processed water (OSPW)	N, S, O_2, O_2S, O_2S_2, NO_2	Anal. Chem. **2010**, 82, 3727–3735
LDI (-) Laser Nd:YAG (355 nm)	12 T FT ICR	Crude oils	N_1, H_1C_1, S_1, N_1S_1, O_1, O_2	Anal. Chem. **2012**, 84, 8587−8594
APPI (-)	9.4 T FT ICR	Oil sands processed water (OSPW)	O_1, O_2, O_3, O_4, O_5, O_6, O_7, O_2S_1, O_3S_1, O_4S_1, N_1O_2, N_1O_3, N_1O_4, N_1O_5	Energy & Fuels **2014**, 28, 1611−1616

APPI (-)	12 T FT ICR	Oil sands processed water (OSPW)	O_2, O_3, O_4, O_5, O_6, O_7, O_8, O_9, O_{10}, O_{11}, O_2S_1, O_3S_1, O_4S_1, O_5S_1, O_6S_1, O_7S_1, O_8S_1, N_1O_3, N_1O_4, N_1O_5, N_1O_6, NO_7.	Energy Fuels **2016**, 30, 3615−3621

Table B4. *Number of molecular formulas ($C_cH_hN_nO_oS_s$) assigned as radical, deprotonated or both type of ions by MALDI FT-ICR. ND=not detected.*

	Number of formulas $C_cH_hO_o$	Percentage %	Total formulas
	F1		
Only Radical ions	171	6.33	2700
Only Deprotonated ions	1207	44.70	
Both	1322	48.96	
	F2		
Only Radical ions	204	6.62	3080
Only Deprotonated ions	1269	41.20	
Both	1607	52.17	
	F3		
Only Radical ions	164	4.92	3335
Only Deprotonated ions	1553	46.57	
Both	1618	48.52	
	F4		
Only Radical ions	222	5.11	4339
Only Deprotonated ions	1963	42.24	
Both	2154	46.64	

F5			
Only Radical ions	262	4.62	5665
Only Deprotonated ions	3002	52.99	
Both	2401	42.38	
F6			
Only Radical ions	58	2.92	1988
Only Deprotonated ions	1905	95.82	
Both	25	1.26	

Table B5. *Number of molecular formulas ($C_cH_hN_nO_oS_s$) assigned as radical, deprotonated or both type of ions by MALDI FT-ICR. ND=not detected.*

MALDI				
Oo Classes				
O_1				
N° Fraction	$[M - H]^-$	$[M]^{\cdot -}$	$[M - H]^-$ and $[M]^{\cdot -}$	Total
1	230	ND	-	230
O_2				
N° Fraction	$[M - H]^-$	$[M]^{\cdot -}$	$[M - H]^-$ and $[M]^{\cdot -}$	Total
1	200	19	165	384
2	288	20	247	555
3	346	25	287	658
4	510	31	317	858
5	911	43	394	1348
6	498	ND	-	498
O_3				
N° Fraction	$[M - H]^-$	$[M]^{\cdot -}$	$[M - H]^-$ and	Total

			[M]$^{\cdot-}$	
1	224	50	223	497
2	217	32	338	587
3	341	45	347	733
4	337	44	464	845
5	627	59	544	1230
6	421	58	25	504
		O_4		
N° Fraction	[M - H]$^-$	[M]$^{\cdot-}$	[M - H]$^-$ and [M]$^{\cdot-}$	Total
1	267	35	291	593
2	285	60	372	717
3	337	44	378	759
4	417	44	504	965
5	739	62	564	1365
6	464	ND	-	464
		O_5		
N° Fraction	[M - H]$^-$	[M]$^{\cdot-}$	[M - H]$^-$ and [M]$^{\cdot-}$	Total
1	259	30	324	613
2	211	44	362	617
3	266	23	359	648
4	330	52	494	876
5	394	44	564	1002
6	338	ND	-	338
		O_6		
N° Fraction	[M - H]$^-$	[M]$^{\cdot-}$	[M - H]$^-$ and [M]$^{\cdot-}$	Total
1	257	37	319	613
2	218	48	288	554
3	263	27	247	537
4	369	51	375	795
5	331	54	335	720
6	184	ND	-	184
		O_7		
N° Fraction	[M - H]$^-$	[M]$^{\cdot-}$	[M - H]$^-$ and [M]$^{\cdot-}$	Total
1	257	36	271	564
2	188	49	149	386
3	ND	130	-	130

4	464	ND	-	464
		O_8		
N° Fraction	$[M - H]^-$	$[M]^{\cdot -}$	$[M - H]^-$ and $[M]^{\cdot -}$	Total
1	217	47	217	481
5	213	ND	-	213
		O_9		
N° Fraction	$[M - H]^-$	$[M]^{\cdot -}$	$[M - H]^-$ and $[M]^{\cdot -}$	Total
1	341	ND	-	341
		O_{11}		
N° Fraction	$[M - H]^-$	$[M]^{\cdot -}$	$[M - H]^-$ and $[M]^{\cdot -}$	Total
5	ND	499	-	499
		N_nO_o Classes		
		N_1O_1		
N° Fraction	$[M - H]^-$	$[M]^{\cdot -}$	$[M - H]^-$ and $[M]^{\cdot -}$	Total
5	628	0	0	628
		N_1O_2		
N° Fraction	$[M - H]^-$	$[M]^{\cdot -}$	$[M - H]^-$ and $[M]^{\cdot -}$	Total
4	601	0	0	601
5	1008	0	0	1008
		N_1O_3		
N° Fraction	$[M - H]^-$	$[M]^{\cdot -}$	$[M - H]^-$ and $[M]^{\cdot -}$	Total
2	465	0	0	465
4	813	0	0	813
5	1166	0	0	1166
		N_1O_4		
N° Fraction	$[M - H]^-$	$[M]^{\cdot -}$	$[M - H]^-$ and $[M]^{\cdot -}$	Total
1	276	54	235	565
2	227	34	271	532
3	656	0	0	656
4	824	0	0	824
5	500	48	687	1235

N_1O_5				
N° Fraction	$[M - H]^-$	$[M]^{\cdot -}$	$[M - H]^-$ and $[M]^{\cdot -}$	Total
1	244	46	280	570
2	251	23	195	469
3	539	0	0	539
4	335	24	439	798
5	1053	0	0	1053
N_1O_6				
N° Fraction	$[M - H]^-$	$[M]^{\cdot -}$	$[M - H]^-$ and $[M]^{\cdot -}$	Total
1	228	48	259	535
N_1O_7				
N° Fraction	$[M - H]^-$	$[M]^{\cdot -}$	$[M - H]^-$ and $[M]^{\cdot -}$	Total
1	236	51	185	472
4	460	0	0	460
N_1O_8				
N° Fraction	$[M - H]^-$	$[M]^{\cdot -}$	$[M - H]^-$ and $[M]^{\cdot -}$	Total MALDI
1	329	0	0	329
O_0S_5				
O_2S_1				
N° Fraction	$[M - H]^-$	$[M]^{\cdot -}$	$[M - H]^-$ and $[M]^{\cdot -}$	Total
2	315	0	0	315
O_3S_1				
N° Fraction	$[M - H]^-$	$[M]^{\cdot -}$	$[M - H]^-$ and $[M]^{\cdot -}$	Total
1	296	0	0	296
2	412	0	0	412
O_4S_1				
N° Fraction	$[M - H]^-$	$[M]^{\cdot -}$	$[M - H]^-$ and $[M]^{\cdot -}$	Total
1	216	50	135	401
2	454	0	0	454
3	470	0	0	470
4	712	0	0	712

O_5S_1				
N° Fraction	$[M - H]^-$	$[M]^{\cdot -}$	$[M - H]^-$ and $[M]^{\cdot -}$	Total
2	329	0	0	329
4	667	0	0	667

Table B6. *Comparison between the number of molecular formulas ($C_cH_hO_o$) assigned by MALDI and ESI FT-ICR. ND=not detected.*

O_2								
	MALDI				**MALDI Vs ESI**			
N° Fraction	**$[M - H]^-$**	**$[M]^{\cdot -}$**	**$[M - H]^-$ and $[M]^{\cdot -}$**	**Total MALDI**	**Total ESI**	**Only ESI**	**ESI and MALDI**	**Only MALDI**
1	200	19	165	384	257	41	216	168
2	288	20	247	555	258	0	258	297
3	346	25	287	658	151	0	151	507
4	510	31	317	858	186	0	186	672
5	911	43	394	1348	283	0	283	1065
6	498	ND	-	498	717	292	425	73
O_3								
	MALDI				**MALDI Vs ESI**			
N° Fraction	**$[M - H]^-$**	**$[M]^{\cdot -}$**	**$[M - H]^-$ and $[M]^{\cdot -}$**	**Total MALDI**	**Total ESI**	**Only ESI**	**ESI and MALDI**	**Only MALDI**
1	224	50	223	497	214	14	200	297
2	217	32	338	587	207	10	197	390
3	341	45	347	733	ND	ND	-	733
4	337	44	464	845	75	0	75	770
5	627	59	544	1230	ND	ND	-	1230
6	421	58	25	504	ND	ND	-	504
O_4								
	MALDI				**MALDI Vs ESI**			
N° Fraction	**$[M - H]^-$**	**$[M]^{\cdot -}$**	**$[M - H]^-$ and $[M]^{\cdot -}$**	**Total MALDI**	**Total ESI**	**Only ESI**	**ESI and MALDI**	**Only MALDI**
1	267	35	291	593	407	134	273	320
2	285	60	372	717	185	0	185	532
3	337	44	378	759	51	0	51	708
4	417	44	504	965	98	0	98	867
5	739	62	564	1365	125	0	125	1240
6	464	ND	-	464	ND	ND	-	464

O_2S								
	MALDI					MALDI Vs ESI		
N° Fraction	**$[M - H]^-$**	**$[M]^{\cdot -}$**	**$[M - H]^-$ and $[M]^{\cdot -}$**	**Total MALDI**	**Total ESI**	**Only ESI**	**ESI and MALDI**	**Only MALDI**
1	ND	ND	-	-	150	150	-	-
2	315	ND	-	315	120	6	114	201
3	ND	ND	ND	ND	27	27	-	-
O_3S								
	MALDI					MALDI Vs ESI		
N° Fraction	**$[M - H]^-$**	**$[M]^{\cdot -}$**	**$[M - H]^-$ and $[M]^{\cdot -}$**	**Total MALDI**	**Total ESI**	**Only ESI**	**ESI and MALDI**	**Only MALDI**
1	296	ND	-	296	175	57	117	179
2	412	ND	-	412	ND	ND	-	412
N_1O_2								
	MALDI					MALDI Vs ESI		
N° Fraction	**$[M - H]^-$**	**$[M]^{\cdot -}$**	**$[M - H]^-$ and $[M]^{\cdot -}$**	**Total MALDI**	**Total ESI**	**Only ESI**	**ESI and MALDI**	**Only MALDI**
1	ND	ND	-	-	271	271	-	-
2	ND	ND	-	-	195	195	-	-
3	ND	ND	-	-	53	53	-	-
4	601	ND	-	601	95	0	95	506
5	1008	ND	-	1008	ND	-	-	1008

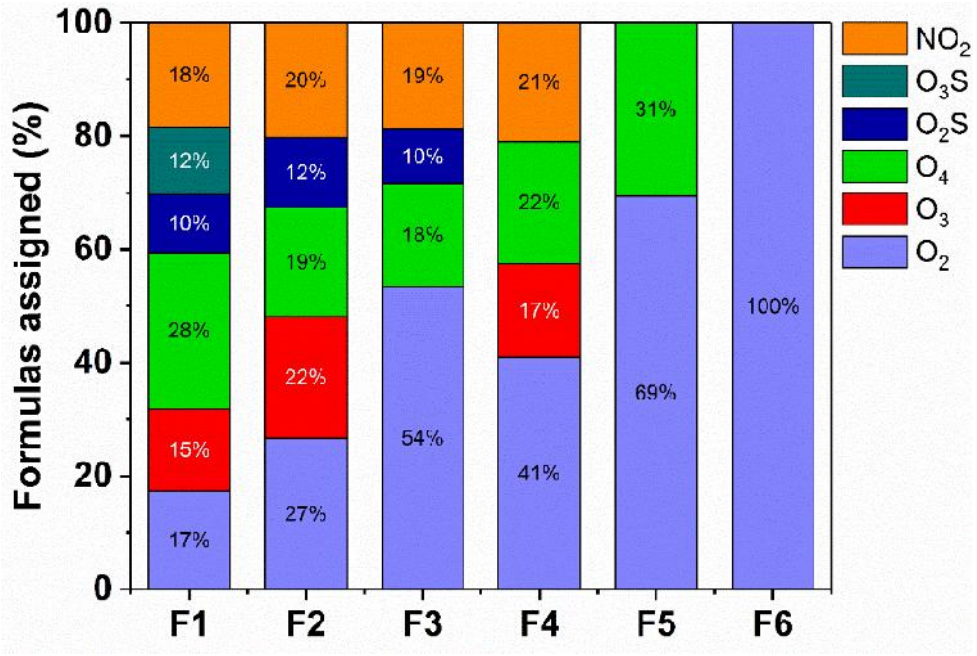

Figure B1. Percentage of molecular formulas assigned by compound classes in the acid fractions (F1-F6) by ESI FT-ICR/MS.

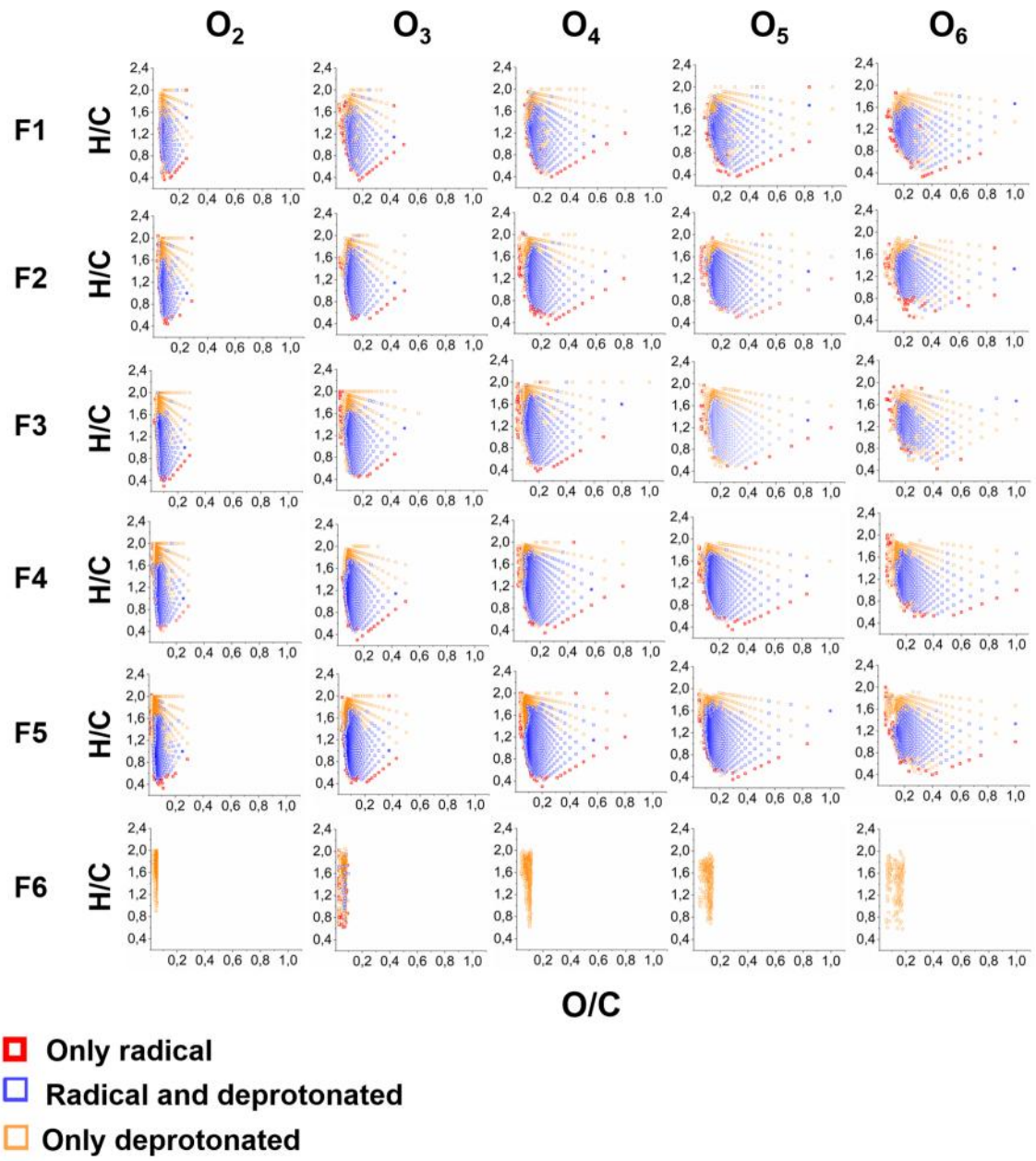

Figure B2. Van Krevelen plots corresponding to individual O_o (o=2-6) compound classes

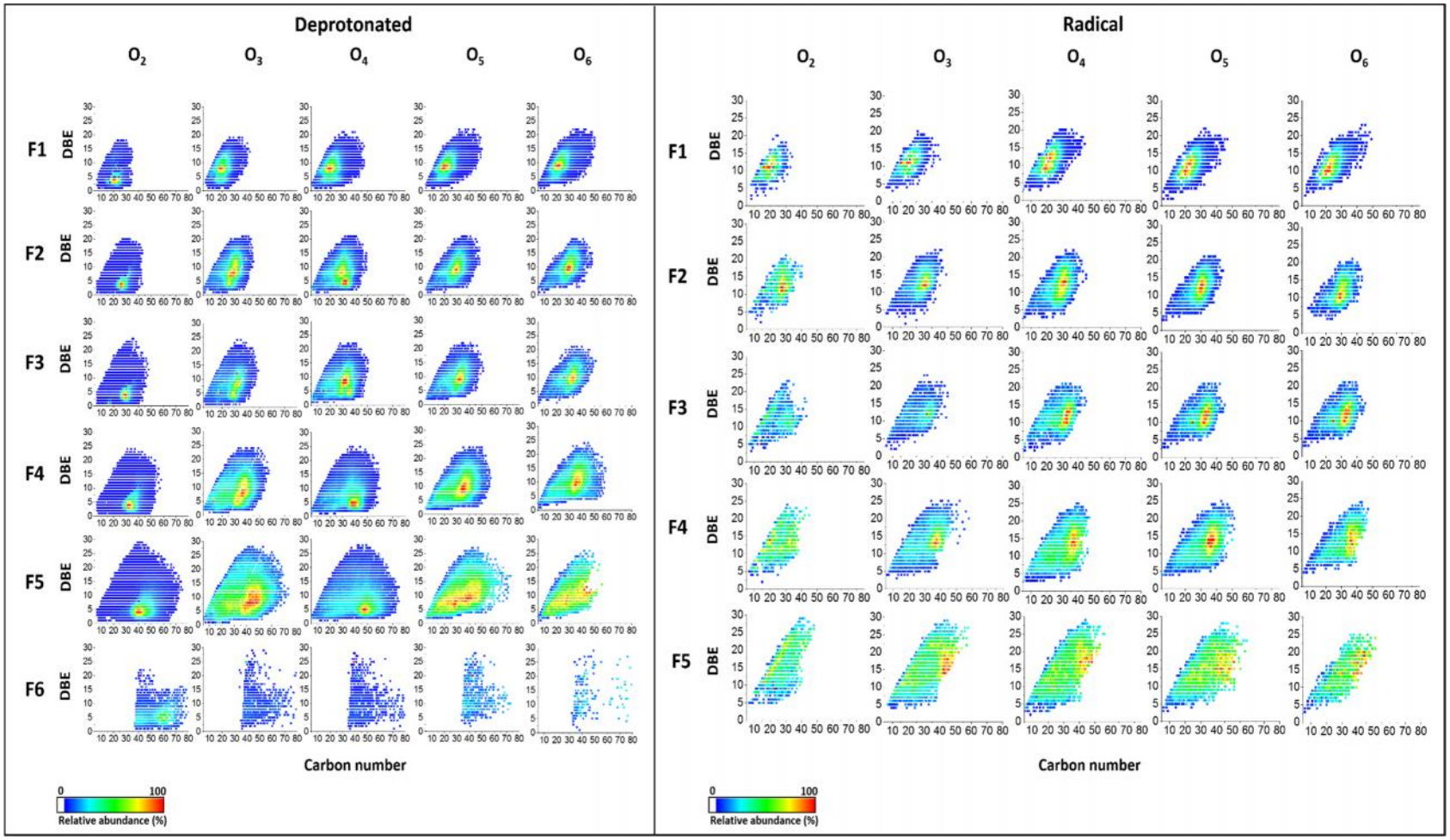

Figure B3. Neutral DBE vs carbon number diagrams for the oxygenated homologous series in fractions F1 to F6 (left – deprotonated molecules-, right –radical anions-)

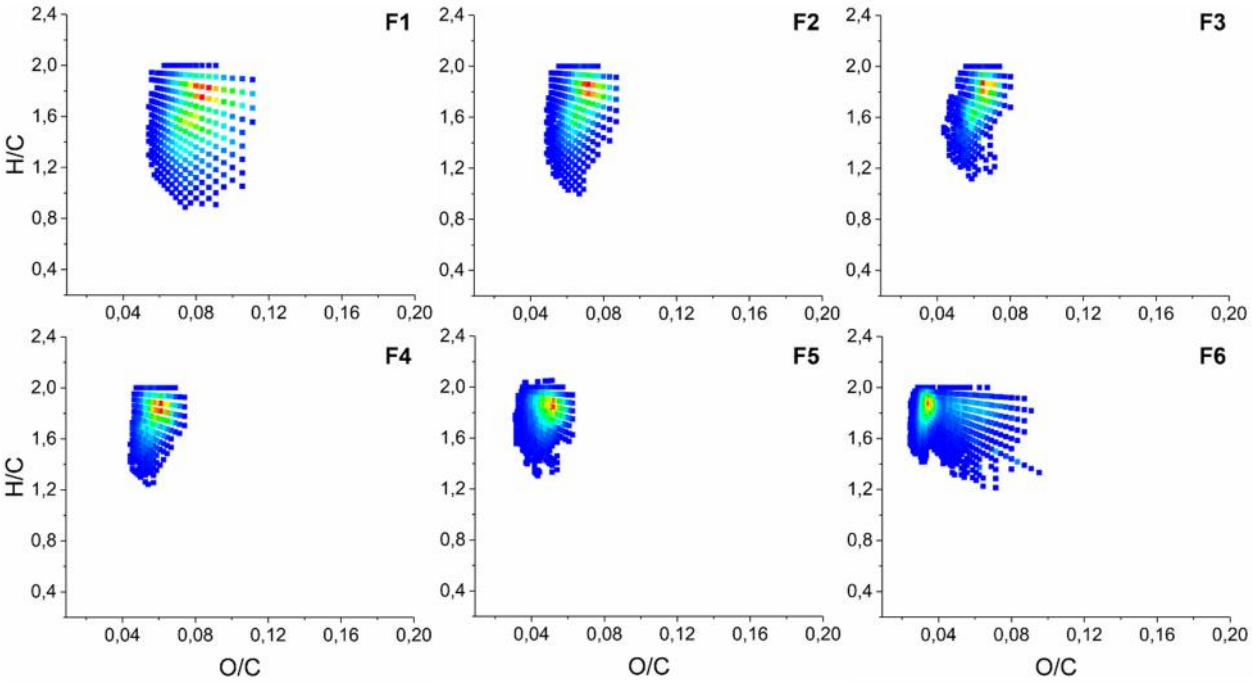

Figure B4. Van Krevelen diagrams of O_2 class detected for each fraction by ESI-FT ICR/MS

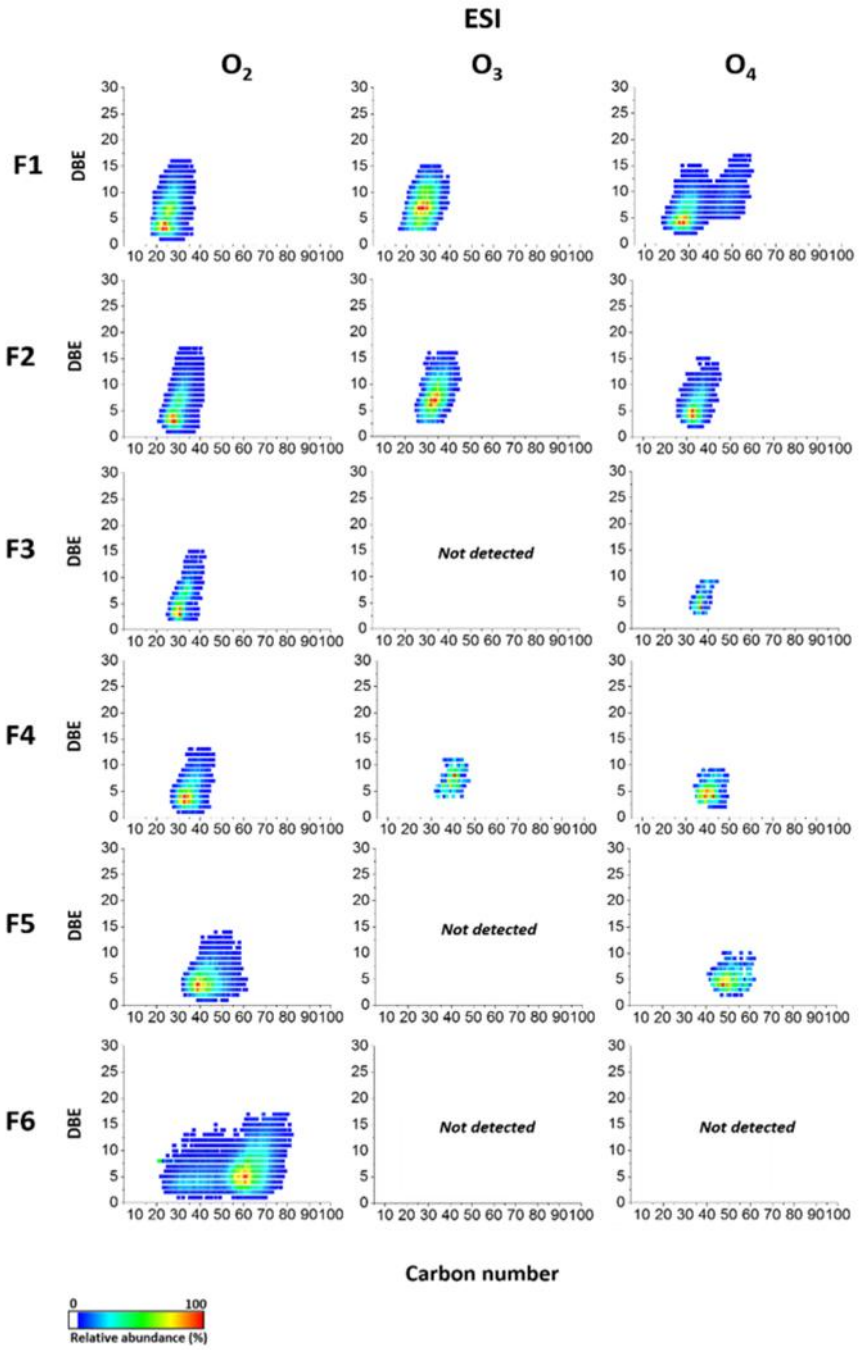

Figure B5. DBE *vs* carbon number contour plots for O_o (o=2-3) species detected by ESI FT-ICR MS.

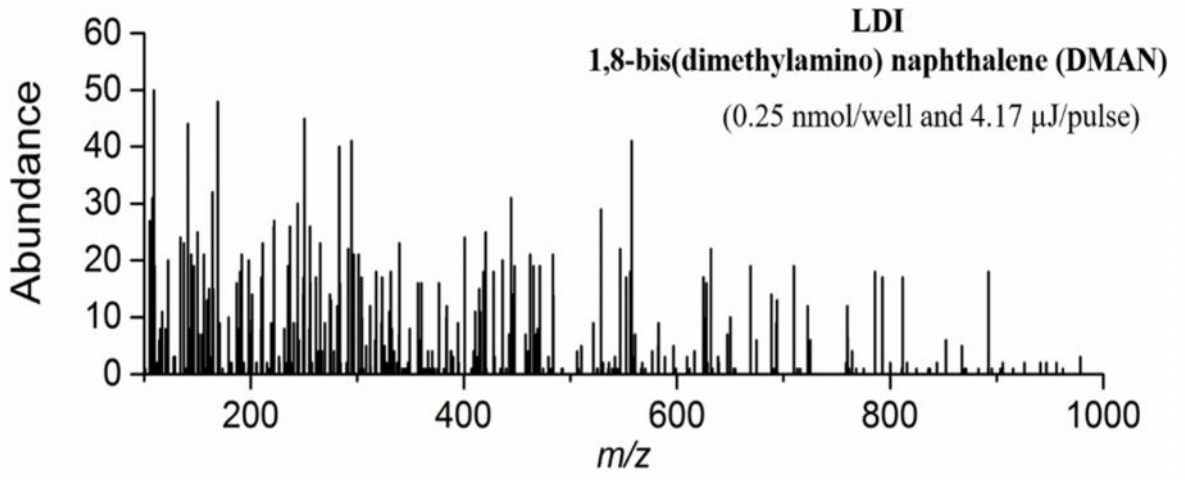

Figure B6. LDI-TOF mass spectrum of the DMAN matrix.

Appendix C. Influence of naphthenic acids in asphaltene heptol/water interfaces and emulsion stability

Interfacial material isolation:

Isolation of the interfacial material was performed by a procedure described by Zhenghe Xu et al(F. Yang et al., 2014) that involves cycles of centrifugation and washings with toluene to extract the most interfacially active compunds that stabilize emulsions. In summary, the prepared emulsion (settled for 1.5 h) with asphaltenes A at 10 g/L is subjected to centrifugation at 2500 rpm for 3 min. After this, the supernatant was removed and the interfacial material with the appearance of a viscous mud was deposited on the bottom of the container without free water observed. Then, the interfacial material was dissolved again in toluene, stirred manually and brought to centrifugation. Finally, the cycle is repeated washing again with toluene. A total of 15 cycles were completed until a colorless supernatant and an interfacial material without free water was observed. The interfacial material was subsequenly dry to remove the trapped water and leave the most interfacially active molecules.

Figures

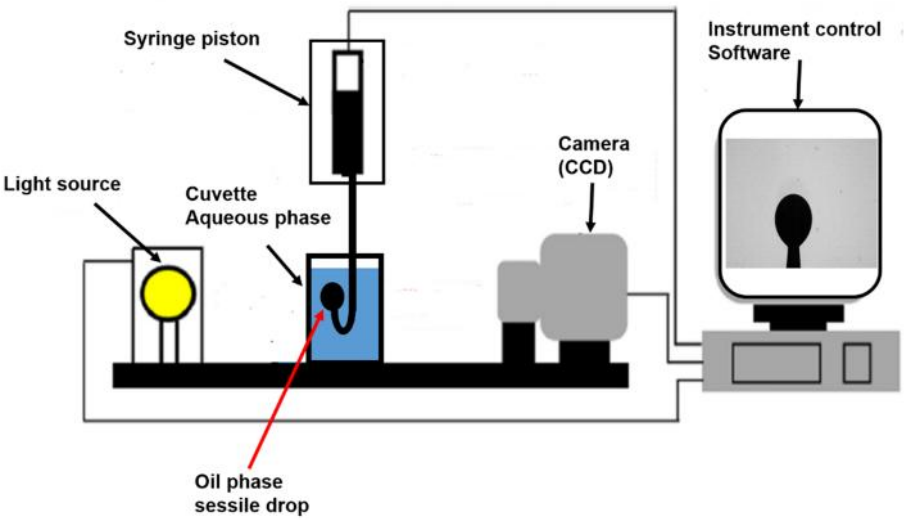

Figure C1. Drop shape analyzer (DSA) apparatus.

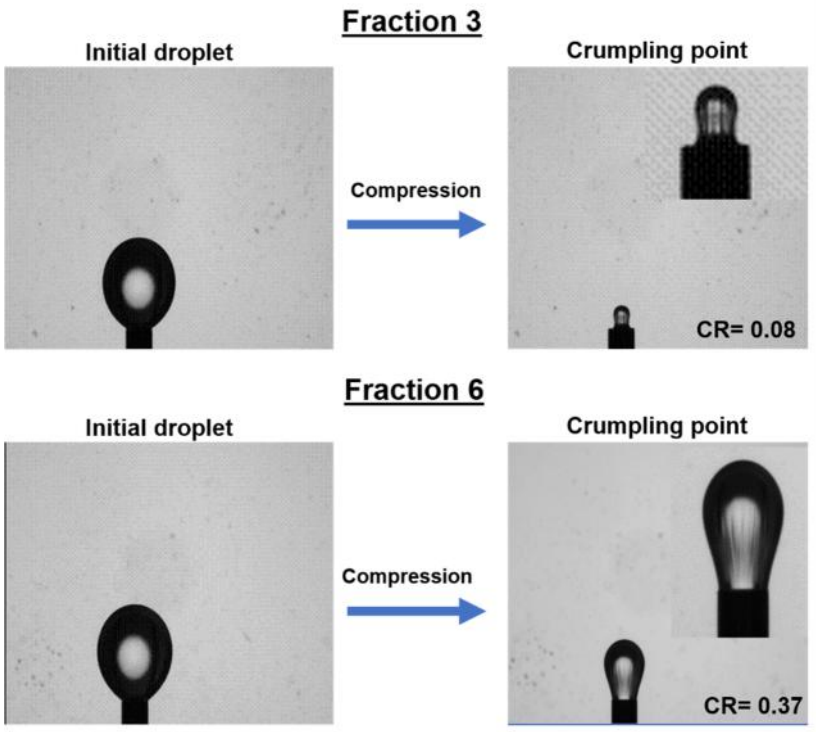

Figure C2. Oil droplets of fraction 3 and 6 (left side) are compressed until their corresponding crumpling points (right side). Inset graphs show magnification images of the oil droplets at the

crumpling points; wrinkles observed on the droplets are related with the formation of a skin that confers some type of elasticity to the films and CR is the crumpling ratio value.

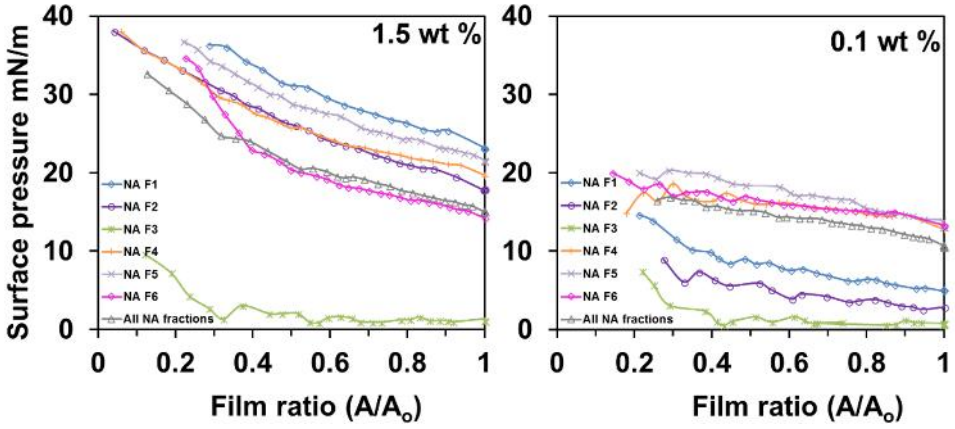

Figure C3. Surface pressure isotherms of naphthenic acids fractions at 1.5 and 0.1 wt %. All solutions were dissolved in heptol (25/75) and aged for 1 h.

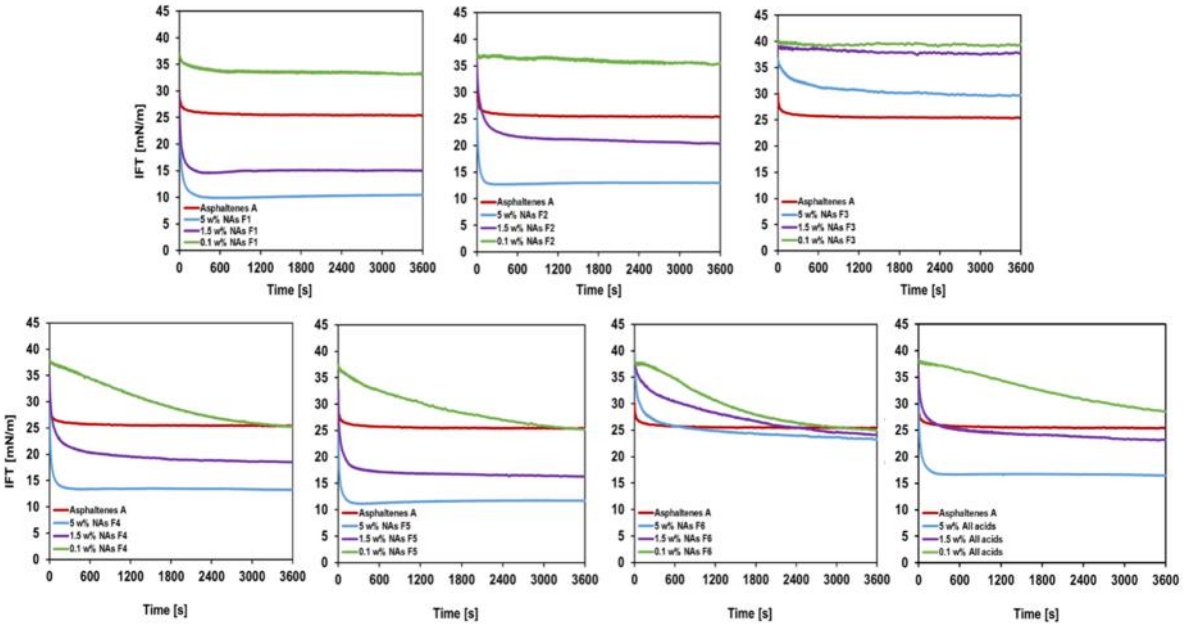

Figure C4. Dynamic Interfacial tension (IFT) for naphthenic acid fractions (1-6) at different concentrations (5 wt %, 1.5 wt %, 0.1 wt %) compared with the asphaltenes A. All samples were dissolved in heptol (25/75).

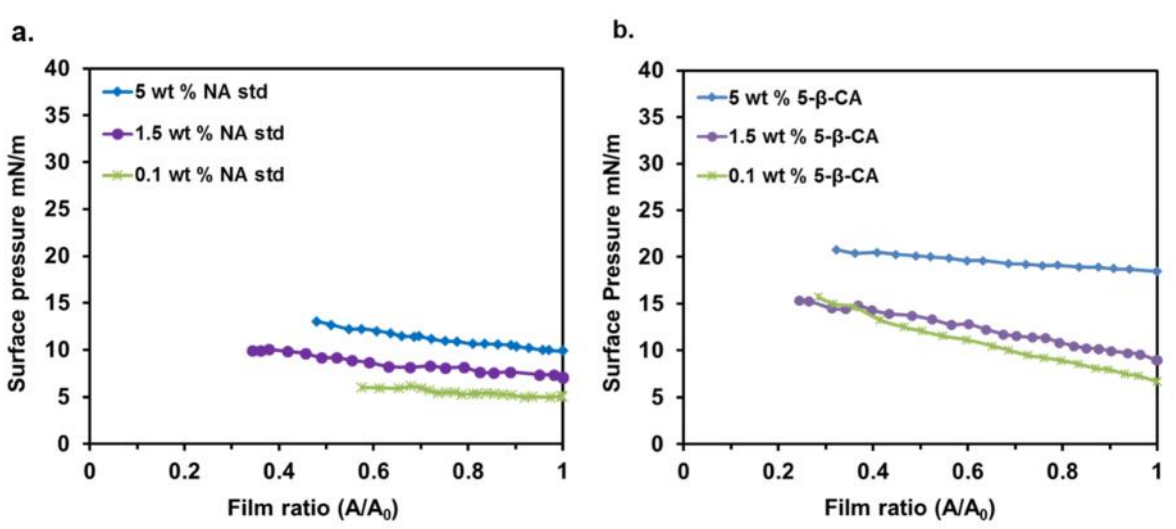

Figure C5. Surface pressure isotherms of a) naphthenic acid (NA) standard mixture and b) 5-β-cholanic acid (5-β-CA) at 5, 1.5 and 0.1 wt %.

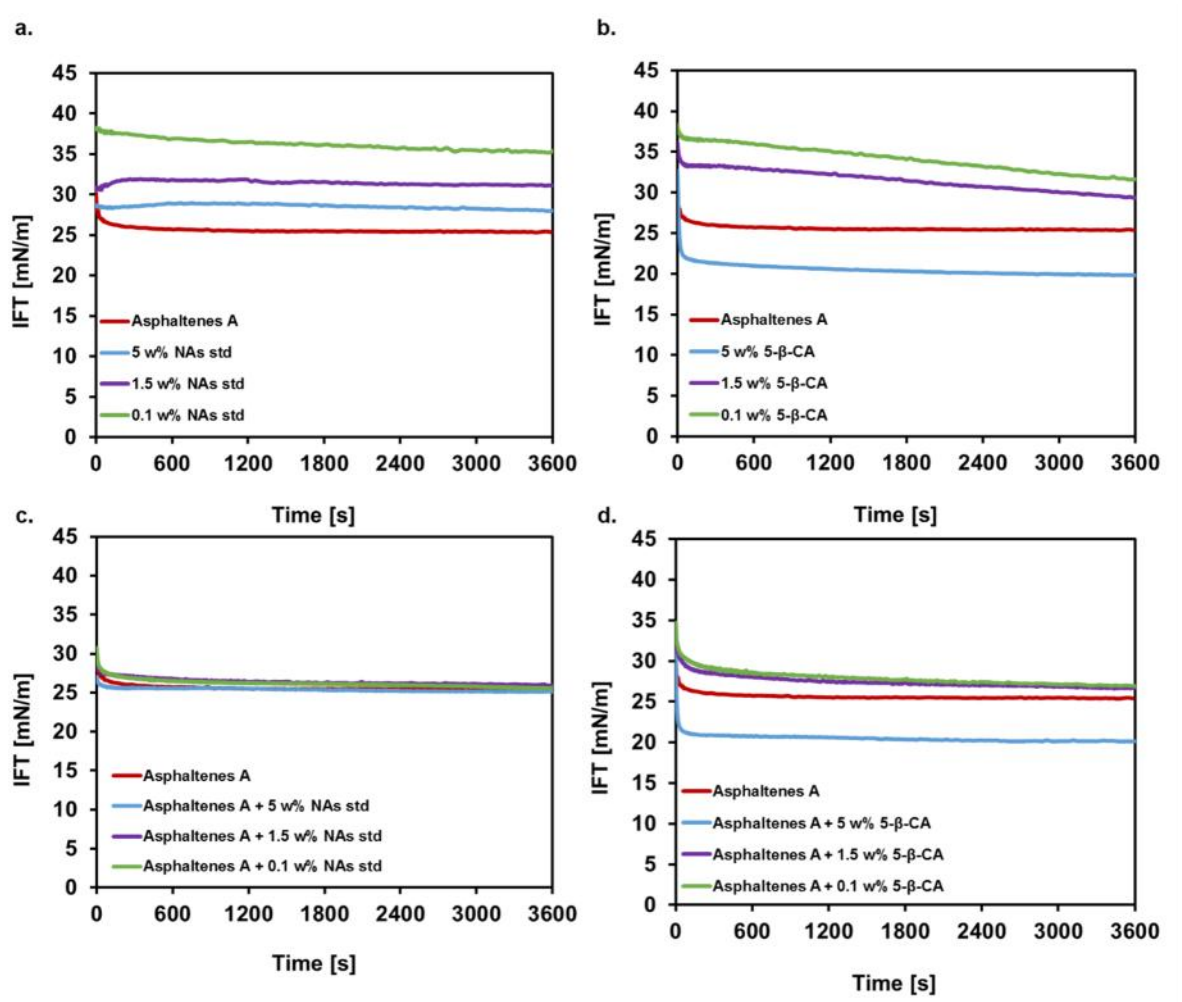

Figure C6. (Top) Interfacial tension measurements of naphthenic acid standard mixture and 5-β-Cholanic acid at 5, 1.5 and 0.1 wt % compared to the asphaltenes A (red trace) without any additives. (Bottom) c) Influence of NA standard mixture and d) 5-β-Cholanic acid on the asphaltenes A films. All samples were dissolved in heptol (25/75) and aged for 1 h.

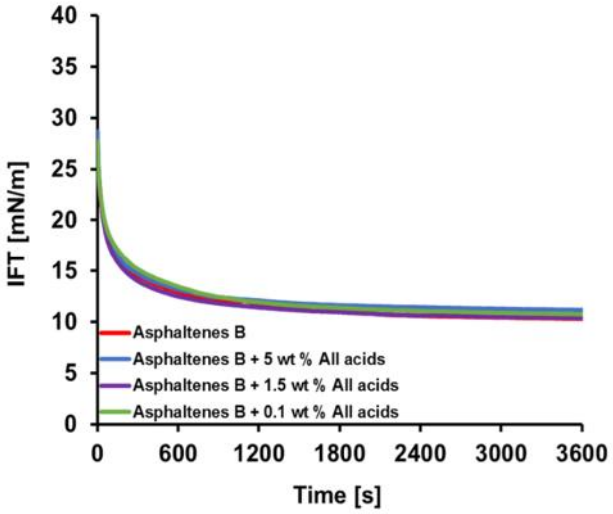

Figure C7. Dynamic IFT of asphaltenes B and the effect of F-all acids at 5, 1.5 and 0.1 wt%.

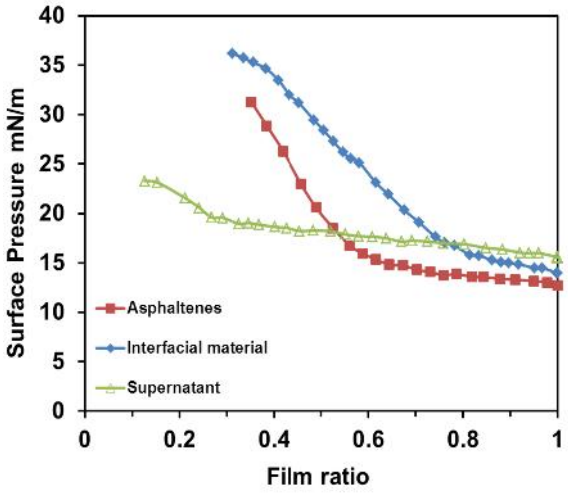

Figure C8. Surface pressure isotherms for the C_7 asphaltenes A (red trace), most adsorbed asphaltenes (blue trace) and the supernatant (green trace) solution isolated from an asphaltenes A-stabilized w/o emulsion. All samples were dissolved in heptol 25/75 at 10 g/L and aged for 1 hour.

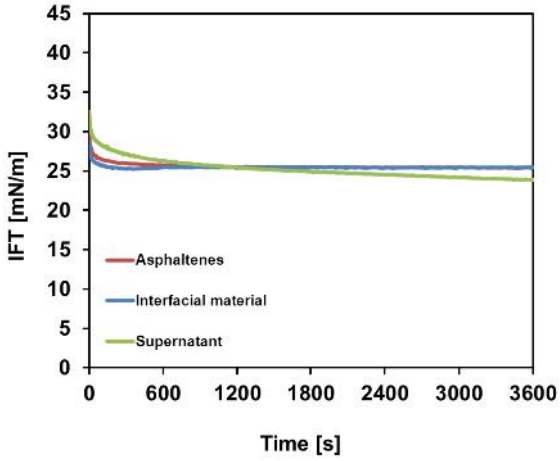

Figure C9. Interfacial tension of C_7 asphaltenes A (red), interfacial material (blue) or most adsorbed asphaltenes and supernatant (Green) isolated from an asphaltene A-stabilized w/o emulsion.

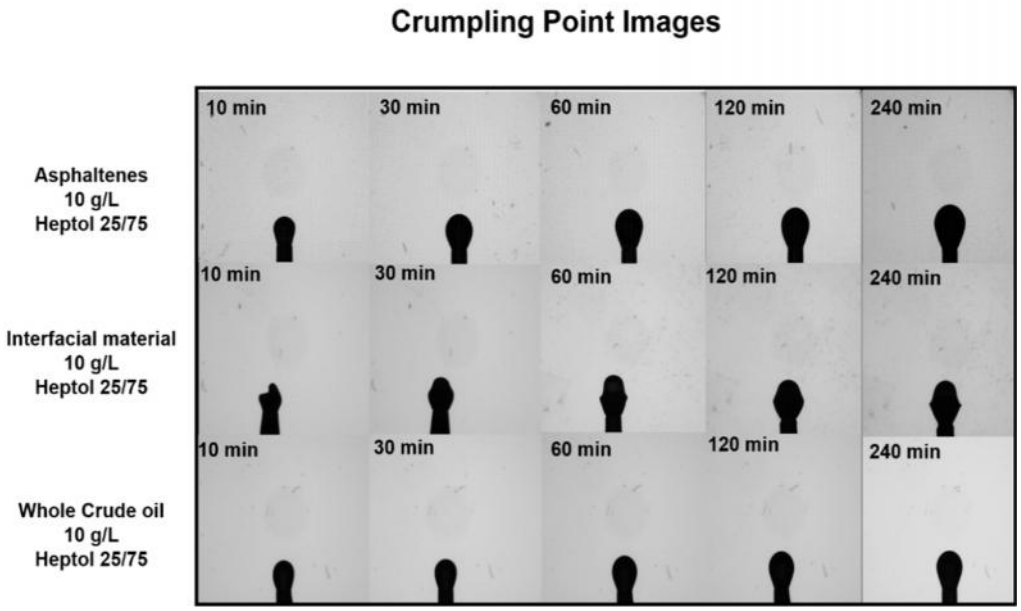

Figure C10. Images taken at the crumpling point by the drop shape analyzer for the fraction of asphaltenes, the most adsorbed asphaltenes isolated from an asphaltene A-stabilized emulsion the whole crude oil A. All samples were dissolved in heptol (25/75) at a concentration of 10 g/ L.

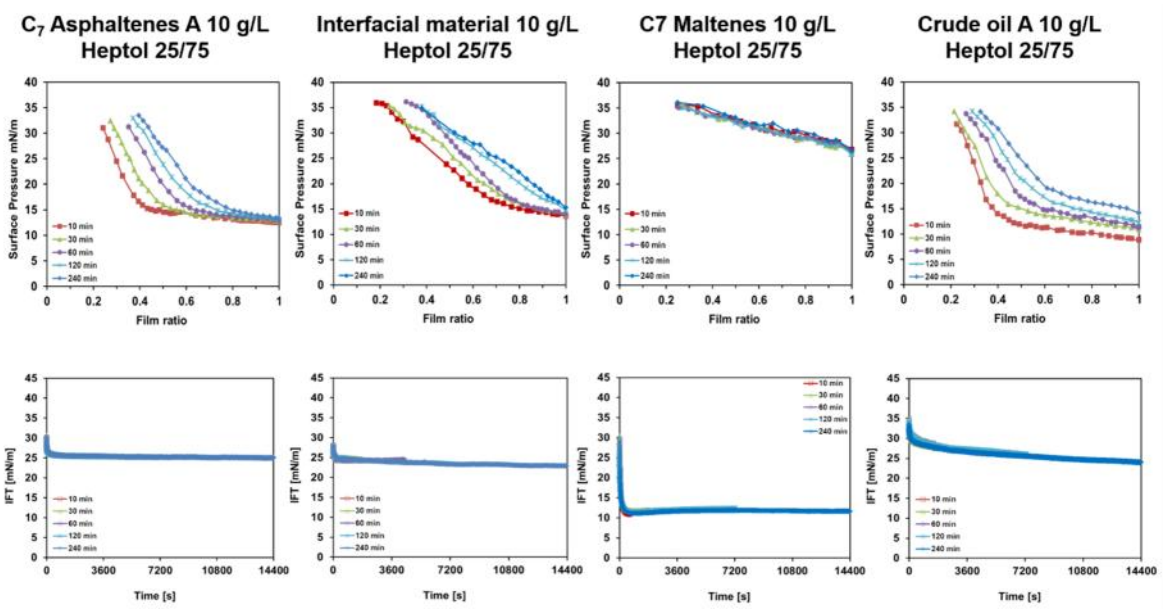

Figure C11. Surface pressure isotherms (top) and dynamic interfacial tension profiles (bottom) for C_7 solid free asphaltenes A, Crude oil A, Maltenes A and interfacial material isolated from an asphaltenes A-stabilized w/o emulsion. All samples were dissolved in heptol (25/75) at 10 g/L.

TABLES

Table C1. *Crumpling point ratio for mixtures of asphaltenes (10 g/L) and acidic fractions at 5, 1.5 and 0.1 wt %.*

Asphaltenes A (10 g/L)
CR= 0.35, 1 hour at 25 °C

Naphtenic acids (NA) concentration wt %	Asphaltenes A + Naphthenic acids fractions	Aged 1 hour at 25°C	
		Crumpling ratio (CR)	
		Mean	SD
5	A+NA F1	0.14	0.021
5	A+NAsF2	0.22	0.007
5	A+NA F3	0.26	0.007
5	A+NA F4	0.16	0.014
5	A+NA F5	0.13	0.014
5	A+NA F6	0.34	0.021

5	A+ All acids	0.15	0.014
1.5	A+NA F1	0.23	0.014
1.5	A+NA F2	0.31	0.007
1.5	A+NA F3	0.34	0.057
1.5	A+NA F4	0.30	0.014
1.5	A+NA F5	0.23	0.014
1.5	A+NA F6	0.34	0.007
1.5	A+ All acids	0.28	0.028
0.1	A+NA F1	0.33	0.000
0.1	A+NA F2	0.34	0.007
0.1	A+NA F3	0.31	0.007
0.1	A+NA F4	0.34	0.007
0.1	A+NA F5	0.33	0.014
0.1	A+NA F6	0.34	0.007
0.1	A+ All acids	0.35	0.007

Table C2. *Crumpling ratio for asphaltenes /standard acids systems*.

Asphaltenes A (0.01 wt%) CR=0.35, 1 hour at 25 °C			
		Aged 1 hour at 25 °C	
Concentration Naphtenic acids %w	Asphaltenes (A) /acids system	Crumpling ratio (CR)*	Standard deviation
5	A+NA standard	0.21	0.007
5	A+5-β-Cholanic acid	0.05	0.028
1.5	A+NA standard	0.28	0.021
1.5	A+5-β-Cholanic acid	0.19	0.000
0.1	A+NA standard	0.33	0.049
0.1	A+5-β-Cholanic acid	0.21	0.014

*Average of two measurements

Table C3. *Crumpling film ratio for asphaltene B and Asphaltene B/F-all acids systems.*

Acidic fraction concentration [wt %]	**Asphaltene B (0.01 wt%) /Acid fraction**
	Crumpling ratio
0	0.08
0.1	0.09
1.5	0.07
5	0.09

Table C4. *Variation of crumpling film ratio of asphaltenes A and B as aging time increases.*

Aging time [min]	**Asphaltene A**	**Asphaltene B**
	Crumpling ratio (CR)	Crumpling ratio (CR)
10	0.24	0.12
30	0.27	0.12
60	0.35	0.08
120	0.37	0.09
240	0.40	0.09

Appendix D. Separation of asphaltene-stabilized water in oil emulsions and immiscible oil/water mixtures using a hydrophobic cellulosic membrane

Table D1. *Description of fixed variables used in the experimental design*

Experimental Variable	Description
Shaking speed	13 000 rpm
Aqueous phase	Synthetic brine
Oil phase	Gasoline
Surfactants	Asphaltene Solution [1000 ppm]

Table D2. *Experimental variables used in the response surface design.*

Symbol	Variable	high level	Intermediate level	Low level
A	% water	50%	30%	10%
B	pH	11	8.6	5.9
C	Emulsifier volume	1 ml	0.55 ml	0.1 ml

Table D3. *ANOVA data for the experimental variables included in the response surface design.*

ANOVA TABLE FOR THE SEPARATE WATER					
Variable	**Sum of squares**	**GI**	**Middle squares**	**Razón - F**	**Value -P**
A: % Water	0,018	1	0,018	0,01	0,9417
B: pH	4,232	1	4,232	1,28	0,2678
C: Emulsifier	208,658	1	208,658	63,34	0
AC	73,96	1	73,96	22,45	0,0001
CC	42,7213	1	42,7213	12,97	0,0014
blocks	0	1	0	0	1
Total error	82,3507	25	3,29403	**R-square= 76,2 %**	
Total (corr.)	411,94	31			

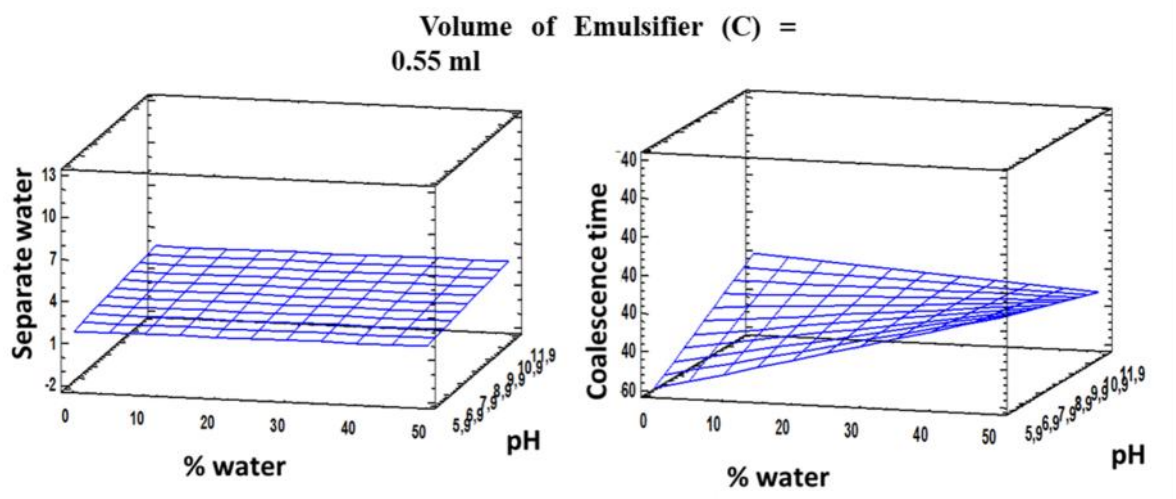

Figure D1. Response surface graphics for the experimental design.

Table D4. *Anova data for the coalescence time variable.*

ANOVA TABLE FOR THE COALESCENCE TIME

Varibale	Sum of squares	GI	Middle squares	Razón - F	Value -P
A: % water	32000	1	32000	8,42	0,0081
B: pH	2880	1	2880	0,76	0,3931
C: Emulsifier	100820	1	100820	26,52	0
AB	42025	1	42025	11,05	0,0029
AC	235225	1	235225	61,87	0
BC	38025	1	38025	10	0,0044
CC	16567,5	1	16567,5	4,36	0,0481
blockes	0	1	0	0	1
Total error	87445	23	3801,96	**R-square= 78,8 %**	
Total (corr.)	554988	31			

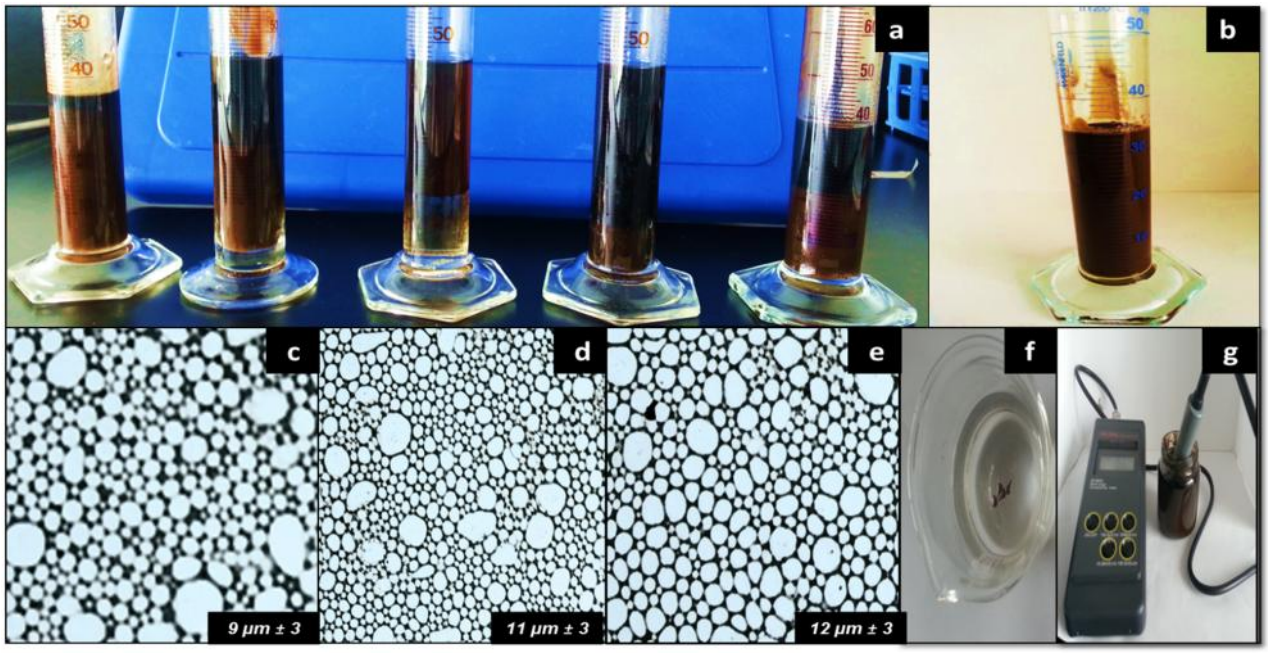

Figure D2. **a)** Bottle tests for emulsion stability experiments**. b)** Photograph of the most stable w/o model emulsion. **c-d)** Images of w/o emulsions with 20/80, 30/70 and 50/50 water/heptol ratios, respectively. **f-g)** Photographs of wettability and conductivity tests.

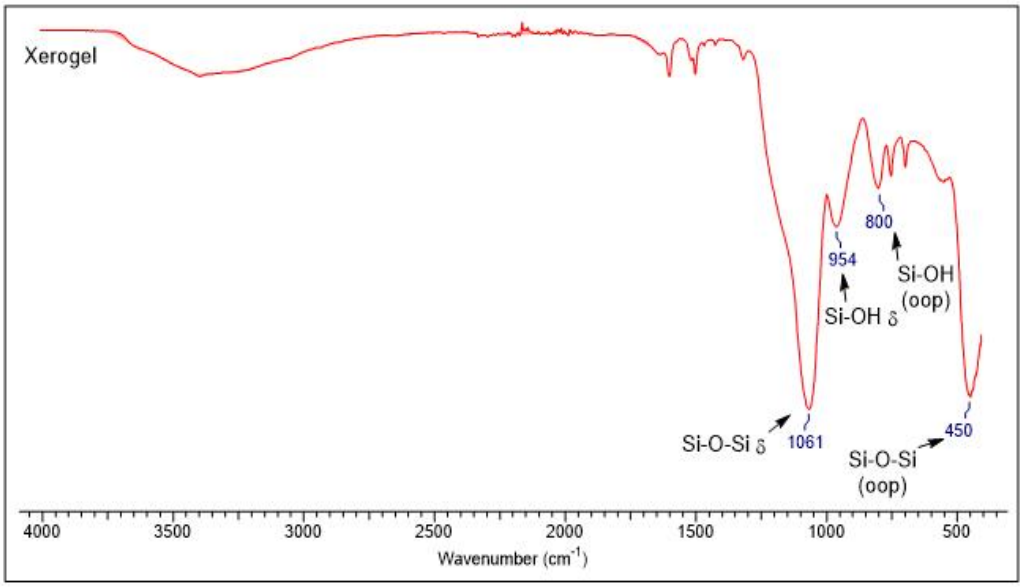

Figure D3. Infrared spectrum of the xerogel obtained after hydrolysis and polycondensation reaction.

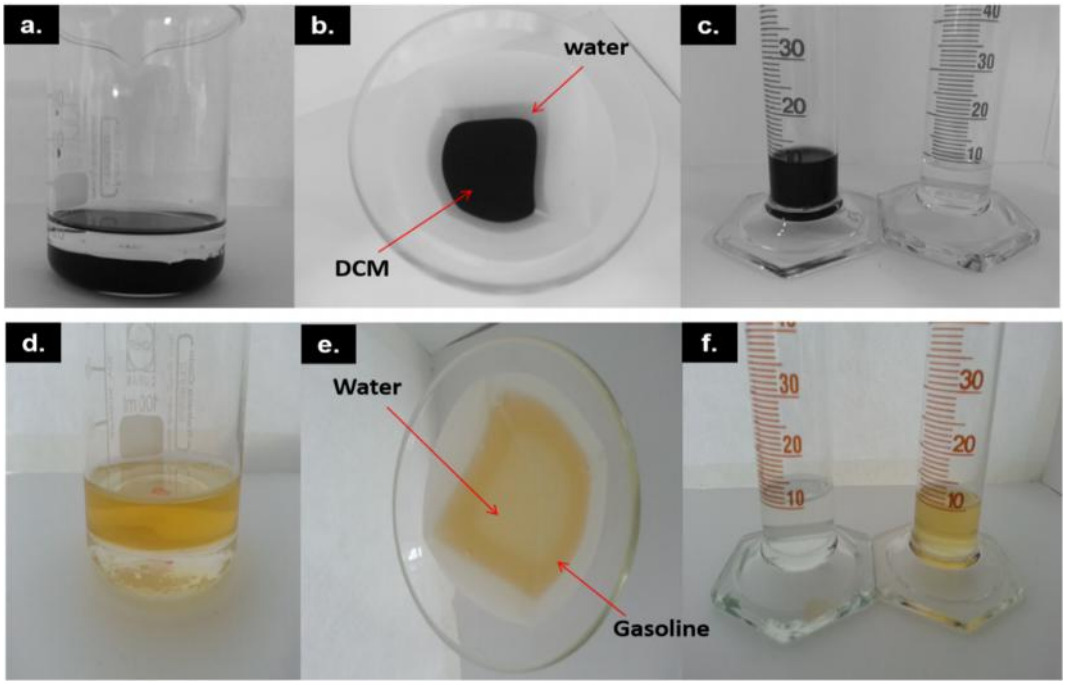

Figure D4. (a-c) Sequence of separation for water/DCM and (d-f) water/gasoline immiscible mixtures driven by gravity filtration using the hydrophobic cellulose filter paper.

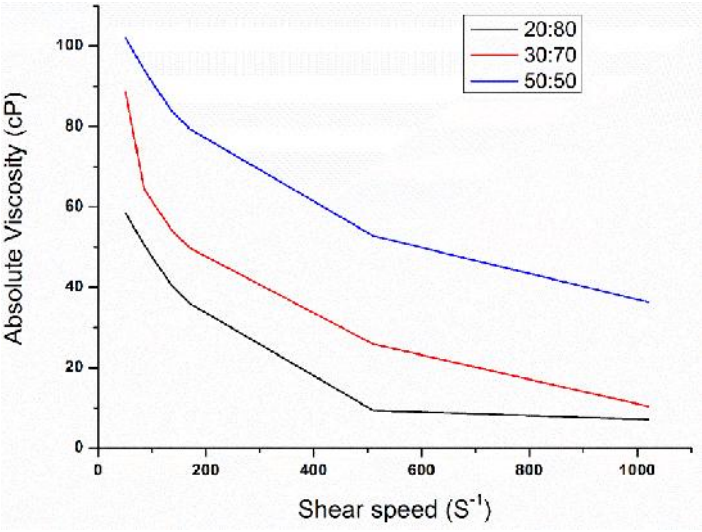

Figure D5. Shear rate vs absolute viscosity of model w/o emulsions stabilized by asphaltenes.

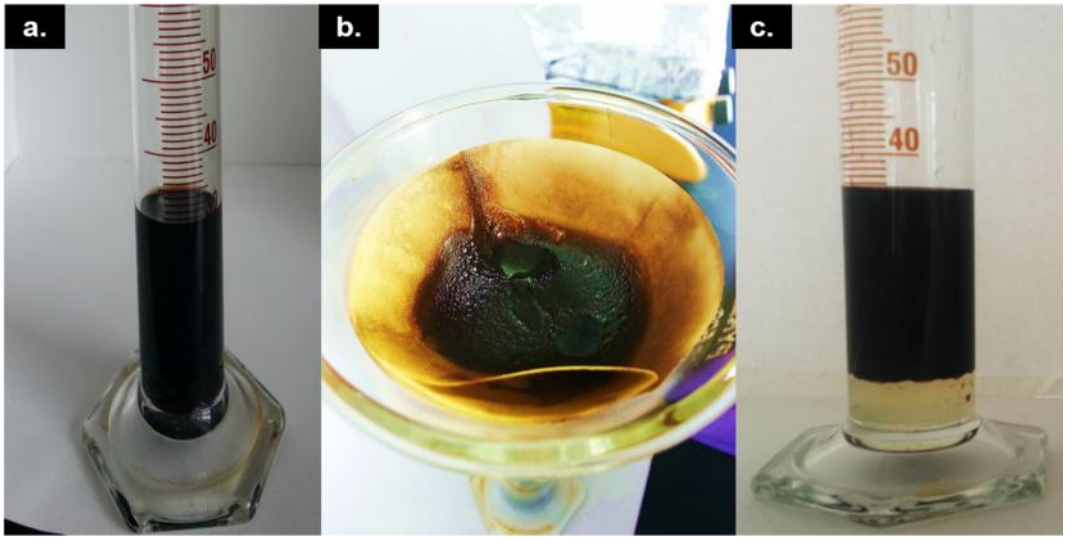

Figure D6. Separation of water in oil emulsions (50 % water content) by gravity filtration using the hydrophobic cellulosic membrane.